Electrode Characterization for Neural Interfaces

Development of a testing platform for reliability and standardization of results, validated via a characterization study of subpar electrodes

Pablo de Anta Dardagan - 5616352

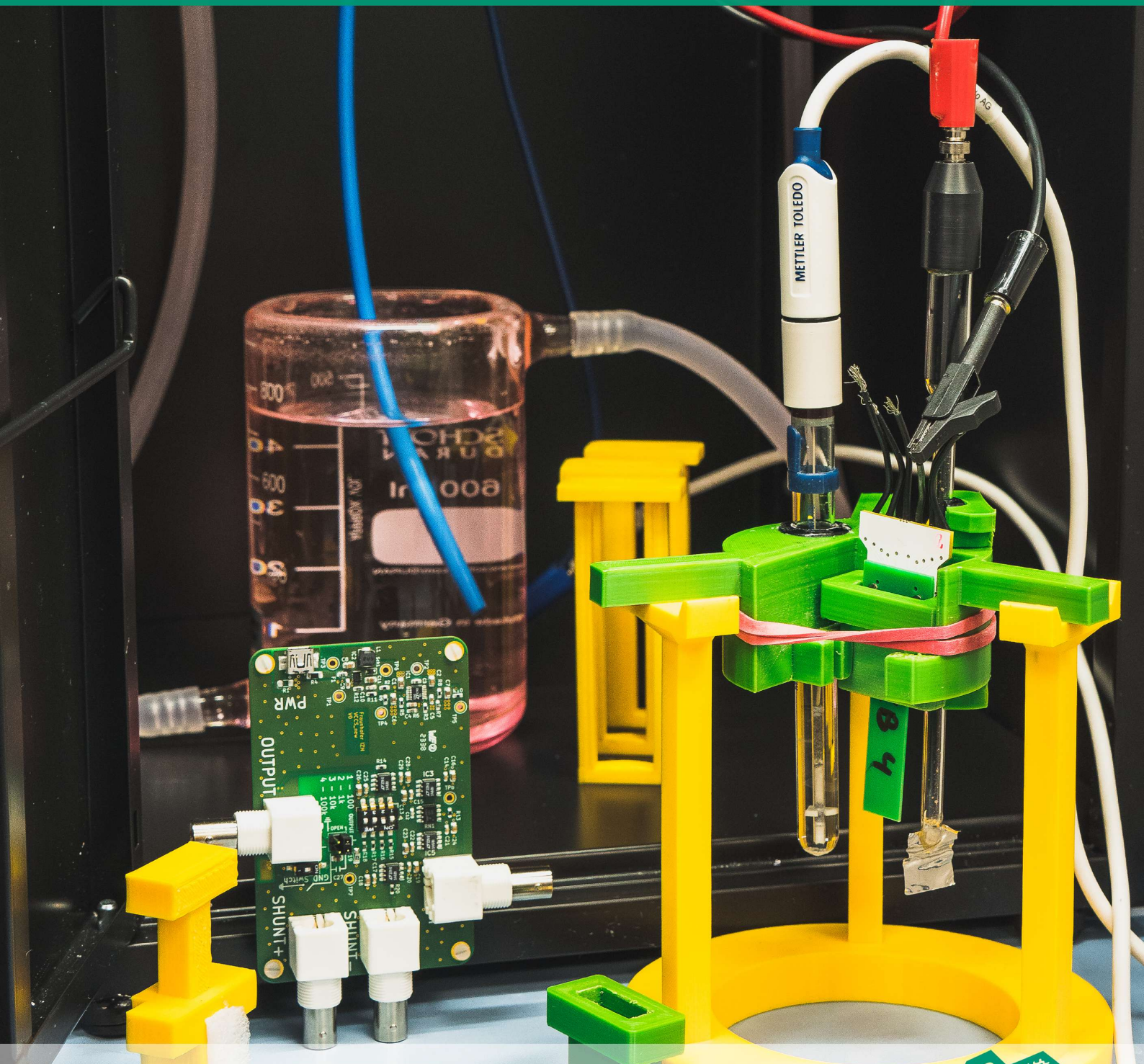

TU Delft
Delft University of Technology

Fraunhofer IZM
Technologies for BioElectronics

Electrode Characterization for Neural Interfaces

Development of a testing platform for reliability and standardization of results, validated via a characterization study of subpar electrodes

by

Pablo de Anta Dardagan

to obtain the degree of Master of Science
at the Delft University of Technology,
to be defended publicly on Tuesday April 16th, 2024 at 9:30 AM.

Student number:	5616352	
Project duration:	January 1, 2023 – December 15, 2023	
Thesis committee:	Prof. dr. V. Giagka,	TU Delft, supervisor
	Dr. J. Wilson,	Fraunhofer IZM, supervisor

Cover:	Photograph of the setup equipment used in this thesis
Style:	TU Delft Report Style, modifications by Pablo de Anta Dardagan & Daan Zwaneveld

An electronic version of this thesis is available at `http://repository.tudelft.nl/`.

TU Delft

Fraunhofer IZM

Technologies for BioElectronics

Preface

Dear reader,

This journey started over a year ago—actually, it started a lifetime ago. So many dreams and goals that were set then came to fruition while working on this MSc Thesis. However, the events that have transpired in the last year have been vital in throwing challenges down my way and making me grow as I overcame them. Both personal and professional, what was achieved - also beyond these pages - **has left a profound mark on me.**

I recall how mid-way through this project; I realized that the lifelong dream of dedicating myself to science and research could already be checked off the list. But, in my effort to constantly do what I do with purpose and meaning, I set myself three objectives that I wished to accomplish by the end of my journey. They have been my daily compass and unwavering support when the storm approached.

Somos enanos a hombros de gigantes.

1. **Be helpful to others.** Whatever you do is for nought if the sole beneficiary is yourself. We are nothing without those who preceded us. Our responsibility with them is to keep the effort moving forward. As my first chance to contribute, my actions were inspired by the potential benefit they could bring to those around me.

Sólo se conoce lo que se ama, y sólo se ama lo que se conoce.

2. It would be trivial to say I entered this journey wanting to learn something new. **What is not trivial is facing the daily challenge with passion and excitement for new horizons**. To learn is to grow, but to really learn, one must do so with love for their learning. Thus, the difference boils down to the attitude with which we face our learning journey and our life. Love what you do, and it will do you well.

Pon en tu vida todo aquello que te traiga Verdad, Belleza, Valor y Bondad.

3. When things are done well, they naturally bring one closer to these four virtues. This is especially true when actions are guided by the previous two objectives and not by the simple wish to attain virtue. **Kept close to my heart, VBVB is why I wish my work to excel.** Although grading matters, it matters less than creating work that resonates with my values. When the latter is accomplished, truth, beauty, value and kindness naturally elevate oneself and its work. This is, in my view, the key to lifelong success.

Only time will tell if what was set as a goal is achieved, but I feel good about this because of everyone who came along for the ride making an impact. They gave me the strength, courage, and passion to pursue what I pursue and how I pursue it. I would really like to appreciate the support by extending my thanks to:

- My supervisors, **Vasso and Josh**, this project would not have existed without your insight. You gave me real examples of what it means to dedicate your life to science and to others. Thank you for always keeping it up.
- **The whole TBE and IZM team.** You gave me the space to try and fail while pushing me to be better and making me grow. Having developed a sense of belonging, I am sure I could not have accomplished my objectives without you. Thank you for welcoming me into your family.
- **Reals, Jumbo, Lunchdate & Berlin friends, and Gilipaeles**. This chapter of my life could be summarised in two: electrodes and you. I would be lost without you. The fun would be lost. The memories would not be worth remembering. The purpose and meaning behind this would be halved at best. I love you all to bits. I can only hope for a life filled with you and everything that follows. Thank you for all the many things.
- **Dad and Mom,** everything I do is only possible because of your support. You are the true giants, and a son can only dream of raising the bar even higher. Thank you once again.
- Those I lost while carrying out this project: **Abuela, Nena and Colly.** Your love and advice have gone wherever I have since your departure. Wherever you are, this success is as much yours as it is mine. Thank you.
- **Paula,** words aren't needed to express what we both know: that I love you and that the thought of carrying out this monumental task without your support belongs in the realm of dreams. Thank you for being a part of this.

With my heart settled on the work done and my eyes locked on the horizon,

Pablo de Anta Dardagan
Madrid, April 2024

Contents

Nomenclature

Abbreviations

Abbreviation	Definition
AC	Alternating Current
ADC	Analog-Digital Converter
AFG	Arbitrary Function Generator
AIBMD	Active Implantable BioMedical Device
AIROF	Activated Iridium Oxide Film
CE	Counter Electrode
CV	Cyclic Voltammetry
DALYs	Disability-Adjusted Life Years
DC	Direct Current
EC	Electrochemical
ECM	Electrochemical Measurements
EIS	Electrochemical Impedance Spectroscopy
ENEPIG	Electroless Nickel Electroless Palladium Immersion Gold
PBS	Phosphate-buffered Saline
PCB	Printed Circuit Board
RE	Reference Electrode
SNR	Signal-to-Noise Ratio
VCCS	Voltage-Controlled Current Source
VT	Voltage Transients
WE	Working Electrode
WW	Water Window

Symbols

Symbol	Definition	Unit
C	Celsius Temperature Degrees	[º]
C_{dl}	Double-Layer Capacitance	[F]
CIC	Charge Injection Capacity	[mC/cm^2]
CSC	Charge Storage Capacity	[mC/cm^2]
CSC_{cath}	Cathodic Charge Storage Capacity	[mC/cm^2]
ESA	Estimated Surface Area	[cm^2]
GSA	Geometric Surface Area	[cm^2]
I	Current	[A]
ISR	Injection to Storage Ratio	Dimensionless
M	Molarity	[mol]
L	Inductance	[H]
P	Power	[W]
PSD	Power Spectrum Density	[dBW/Hz]
R_{Ω}	Cell medium Resistance	[Ω]
R_{ct}	Electron Transfer Resistance	[Ω]
V	Voltage	[V]
V_{a}	Access Voltage	[V]
V_{msn}	Microelectrode System Noise	[V]
V_{ni}	Total Instrumentation Noise	[V]
V_{np}	Single Reference Electrode Noise	[V]
$V_{\text{nμ}}$	Microelectrode noise	[V]
V_{OFFSET}	Offset Voltage	[V]
V_{r}	Reaction Voltage	[V]
V_{rsn}	Reference System Noise	[V]
Z	Impedance	[Ω]
Z_{CPE}	Constant Phase Element	[Ω]
Z_{W}	Warburg Impedance	[Ω]
θ	Phase Angle	[º]

I Abstract

Characterizing electrodes for neural interfaces is an essential step of the prototyping and manufacturing process. Sample performance can be modelled by conducting electrochemical measurements such as Electrochemical Impedance Spectroscopy, Cyclic Voltammetry, Voltage Transients and Noise characterization, providing insights for future use scenarios. However, parameters, techniques, and scientific reporting of results often fall short of a complete characterization and do not adhere to any standard. A platform for accurate, reliable, and standardized electrode characterization was conceived to overcome these obstacles. It allows complete electrochemical characterization while providing a modular 3D-printed solution to securing the electrodes above the beaker. Additional parameters, such as electromagnetic isolation and control of the medium, are also accounted for. A complete characterization study of ENEPIG electrodes was carried out to validate the setup. Manufactured as circuit boards, not electrodes, several aspects of their electrochemical performance were lacking - mainly their survivability to the stress applied by the tests carried out. Testing parameters had to be determined to minimize structural damage while maximizing performance, akin to what would be desirable in a clinical setting. Sensing characterization experiments identified a double-layer electrode structure and revealed that smaller electrodes exhibit capacitive behaviour in bandwidths one order of magnitude wider than larger ones. Stimulation characterization experiments ascertained that charge surface distribution would predominantly accumulate along the perimeter of the electrode. In conjunction with surface characterization, results indicate the flat surface of the electrodes prevents charge from being stored and injected optimally. Ultimately, the performance of the ENEPIG electrodes was measured with the injection-to-storage ratio at 10%, significantly inferior to other Au electrodes reported in the literature and utilized *in vivo*. As results accurately represented the sample population, characterization was deemed successful - validating the experimentation setup developed for this project.

II Introduction

According to the Global Burden of Disease study, there were nearly 10 million deaths related to neurological disorders in 2019, costing 210 million disability-adjusted life years (DALYs) and showing a significant increase compared to data from 1990 [1, 2]. Two approaches exist to address this: pharmaceutical and bioelectronic solutions. Although pharmaceuticals have been used for over a century, they are known for provoking undesired effects and lacking specificity [3, 4, 5, 6, 7]. Meanwhile, bioelectronics aims to close this gap by having significantly fewer side effects and high site-specificity at the cost of invasiveness [8, 9].

Neural interfaces are bioelectronic devices that can read changes in neural activity and modulate it through their active elements. Using these two modes, they can effectively record neural activity and provide therapy by activating or inhibiting neural networks - in a process known as neuromodulation [8]. Most neural interfaces interact with neural tissue in the electrical domain. This is achieved via electrodes implemented using various materials (usually metals, although some other materials such as conductive polymers are possible), which act as electrochemical transducers [10]. Changes in the chemical environment of an electrode may be reflected in the electrical domain and vice-versa. Their ability to perform this transduction determines how well they can record neural signals or safely inject charge to elicit a neural response [11, 12]. As neurological disease challenges are met with active efforts to create better neural interfaces, improving electrode performance is at the centre of the efforts of the scientific community.

Before *in vivo* use, the quality of the electrode must be characterized. That is to say, figures of merit indicative of required performance criteria must be selected and measured. For characterization to be valid, it must be performed accurately, reflecting the use case and sufficiently reproducible to enable broad comparison between a range of samples measured in different laboratories [13, 14]. There are many challenges to achieving such tests, including equipment accuracy, test sample design and selecting test parameters [11, 15]. Comprehending and overcoming these challenges is the basis of performing a correct sample characterization.

When reading through literature (both old and new), there is no consensus around electrode characterization for neural implants. Precisely because of the challenge in trying to unify characterization practices, several guideline-type papers for adequate electrode characterization have been published, with notable examples from Cogan *et al.* in 2008 and Boehler *et al.* in 2022 [10, 11, 13, 15, 16, 17]. Despite these efforts, factors such as different measurement setups, a vast range of test parameters, and poor scientific reporting have prevented electrochemical electrode characterization from reaching any standard. Even some of the most reported metrics, like the Impedance value at 1 kHz (Z @ 1 kHz), are under heavy scrutiny due to the limited information they provide [13]. Thus, there is still a strong need to establish good characterization practices and how they should be performed.

Inspired by the above, we developed a testing platform for standardized and reliable electrode characteri-

zation tailored to neural interfaces. It features modules to perform electrochemical impedance spectroscopy (EIS), cyclic voltammetry (CV), voltage transients (VTs) and noise measurements in phosphate-buffered saline (PBS) solution at a controlled temperature. It can extract parameters such as electrode impedance (Z), charge storage capacity (CSC), and charge injection capacity (CIC). It was designed following the guidelines proposed by relevant literature, [11, 13, 15] and then tested by characterizing printed circuit board (PCB) electroless nickel electroless palladium immersion gold (ENEPIG) electrode samples of different sizes. These samples were manufactured as regular PCBs, not meant to be used as electrodes. Because of this, aspects such as manufacturing reliability, survivability or electrochemical performance do not match those of commonly used electrode materials. This non-ideal behaviour was also used to test the integrity and validity of the setup itself, as tests should reflect sample-type peculiarities while still exhibiting shared trends. Data plotting and analysis steps were also included to further look into the behaviour trends of these unusual electrodes and determine if the setup measurements accurately represented the samples.

III Methods

A summary of all the characterization tests carried out in this project can be found in Figure 1.

1. Electrode Characterization Setup

A dedicated setup was built to characterize electrodes in a repeatable configuration, replacing the previous unreliable and troublesome setup (Appendix C.1). Repeatability matters to ensure reliable characterization results that can be compared across our measurements and is a necessary step for developing a standardized characterization method. Additionally, comparing measurements to literature was a priority, which demanded control of:

- **Electromagnetic isolation.** Electrochemical measurements are susceptible to interference by external electromagnetic sources [18]. Specifically, 50 Hz power line interference (PLI) was an issue due to other equipment near the setup being used [19, 20]. The setup was efficiently isolated using a grounded Faraday cage, removing external interferences.
- **Testing medium.** The condition of the medium directly influences the kinematics of the electrochemical reactions occurring. Thus, it must achieve conditions similar to *in vivo* environments and do so reliably. Several parameters influence the medium:
    - **Medium Temperature.** As the human body has a rather constant temperature of 37° C [21], testing conditions mimic this by employing a thermostat heating up a double-glass walled beaker and a thermometer immersed in the testing medium.
    - **Medium concentration and pH** play a very large role in determining reaction kinematics [22]. PBS solution is recommended because even if the specific *in vivo* electrolyte is not replicated, the ionic composition and conductivity are sufficiently close to provide accurate and reproducible measurement data [11, 13]. Carl-Roth ROTI©Fair PBS 7.4 (pH of 7.4, 0.1 M) dissolving tablets were used.
    - **O_2 degassing.** Otherwise known as sparging, an inert gas (N_2) is bubbled through a liquid (PBS) to remove a reactive species (O_2) it contains [23, 24, 25]. Sparging O_2 for electrode characterization matters because tissue concentration of O_2 is lower than in PBS at ambient conditions [13, 26]. Accurate characterization should account for it by sparging O_2.

Figure 2 encompasses all the components used in the setup, including a thermostat with a double-glass walled beaker, a N_2 probe for sparging O_2, a custom modular 3D-printed electrode holder and a Faraday cage with ports for all the connections. Several 3D-printed pieces were designed to adapt to different sample types and use scenarios, building on the modular design. Schematics are in Appendix C, from C.11 to C.27.

To ensure the setup was prepared in a standard, safe and efficient manner, the electrode characterization testing platform protocol was written and followed for all the experiments in this thesis (Appendix E.1). It is also intended to guide future users and ensure their measurements are reliable.

Before testing for data acquisition, the Solartron Modulab XM+ was calibrated. The test cell with an ideal electrode circuit (Appendix C.5) was connected to both the Modulab XM+ and a separate impedance analyzer (Keyence Insight). EIS tests were performed on both instruments, maximizing their respective frequency ranges: 0.1 to 100 kHz for the Modulab XM+ and 20 to 100 kHz for the Keyence. The test cell circuit was modelled in LT Spice, and its EIS was simulated.

Additional test parameters on how each electrode type can be most accurately characterized were determined before data acquisition.

The ultimate goal of characterization is to predict the performance of an electrode in its final setting (often clinical, *in vivo*). Therefore, *in vitro* testing parameters must reflect that too. To optimize performance, electrode types are operated within their Water Window (WW), and they should be characterized and compared accordingly. The WW is defined as the voltage range where water electrolysis does not occur for a particular electrode type. It is used to define a voltage window for the safe operation of the electrode (within the WW bounds). It was determined according to the indications from Boehler *et al.* [13]. Each

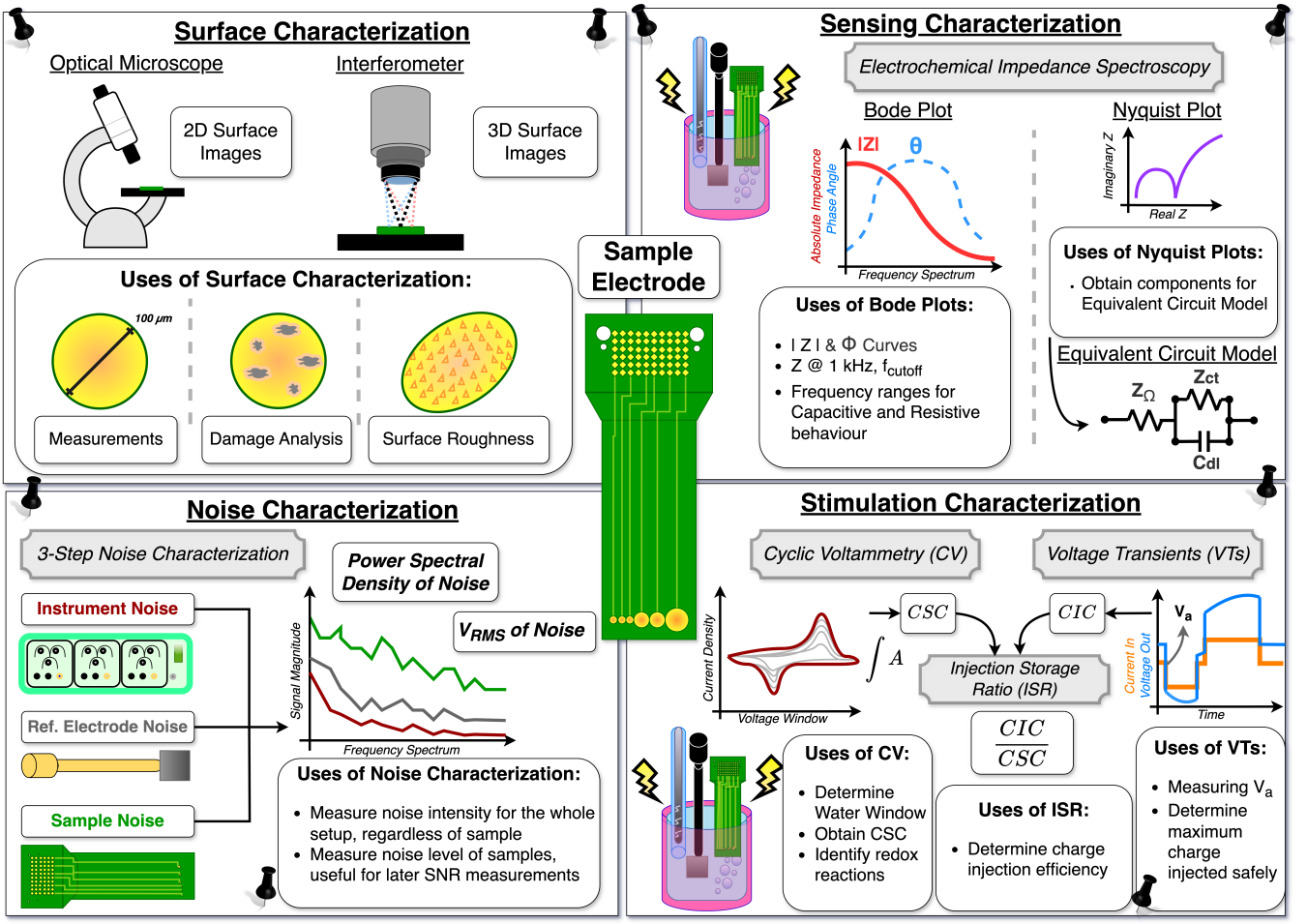

Figure 1: Summary figure of the main characterization tests carried out in this thesis. **Surface Characterization** concerns evaluating the surface of the electrode through imaging techniques. **Sensing Characterization** aims to define the capabilities of an electrode to detect field oscillation in its environment. **Noise Characterization** applies to both the measurement setup and samples, as they should have their basal noise level measured. **Stimulation Characterization** studies the capabilities of an electrode to store & inject charge.

bound of the WW needs individual testing, so two cyclic voltammograms were needed. In a single voltammogram, the sample was driven from 0 V to $\pm$ 1.5 V, past the required voltage to hydrolyze water molecules, driving an irreversible reaction. By observing when this reaction shows in the voltammogram as a peak [17, 27, 28], the maximum bound value for the safe operation of the electrode was determined. Ideally, reactions happen reversibly when an electrode operates within its WW, so its electrochemical structural integrity should remain intact [11, 17, 29, 30]. This is important both for characterization purposes and biocompatibility issues.

VT tests aim to determine the maximum charge injected safely by an electrode. A charge-balanced biphasic pulse is applied through a current stimulator PCB, and the maximum polarization reached, either at the cathodic or anodic ends, is determined [31]. The asymmetry ratio between the currents for the cathodic and anodic pulses is a crucial parameter determining how much charge is injected. Depending on the type of electrode tested, Cogan *et al.* proved it is possible to maximize the charge injected safely by an electrode by tweaking the asymmetry ratio of the pulses [32, 33, 34]. Ratios of 1:1, 1:2, 1:4 and 1:8 were tested while keeping the pulses charge-balanced and within the WW of the electrode. The maximum injected current was compared for each ratio and which WW bound (cathodic or anodic) was first reached. Acquiring data from VT tests was then conducted using the chosen ratio to compare CIC results.

Electrochemical noise characterization was achieved by measuring the noise signal of each category. The noise signal introduced by samples or instruments was characterized by its power spectrum density (PSD) and its root mean square voltage (V_{RMS}). The PSD of a noise signal indicates the power of the noise signal across the frequency spectrum it is used in [35], while the V_{RMS} of a noise signal (AC) gives an estimate of the equivalent voltage in DC that is required to produce the same power effect [36].

To measure the noise a sample introduces, it is necessary to know the noise contributions of the rest of the setup: the measurement instrument, the reference electrode used during testing and common equipment such as cables, adapters or ports. The following 3-step noise characterization method described by Gabran *et al.* was followed [37].

1. **Instrumentation Noise.** Defined as V_{ni}, by short-circuiting the front end of the amplifier, the noise voltage of the instrumentation can be recorded.
2. **Reference System Noise.** Defined as V_{rsn}, it is measured by employing two identical reference electrodes. Two Pt flag foil electrodes were manufactured in-house, with a total active surface area of 1.2x1.2 cm. Figure C.10 shows images of the manufacturing electrodes. Due to their large active area and identical build, the noise contributions of each Pt electrode (V_{np}) should be the same. Following Equation 1, the individual noise contributions of one reference electrode can be determined.
3. **Microelectrode System Noise.** Defined as V_{msn}, it is the total noise sum of the instrumentation noise V_{ni}, the contribution of a single reference electrode V_{np} and the noise contribution of the microelectrode of interest ($V_{\text{n}\mu}$). Thus, following Equation 2, it is possible to characterize the noise signal of a sample electrode by identifying all the individual contributions in the measurement of the system.

$$V_{\text{rsn}} = V_{\text{ni}} + 2V_{\text{np}} \tag{1}$$

$$V_{\text{msn}} = V_{\text{ni}} + V_{\text{np}} + V_{\text{n}\mu} \tag{2}$$

Once steps 1. and 2. were performed, different electrode samples were characterized in a single measurement. Swapping the microelectrode sample tested in step 3. does not affect prior results for V_{ni} and V_{np}, as noise contributions are independent [37, 38].

2. Sample Design and Manufacturing

To test and validate the characterization setup, a batch of 15 sample PCBs with ENEPIG openings of different sizes was ordered from Würth Elektronik. Of the 15 samples, two had their openings destroyed during manufacturing; five were used to determine testing parameters before the sample study; seven were characterized with EIS, CV and VT testing, and one sample was used for noise characterization. The six circular opening sizes were designed to go from the smallest diameter possible for the tooling employed (200 µm) to 900 µm - diameters larger than 1mm would not be considered microelectrodes. Opening diameters were evenly spaced out in the log scale between these two openings. The total progression of theoretical opening sizes was set to be 200, 270, 370, 500, 670 and 900 µm. The Gerber file design used in manufacturing the samples is in Appendix D.1.

As PCBs, openings were manufactured to be used as soldering pads, not electrodes. Thus, ENEPIG was the only available material for the openings, which is considered a gold-standard material to solder on. ENEPIG contacts consist of three thin metal layers stacked on one another on top of a substrate with Cu wiring. Standard ENEPIG plating starts at the bottom Ni layer (3 - 6 µm thick), followed by the Pd mid layer (0.05 - 0.30 µm thick) and finished with a Au layer as its surface finish (≈0.30 µm thick) [39, 40, 41]. Regardless of their thin profile, they are regarded as strong contacts for soldering and wire bonding partly due to their flat surface profile [42, 43, 44].

3. Surface Characterization

Circular openings with different diameters were designed for the electrodes, leading to different geometric surface areas (GSA). Although the GSA for the electrodes should be the same for each size category, various fabrication techniques and variations within each process made their opening sizes different. Optical microscopy was performed on all samples to determine their opening size and establish their estimated surface area (ESA). The ESA value for each sample then replaced their GSA when producing characterization results dependent on the opening area [11, 13].

Additional surface characterization was performed using a Leica DC8 Interferometer. Both confocal and interferometry imaging were carried out to study the surface topology of electrodes before and after their electrochemical characterization. Blue light was used, with selected intensities between 10% and 11%.

4. Electrochemical Characterization

Three electrochemical measurements (ECM) were performed for each sample microelectrode: EIS, CV and VTs. To best simulate the human internal environment [11, 13, 15], tests were carried out in PBS at 37º C. For EIS and CV, a three-electrode setup is needed. The setup is comprised of the sample working electrode (WE), an in-house built large Pt foil flag counter electrode (CE) for minimum impedance contribution, and a glassy-carbon tube Ag/AgCl reference electrode (RE) from Mettler Toledo. The three electrodes, held in place by the electrode holder, can be seen in Figure 2E and Appendix C.15. VTs only require a WE and a CE, as the oscilloscope provides the reference (Figure 2B).

EIS tests measured impedance changes across the WE-CE pair against the RE using the Modulab XM+ ECS testing platform by Ametek, with its proprietary Femto Ammeter module (Fig. 2A). Frequency sweeps were set to the whole bandwidth of the instrument (0.1 Hz to 100 kHz), with a V_{RMS} of 10 mV at each point, considered a standard value for this test [13, 45, 46]. A total of 20 points

per decade were measured and spaced evenly on the frequency log scale. Tests were repeated thrice, and results were later averaged for each studied sample. It allowed us to gain statistical information on the possible measurement variations in absolute impedance and phase angle ($|Z|$ and θ) for a single sample.

EIS results were then plotted as Bode plots with the average values and deviation spectrum using a dedicated Matlab code (Appendix B.1). Their Z @ 1 kHz and cutoff frequency (f_{cutoff}) were extracted as figures of merit, as they are considered standard metrics to report EIS tests - yet also criticized for misuse [13, 47, 48, 49]. Additionally, the real and imaginary components of $|Z|$ (ReZ and ImZ) were plotted in Nyquist plots. Analysis of features in these graphs, such as maxima, minima and slopes, led to extracting values for their equivalent circuit components - further details on the method used can be found under Appendix D.12. Circuit models were built from these components, closely following relevant literature on the topic [16, 50, 51, 52, 53, 54, 55].

CV measures the current output between the WE-CE pair as a sweeping voltage is applied using the Modulab XM+ ECS (Femto Ammeter module, Ametek) (Fig 2A). The WW determined the cycle bounds, which were previously measured (Fig 3C & D). Cycle after cycle, the surface of the electrode activates until theoretically settling in a stable cycle path [17, 56]. As this cycle is employed for extracting figures of merit to characterize the sample, criteria for stability need to be established. A Matlab code was written to analyze the difference between the minimum and maximum values between each pair of consecutive cycles in a CV (this and the entire CV Matlab code may be found in Appendix B.4). For a cycle to be deemed stable, the selected difference between the minima and maxima must be less than 0.5% of the previous values.

Each sample was also tested with three different scan rates: 50 mV/s, 200 mV/s and 500 mV/s. When a sample electrode is swept at a slower rate, it is more able to recruit structures in its surface with lower exposure to the medium, as chemical species have a longer time to interact at the interface of the electrode [13, 28, 57, 58]. Employing several rates is helpful to gain information on the surface features of a sample and whether its performance varies according to the stimulation protocol employed [11, 28, 29, 30].

The stable cycle at each scan rate for every sample is then used to obtain the charge storage capacity (CSC, [mC/cm^2]) of the electrode. The total charge stored in that cycle is determined by integrating the area enclosed by the CV curve. As charge is especially relevant to electrodes employed under stimulation protocols, the cathodic contribution may be prioritized over other charge metrics [11, 13, 17]. Hence, the cathodic charge storage capacity (CSC_{cath}, [mC/cm^2]) can also be calculated by taking the integral of only the cathodic section of the curve (negative current in our convention). Besides charge quantification, current density peaks were evaluated to study EC reactions happening at the interface [17, 27, 59, 60]. The voltages at which reaction peaks occur (V_{r}) were used to identify the reactions. In contrast, their width was used to assess the kinetics of the electrochemical species during the EC process.

To quantify the injected charge in a VT test, the maximum CIC achieved while ensuring safe stimulation (within WW bounds) was determined by measuring the access voltage (V_{a}) using a custom PCB and a Tektronix MDO34 oscilloscope. The PCB is an improvement on another previous PCB for a voltage-controlled current source (VCCS) [61, 62], adding better signal stability, portability, and tuning capabilities to accommodate samples with a more extensive range of impedances. The diagram of this PCB may be found in Appendix C.30 and C.31. Controlled via Python code (Appendix B.5), the arbitrary function generator (AFG) of the MDO34 sent biphasic voltage pulses to the VCCS PCB. The VCCS PCB then delivered the same pulse profile to the WE-CE pair but as a current pulse. Parameters were set in-code, with a cathodic lead pulse, a pulse asymmetry ratio of 1:4, a cathodic pulse duration of 200 µs and an interphase delay of 20 µs being kept constant for all tests. These parameter values have become standard for VT characterization practices as they represent standard clinical electrode stimulation protocols [11, 33, 34, 63, 64, 65, 66, 67].

V_{a} is defined as the immediate shift in voltage observed in an electrode as a current pulse is applied. It is a result of the ohmic drop resistance (R_{i}) of the electrode, expressed in Equation 3 [11]. VTs were carried out by increasing the current pulse amplitude until V_{a} reached the value of either the cathodic or anodic WW bound (further information on the actual procedure followed may be found in Appendix E.1) [13, 68].

$$V_{\text{a}} = i_{\text{c}} * R_{\text{i}} \tag{3}$$

Determining whether V_{a} had reached its safe maximum was achieved by inspecting the output transient with the measurement tools of the oscilloscope [69, 70]. The same measurement procedure, described in the Electrode Characterization Protocol (Appendix E.1), was followed for all tests to ensure data was comparable despite the manual procedure. Then, data was exported with the Python code and further analyzed with a complementary Matlab code (Appendix B.6) where the CIC of the electrode was calculated as in Equation 4.

$$CIC = (i_{\text{pulse}} * t_{\text{pulse}})/ESA = Q_{\text{inj}}/ESA \tag{4}$$

The charge injected (Q_{inj}, [mC]), calculated by multiplying the current pulse amplitude reached by the pulse time, was divided by the ESA, resulting in charge injection capacity per unit area [mC/cm^2].

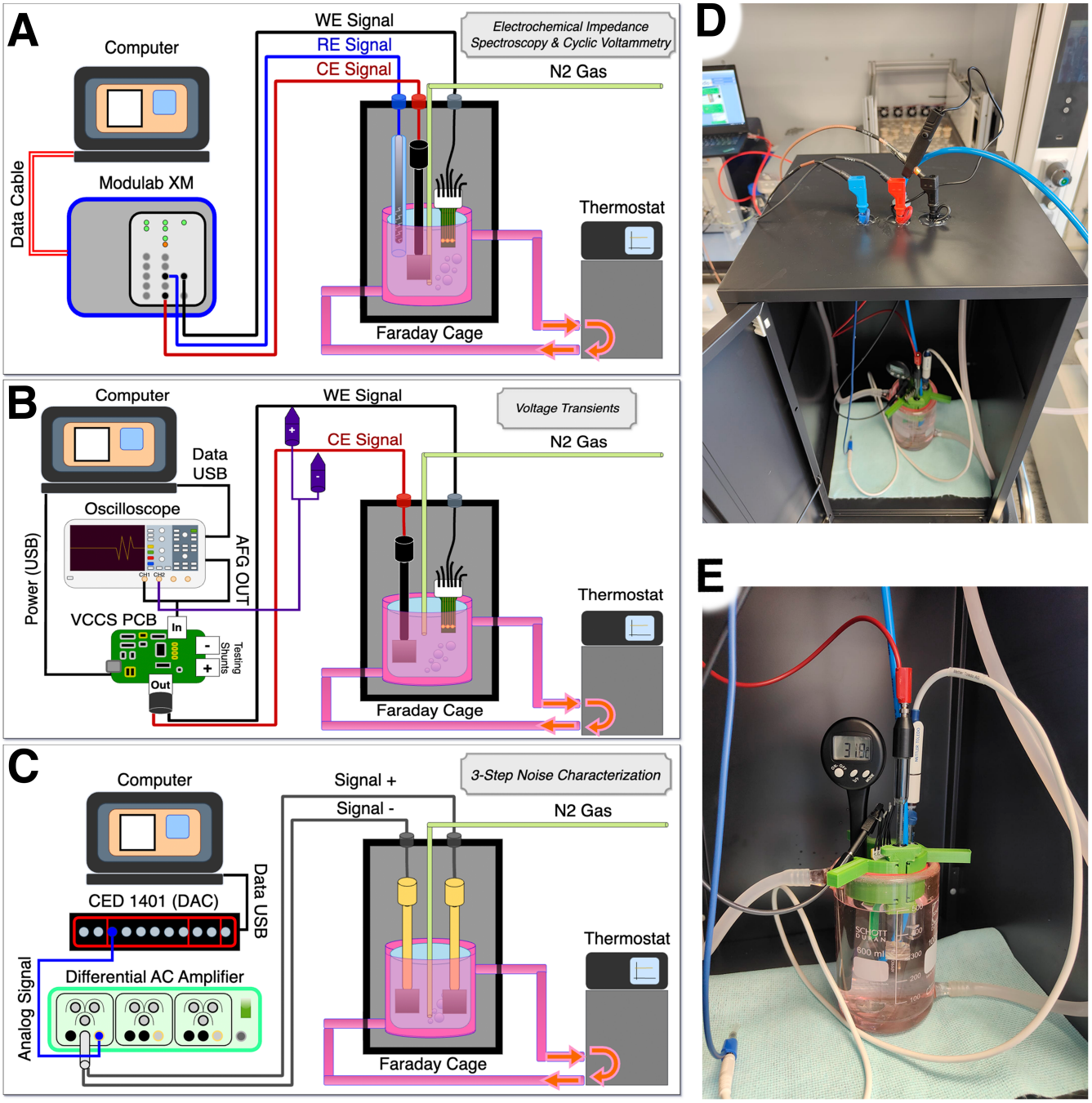

Figure 2: Electrode Characterization setups used for the different tests conducted in this thesis. Pictures of the complete set of required equipment are found in Appendix C, from C.2 to C.9. Common elements include the thermostat and double-glass walled beaker for temperature control, a N_2 probe for O_2 sparging of the medium, a Faraday cage for electromagnetic isolation, the PBS medium with a pH of 7.4 and the computer for data acquisition. **A -** Electrode Characterization setup diagram used with the Modulab XM+ testing platform to perform EIS and CV tests. A three-electrode setup comprised of a WE, CE and RE is needed. **B -** Electrode Characterization setup diagram used with the MOD34 Oscilloscope and the voltage-controlled current source (VCCS) PCB to perform VT tests. The MDO34 receives signal data from the computer and then relays it with its arbitrary function generator output to the VCCS PCB. A WE and CE are needed, while the MDO34 provides the reference. **C -** Electrode Characterization setup diagram used with the Amplifier+ADC pair to perform noise characterization tests. The diagram shows the second step of noise characterization, where the reference system noise is measured. The two Pt foil flag electrodes differ from the CE used in other tests. Because they need to be identical to each other, they were built specifically for noise characterization tests. **D -** Image from the outside of the Faraday cage, showing the electrical and N_2 port interface of the cage. Crocodile grippers attach to the shielding of the WE signal cable to electrically ground it to the Faraday cage. Ports for the heated liquid of the thermostat are located at the backside of the cage. **E -** Image of the interior of the Faraday cage with the three electrodes setup in the thermoregulated beaker. A thermometer is placed during warm-up to monitor the medium temperature.

5. Additional Electrode Characterization Data Analysis

Additional analysis of the obtained electrode characterization data was done to understand trends and gather insight on advanced characterization metrics.

- EIS was performed on each electrode sample 3 times. Results were then averaged to obtain its figures of merit (Z @ 1 kHz, f_{cutoff}). To obtain results for each size category, figures of merit and $|Z|$ & θ curves for 5 samples within that size category of interest were again averaged. Standard deviation was also computed across the 5 samples.
    - Z @ 1 kHz was averaged over the opening size and PCB sample.
    - f_{cutoff} values were first identified as either belonging to the low- or high-frequency spectrum and then averaged out per opening size
    - An average equivalent circuit model of a double-layer Randles circuit was built by averaging values for the circuit components across three models per opening category.
- CSC data from CV tests was analyzed by scan rate, opening size, and PCB sample.
- CIC data from VTs was averaged over opening sizes and PCB samples.

To understand the overall stimulation properties of the electrode, one last metric was introduced: the injection-to-storage ratio (ISR). Expressed as a ratio of the injected to stored charge (Equation 5), the ISR of an electrode was used to understand the stimulating efficiency of its material surface. Ganji *et al.* showed how high-CSC/low-CIC electrodes demand more power for delivering the same neuromodulation pulse, resulting in shorter battery lifespans for implantable neural interfaces [71]. By relating how an electrode stores and then injects charge through charge capacities, sample geometry does not influence ISR. Instead, other factors relating to charge storage and injection, such as electrode material choice and surface roughening features, are reflected when using the ISR. ISR was calculated using the CIC & CSC (at each scan rate) results of each sample, then averaged over five samples per opening size category.

$$ISR = CIC/CSC \tag{5}$$

IV Results

1. Electrode Characterization Setup

Figure 3 and Table 3 show results obtained while testing the platform to research fundamental aspects required for the correct characterization of samples.

Figure 3A shows calibration testing of the Modulab XM+ with its test cell. It showed accurate readings, better than the Keyence in the high-frequency spectrum, and overlapped the LT Spice model measurement.

Figure 3B demonstrates the efficacy of the built Faraday cage by comparing EIS measurements with and without using the cage. Removal of the PLI 50 Hz phase peak can be observed in the caged measurement. $|Z|$ and θ curves show less disturbance in the lower frequency spectrum. When measured without the cage, the $|Z|$ curve tends to show sudden changes in its slope, but these artefacts disappear when adequately caging and grounding the setup.

Figures 3C & D show the recorded cycles in CV WW testing. Red dotted line arrows indicate the hysteresis direction when performing the voltage cycle. Figure 3C is for the negative bound test. It showed a curve shape characteristic of ENEPIG electrodes with current densities increasing in amplitude as the voltage reaches extreme values [59]. As it was not helpful for peak identification, additional tests focusing on studying structural integrity when testing a sample to different negative bounds (Appendix D.11) led to choosing -0.6 V as the negative bound for the WW. Figure 3D is for the positive bound test. The positive bound of the WW was determined by observing the peak shown in the graph at +0.4 V. To ensure a safe testing bound, the bound was set at +0.3 V.

Table 3 indicates the maximum current injection achieved during VT tests with different pulse asymmetry ratios. Current is expressed in terms of the maximum current achieved for the tested sample (PCB 2, 270 µm, 370 µm, 500 µm, 670 µm openings) throughout all tests. Additionally, the WW bound where V_{a} first maximized its value for safe injection is noted.

As 1:4 was the smallest ratio with maximized injected current while only reaching a single bound (easier detection, safer operation), it was chosen as the VT asymmetry ratio for all further characterization tests.

2. Surface Characterization

Figure D.2 in Appendix D shows optical microscope images of the ENEPIG sample electrodes. Images were taken using Dark Field lighting. Using the microscope images, the diameter of the electrode openings was measured and used to determine the ESA of each sample. Table D.1 in Appendix D collects the average measured diameter value for each size category and the standard deviation between all samples.

Figures D.3, D.5 and D.4 in Appendix D show results from confocal and interferometry imaging used to characterize the surface of the electrodes. The ENEPIG finish presents roughness features < 1 µm tall and $\approx$ 10 µm across, while residues deposited after testing measure 5 to 10 µm in height. Additionally, damages like surface warping and removal of metal layers are profiled.

Table 3: CIC asymmetry ratio testing results. At each asymmetry ratio, it was tested whether the sample electrode first reached its cathodic or anodic WW bound and the relative value of the injected current to the maximum injected current across all ratios tested.

CIC Ratio	Current Injected (% of max)	Bound Reached
1:1	66.8%	Anodic
1:2	100%	Anodic & Cathodic
1:4	100%	Cathodic
1:8	100%	Cathodic

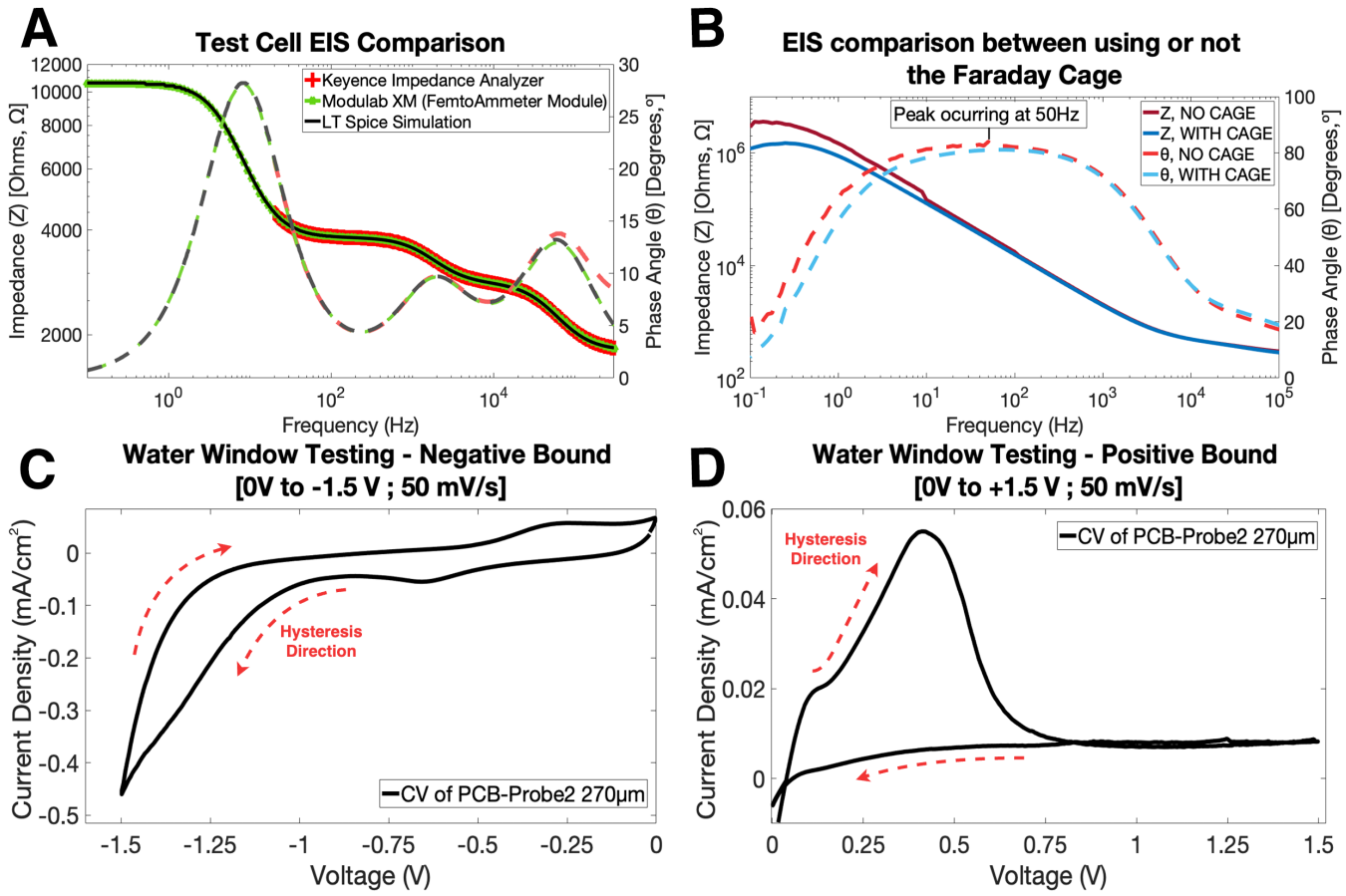

Figure 3: Electrode Characterization platform validation testing. In CV plots, red dotted line arrows indicate the hysteresis direction. **A -** Modulab XM+ calibration testing was performed by comparing EIS measurements of the test cell between the Modulab XM+ (green curves), the Keyence Impedance Analyzer (red curves), and the theoretical EIS curve obtained by simulating the circuit in LT Spice (black curves). $|Z|$ measurements are plotted with solid lines, while θ is plotted with dashed lines. The test cell circuit may be found in Appendix B C.5. **B -** Testing the Faraday cage by performing an EIS with and without the grounded cage shows how the cage can remove PLI at 50 Hz and smooth out $|Z|$ and θ curves, especially at the lower frequency spectrum. **C -** CV WW negative bound testing, the sample is swept from 0 V to -1.5 V to 0 V for a single cycle. **D -** CV WW positive bound testing, where the sample is swept from 0 V to +1.5 V to 0 V for a single cycle.

3. Electrochemical Characterization Measurements

Figure 4 and Table 4 show results obtained during electrode characterization of the samples (EIS, CV, VT and Noise tests). Additional examples of ECM for single samples are in Appendix D.8, D.9 and D.10.

Figures 4A & B show Bode plot EIS measurements averaged over 5 sample measurements for 3 electrode size categories (200, 500 and 900 µm). The colour-coded shading of each curve indicates the standard deviation. Complete graphs plotting the six size categories may be found in Appendix D.6. Figure 4A shows $|Z|$ curves, while Figure 4B shows θ curves. Equivalent circuit models were built following Nyquist plots from EIS data. The circuits, accompanied by illustrative Nyquist plots, may be found in Appendix D.14 and D.15. Measurements indicate a double-layer behaviour, expected in coated materials like ENEPIG [53]. Some samples present Warburg impedance (Z_W) elements at lower frequencies, indicating a mass transfer process. In one sample measurement, inductance at low frequencies indicates the adsorption of species to the sample [16, 54].

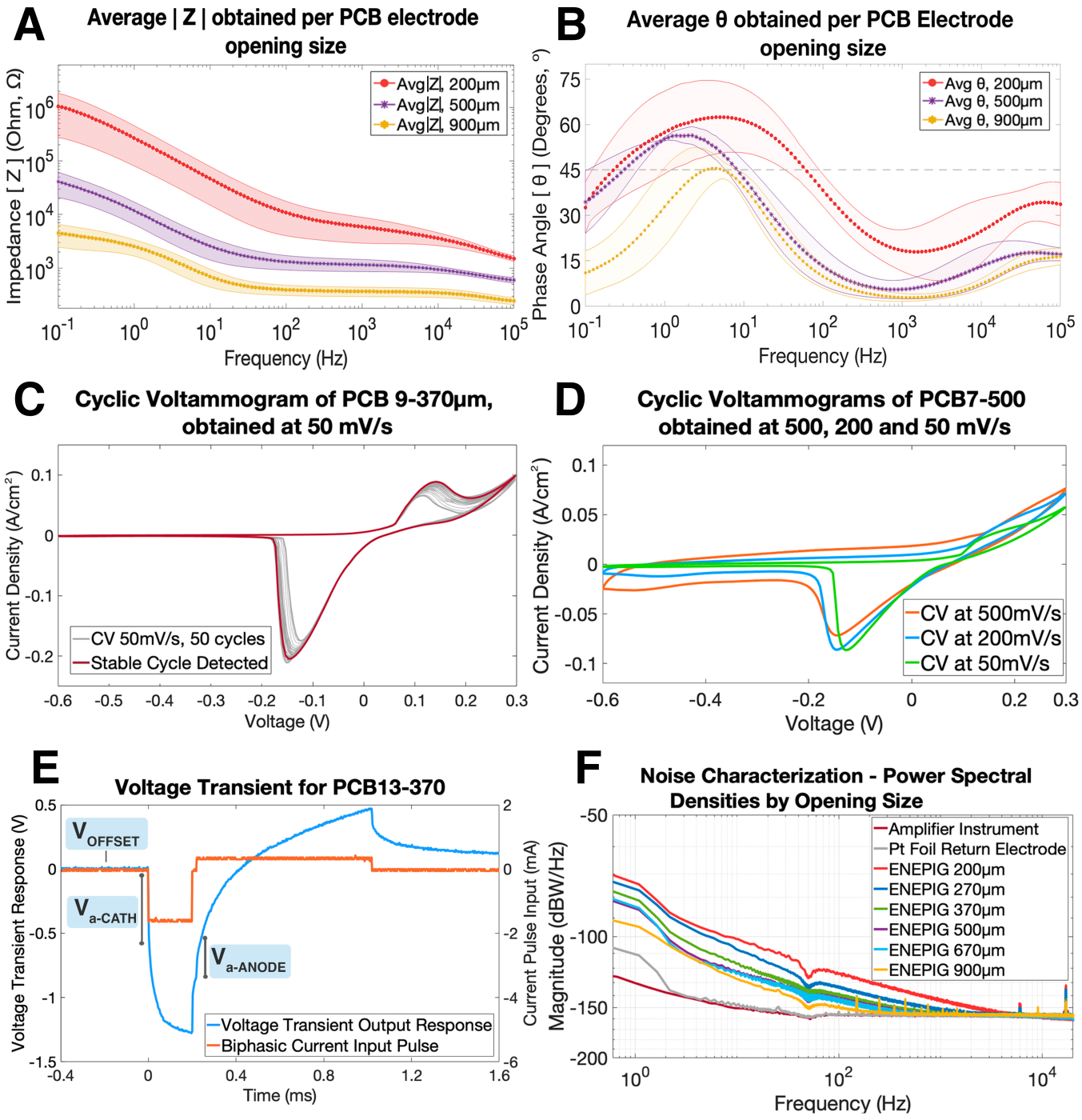

Figure 4: Electrode Characterization testing results. **A -** Average $|Z|$ (solid lines) obtained per electrode opening size. Only 3 out of 6 opening size category sizes are shown for clarity. Full graphs in Appendix D.6. Standard deviation across the averaged samples is shown as shading, with the same colour as the curve to which it belongs. **B -** Average θ (dashed lines) obtained per electrode opening size. Only 3 out of 6 opening size category sizes are shown for clarity. Full graphs in Appendix D.6. Standard deviation across the averaged samples is shown as shading, with the same colour as the curve to which it belongs. **C -** Example CV obtained from PCB9-370µm. The highlighted cycle in red indicates the detected stable cycle, which was later used to obtain the CSC of the electrode. The rest of the CV scan cycles are shown in light grey. **D -** Comparison of CVs obtained for the same electrode, but at three different testing rates: 500 mV/s in orange, 200 mV/s in blue, and 50 mV/s in green. **E -** Example Voltage Transient graph, where both the biphasic current input pulse (orange, right axis) and the output voltage transient (blue, left axis) are plotted. Added labels indicate the voltage drop associated with V_a, both in the cathodic and anodic edges and the resting voltage offset of the output voltage transient, named V_{OFFSET}, is also indicated. **F -** Noise characterization of the different size openings following the 3-step noise characterization procedure. The power spectral densities are plotted over the full frequency spectrum the recording setup could measure (0.55 Hz to 20 kHz), and the measurement of the noise of the amplifier and one single Pt foil large return electrode are also added.

Table 4: V_{RMS} obtained from the noise signals for each element and PCB opening size, following the 3-step noise characterization method.

Element	V_{RMS}
Amplifier Instrument	1.949 µV
Pt Foil Return Electrode	1.839 µV
ENEPIG 200 µm	349.141 µV
ENEPIG 270 µm	251.262 µV
ENEPIG 370 µm	155.984 µV
ENEPIG 500 µm	91.789 µV
ENEPIG 670 µm	101.321 µV
ENEPIG 900 µm	32.276 µV

Figure 4C shows a CV reference example measurement. The complete 50 cycles of CV performed on the sample are plotted in light grey, while the cycle detected as stable is highlighted in dark red. Note that CV cycles occur after the detected stable cycle, as stability was achieved in cycle 32. The CSC & CSC_{cath} for this cycle are 30.44 & 21.51 mC/cm^2 respectively, and the reaction peaks for the adsorption and release of H^+ and O^{2-} can be seen at +0.15 V and -0.16 V respectively [17, 27].

Figure 4D shows the highlighted cycles of three CV measurements of the same electrode obtained at three different scanning rates. It can be observed how curve features such as the resting voltage value from -0.6 V to -0.2 V, or the width of the reaction peak happening at -0.2 V, change with the scan rates. These then translate directly to the calculated CSC values, with CSC measured values for 500 mV/s, 200 mV/s & 50 mV/s resulting in 28.25, 20.05 & 13.11 mC/cm^2 respectively.

Figure 4E shows a VT measurement plot. Both the input biphasic current pulse and output voltage transient response are included. Additional labels indicate the V_{OFFSET} and the measured V_{a} on both the cathodic and anodic ends.

Figure 4F shows the whole set of measured noise signal PSD. Reference measurements needed for the 3-step noise characterization protocol (Noise contributions from the amplifier and the Pt foil large return electrode) and measurements for each size opening category are plotted. Additionally, Table 4 collects V_{RMS} values for each noise signal measurement.

4. Additional Electrode Characterization Data Analysis

Figure 5 collects all the graphs obtained through data analysis of the electrode characterization tests performed on the sample population.

Figure 5A shows boxplots of CIC values per electrode opening category. Complimentary to 5A, are 5B & 5C. Figure 5B plots the normalized current over area ratio in dark red and the normalized perimeter over area ratio in grey, revealing both normalized ratios follow a similar trend. Figure 5C plots the normalized average injected current in dark red versus the normalized average area opening in grey for each size category.

Figures 5D, E, and F collect boxplots for the CSC values obtained for each electrode opening at the three tested scan rates. The sample population used in these plots is a selection of the entire set, based on results from 5H - complete population graphs in Appendix D.17. Figure 5D represents CSC data obtained at 500 mV/s, figure 5E represents CSC data obtained at 200 mV/s, and figure 5F represents CSC data obtained at 50 mV/s.

Figures 5G & H show average CSC data, categorized by different electrode opening sizes (5G) and by the PCB sample measured (5H). Separate bars illustrate the three scanning rates used. Although the value progression observed in Figure 5G mimics those observed in Figures 5D, E and H, figure 5H shows how CSC data values can vary from sample to sample. Similarly to 5H, figure 5I shows how EIS is also affected by which PCB is tested. The value of Z @ 1 kHz obtained for the six size openings of each PCB was averaged, producing the average Z @ 1 kHz per PCB metric. High variation between tested samples can be observed despite shared parameters and opening size categories. f_{cutoff} are compiled under the Appendix Table D.2, while the average double-layer Randles equivalent circuit models for each opening size are found in Appendix D.13.

Figure 5J plots the ISR calculated at each size opening for the three scan rates used in the CV tests. The CSC data is also a selection of the whole population, with a graph of the entire sample data set available in Appendix D.16. Across the three rates, the ISR tends to increase slightly as the opening size decreases and presents a sudden increase in the 200 µm size category.

V Discussion

1. Electrode Characterization Setup

Results from testing done on the electrode characterization setup indicate that measurements are reliable and that the infrastructure developed improves their accuracy and reliability.

Calibration of the Modulab XM+ using the test cell (Fig 3A) shows a complete overlap between the theoretical

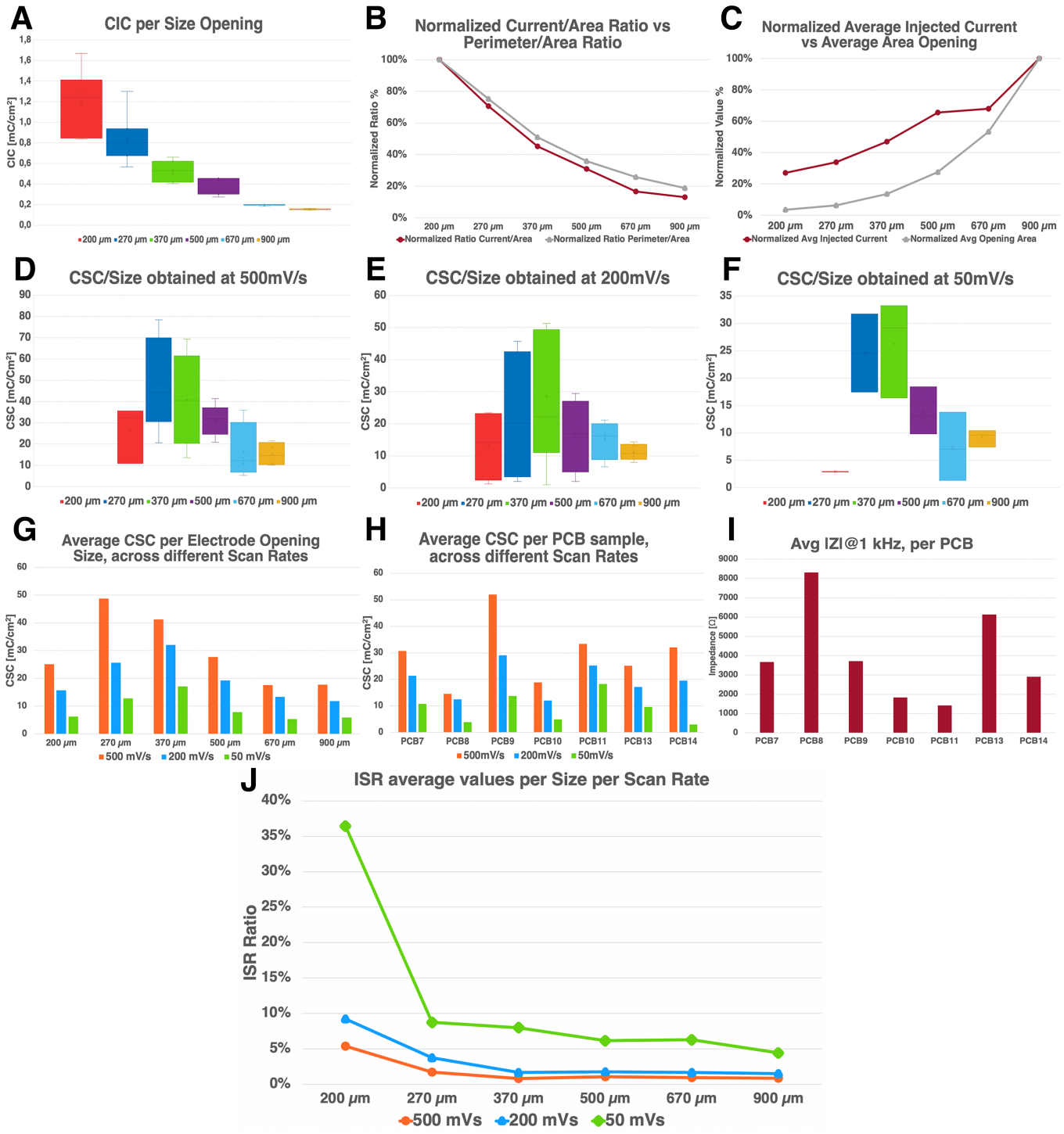

Figure 5: Additional data analysis performed on the electrode characterization data. **A -** Boxplots of the CIC values obtained by electrode opening. **B -** Plot comparing the normalized ratios obtained across the different electrode openings for current over area of the opening, and for the perimeter over area of the opening. **C -** Plot comparing the normalized values obtained across the different electrode openings for the average injected current per opening and the average opening area. **D -** Boxplot of a selection of CSC values obtained per electrode opening at 500 mV/s. **E -** Boxplot of a selection of CSC values obtained per electrode opening at 200 mV/s. **F -** Boxplot of a selection of CSC values obtained per electrode opening at 50 mV/s. **G -** Average CSC values obtained per electrode opening and scanning rates. **H -** Average CSC values were obtained per PCB sample characterized and scanning rate used. **I -** Average Z @ 1kHz values across opening sizes, per PCB sample characterized. Values obtained for the individual six openings of each PCB were averaged, producing the average Z @ 1 kHz per PCB metric. **J -** ISR average values were obtained at different scanning rates per electrode opening category.

model and the measurement of the XM+. It even outperforms the Keyence Impedance Analyzer in the higher frequency spectrum, as the measured phase of the Keyence differs from the model. Coupled with the capability of the XM+ to measure lower frequencies, the positive results of the calibration test proved that the XM+ was the best instrument at our disposal for the setup. If attempting to calibrate other impedance analyzers, the alternative method would be building an electrical circuit simulating an electrode (similar to those found in Appendix C.5, D.13 and D.14) and performing on it impedance measurements. Then, the circuit should be modelled *in silico* and its impedance response simulated. One may be sure their instrumentation is calibrated by studying the overlap between theoretical and empirical curves.

Testing the efficiency of the Faraday cage yielded positive results, too (Figure 3B). Not using a grounded cage would result in the EIS measurement showing several artefacts. Notably, a peak in θ at 50 Hz would consistently show as a consequence of PLI. θ measurements at the lower end of the frequencies would also present additional noise. The $|Z|$ curve presented artefacts, too, measured as sudden increments that made the final slope seemingly divide into segments. Testing inside of the cage and grounding it effectively eliminated all these nondesired phenomena.

However, other parameters related to electrode characterization could have been better controlled and would have improved the setup further. O_2 sparging was a procedure step that, although included, was not quantified in this work. Including a sensor to measure the dissolved O_2 concentration in the PBS media would add an extra layer of control and accuracy to the experimental platform [11, 13, 24, 25, 26].

Moving onto sample-related parameters necessary for characterization, determining the WW was not achieved solely through the theoretical method. The test for the positive bound (Figure 3D) showed a peak in the voltammogram, setting the positive WW bound to 0.3 V. However, the characteristic shape of the negative WW test voltammogram made it necessary to use other methods, as no clear peak could be observed (Figure 3C) [59]. Testing was greatly limited by the degradation of samples during characterization, CV being the most stressful [11, 17, 29, 30]. Thus, the negative bound was determined by CV testing the samples for 15 cycles and observing the survival rate at each tested bound. Samples were observed under the microscope for surface defects after the tests. Based on the results (Appendix D.11), the negative bound was set at -0.6 V. However, selecting a WW that does not adhere to standard guidelines to determine it raises a few issues to achieve standard characterization:

1. Not studying the samples with their correct WW prevents accurate comparisons between sample types. As samples are intended to maximise their WW when used in clinical settings, we cannot be certain the ENEPIG electrodes are operated at the desired standard conditions. It is impossible to characterize the ENEPIG electrodes under the same conditions as other materials (regular Au, Pt, AIROF). Accurately defining the WW would be imperative if samples were to be used in clinical settings, akin to other commercial electrodes.
2. But beyond comparison to other sample types and standardization, sample degradation mid-test obstructs carrying out the characterization study. If solely attempting to characterize ENEPIG samples and compare results, two factors must be considered to ensure reliable results: samples must survive for accurate results, and conditions should be repeatable between experiments. This is why the criteria to determine the negative voltage WW bound through the survivability of the samples was chosen. By keeping that bound consistent throughout testing, it was possible to move forward with the study reliably.
3. If not able to determine the exact bound of the WW, the chosen bound may fall to either side of it. If the chosen bound exceeds the WW, water electrolysis is bound to happen. This would lead to irreversible charge transfer processes, altering the chemistry of the medium and damaging the electrode. If the chosen bound is within the WW, irreversible reactions are much less likely to occur, preserving the structural integrity of the sample.

Therefore, as samples were never intended to work as clinical electrodes but rather as a tool to validate the characterization setup, reliable WW bounds were prioritized over accurate ones. Additionally, by choosing sample survivability as the factor determining the WW bound, we can assume that the selected bound is within the theoretical WW, as no damage from irreversible reactions is observed. Although characterization results may not be standard and comparable across electrode types, they sufficiently adhered to guidelines to proceed with the research and study samples among themselves.

VT asymmetry ratio testing (Table 3) yielded three ratios that achieved maximum injected current. However, the smaller ratio achieved the maximum current while simultaneously reaching both the anodic and cathodic ends of the WW. With two bounds to account for, the chances of damaging the sample and exceeding the window while testing increases [11, 31]. Therefore, having a single bound to look out for leads to a safer and more reliable characterization protocol [13]. On the other hand, to optimize the time profile of the pulse, the smaller ratio with a single bound reached was chosen and set for VT characterization: a 1:4 pulse phase ratio.

2. ENEPIG Sample Characterization & Analysis

ENEPIG sample characterization results showed common trends across the tested samples.

EIS tests showed $|Z|$ curves had two main slopes, corresponding to a double-layer behaviour (Figure 4A). Across sizes, the first slope started before 1 Hz and extended from 10 Hz up to 500 Hz in some cases. The second slope can be observed to start past the 30 kHz mark. This double-layer behaviour is also reflected in the θ plots (Figure 4B), where two peaks at around 10 Hz and around 60 kHz can be observed in all size openings. One critical remark is that the high-frequency phase peak remains low in value, in most cases below 45º. Therefore, samples indicate a predominantly resistive behaviour after the first slope flattens. Still, a significant issue in studying the double-layer impedance behaviour of these samples is that the frequency bandwidth seems not large enough to show the impedance curves settling at both the low- and high-frequency end of the spectrum [13]. To study a sufficiently broad impedance spectrum, future work on similar samples should try to extend the band from 10^{-2} Hz to 10^{6} Hz.

Another important takeaway from the graphs is the relationship between the observed impedance and the size of the samples. $|Z|$ curves show higher values as openings get smaller (Figure 4A), with Z @ 1 kHz for the 200 µm opening being over an order of magnitude larger than for the 900 µm opening (Appendix D.2). Looking at the θ curves by the opening size, θ values are also higher for smaller electrodes. The difference is such that not all size categories get to cross the threshold for f_{cutoff} at 45º the same amount of times, with some larger sized samples not having a single f_{cutoff} (Appendix D.2). Another consequence of this is that the second time the phase curve crosses 45º differs over an order of magnitude between the larger openings (541 Hz for the 900 µm curve averaged from 5 sample curves) and the smaller openings (15.2 kHz for the 200 µm curve averaged from 5 sample curves). This implies that the frequency band in which samples are in their capacitive domain is over an order of magnitude wider for smaller openings. Thus, the results indicate that there is also a relationship between opening size and the resistive-capacitive behaviour of samples: larger opening samples behave mostly in the resistive domain, while smaller opening samples are prone to exhibit a stronger capacitive behaviour and a larger bandwidth - to understand why, it is best to continue by looking at the Nyquist plots. As capacitive EC reactions allow for reversibility while faradaic EC reactions are prone to induce non-reversible reactions [11, 13, 16], smaller electrodes from the sample batch would be better suited for safe cell signal recording despite their higher impedance.

These findings are also reflected in the study of data through Nyquist plots and their corresponding equivalent circuits in Appendix D.14. By examining the circuits built as averages of the other circuits for the same-sized electrodes (Appendix D.13), trends appear to reflect the same conclusions as above.

- Electrodes are best modelled by a double-layer Randles circuit, indicating that samples have at least two contributing materials [16, 50]. Although the capacitance values between these layers do not differ much, the resistance difference between layers goes from one to three orders of magnitude. Usually, this refers to materials with a coating layer [55]. This is consistent with the double slope in the Bode plots and the ENEPIG material of the samples, as they have a Au finish (lower impedance), and two layers below made out of Pd and Ni, known for their higher impedance [72, 73].
- Size is also related to the modelled circuits. Resistances increase significantly with the decrease in size, reflecting how the impedance curves did, too. Capacitors decrease slightly with smaller sizes. The critical factor here is the relationship between the electron transfer resistance (R_{ct}) and the double-layer capacitance (C_{dl}): the ratio of R_{ct} to C_{dl} in smaller openings is over an order of magnitude larger than in larger openings. This explains why smaller electrodes act in their capacitive domain in a broader frequency spectrum [16, 45, 53]. However, why resistance varies significantly with size while capacitance does not, remains unanswered. Further testing would be required to research how and why the relationship of R_{ct} to size is stronger than that of C_{dl}.
- Issues such as not having a wide enough bandwidth also show. As the entire impedance behaviour cannot be studied, not all circuit components can be modelled accurately. The lack of lower frequencies for the second electrode circuit meant an incomplete Nyquist plot from which to model. R_{ct} and C_{dl} of these models can only be estimated and are most likely underestimated.

Nyquist plots and their circuit models become very useful in illustrating the differences between samples working as intended and faulty samples [53]. Appendix D.15 contains some Nyquist plots with their circuit models of data whose measurement was out of the norm in one way or another.

- D.15A shows that sample 8-200 behaved like a double-layer electrode, but the high resistance and similarities between layers seem to indicate that the Au surface is not reacting in this process as it has better performance than other possible reacting materials [53]. Future work should study samples exhibiting this behaviour to confirm if the two layers may have originated from the Pd and Ni

layers present in ENEPIG finishes or if the Au layer was damaged.

- D.15B shows other circuits with an inductance element. When present at low frequencies, it is associated with the adsorption of species to the reactive surface [16]. More work should be done to identify these measurements on-site and do surface characterization tests similar to Appendix D.5 to determine the exact process occurring and study potential residues before being washed off.
- D.15C, and D show circuits where a Warburg impedance (Z_W) component has been introduced in the second circuit. Z_W represents the difficulty of mass transport experienced by the ionic species involved in the redox process, limited by a semi-infinite linear diffusion process [16]. It appears at the lower end of the frequency spectrum and is expressed by its coefficient σ. It was also the case in D.15D that the frequency spectrum was not low enough to accurately characterize Z_W [54].

The main challenge behind CSC computing of the CV cycles was determining the cycle to be considered stable (Figure 4C). The developed algorithm (Appendix B.4) used an arbitrary threshold criterion (0.5% difference) set to work with most sample data, but it did not always succeed. Some of the reasons for this are:

- Some samples did not stabilize at all during the set amount of cycles
- In some cases, samples would seem to stabilize, but shortly after, would break apart due to the accumulated stress of the whole characterization procedure [11, 31]. As the algorithm checks a few cycles ahead of the selected cycle, it may deem it unstable. This was especially prevalent at the 50 mV/s test, as it was the last and most stressful (longer) test performed.
- Other tests did pass the criterion to be determined as stable, but they would continuously slowly drift. Thus, stability was not achieved, but it was detected.

Future versions of the algorithm should be able to measure the whole curve difference between one cycle and the other and analyze the overall curve drift progression to determine whether overall stability was achieved despite local results.

The comparison of CV tests performed at three different scan rates revealed both sample and testing insights (Figure 4D). The consensus around scan rates is that slower rates allow for better recruitment of fine surface structural features, leading to slower rates yielding higher CSC values [11, 13, 17, 28, 58]. However, if the three CSC values of the measured curves were compared, the results would suggest otherwise. Upon further analysis, two findings helped explain the observations:

1. The sample´s surface is majorly flat, with surface features measuring < 1 µm in height and ≈10 µm in length, as shown in several images (Appendix D.3,D.4). With a 1:10 aspect ratio, they can barely benefit from slower rates having higher feature recruitment - ionic species can easily access the most active surface features despite using fast scan rates. [11, 17, 74]. So, the amplitude of the reaction peaks remains similar between scan rates.
2. As both the scan rate and the electrochemical kinematics are time-related processes, using faster scan rates affects kinematics, which can determine curve features [75, 76].
    - Once the sample undergoes several cycles and the measured cycle stabilizes, fast-rate scan regions with a near-zero current response will still have species incurring minor reactions.
    - As the sample approaches the reaction voltage (V_r), a peak shows in the curve. However, as scan rates increase, the ionic species will start reacting at voltages further away from the V_r due to the speed at which V_r is approached. This leads to wider reaction peaks for faster rates and narrower peaks for slower rates.

Combining these two effects supports the results observed without contradicting prior literature. As the flat interface of the sample does not benefit from slower rate feature recruitment, and the speed of faster rates results in the area under the curve increasing at certain sections, the computed CSC increases with the scan rate. If the surface were to present a more complex 3D geometry, surface feature recruitment would translate to a higher amplitude peak [28, 29, 30, 57, 58]. Then, the curve area to scan rate progression would be similar to what is reported in the literature for more complex electrodes.

Noise characterization showed a strong trend between larger openings linked to lower noise levels, except for the 500 & 670 µm openings. Their V_{RMS} values (Table 4) indicate that 500 µm has lower noise than 670 µm. This is the opposite of what is expected and what can be observed in the rest of the measurements [35, 38]. Two important observations are made:

1. When observing the PSD (Figure 4F), it is clear that the 670 µm noise measurement presents a higher variance. Additionally, its curve tends to overlap the 500 µm noise PSD curve. These results indicate that the faulty measurement should be from the 670 µm, not the 500 µm opening.
2. Noise characterization measurements were performed only once per electrode opening size.

Given these two observations, it is hypothesized that the noise measurement for the 670 µm was faulty for some

reason, like high environment noise or unreliable manufacturing. A new measurement would be required to assess if the V_{RMS} value for this size category is, in fact, smaller. Nevertheless, as it is only a single data entry identified to be erroneous, the expected trend of noise decreasing for larger size openings would still hold.

Moving on to the analysis of the whole sample population, the main obstacle throughout the study of the samples was their low manufacturing reliability. As the PCB manufacturer never intended to make electrodes, aspects such as opening edge profile, opening area, or sample survivability to electrode testing varied considerably between similar samples. These combined factors resulted in sample performance differing vastly from sample to sample. Further data from Figures 5H & I proves how PCBs, in principle identically manufactured, can vary significantly in their performance. Calculating the average value for the CSC or the Z @ 1 kHz obtained across all openings shows how performance in a characterization test can be consistently relatively high or low compared to the whole population. Thus, the low manufacturing reliability of the samples is one of the main factors behind data variance when trying to evaluate trends across similar electrodes (opening sizes).

The first trend of interest is that CIC seems to increase as size opening decreases (Fig 5A). However, upon further analysis of the CIC-related metrics, we can see that:

- The normalized ratio between the current injected and the area of the opening (CIC) closely follows the same trend as the normalized ratio between the perimeter and the area of the opening (Figure 5B).
- If solely the charge injected is observed (not the charge capacity), it is clear that larger openings do inject more charge (Figure 5C).

It thus seems that what we can observe in Figure 5A is the result of dividing the total charge injected by electrode area (smaller areas yield higher CIC if charge remains constant) and the documented phenomenon of charge distribution heterogeneity [11, 33, 63, 77, 78]. As charge accumulates on sharp surface features (edges, spikes) rather than on the bulk of it, and as these electrodes are primarily flat, CIC closely follows the same relationship as the one between the perimeter to the area of the opening. Results seem to indicate that Q_{inj} in the sample electrodes would happen mainly at their edges.

When studying CSC results across the sample population (Figures 5D, E & F), it must be mentioned that the high electrochemical stress of the CV test [11, 17, 28, 29, 30], the low survivability of the samples (Appendix D.11), and the lack of reliability in achieving and then detecting a stable cycle, led to initial results lacking any significant trend. To clean the data, a selection of entries based on which PCB the electrode belonged to (Figure 5H) and whether the sample achieved stability was made. Equivalent graphs to Fig 5D, E & F but obtained with the entire data population can be seen in Appendix D.17.

Studying the boxplots, CSC increases as the opening size gets smaller. Figure 5G illustrates this trend using averages at each opening size category and scan rate. However, there are two important remarks:

1. At the smallest opening size (200 µm), CSC seems to drop drastically.
2. Other small opening sizes (270, 370 µm) also present a high variance between the measured results.

Again, the reason behind these remarks is the lack of manufacturing reliability of the samples. According to the manufacturer, 200 µm was the smallest possible dimension their drilling tool could manage. Further evidenced by the irregularity of the edges of these openings (Appendix D.2), it backs why the reliability at 200 µm is low. Thus, as CV is a stressful electrochemical test, poorly manufactured electrodes can be expected to perform poorly. Regarding the 270 & 370 µm openings, as their scale is not pushing the tooling limits, reliability improves marginally - with issues like edge smoothness and opening size variation still present. As sizes get larger, sample variations such as edge smoothness and opening size become relatively minor to the whole electrode, reducing their effect on performance. Due to the relationship of the scale of the electrode with manufacturing reliability issues, CSC results for the smaller sizes present a very high variability - with 200 µm not being able to function correctly at all.

The ISR was calculated to obtain additional insights into the performance of the electrodes; however, as a metric resulting from the CIC and CSC, issues mentioned before limited the usefulness of these results. CIC and CSC trends must be understood to understand the plots adequately. While the CIC follows an increasing trend as the opening sizes get smaller, CSC results lack any trends because they are strongly related to sample manufacturing issues. Therefore, inconsistencies across the ISR results are better understood by analyzing CSC results. The same sample selection for CSC figures is also made here - the graph with the entire sample data population is in Appendix D.16.

1. At 200 µm, the ISR suddenly increases. Although CIC is at its highest at 200 µm, the sudden rise is an effect of the abnormally low CSC recordings at 200 µm. As previously discussed, this effect is attributed to manufacturing issues rather than an accurate measurement of their CV. Were 200 µm openings manufactured reliably, their CV measurements would theoretically be in trend with the rest of the size categories, leading to similar ISR results across opening sizes.

2. It can be observed that faster scan rates yield smaller ratios, as CSC values are higher for these samples.
3. For other opening sizes, the ISR remains relatively constant, with a slight increase as opening sizes decrease for a given scan rate.

ISR seems to be a property intrinsic to the material and surface of the electrode, as suggested by theory - further experimentation with other surface materials is needed to claim it properly. The minor increase observed as sizes decrease could be because charge injecting is more strongly affected by current distribution heterogeneity (e.g., perimeter-to-area ratio). In contrast, the storage of charge activates the bulk of the surface - more so at slower rates [23]. This also reaches similar conclusions to the findings of Ganji *et al.* [71], where if we wanted to significantly increase the ISR without changing the material, increasing surface roughness would be the way. Increasing the number of features in the activated surface of an electrode due to its heterogeneous current distribution heavily benefits injecting over storing charge ratio. Compared to other studies with Au electrodes (no surface modifications), the ENEPIG electrodes performed poorly, with an ISR of below 10%. In contrast, studies from Ganji *et al.* and from Du *et al.* reported values of 30% and 100% respectively [71, 79].

Further tests should be conducted to study and compare ENEPIG samples to other types of Au electrodes (Sputtered, Plated, Fuzzy). As surfaces roughen, CSC will also see a reversal in the trend of faster rates with higher values than slower ones. This would then reflect on other metrics, such as ISR. Understanding how these trends relate to surface roughness and what scan rate is better suited to characterize the sample should also be studied.

VI Conclusion

As a project revolving around EC characterization, the scope was double: to successfully build a characterization setup that was reliable, accurate, and standard in performing common measurements and test it by performing a characterization study on subpar ENEPIG samples to highlight the capabilities of the setup, ensuring its measurements can accurately represent the samples.

Reliability was achieved by building a dedicated characterization setup capable of quickly adapting to many possible samples while offering adequate testing conditions and by developing a user guide protocol to ensure procedures such as setup, parameter selection and one-time experiments (WW testing) are performed correctly. By also aiding upcoming users of the setup in following the same testing guidelines while still accommodating their needs, future measurements should be trustworthy despite a lack of user experience. It was also ensured that the measurements produced were accurate, performing calibration measurements on the setup instrumentation and other necessary equipment such as the shielding effect of the Faraday cage. Furthermore, published guideline papers such as Cogan *et al.* 2008, Boehler *et al.* 2022 and Schiavone *et al.* 2020 were closely followed to create a setup that would produce standard characterization measurements, giving control over setting conditions (medium temperature, O_2 sparging), selecting testing parameters accordingly and performing initial tests to determine the optimum characterization test for each sample type.

A characterization study of ENEPIG electrodes was done to validate the setup. Manufactured as PCBs with no intent of working as electrodes, their performance, survivability and reliability were sub-par to that of microfabricated electrodes found in the literature. Nevertheless, as characterization is the method of measuring such aspects, meaningful conclusions were reached. The characteristic layered structure of ENEPIG was identified and modelled through EIS while still indicating a trend between observed impedance and the size opening of the sample. Due to the high EC stress applied, the study of the stimulating capabilities of the samples revealed issues with sample survivability and the reliability of the manufacturing process. After performing a smaller population study without data from outlier PCBs, characterization results were related directly to surface and fabrication features. In the end, the stimulation efficiency of ENEPIG (10%) was evaluated as highly inferior to that of commonly used non-modified Au electrodes (30%-100%). The study was also helpful in indicating how EC performance could be improved by incorporating surface modifications if these samples were to be still used.

By carrying out complete characterization testing on the samples, it was possible to characterize them on an individual level and still identify issues showing on a population level. Were these samples to work as electrodes, the tests performed would have evidenced their inadequacy to the *in vivo* environment and the exigence of therapy protocols in neural interfaces. These results mirror what was expected from ENEPIG openings that were never meant to be employed under such conditions, indicating a successful characterization procedure.

Bibliography

[1] C. Ding, Y. Wu, *et al.*, “Global, regional, and national burden and attributable risk factors of neurological disorders: The global burden of disease study 1990–2019,” *Frontiers in Public Health*, 2022.

[2] J. Dumurgier and C. Tzourio, “Epidemiology of neurological diseases in older adults,” *Revue Neurologique*, 2022.

[3] P. Ortinski and K. J. Meador, “Cognitive side effects of antiepileptic drugs,” *Eplisepsy Behaviour 5*, 2003.

[4] R. Makins and A. Ballinger, “Gastrointestinal side effects of drugs,” *Expert Opinion on Drug Safety*, 2003.

[5] I. L. Michael Kuhn *et al.*, “The sider database of drugs and side effects,” *Nucleic Acids Research*, 2015.

[6] S. Reardon, “Electroceuticals spark interest,” *Nature*, 2014.

[7] S. Mishra, “Electroceuticals in medicine – the brave new future,” *Indian Heart Journal*, 2017.

[8] A. Majid, *Electroceuticals - Advances in Electrostimulation Therapies*. Springer International Publishing, 2017.

[9] G. Yao *et al.*, “Flexible bioelectronics for physiological signals sensing and disease treatment,” *Journal of Materiomics*, 2020.

[10] M. Zhang *et al.*, “Electronic neural interfaces,” *Nature Electronics*, 2020.

[11] S. F. Cogan, “Neural stimulation and recording electrodes,” *Annual Review Biomedical Engineering*, 2008.

[12] J. P. Donoghue, “Connecting cortex to machines: recent advances in brain interfaces,” *Nature Neuroscience*, 2002.

[13] C. Boehler *et al.*, “Tutorial: guidelines for standardized performance tests for electrodes intended for neural interfaces and bioelectronics,” *Nature Protocols*, 2022.

[14] T. D. Y. Kozai, “The history and horizons of microscale neural interfaces,” *Micromachines*, 2018.

[15] G. Schiavone *et al.*, “Guidelines to study and develop soft electrode systems for neural stimulation,” *Neuron*, 2020.

[16] A. C. Lazanas and M. I. Prodromidis, “Electrochemical impedance spectroscopy–a tutorial,” *ACS Measurement Science Au*, 2023.

[17] N. Elgrishi *et al.*, “A practical beginner’s guide to cyclic voltammetry,” *Journal of Chemical Education*, 2018.

[18] J. M. DeFreitas, T. W. Beck, and M. S. Stock, “Comparison of methods for removing electromagnetic noise from electromyographic signals,”

[19] S. Kumar, R. Bhooshan, S. Varshney, C. Verma, and L. Gideon, “Faraday cage for EMC improvement of electronic devices,”

[20] M. W. Glasscott, E. W. Brown, K. Dorsey, *et al.*, “Selecting an optimal faraday cage to minimize noise in electrochemical experiments,”

[21] C. A. Wunderlich, *On the Temperature in diseases*. New Sydenham society.

[22] J. O. Bockris, “Kinetics of activation controlled consecutive electrochemical reactions: Anodic evolution of oxygen,”

[23] E. M. Hudak *et al.*, “Electron transfer processes occurring on platinum neural stimulating electrodes: calculated charge-storage capacities are inaccessible during applied stimulation,” *Journal of Neural Engineering*, 2017.

[24] B. Chakraborty, A. Joshi-Imre, and S. F. Cogan, “Charge injection characteristics of sputtered ruthenium oxide electrodes for neural stimulation and recording,”

[25] G. U. Balcke, M. Hahn, and S. E. Oswald, “Nitrogen as an indicator of mass transfer during in-situ gas sparging,”

[26] M. K. Puglia and P. K. Bowen, “Cyclic voltammetry study of noble metals and their alloys for use in implantable electrodes,”

[27] J. P. Hoare, “A cyclic voltammetric study of the gold□oxygen system,” *The Electrochemical Society*, 1984.

[28] K. K. Justyna Lipus, “Challenges and limitations of using charge storage capacity to assess capacitance of biomedical electrodes,” *Measurement*, 2022.

[29] R. Chattot *et al.*, “Beware of cyclic voltammetry! measurement artifact in accelerated stress test of fuel cell cathode revealed by operando x-ray diffraction,” *Journal of Power Sources*, 2023.

[30] R. Sharma and S. M. Andersen, “Quantification on degradation mechanisms of polymer electrolyte membrane fuel cell catalyst layers during an accelerated stress test,” *ACS Catalysis*, 2018.

[31] S. Brummer and M. Turner, “Electrical stimulation of the nervous system: The principle of safe charge injection with noble metal electrodes,” *Bioelectrochemistry and Bioenergetics*, 1975.

[32] S. Cogan, T. Plante, and J. Ehrlich, “Sputtered iridium oxide films (SIROFs) for low-impedance neural stimulation and recording electrodes,” *IEEE*, 2004.

[33] S. F. Cogan *et al.*, “Potential-biased, asymmetric waveforms for charge-injection with activated iridium oxide (airof) neural stimulation electrodes,” *IEEE*, 2006.

[34] S. Cogan, “In vitro and in vivo differences in the charge-injection and electrochemical properties of iridium oxide electrodes,” *IEEE TRANSACTIONS ON BIOMEDICAL ENGINEERING*, 2006.

[35] A. Suarez-Perez, G. Gabriel, B. Rebollo, *et al.*, “Quantification of Signal-to-Noise Ratio in Cerebral Cortex Recordings Using Flexible MEAs With Co-localized Platinum Black, Carbon Nanotubes, and Gold Electrodes,” *Frontiers in Neuroscience*, 2018.

[36] E. Huigen, A. Peper, and C. A. Grimbergen, “Investigation into the origin of the noise of surface electrodes,” *Medical and Biological Engineering and Computing*, 2002.

[37] S. Gabran, M. Salam, J. Dian, Y. El-Hayek, *et al.*, “3-d flexible nano-textured high-density microelectrode arrays for high-performance neuro-monitoring and neuro-stimulation,” *Neural Systems and Rehabilitation Engineering, IEEE Transactions on*, 2014.

[38] J. P. Neto *et al.*, “Does impedance matter when recording spikes with polytrodes?,” *Frontiers in Neuroscience*, 2018.

[39] A. Menahem Ratzker, M. Pearl, M. Osterman, *et al.*, “Review of capabilities of the enepig surface finish,” *The Minerals, Materials and Metals Society*, 2014.

[40] B. A. Circuits, “Enepig plating – a guide to the evolution of pcb finishes,” 2024.

[41] K. P. L. Pun, M. N. Islam, C. W. Cheung, *et al.*, “Solid-state growth kinetics of intermetallic compounds in cu pillar solder flip chip with ENEPIG surface finish under isothermal aging,” 2017.

[42] J.-H. Back and J.-W. Yoon, “Comparative study of normal and thin au/pd/ni(p) surface finishes with sn–3.0ag–0.5cu solder joints under isothermal aging,” no. 20, pp. 24790–24800, 2021.

[43] T.-T. Chou, C. J. Fleshman, H. Chen, *et al.*, “Improving thermal shock response of interfacial IMCs in sn–ag–cu joints by using ultrathin-ni/pd/au metallization in 3d-IC packages,” 2019.

[44] C. E. Ho, S. J. Wang, C. W. Fan, *et al.*, “Optimization of the ni(p) thickness for an ultrathin ni(p)-based surface finish in soldering applications,” 2014.

[45] C. M. Brett, “Electrochemical impedance spectroscopy in the characterisation and application of modified electrodes for electrochemical sensors and biosensors,” *Molecules*, 2022.

[46] M. E. Orazem, “University of Florida Lecture: Electrochemical Impedance Spectroscopy,” 2018.

[47] G. Buzsáki, *Rhythms of the Brain*. Oxford University Press, 2006.

[48] A. Lasia, *Modern Aspects of Electrochemistry n32*, ch. Electrochemical Impedance Spectroscopy and its Applications, p. 435. 2002.

[49] M. J. Barsoukov E, *Impedance Spectroscopy Theory, Experiment, and Applications, 2nd Edition*. Wiley-Interscience, 2005.

[50] B.-A. Mei *et al.*, “Physical interpretations of nyquist plots for edlc electrodes and devices,” *Journal of Physical Chemistry*, 2018.

[51] T. K. Zoltán Lukács, “A generalized model of the equivalent circuits in the electrochemical impedance spectroscopy,” *Electrochimica Acta*, 2020.

[52] F. Ciucci, “Modeling electrochemical impedance spectroscopy,” *Current Opinion in Electrochemistry*, 2019.

[53] H. H. Hernández, A. M. R. Reynoso, J. C. T. González, *et al.*, “Electrochemical impedance spectroscopy (eis): A review study of basic aspects of the corrosion mechanism applied to steels,” 2020.

[54] H. S. Magar, R. Y. A. Hassan, and A. Mulchandani, “Electrochemical impedance spectroscopy (eis): Principles, construction, and biosensing applications,” *Sensors*, 2021.

[55] W. Choi, H.-C. Shin, J. M. Kim, *et al.*, “Modeling and applications of electrochemical impedance spectroscopy (eis) for lithium-ion batteries,” *Journal of Electrochemical Science and Technology*, 2020.

[56] A. Achour *et al.*, “Nanostructuration and band gap emission enhancement of zno film via electrochemical anodization,” *Thin Solid Films*, 2014.

[57] M. B. Davide Reato, Asif Rahman and L. C. Parra, “Effects of weak transcranial alternating current stimulation on brain activity—a review of known mechanisms from animal studies,” *Frontiers in Human Neuroscience*, 2013.

[58] A. Sukasem *et al.*, “The effects of low-and high-frequency non-invasive transcutaneous auricular vagal nerve stimulation (tavns) on gastric slow waves evaluated using in vivo high-resolution mapping in porcine,” *Neurogastroenterology and Motility*, 2020.

[59] H. Lee, S. Lee, K. Kim, *et al.*, “Investigation of surface defects of electroless Ni plating by solder resist dissolution on the ENIG process,” *Microelectronic Engineering*, 2018.

[60] J. K. Andreas Weltin, “Electrochemical methods for neural interface electrodes,” *Journal of Neural Engineering*, 2021.

[61] J. M. Späth, K. K. Kouri, L. Holzapfel, R. Thewes, and V. Giagka, “Stand-alone broad frequency range charge-balancing system for neural stimulators,” in *2023 IEEE Biomedical Circuits and Systems Conference (BioCAS)*, 2023.

[62] J. M. Späth, “Development of a stand-alone charge balancing system for nerve conduction block stimulators,” 2023.

[63] S. F. Cogan *et al.*, “The influence of electrolyte composition on the in vitro charge-injection limits of activated iridium oxide (airof) stimulation electrodes,” *Journal of Neural Engineering*, 2007.

[64] T. Rose and L. Robblee, “Electrical stimulation with pt electrodes. viii. electrochemically safe charge injection limits with 0.2 ms pulses (neuronal application),” *IEEE*, 1990.

[65] I. C. Stefan *et al.*, “Theoretical analysis of the pulse-clamp method as applied to neural stimulating electrodes,” *Journal of the Electrochemical Society*, 2001.

[66] E. J. Tehovnik, “Electrical stimulation of neural tissue to evoke behavioral responses,” *Journal of Neuroscience Methods*, 1995.

[67] J. B. Ranck, “Which elements are excited in electrical stimulation of mammalian central nervous system: A review,” *Brain Research*, 1975.

[68] A. Cisnal, J.-C. Fraile, *et al.*, “A measurement setup and automated calculation method to determine the charge injection capacity of implantable microelectrodes,” *Sensors*.

[69] S. Mottaghi *et al.*, “Modular current stimulation system for pre-clinical studies,” *Frontiers in Neuroscience*, 2020.

[70] J. S. Nathan Cermak, Matthew A. Wilson and J. P. Newman, “Stimjim: open source hardware for precise electrical stimulation,” *bioRxiv*, 2019.

[71] M. Ganji *et al.*, “Scaling effects on the electrochemical stimulation performance of au, pt, and pedot:pss electrocorticography arrays,” *Advanced Functional Materials*, 2017.

[72] C.-Y. Ho and J.-G. Duh, “Optimal ni(p) thickness design in ultrathin-ENEPIG metallization for soldering application concerning electrical impedance and mechanical bonding strength,” 2014.

[73] C. E. Ho, C. W. Fan, and W. Z. Hsieh, “Pronounced effects of ni(p) thickness on the interfacial reaction and high impact resistance of the solder/au/pd(p)/ni(p)/cu reactive system,” 2014.

[74] A. J. Bard and L. R. Faulkner, *Electrochemical methods: fundamentals and applications*. Wiley, 2001.

[75] J.-M. Savéant, *Elements of Molecular and Biomolecular Electrochemistry: An Electrochemical Approach to Electron Transfer Chemistry*. John Wiley & Sons, 2006.

[76] “Equilibrium electrochemistry and the nernst equation,” in *Understanding Voltammetry*, IMPERIAL COLLEGE PRESS, 2010.

[77] S. L. Thompson *et al.*, “A review of parameter settings for invasive and non-invasive vagus nerve stimulation (vns) applied in neurological and psychiatric disorders,” *Frontiers in Neurscience*, 2021.

[78] D. Klooster *et al.*, “Technical aspects of neurostimulation: Focus on equipment, electric field modeling, and stimulation protocols,” *Neuroscience and Biobehavioral Reviews*, 2016.

[79] Z. J. Du *et al.*, “Poly(3,4-ethylenedioxythiophene)-ionic liquid coating improves neural recording and stimulation functionality of meas,” *Royal Society of Chemistry*, 2015.

VII Future Work

Throughout this project, several issues that should be further improved were identified. They range from issues concerning the design of the characterization setup to how the samples were made, how the characterization experiments were carried out, and how the analysis of these results was conveyed. These improvements aim to gain more information about the samples by directly generating more data from them or studying similar electrodes that will provide additional results.

Although the setup allows performing O_2 sparging by flowing N_2 gas through the PBS, **there is no way to quantify this process**. Incorporating an O_2 sensor into the setup could quantify the partial pressure of the gas dissolved in the PBS solution. This way, adequate medium conditions, reflective of the *in vivo* tissue environment, could be monitored during the preparation and warm-up of the setup. Characterization tests shall only be started once dissolved O_2 levels mimic *in vivo* conditions to represent future performance better. An important consideration is that the sensor should be self-powered through a battery. This would avoid additional issues with porting through the Faraday cage and minimize electromagnetic interference.

An obstacle throughout the project was the **ENEPIG samples and their low reliability in testing**. Manufactured as openings meant to be soldered on, the electrochemical stress induced by characterization testing (especially CV) would often irreversibly damage the openings, and the reliability of crucial features, such as the opening edge, was subpar. This is not the case with other electrodes manufactured according to their purpose, such as pure Au electroplated circular opening electrodes. Additionally, throughout the literature research, no team used ENEPIG as the finishing material for their Au-based electrodes. As Au is only used as a coating layer, it is expected to have low survivability, while the other metal layers underneath (Pd and Ni) hamper its electrochemical performance [39]. ENEPIG surface finish also cannot present a high degree of surface roughness features to increase its charge-injecting performance, as it is intended to be used as a solder connecting pad. For all these reasons, further validation of the characterization setup would be possible if other Au-based samples were characterized. Fewer reliability issues during testing would be expected, and the similar yet different electrodes would provide exciting results to compare to.

Regarding the characterization testing process, a few issues related to the several experiments have been identified.

- A major setback in characterizing the samples while representing ideal *in vivo* conditions was **determining the WW of the ENEPIG electrodes**. Coupled with their low survivability to the stress applied by CV, determining the negative WW bound according to the proposed methodology from literature [11, 13] was impossible. As the voltammogram was not different from other reported CV scans on ENEPIG electrodes [59], and the standard profile of the curve in the negative voltage domain does not suffice for water hydrolysis detection, an alternative needs to be developed. Current alternatives are to either incorporate a sensor to measure when water hydrolysis happens or manufacture ENEPIG samples with a higher electrochemical stress resistance to avoid breaking down from the test and measure surface chemical changes due to irreversible reactions.
- When modelling electrodes with EIS measurements, a common setback to accurate models came from **the bandwidth of the test being a few orders of magnitude short**. As multiple layers play a part in the electrochemical process, the features of the layers that are not exposed only show at the lowest frequency end. Incrementing the testing bandwidth from 10^{-2} to 10^{6} Hz may result in more accurate models, leading to a better understanding of the contribution of the covered metal layers.
- Additional research into the **relationship of R_{ct} & C_{dl} to size** is needed. It is already understood that these factors vary with the opening size and do so differently. However, no current explanation exists for why or how the opening area affects more R_{ct} than C_{dl}. EIS testing of electrodes with equal surface area but other structural differences (different opening geometry, different ENEPIG layer thickness profiles, raised versus recessed profiles) may show changes in the current observed trend. Once significant differences are observed between these factors, another size study would be required to understand how they change differently with size, leading to potentially answering why this happens.
- Calculating the CSC for each sample was only as good as the process of **determining the CV cycle where stability was achieved**. One way to improve this process would be to have samples that stabilize instead of breaking down mid-test. As enhancing the samples has already been mentioned, the alternative would be to refine the algorithm further to detect stable cycles. Adding features such as evaluating the whole scan before measuring differences between cycles could help identify samples that do not achieve proper stability. Stability detection could be further improved by making the difference criteria adaptable to the specific values of the

measurement cycles. Lastly, with a sufficiently large pool of CV data, an artificial intelligence model could be trained in stable cycle detection.

- As previously reported in the literature, the biggest challenge in obtaining accurate VT test results lies in **accurate detection and extraction of V_a**. Done manually for this project, V_a extraction could be automated in code for higher reliability across different samples tested. An iterative loop where pulse current amplitude is increased step by step while edge detection thresholding is performed to measure V_a is proposed.
- Although integration with the previous suggestion is complex under the current setup configuration, **it would benefit VTs if a third electrode were used for an actual 3-electrode setup configuration**. Currently, the MDO34 oscilloscope provides the reference against which to measure. More reliable and accurate measurements could be achieved if an Ag/AgCl RE electrode could be incorporated into the VT setup. However, as the current configuration does not allow using the third electrode, it would change how the experiment is carried out and could prevent incorporating automated V_a extraction.

Lastly, the characterization sample population study could also be improved in a few ways.

- To identify stronger trends in CSC values across opening sizes, **having a higher statistical power could be useful to identify outlier samples better**. Coupled with the previously proposed sample improvements, testing more PCBs would make trends more significant. If outlier samples are an oddity, a vast number of similar results would make it easier to discard samples that do not represent the population. In the case of samples presenting high variance across all samples, they would not be deemed outliers anymore and should be included in the analysis.
- Although theory seems to indicate that ISR should be a property directly related to surface-finish and material used, **additional sample types should be studied to add evidence to this claim**. Studying other Au-based electrodes with different surface finishes would be helpful in determining how various features affect the ISR. In the case of having a repeatable surface finish (flat, jagged structures, deposited nanoparticles), testing different materials with the same finish would also be required. Little research has been done on this metric, yet it seems it could revolutionize how stimulating electrodes are understood and reported.

A Literature Review

Document A.1: Literature Review conducted on Electrode Characterization techniques, emphasising Au electrodes and standardization.

Title: Characterization of Gold Electrodes for Neural Interfaces - Test Settings and Standardization.

Figure A.1: Literature Review on Electrode Characterization researched before conducting this MSc Thesis research project. It focuses on the three main electrochemical characterization techniques used for electrodes in neural interfaces: Electrochemical Impedance Spectroscopy, Cyclic Voltammetry and Voltage Transients. It also pays close attention to issues in standardizing these measurements and focuses on reported metrics in previous literature for Au electrodes.

1 INTRODUCTION TO ELECTRODE CHARACTERIZATION

1.1 MOTIVATION

According to the Global Burden of Disease study of 2022, around 10 million deaths related to neurological disorders were recorded in 2019. 6.5 million were attributed to stroke, while 2 million were related to Alzheimer's, dementia, epilepsy, and Parkinson's disease. The human cost these disorders (migraine here is included too) have in terms of disability-adjusted life years (DALYs) reached 210 million DALYs, and when comparing these results to data from 1990 it becomes clear that the burden they hold on the world population is only growing [1, 2]. To be able to diagnose these conditions accurately, early, and potentially treat them, we rely on drugs and/or neural interfaces. Drugs have been used for over a century, and although they are easier to deliver to the patient, they have many drawbacks. Due to their chemical nature, drugs are less capable of targeting specifically the desired site, reducing their therapeutic potential - sometimes even having a difficult time reaching their destination. While travelling through the whole system of the patient, they can also induce many side effects that can range from minor annoyances to severe conditions [3–5]. Conditioned by both each patient's physiology and other drug-drug interactions, the complexity behind effective and harmless drug therapy has pushed researchers to look for alternatives [6, 7]. Neural interfaces, also named in comparison to traditional drugs as "electroceuticals", are essentially medical devices that use electricity to tap into the neural tissue of patients for diagnosis and therapeutical purposes. The advantage of these devices is that it is possible to provide therapy in a targeted manner, with some local side effects and near no systemic side effects [8]. Of course, the main drawback of said devices is that they require surgical implantation, but the overall lesser impact they have on a patient has kept the researcher´s interest high. Although many options are available, the default method neural interfaces have of interacting with tissue is through electrodes [9]. Improving these electrodes has become one of the main areas of research for improving neural interfaces, with the hope of addressing the growing concern of neurological disorders.

Yet, when it comes to electrode research and development, it is often found in modern literature that not all research teams conduct full testing of electrode prototypes. Tests also often lack appropriate parameter settings that enable results to be translatable to future clinical applications [10]. And when it comes to finally reporting said data, it can be omitted or reduced to the point where it is not useful to the whole scientific community trying to tackle the pressing issue. By not carrying out testing and reporting appropriately, scientific progress is hindered: teams may find out at a later stage that their electrode is not suitable for patients and overall progress is staggered.

This literature review aims to collect all the available information and recommendations on how to perform testing and characterization for electrodes in neural implants. Additional focus on Au as an electrode material will be given at the end of each test section, due to its versatility, availability, biocompatibility, and relevance in novel, flexible electrodes. As the current electrode material being experimented on by the team of Technologies for Bioelectronics at the Fraunhofer IZM in Berlin; this review serves the purpose of highlighting good and bad practices in electrode testing and reporting, showcasing additional uses behind said tests, and establishing the groundwork for standardizing these practices.

1.2 THEORETICAL BACKGROUND FOR NEURAL INTERFACES

OVERVIEW OF NEURAL TISSUE

Since humans were able to observe neural tissue on the microscopic scale, thanks to Santiago Ramón y Cajal using a modified Golgi stain in 1887, neural tissue has been a subject of intense study. Yet, it seems to hold the answers to some of today's biggest challenges in the medical field, such as Parkinson's disease, schizophrenia, neuropathic pain, depression, OCD, and all neurodegenerative diseases [11, 12]. Coupled with its high complexity, it has pushed researchers to develop new and improved technologies to better study this tissue [13]. Although other tissues may be easily understood through visual methods in order to assess their structure, neural tissue's function lies in its excitability.

Neurons are capable of communicating with one another through the so-called "action potentials": a fast and discrete membrane depolarization caused by a change in the concentration ratio of chemical species in the extra-cellular and intra-cellular medium [14, 15]. It is precisely such excitable nature of the tissue that must be researched and understood to unlock future potential diagnoses and therapies. But in order to study the activity of neurons, researchers need to be able to detect the electrochemical impulses used in cell-to-cell communication (other methods besides electrodes include functional magnetic resonance imaging and

focused ultrasound(fMRI, FUS)), and then stimulate said cells in a way that elicits an appropriate biological response [16, 17]. As neurons communicate through the exchange of chemicals in their medium, altering concentration values for local species such as Na^+ and K^+, a tool capable of detecting changes in chemical concentration is needed [15, 16].

The high frequency at which neurons fire, the low amplitude and high background noise of said signals, and the number of individual signal sources that can be encountered in a section of tissue, call for a precise, fast, and robust method to keep up with the biological tissue [11, 17]. To date, the best domain to work with such signals is the electrical domain, where with the help of computers it is possible to acquire, process, and generate signals at a scale comparable to that of neural tissue.

NEURAL IMPLANTS

In order to study how neural tissue behaves and provoke it with desired responses, researchers have at their disposal several technologies, but not all have the same purpose. At larger scales (tissue, general brain activity), the use of magnetic resonance imaging (MRI) and electroencephalogram (EEG) allows clinicians to study the neural anatomical and physiological state of patients. However, these techniques still struggle when it comes to treating and diagnosing at the microscopic and cellular levels. At this scale, the standard technology has become neural implants. Although they may differ from one another, they all share the common ability to transduce information back and forth from the chemical domain of cell communication to the electrical domain where humans can have control and process information [13, 16, 17]. As they need to be directly in contact with the living tissue, and because they also serve as the interface between tissue and man-made machine, neural implants are also called neural interfaces. Both names can be used interchangeably for most matters, although the former refers to the whole physical device and its components, while the latter can be used in context to refer to the portion of the neural implant that is directly in contact with the tissue.

As with any implant, neural implants are designed to minimize eliciting undesired responses when they come in contact with tissue. This becomes even more important when it is considered that although device testing and some therapies may be run in acute settings, research and therapies almost always have a chronic goal in mind [17]. Being able to acquire information from neural tissue for prolonged periods of time with minimal interference in their natural processes is the ideal scenario for any neural implant [18]. This serves as well as the main challenge driving current research and manufacturing efforts: to perform better in the electrochemical domain, leading to increased diagnosis and therapeutic capabilities; to do so in the safest and least intrusive way; and to achieve high efficiency leading to longer time spans where the device may be implanted in a patient [11].

Although each neural implant may have a different design, as active implantable biomedical devices (AIBMDs), most of them share standard components. These would be the stimulation circuit, the recording circuit, a communications module, a system control unit, and power management, represented in Figure 1 [19].

The stimulation circuit is responsible for transforming the charge from the power source into usable charge by the stimulating elements (electrodes or ultrasound transducers, for example). It usually requires its own control circuit in order to deliver charge in a controlled and precise manner. The stimulation circuit and its stimulation elements are critical for the correct function of an AIBMD, and they will be the subject further discussed in this review [19].

As active devices are capable of modifying their output based on the change in their surroundings, they require a closed-loop design. Closed-loop designs need a recording circuit to have inputs of their surroundings, which can then be used to modify a certain output. They usually require amplifiers and some kind of analogue-to-digital converter (ADC) in order to acquire external biological signals and transform them into usable information. To sense the physiological signal, they often rely on the same elements as the stimulation circuits as long as they have both stimulating and sensing capabilities, like electrodes [19].

Communication modules are also essential to send data back and forth between the AIBMD and the external world. In the case of implants, wireless solutions are preferred to avoid patients undergoing constant intrusive procedures in order to acquire data and modify possible therapy protocols. This means that elements such as data encoders, decoders, and radio frequency emitters and receivers are standard requirements for AIBMDs [19].

As with any electronic device, the system control unit is essential for the correct functioning of the device. It regulates all of the operations carried out and performs most of the calculations necessary. It is responsible for the adequate closed-loop stimulation protocol, data processing, and general function of the implant [19].

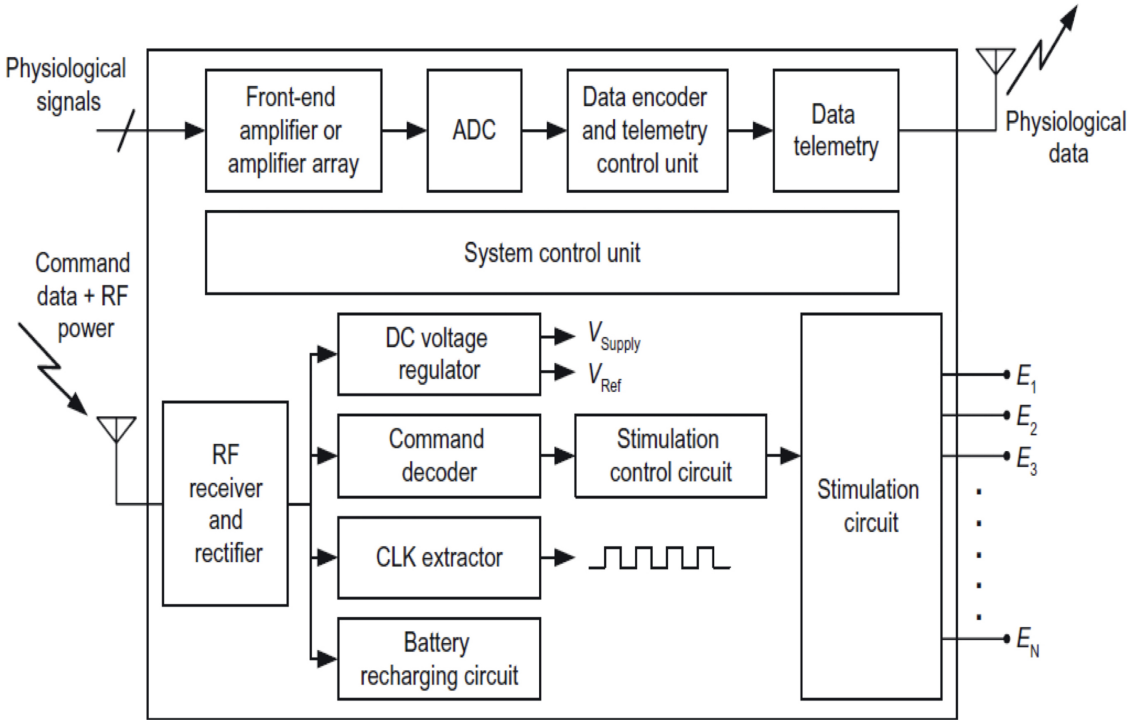

Figure 1: Schematic of the standard components needed to build an active implantable biomedical device. Adapted from [19]

Finally, the power management unit is needed for any standalone device. Additional circuitry for efficient use of the energy available and to minimize losses is added in order to have long-lasting implants, capable of operating autonomously for several years [19].

All these components play an important role in the neural implant's function and are carefully designed to work optimally with one another. This work will focus on understanding what makes a neural implant have good recording and stimulating elements and how these can be measured.

ELECTRODES

There are a few options when it comes to interfacing elements of neural implants, but electrodes became the field's standard decades ago due to their simple action mechanism. Electrodes are a type of transducer, capable of exchanging electrical charge for ionic chemical species. Thus, they are able to detect chemical concentration variations in the cellular media and transform these changes into a measurable electrical current. They can also stimulate cells, as when a current profile is applied to them, they will generate a proportional amount of ionic species capable of exciting neurons [9, 10, 17]. This phenomenon of back-and-forth electrochemical communication between electrodes and cells is known as the electrode-tissue interface and is the basis for neural recording and stimulation.

Usually, electrodes are made out of metals (Au, Pt, Ag, TiN) that are capable of this electrochemical transduction at their surface - although other material types such as conductive polymers or graphene have been found to also work well [9]. Different electrode types perform differently in the electrochemical domain, opening the door for researchers to figure out which type has the best properties for certain scenarios. Understanding how a certain electrode behaves at the electrode-tissue interface has been for a long time a heavy topic of research, as the need for better devices implies the need for better electrodes.

WHAT MAKES A "GOOD" ELECTRODE?

Because electrodes are the elements of neural implants providing them with function, efforts of researchers to improve electrodes are focused on their performance. Specifically, the electrochemical properties of electrodes which govern the interaction with tissue. Yet, it is important to note first that the requirements for recording and stimulating electrodes are not the same.

Recording electrodes need to be able to pick up the physiological signals from their environment, while still not being affected by the background noise present in living tissue. An electrode´s levels of thermal noise in a certain setting will be directly proportional to the minimum measurable modulus of the surrounding signals. This capability is expressed in electrical terms with the concept of impedance, i.e.: the resistance experienced by the electrode to record physiological signals at a certain frequency [9, 10, 20]. Electrodes displaying very high impedance will struggle to detect low-amplitude activity over their noise baseline, rendering them incapable of signal recording. It is also important to know how the impedance changes across the measured frequency spectrum because it will produce in the recording electrode a filter-like behaviour. Suppose the recording electrode presents elevated impedance at the frequency range of interest, or it significantly distorts the sensed signal across its spectrum. In that case, it may not be usable for adequate signal recording [9, 10].

Stimulating electrodes aim to inject charge into the tissue they are in contact with. How much charge are they able to inject safely during a duty cycle, how does the charge distribute across the electrode's surface and how efficient are they when delivering the charge are some of the main characteristics to look out for in stimulating electrodes. Good stimulating electrodes should have wide potential operating windows for their safe operation while still injecting as much charge as possible with optimal energy efficiency [9, 10].

Still, due to the intrinsic link between the form and function of electrode materials, the capabilities of a specific electrode are conditioned by its design and manufacturing process. Hence, although the characteristics of an electrode that researchers ultimately care about are electrochemical, how they are improved is through experimenting with the material, structures, device design, and test parameters.

TESTING AN ELECTRODE'S PERFORMANCE

As the manufacturing process of an electrode is linked with its later performance (which can also not be accurately predicted beforehand) testing electrodes is essential [9]. The objective of said tests should be more than simply evaluating performance, but rather to do so in a way that makes results translatable to real, clinical scenarios. This can be challenging as initial experimentation should always start in-vitro, where conditions are vastly different from the final in-vivo setting. Thus, test parameters should be tailored to better reflect final use scenarios [10]. The practice of testing and defining an electrode's capabilities (either in-vitro or in-vivo) to be able to predict its performance for future uses is known as characterization.

Special attention must be paid to the test setup itself: adequate protocol, test conditions, and parameter setting are necessary to perform good tests. Because results should be comparable despite the complexity of the test, these precautions are necessary to ensure the test's repeatability and reliability of the obtained measurements [10, 20]. Therefore good characterization practices entail both obtaining useful information about a sample electrode and doing so in the most standardized manner.

Due to their inherent risk factor and performance requirements, as long as electrodes have been manufactured for neural interfaces, there has been a need to characterize them. Characterizing an electrode has proven to be a useful practice for a field that has seen constant innovation in materials, approaches, and designs over almost 50 years [21, 22]. It has opened the door to comparing different electrodes and choosing optimal configurations and designs, without having to test on patients. It also has allowed the field to move forward by giving researchers the ability to identify which areas of a certain electrode may need improvement. Decades of iterative electrode manufacturing, characterization, and clinical implementation have made it clear that developing more accurate and representative characterization methods will lead to a deeper understanding of electrodes and their potential, further pushing the boundaries of neuroscience [10].

1.3 TYPES OF CHARACTERIZATION

Being able to determine the functional properties of an electrode in a controlled setting that mimics real-life use cases, before having to actually use it, is essential to the present and future of neuroscience. These studies propel electrode manufacturing forward and enable new materials and manufacturing techniques to be considered in practice due to their improvement over the previous standard. As such, these controlled experiments aim to gain information on the key properties that make an electrode better or worse. Characterization can be subdivided into three main types: Electrochemical (EC) Characterization, Surface Characterization, and Mechanical Characterization

ELECTROCHEMICAL CHARACTERIZATION

Electrochemical Measurements (ECM) are used to test the performance of the electrode under working conditions. By observing the electrode's output in the electrical domain, it is possible to determine and quantify what are the thresholds for its safe stimulation of surrounding tissue, how efficient it is delivering charge, or the impedance it will have when recording neural signals [23, 24]. These characteristics of an electrode directly relate to how useful and capable it is in recording and stimulating neural tissue. Heavy research goes into these tests as they are the ones determining whether a novel electrode will have a therapeutical advantage over another one.

SURFACE CHARACTERIZATION

Surface Characterization refers to the use of a diverse set of tools intended to obtain information from the most external layer of an electrode. Microscopes and other imaging instruments such as Atomic Force Microscopy (AFM) are used in order to gain insight into the micro- and nano-structure of the electrode. Example images of a Au electrode can be found in Figure 2. Besides imaging, chemical tests such as X-ray Photoelectron Spectroscopy (XPS), Auger Electron Spectroscopy (AES) or Secondary Ion Mass Spectroscopy (SIMS) may be carried out to identify the individual species present on a sample´s surface. As the electrode's surface is the only active portion in direct contact with the tissue, and electrode activity is a process happening uniquely at the interface, surface studies are a fundamental part of electrode characterization. By examining its integrity, surface features, composition, or the existence of defects, researchers are able to assess the quality of the manufacturing process of both simple deposited metal layers or complex nano-structures[25–27].

MECHANICAL CHARACTERIZATION

Mechanical Characterization looks into the mechanical properties of an electrode. As the electrodes come in direct contact with the body, adequate mechanical performance is needed to avoid damage to both electrodes and tissue, especially with repeated uses or special use scenarios like peripheral nerve cuffs [28]. Current interests in miniaturizing technologies to make them implantable means that a full-on study of the device's mechanical behavior is needed for optimal biocompatibility and reliability. Additionally, flexible electrodes require new characterization tests to determine their integrity and flexible capabilities, while for electrodes coated in other 3D materials - especially those with conductive polymers like PEDOTs - a delamination test is needed to study the adhesion of the coating [29].

Yet, although these types of characterization may seem independent, they are intrinsically linked [9, 27]. Surface features will translate to changes in performance in the EC domain, and questions about why a certain electrode under-performs or improves a similar one may only be answered after examining them visually and mechanically. Hence, for a complete characterization of an electrode, all are needed as they complement each other. Yet, the current challenge in the field of electrode characterization, and the one that is trying to be addressed in this review is that of EC characterization. This is mainly due to the fact that not only do these tests give the most crucial information to assess whether an electrode improves upon a previous one, but the complexity in parameters of such experiments makes EC characterization a non-standardized practice [10, 20]. Not all teams perform the same tests, nor in the same manner, making results difficult to compare and build upon.

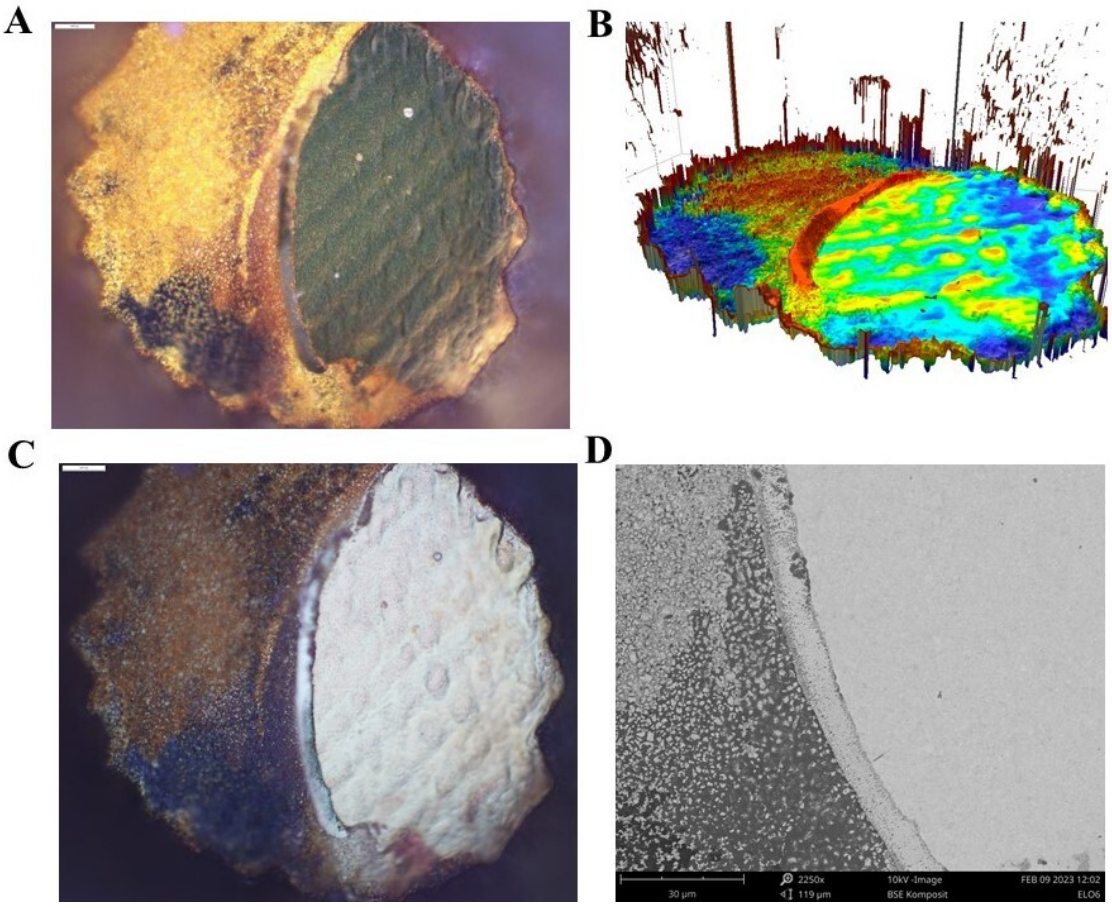

Figure 2: Surface Characterization techniques for a Au circular opening electrode. Techniques used are A: Optical Microscopy, B: Interferometry, C: Dark Field Microscopy, D: Scanning Electron Microscopy.

1.4 ELECTROCHEMICAL CHARACTERIZATION OF ELECTRODES

The following section will be an overview of the most commonly used techniques and equipment involved in electrochemical characterization for neural interface electrodes: electrochemical impedance spectroscopy, cyclic voltammetry, and voltage transients. Additionally, as the ultimate application of this review is characterizing Au electrodes, the specific behaviour of Au in these tests will be further explored. Relevant research was studied, and values for the reported figures of merit were extracted from the text or, in the absence of literal values, figures.

Although these three tests are performed differently, they do share common factors that are worth exploring before looking into each specific test. In all cases, the fundamental aspect of an electrochemical test involves applying some current or potential from our electrode of interest, commonly referred to as a Working Electrode (WE), to a Counter Electrode (CE). This CE is usually chosen to be of good conducting material that is also inert to avoid interfering with the electrolyte kinetics. This is why materials like Pt or graphite are preferred to others like Cu. Additionally, CE's are made with a much larger dimension than the WE to avoid it being a source of impedance in the test [10]. Besides these two electrodes, it is also common to use a third Reference Electrode (RE) to measure against, giving measurements higher repeatability and reliability. Using Ag/AgCl electrodes as the RE has become a very widespread practice, which has the added benefit of making results from different groups more comparable - yet many other possible RE electrode materials are possible. Hence, this setup is referred to as a 3-Electrode Setup and is standard practice for EC experiments [9]. Note it is also standard to always report the full electrode setup when sharing findings, as results are strongly linked to them.

The other main common factor across all of the tests of interest is that of the medium through which tests are run. In-vitro tests are the easiest to perform, but it is key that the conditions of the medium can be somewhat translatable to future in vivo environments. Although living tissue is characterized by having many chemical species in different concentrations, they do not seem as relevant when testing for the immediate EC

performance at the electrode's interface for short-term time spans [10]. As this is the scale of most scenarios for these tests, a phosphate-buffered saline (PBS) solution is deemed suitable. A common range for the solution's pH, trying to mimic an in vivo environment, is between 7.2 to 7.4 [30–33]. For longer-term testing, the medium should better mimic that of living tissue, as species like carbonate ions or nutrients are absent in PBS. Alternative solutions, such as extracellular fluid (ECF) contain these factors that have been shown to have an effect on electrode performance due to protein adsorption and electrode biofouling [34]. Additionally, tissue anisotropy can also be overlooked when testing in vitro [35]. This all leads to an increased interest in performing these ECM in vivo instead of in vitro. But the change in medium has several drawbacks besides getting approval for in vivo testing. For instance, it is usually not possible to include a RE in the experiment setup [10], limiting the control precision of the WE's potential. This makes taking measurements regarding the sensing capabilities of the WE (such as EIS) a major challenge. And for stimulation tests, in-vivo experiments also hold risks related to stimulating tissue over the safety thresholds [36]. As the goal of ECM for stimulation capabilities is often to find this threshold, it is quite possible to reach harmful potentials during electrode characterization in vivo. These limitations, coupled with the need to still carry out in vivo recordings, have pushed researchers to develop alternatives such as growing living cells on top of the electrodes [37, 38]. As each test presents different challenges when trying to be carried out in vivo, the practice of in vivo ECM will be evaluated separately within each test.

2 ELECTROCHEMICAL IMPEDANCE SPECTROSCOPY

Electrochemical impedance spectroscopy (EIS) is an EC measurement test where the impedance and phase angle response of an electrode of interest is measured across a frequency range. As the impedance is a result of the electrochemical kinetics at the electrode's interface, it is also a measure of the electrolyte itself. To be able to characterize an electrode with EIS and later compare measurements, it is imperative to fix the medium conditions (pH, concentration, positioning, temperature). EIS is mostly used as a test to describe the capabilities of electrodes that will be used for recording applications.

2.1 PERFORMING EIS

To conduct the test, a sinusoidal potential or current is applied to the WE over a frequency range - usually for neural interfaces, it ranges from 0.1 Hz to 100 kHz [9]. In order to estimate the electrode impedance, a comparison between the input excitation value and the measured output of the circuit is needed. From that data, both amplitude and phase $(|Z|, \varphi)$ for the electrode's impedance can be calculated following

$$|Z| = \sqrt{Re\{Z\}^2 + Im\{Z\}^2} \tag{1}$$

$$\varphi = arctan(Im\{Z\}/Re\{Z\}) \tag{2}$$

where $Re\{Z\}$ and $Im\{Z\}$ refer to the corresponding real and imaginary components. As the excitation used to measure impedance is small in magnitude, the impedance response of the electrode remains linear for each frequency point, as seen in Figure 3. For EIS, the root mean square of the voltage is most commonly set to 10mV, and values higher than 100mV are discouraged [10], as the linear relationship disappears. Doing this across a window of frequencies produces a spectrum of impedances, describing the electrode's recording capabilities.

Other secondary test parameters can be tweaked based on the setup available, such as the number of frequency points measured, or over how many cycles of measurement the final impedance value is averaged after. These aim to produce more robust results but do not change the fundamental aspect of how is the test performed. For instance, Bret *et al.* recommend cycling 5 times at each frequency point for better measurements [40].

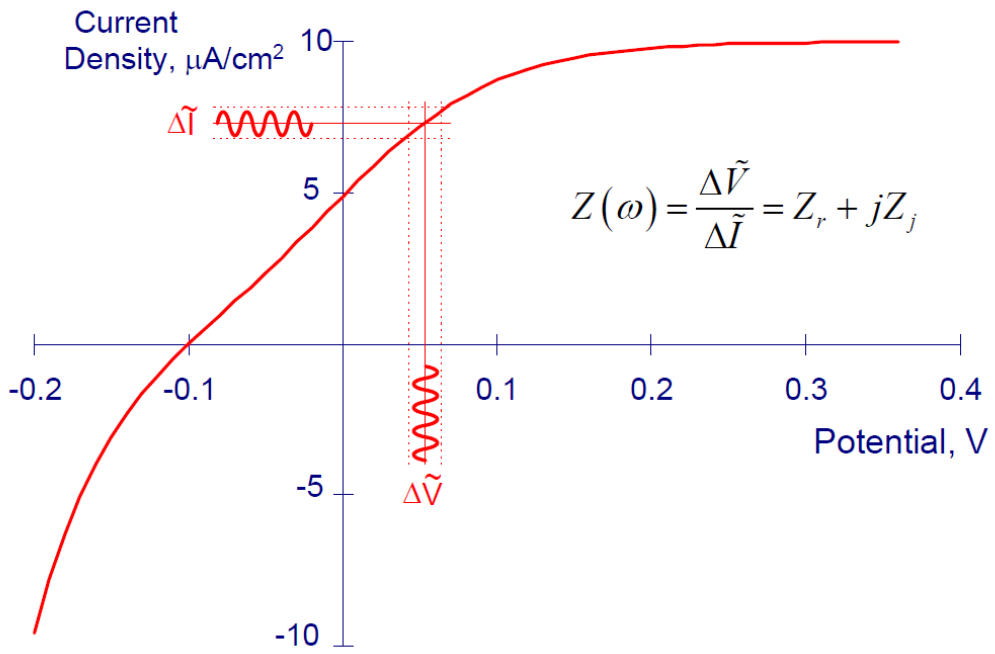

Figure 3: Graph depicting the linear relationship between current and potential for calculating impedance over low magnitude sinusoidal excitation. Adapted from [39].

2.2 REPORTING OF EIS DATA

EIS results can be shared in literature in many different ways, yet they all aim to depict the general behaviour across the whole frequency range measured. The results of EIS are typically presented in three separate ways.

BODE PLOTS: ABSOLUTE IMPEDANCE AND PHASE ANGLE

The most common and straightforward method plots impedance in two separate graphs, one for the absolute value of the impedance, usually plotted in a logarithmic scale, and another for the phase angle. This is known as a Bode plot. Figure 4 depicts a standard Bode plot for a single Au electrode with both variables in a combined graph. Impedance starts high at lower frequencies, decreasing as frequency increases in a linear fashion when plotted in a logarithmic scale, and staying rather constant after a certain frequency value (in Figure 4 around 10 kHz). Due to the capacitive behaviour of the electrode-tissue interface, the phase angle is measured to be negative in value across the whole frequency spectrum. It is common to change the sign of this component to make it positive. Standard phase angle recordings are a result of the interplay between the resistive and capacitive contributions in the standard impedance curve described previously. The expected profile of such phase angle will start in the predominantly resistive behaviour region if the measured frequencies are low enough. As intermediate frequencies are reached, a shift to predominantly capacitive behaviour will be represented by a decrease in phase angle, eventually plateauing close to -90º and rising back as it approaches the high-frequency region. Lastly, as the electrode will have a predominantly resistive behaviour in the high-frequency region, phase angle values will approach 0º. Most importantly, when measured from low enough frequencies, it is expected that the phase angle shall cross the -45º threshold twice, indicating the changes of behaviour in the electrode (more on this in section *2.4*). Evaluating the magnitude of the impedance element at a certain frequency or the shape of the phase curve can be useful for direct comparisons between electrodes. More so, these graphs are usually presented together with the figure of merit of the electrode's impedance at 1kHz - or in some cases, substituted by it. Although not perfectly representative of the electrode's performance for actual neural activity recordings [10], it has become the standard value to be shared and used as a reference for a certain electrode type.

Another possibility is to normalize this impedance by the unit area of the electrode, typically expressed in $\Omega * cm^2$. Normalization allows researchers to express the impedance as a function of area, opening the door to comparing differently sized electrodes. Although it is common in most tests to normalize by dividing by area, this is not the case for impedance. Instead, normalized impedance is calculated by multiplying by the area and

the reasoning for such calculation lies in the definition of impedance itself. Impedance is defined as

$$Z = \delta V / \delta I \tag{3}$$

where dV represents the immediate change in voltage and dI the immediate change in current (Equation 3). To normalize impedance, the current is substituted by current density (J), effectively dividing current by area as

$$J = I / A \tag{4}$$

If we then want to calculate the normalized impedance (Z'), we write equation 4 into equation 3, as

$$Z' = \delta V / \delta J = \delta V / (\delta I / A) \tag{5}$$

$$Z' = Z * A \tag{6}$$

Thus, to obtain directly the normalized impedance it can be done by following equation 6, where the impedance is multiplied by the geometric surface area of the electrode [41]. By normalizing EIS data, it is possible to compare electrodes manufactured in different sizes and with different techniques.

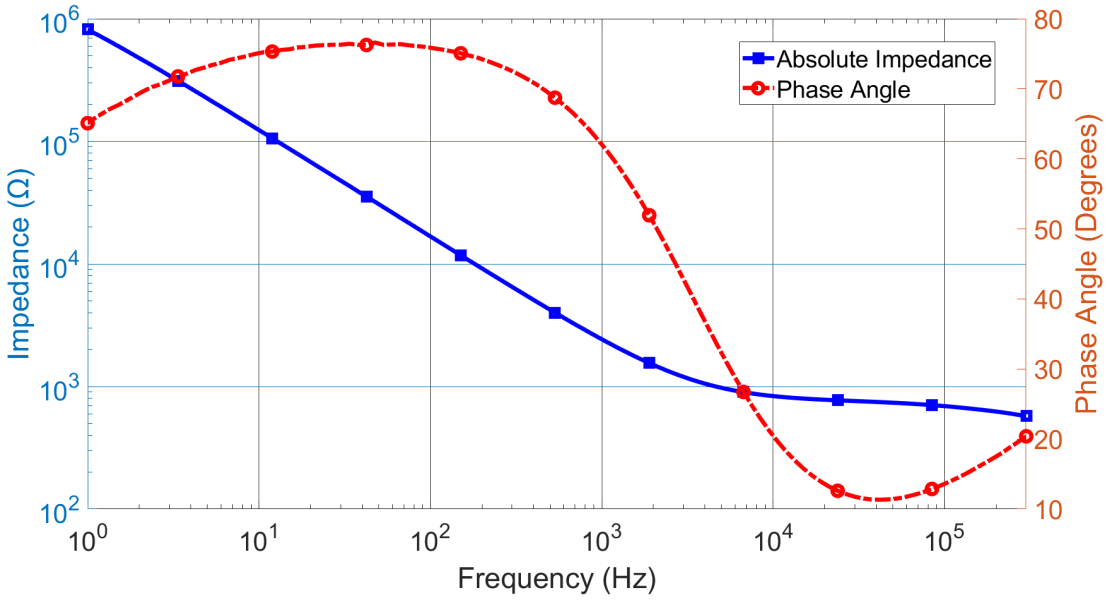

Figure 4: Graph showing EIS for an electrode by plotting its absolute impedance and its phase angle components.

NYQUIST PLOTS: REAL AND IMAGINARY COMPONENTS OF IMPEDANCE

An alternative method to view EIS data would be to combine impedance and phase angle data into a single Nyquist plot, with the X-axis being the real part, and the Y-axis being the imaginary part of the impedance measurement. These values can be obtained in a variety of ways, from the measurement setup directly, to transforming from the polar format expressed before (Z and Phase Angle φ) to its rectangular counterparts (namely, ReZ and ImZ) as shown in

$$Re\{Z\} = |Z| * cos(\varphi) \tag{7}$$

$$Im\{Z\} = |Z| * sin(\varphi) \tag{8}$$

The benefit of the Nyquist plot is that the real part of the impedance is directly related to the resistive behaviour of the electrode, while the imaginary part reflects the capacitance behaviour. The combined contribution of

both charge transfer methods gives electrodes a characteristic shape to their Nyquist plot: a semicircle. As the relationship between real and imaginary counterparts of impedance is related to the resistive and capacitance charge transfer methods; points where the imaginary component is at a minimum will display impedance solely from the real component. Similarly, when the plot reaches maximum values in the imaginary axis, it is indicative that the contribution of the capacitive behaviour is at its maximum. By observing features of the Nyquist plot we can directly extract values for a simple model of the electrode, as indicated in Figure 5 from Brett *et al.*'s paper [40]. Cell resistance (R_Ω) indicates the resistance component of the medium the electrode is immersed in and can be obtained by observing the minima of the semicircle at very high frequencies (lower values for real and imaginary components). The electron transfer resistance (R_{ct}) is another key component of an electrode's model and reflects the resistance electrons encounter when transferring over the interface boundary. It can be obtained by considering that the minima of the semicircle corresponding to a higher value for the real impedance is a sum of both resistive components. Double-layer capacitance (C_{dl}) is a result of the electrolyte and the charged electrode interface acting as two separated and charged layers, effectively behaving as a capacitor able to store and effectively transfer charge. By observing the maxima of the imaginary impedance component, we can deduce the C_{dl} following equation 9.

$$\omega R_{ct} C_{dl} = 1 \tag{9}$$

The ability to determine values for elements of the model of the electrode at a single glance, makes Nyquist plots a useful tool to give more detailed information about the electrode [42]. Similarly to impedance modulus and phase angle plots, Nyquist plots can be used to assess how modifications of the electrode affect performance, but their presentation of the real and imaginary parts of the impedance makes them redundant for simple characterization purposes. When not trying to simply display impedance measurements, the presence of Nyquist plots is used to build electrode models from the information contained in them [43, 44].

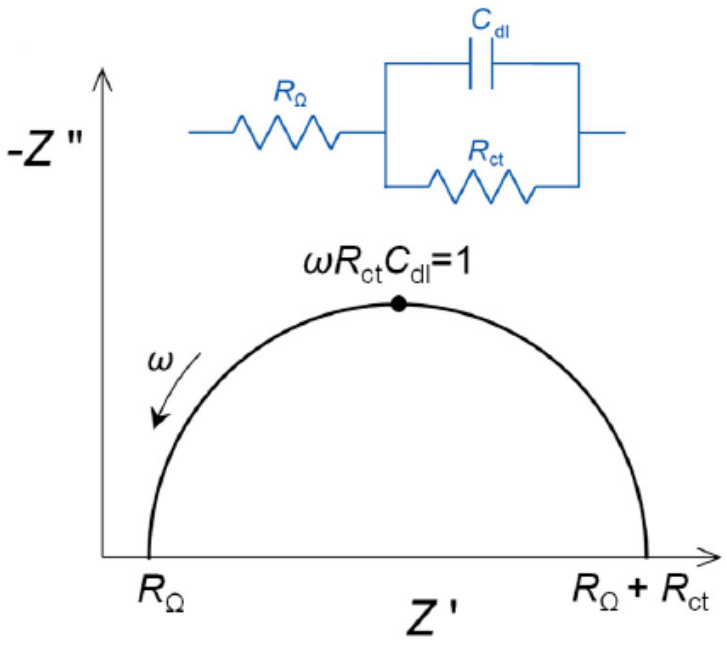

Figure 5: Illustration of how basic elements of the simple electrode model can be extracted from the Nyquist plot of an electrode undergoing an EIS characterization test. R_Ω: cell resistance, R_{ct}: electron transfer resistance, C_{dl}: double-layer capacitance Adapted from [40]

BUILDING EQUIVALENT CIRCUIT MODELS

The third way to compile the information gathered from an EIS test would be to model an equivalent circuit of the electrode, with fitting impedance elements. By representing an electrode with an ideal electric circuit model, it is possible to represent the electrode's behavior simply. Obtaining a simple model is usually a simple task that can be carried out by available software or by plotting out the Nyquist plot of the electrode, as mentioned before and illustrated in Figure 5 [43].

The most simple electrode model, consisting of a resistor for the cell's resistance, in series with a resistor with the electron transfer resistance in parallel with a capacitor for the double-layer capacitance, can be fitted to almost all electrode EIS data. And all it needs to be built is contained in its Nyquist plot. But as the electrode and its interface interaction become more complex, it can be difficult to represent all the different elements at play [40].

It is also important to take into account that these models still present themselves as black-box models that may not take into account all the parameters involved in the EC reaction, missing out independent elements, or grouping under one component many individual sources [43]. It is possible to arrive at different models that both provide a correct fit, making it difficult for researchers to decide which one is the correct one. Figure 6 shows 4 equivalent circuits Lempka *et al.* built to model an electrode's EIS behaviour [45]. All of them are valid but with varying degrees of error and robustness. This is in summary why, when it comes to using it as the way to characterize EIS results, there are many critiques to its solo use [46, 47]. It "does not provide a complete analysis of data" [48].

Still, there is one particular scenario where equivalent circuit modelling provides insight that previous methods do not: circuit design. By knowing the equivalent circuit model of the electrode, it is possible to make an informed approximation for representing the electrode in circuit design schematics. In these scenarios, modelling electrodes is necessary to understand the system's requirements for optimal performance and design accordingly. But even then, there may be marginal benefits to obtaining high-precision models, at the price of increasing complexity.

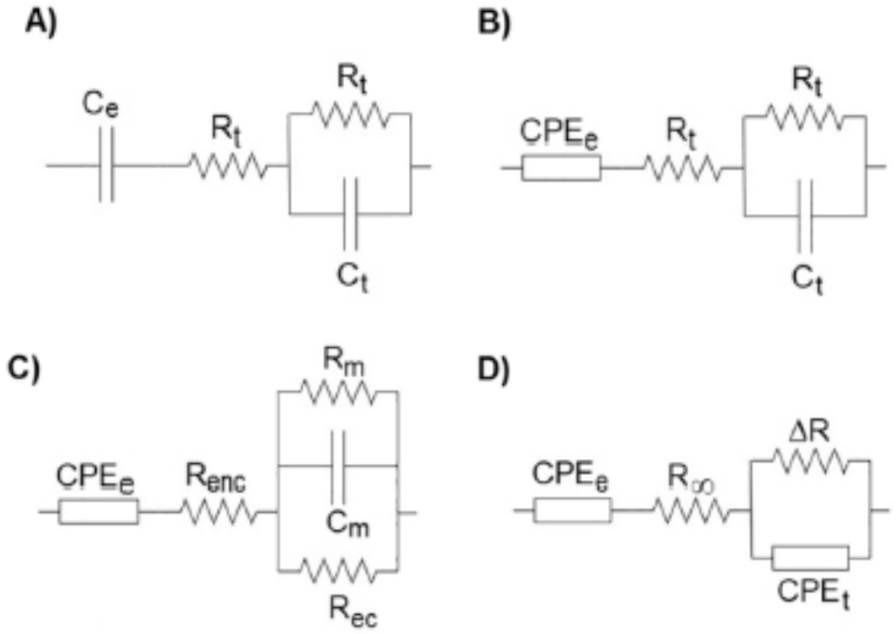

Figure 6: Examples of four Equivalent Circuits developed to fit the same electrode EIS data. C – capacitance, CPE – constant phase element, e – electrode, ec – extracellular, enc – encapsulation, m – membrane, R – resistance, t – tissue. ∞ – infinite frequency, Δ – difference between a parameter at DC and at infinite frequency. Adapted from [49]

2.3 PERFORMING EIS ON LIVING TISSUE

The use of EIS as a means to characterize electrode-to-tissue performance is broad, but it serves a slightly larger purpose than characterization performed in a prepared medium - like PBS. Taking EIS measurements of in vivo environments to characterize the isolated electrode's performance would be very complex, as many factors come into play when trying to replicate the three-electrode setup common to an electrolytic cell described previously in this section. Instead, EIS has two main uses when applied to living tissue: directly comparing performance between electrodes and using it to characterize the electrode-tissue interface. Taking impedance measurements of cellular recordings (in vitro extracellular, or in vivo) with developed electrodes to see which ones pick up a better signal has become a widespread practice [37, 50] (although it is discussed in section *2.4* that lower impedance does not always equate to better performance). Still, it is challenging to obtain accurate recordings of living tissue. Specifically for in vitro extracellular recordings, one of the most common

approaches to solve this challenge is growing culture cells directly on top of the electrode itself. These experiment setups are still conditioned by the electrode's material, surface, and other interface properties as they condition cell growth [38].

On the other hand, EIS has seen more use as a tool to characterize the electrode-tissue interface at any given time. By modelling EIS behavior before, throughout, and some time after implantation, Lempka *et al.* were able to use this data to determine the interfacial state of the electrode from electrochemical data [45]. This allowed clinicians and researchers to determine the encapsulation rate of the electrode due to the foreign body response of the host. Further progress has been made to determine other scenarios such as cell differentiation, proliferation, recognition, and death based on impedance measurement shifts[49, 51].

2.4 ISSUES WITH EIS

Even after using EIS for decades, being a standard test to conduct electrode characterization, there is still ongoing debate about some of its fundamental aspects.

SELECTING AN IDEAL REPORT FORMAT

The ways of representing EIS data have varying utilities depending on their scenario, which has made it difficult for researchers to settle on one single method. For EC electrode characterization and possible comparisons, Bode plots showing absolute impedance and angle have become the standard among researchers, with a secondary interest in showing an equivalent circuit model to be able to quantify performance using traditional circuit components. This is because displaying impedance in an absolute manner better reflects the outcome when using the said electrode for recording: it should be able to pick up better or worse the signals in the surrounding medium without filtering them excessively; while phase provides insight into the governing charge transfer mechanism (Faradaic or Capacitive) at a certain frequency. The additional urge in academia to share information in a useful condensed manner made absolute impedance plots the preferred reporting format for electrode manufacturers. On the other hand, when trying to solve problems arising from circuit design, it is more common to observe the use of Nyquist plots and a strong interest in developing accurate electrode models. This preference change happens due to the same prioritization in condensing useful information: electrical circuit components convey more usable information for circuit designers.

IMPEDANCE AT 1KHZ AS A FIGURE OF MERIT

The use of the impedance at 1 kHz as a figure of merit for EIS is done for practical purposes, but also as it is also commonly shared when reporting EIS data from other instruments, such as batteries [52]. Yet, for biological purposes, the signal spectrum is mostly lower than 1 kHz [53]. A collection of biological signals, and their corresponding recording frequency spectrum, are presented in Table 1 [54, 55]. This means that the impedance profile of an electrode works as a filter of sorts across the whole frequency spectrum, as the difference in impedance between high frequencies and low frequencies can be of several orders of magnitude. Because of this, Boehler *et al.* recommend shifting from the figure of Z_{1kHz} to the cutoff frequency (f_{cutoff}). f_{cutoff} can be defined for electrodes as the frequency, starting from high-frequencies as they have pass-band behaviour, at which the phase angle is -45º (Fig 7). This point is also coincidentally the point at which the electrode transitions from a predominantly resistive behaviour to a predominantly capacitive one, signalling the shift to a predominantly non-linear distortion in the recorded signals [10]. Hence, this figure of merit can better convey what signal environment is the recording electrode good for.

IMPEDANCE AND IMPROVED NEURAL ACTIVITY RECORDINGS

There are also substantial critiques of the assumption that better impedance response equals better recordings in vivo. There is a sound basis for this idea, as impedance is intrinsically linked with the electrode's signal-noise ratio (SNR). This is because, at the recording electrode site, the contribution to noise is solely thermal noise (v_n)[56]. Thermal noise is directly related to impedance, as shown in equation 10, where k represents the Boltzmann constant, T the temperature in Kelvin degrees, and Δf the bandwidth.

$$v_n = \sqrt{4kT\Delta f Re\{Z\}} \tag{10}$$

Equation 10 shows that it is possible to obtain high SNR recordings when the recording electrode's impedance is low. Yet, recent studies have shown that differences in impedance may not translate directly to better recordings. In a study with polytrodes by Neto *et al.* [57], it was observed that having better impedance electrodes did not relate to neural recordings having a higher SNR ratio. To explain this counter-intuitive phenomenon,

Table 1: Table containing some of the most relevant biological signals and their corresponding frequency range in Hz at which they can be recorded. Adapted from [54, 55]

Type of Signal	Frequency Range (Hz)
Blood Pressure	0-60
Electroretinogram	0-50
Electrocardiogram	0.1-250
Electromyogram	20-1k
Electroneurogram	250-5k
Delta Brain Waves	0.1-3.5
Theta Brain Waves	4-8
Alfa Brain Waves	8-12
Beta Brain Waves	12-30
Gamma Brain Waves	30-90

Table 2: Table collecting available normalized impedance values from the literature for bare Au electrodes. Adapted from [30, 33, 37, 38, 58–60]

Electrode Description	Z' @ 1 KHz ($\Omega * cm^2$)	Author
20 µm radius sputtered Au	10.1	Martin *et al.*, 2002
Compact Au electrode tip	6.84	Seker *et al.*, 2010
30µm diameter bare Au	0.11	Kim *et al.*, 2015
Bare Au electrode	0.88	Kim *et al.*, 2017
Planar circular Au electrode	3	Won *et al.*, 2018
Planar Au electrode	0.3	Won *et al.*, 2018
Planar Au electrode	1.4	Won *et al.*, 2018
10 µm radius raised bare Au	6.28	Wolfrum *et al.*, 2021
100 µm radius raised bare Au	9.42	Wolfrum *et al.*, 2021
1,25mm radius bare Au electrode	15	Gryszel *et al.*, 2022
50x50µm bare Au electrode	10	Gryszel *et al.*, 2022

the research team argues that thermal noise (related to impedance in Eq 10) will have little contribution to the overall recording, as the neural signals would elicit higher amplitude recordings at the electrode when originating from proximal neurons than the contribution of thermal noise. Improving impedance further would not report significant benefits to these recordings, at the cost of more complex electrodes [57].

These points illustrate that despite EIS being a widespread technique for characterization, there are still aspects that are not being taken into account when conducting tests. More importantly, it is how this data is reported and the weight that researchers give to the results that are missing the context of clinical application.

2.5 EIS OF AU ELECTRODES

Reported values for bare Au electrodes - consisting of a simple Au layer interface - may vary due to electrode size, so results are normalized by multiplying by the electrode's area. We compiled relevant literature and calculated the normalized impedance by extracting data from the text and figures presented, summarized in Table 2. Normalized Z at 1kHz for bare Au electrodes present on average a value of 5.76 Ωcm^2 [30, 33, 37, 38, 58–60], spanning over two orders of magnitude, from 0.11 Ωcm^2 [37] up to 15 Ωcm^2 [59].

Additionally, researchers have tried to improve Au's performance by modifying its surface to improve its ESA/GSA ratio. Techniques such as making "Fuzzy Au", attaching Au nanoparticles, or etching the Ag of a thick Au-Ag layer to obtain a nanoporous Au electrode are some of them, summarized in Table 3. In general terms, these modifications seem to improve the Normalized Z at 1kHz by one order of magnitude, with the calculated average normalized Impedance at 0.47 Ωcm^2, minima at 0.09 Ωcm^2 [37], and maxima at 1.24 Ωcm^2 [60]. Utilizing surface modifying techniques allows for giving Au-based electrodes similar performance to other materials favoured in the field, such as modified platinum or some conducting polymers [37, 38, 61–65].

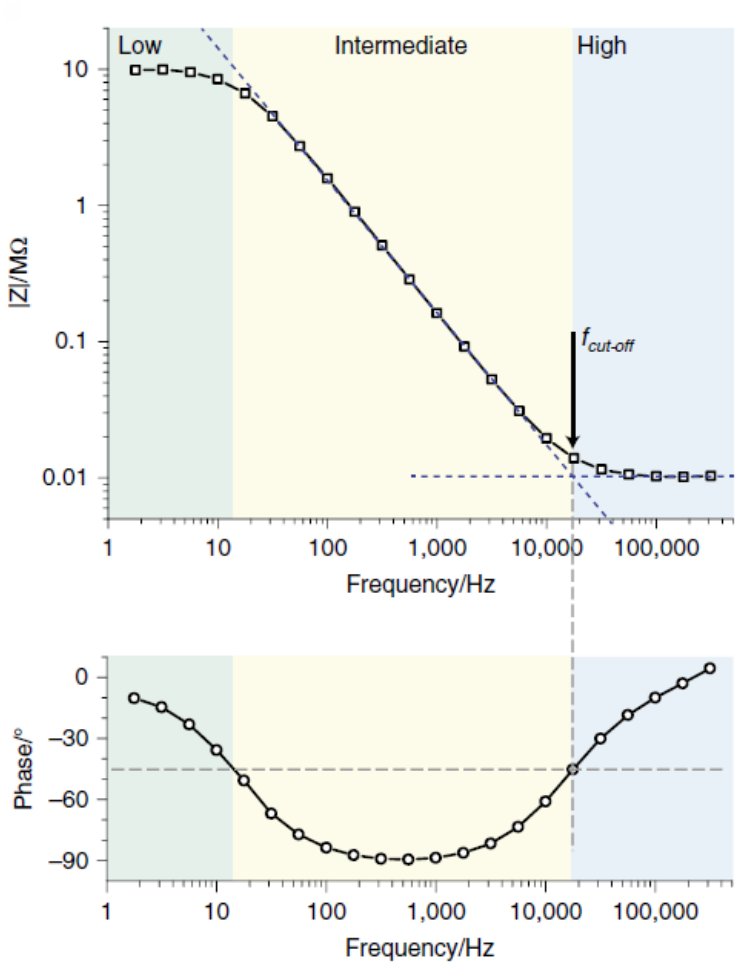

Figure 7: Bode plot of an EIS measurement, indicating where the cutoff frequency would be located, both from the 45° point and the intersection of resistive and capacitive regions. Adapted from [10].

3 CYCLIC VOLTAMMETRY

Cyclic Voltammetry (CV) is an EC measurement test where the current response of an electrode of interest is measured as we apply a voltage potential in steps, cyclically sweeping across a voltage window at a constant sweep rate. CV is used to determine what kind of electrochemical reactions happen at the electrode's surface within certain voltage ranges and, most commonly reported, quantify the amount of charge available in the electrode for injection during stimulation applications. Other information, such as identifying the electrochemical reactions happening, their reversibility, and the electrode's stability after stimulation, can also be obtained from CV [9].

3.1 PERFORMING CV

To perform a CV test, a 3-electrode setup is required. The voltage is swept back and forth from each of the voltage window's extremes, across the electrode pair WE|CE, while the RE|WE pair is used to measure the current response. If only two electrodes were employed, as the WE needs to be under stimulation in pair with another electrode, it would not be possible to accurately measure its current response. Thus, the RE|WE pair must study the current response to the applied voltage [29]. Voltage is used as a driving force for the electrochemical reactions that happen at the electrode's surface. Sweeping the potential (V/s) across a potential window drives different, characteristic redox chemical reactions. The kinetics of these reactions are related directly to the current response, which is measured [29]. Hence, it is possible to identify the redox reaction happening at the electrode's surface and determine the amount of electrochemical charge the electrode was holding throughout an entire cycle. It is important to note that the current will be the result of both faradaic and capacitive

Table 3: Table collecting available normalized impedance values from the literature for modified Au electrodes. Adapted from [30, 37, 58–60]

Electrode Description	Z' @ 1 KHz ($\Omega * cm^2$)	Author
Fuzzy Au 20 µm radius	1.24	Martin *et al.*, 2002
Au with 304 nm Au nanoparticles	0.24	Seker *et al.*, 2010
Au with 112 nm Au nanoparticles	0.56	Seker *et al.*, 2010
Au nanoparticles on Au	0.09	Kim *et al.*, 2015
Au with Au nanorods	0.46	Won *et al.*, 2018
50x50 µm Au with nanoparticles	0.2	Gryszel *et al.*, 2022
50x50 µm nanoporous Au	0.5	Gryszel *et al.*, 2022

reactions. Capacitive current, defined as

$$i_c = C_{dl} * \delta v / \delta t \tag{11}$$

is constant for any process with a constant potential change ($\delta v / \delta t$), so it will yield a constant positive or negative current in the respective anodic or cathodic sweep. Capacitive processes are the ideal charge transfer methods for neural interfaces because they do not introduce chemical species in the environment or themselves [66]. On the other hand, faradaic reactions depend directly on the potential at which they occur, meaning they will change with it. As the potential reaches that of an electrochemical reaction (V_r), and when the reaction is limited by kinetics, the current response will rapidly increase as the reaction equilibrium potential is reached. As the potential moves away from V_r, the current response decreases [10]. This behaviour results in chemical reactions appearing as peaks in the voltammogram. As such, it is easy to determine whether an electrode is behaving as intended by examining the peaks present and the voltages they happened at. If they align with the expected redox reactions for that certain type of material, the adequate performance of an electrode can be assessed [29].

It is also worth noting that in altered mediums, as reaction kinetics change, so can the current response. For instance, degassed mediums aim to reduce the amount of 0_2 dissolved in the medium. Limiting the electron transfer kinetics will require a larger potential (in absolute value) for the reaction to occur, shifting the current peak. In this case, at the potential region for O_2's adsorption, mass transfer kinetics (governed by diffusion) may surpass electron transfer kinetics, leading to an irreversible charge transfer process [29]. Media with an excessively high concentration of a species should not affect the reversibility of the reaction as kinetics for electron transfer surpass those of mass transfer. The current response shall happen at a similar potential to that of a medium with ideal species concentration, but the peak's width and amplitude may grow as species are more available to react.

3.2 ELECTRODE CHARACTERIZATION WITH CV

When it comes to characterizing an electrode, CV does so in two distinct ways: the first is that it allows identifying which electrochemical reactions are happening at the electrode's surface, and the second is that it can quantify the charge available for stimulation.

IDENTIFYING EC REACTIONS

Identifying electrochemical reactions through peaks in the voltammogram curve can be a complex topic, as one needs to understand all the chemical species in the process and at which potential they are expected to happen [9, 29]. But as they are related directly to the electrode material, they are available in the literature and should not vary between different electrodes made of the same material. So the common approach is usually that of using the presence of these reactions as a qualitative indicator of the electrode (i.e.: whether it is behaving as expected for that material). Thus, by observing roughly the curve's morphology one can differentiate electrode types. Figure 8 showcases how curves for three different electrodes can be very different despite keeping other parameters constant across tests. Still, as minor changes in the electrode can produce shifts in the curve and its signature peaks, observing faradaic reaction peaks should not be used lightly. For further insight, all possible species and electrochemical processes should be taken into account when justifying a behaviour. This hints at the other main challenge when trying to identify reactions in an unknown or novel electrode. A study of the full range of electrochemical reactions happening throughout the tested window should accompany every new electrode type, as it may not be possible to rely on past references. Con-

sidering the influence of the capacitive charge transfer versus the faradaic charge transfer processes is also key to understanding the expected shape of such peaks [10, 67].

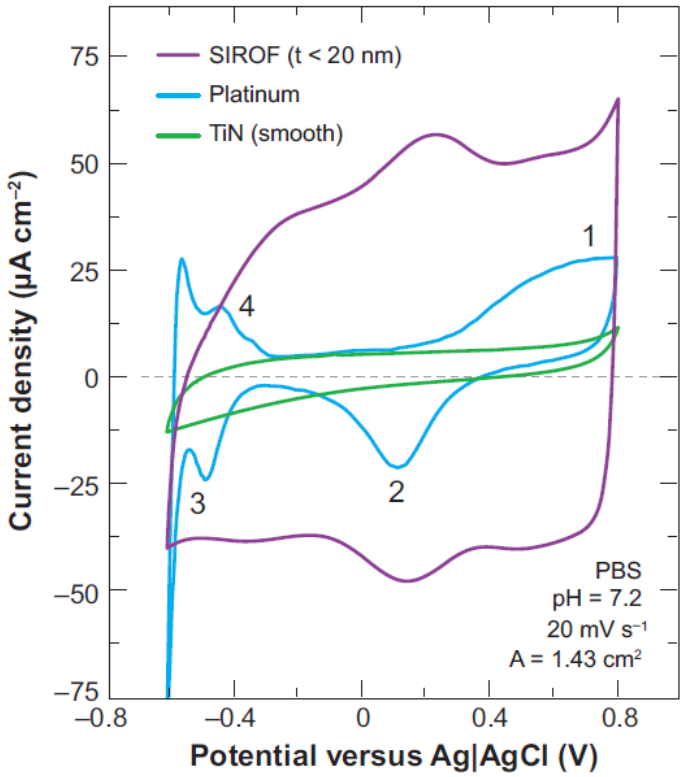

Figure 8: CV measurement of three distinct electrode types, in PBS at a rate of 20 mV/s. The numbers indicate characteristic faradaic reactions for the Pt electrode: 1 indicates Pt oxidation, 2 indicates Pt reduction, 3 indicates H atom plating and 4 indicates H atom stripping. Adapted from [9].

QUANTIFYING AVAILABLE CHARGE

Quantifying available charge is the most reported use of CV for electrode characterization. To do this, Charge Storage Capacity (CSC), expressed usually in mC/cm^2, is computed from the integral of the voltammogram curve. It represents the amount of charge available at the interface per geometric unit area. Most commonly, as the charge that is of interest is that which is available for stimulation, it is also expressed through Cathodic Charge Storage Capacity (CSC_{cath}), defined as the total amount of charge per geometric unit area while operating the cathodic region, resulting in negative values for the current response. By computing the time integral of only the negative portion of the CV curve, shown in Figure 9, CSC_{cath} can be calculated. CSC_{cath} can be useful to compare different electrodes' performance, as it solely presents a quantifiable amount of charge per unit area. It is thus the most reported metric from CV tests, sometimes reducing the whole test to it. But using it as a standalone value, even if it is the only comparable metric, is an incomplete description of the electrode's capabilities [10]. The need to check for the curve's morphology as an indicator of the adequate performance of the electrode, and the high susceptibility of numerical metrics to the parameters used in CV demand that the full test information must be disclosed, discussed in section *3.3*.

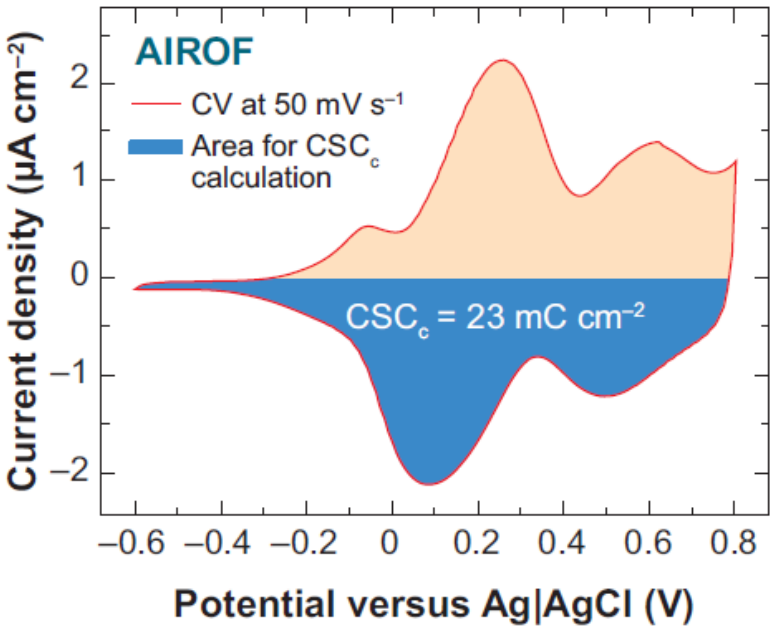

Figure 9: CV curve of an activated iridium oxide film (AIROF) electrode with the cathodic contribution highlighted in blue. By computing its integral, it can be known that this electrode has a CSC_{cath} of 23mCcm^{-2}. Adapted from [9].

3.3 KEY PARAMETERS IN CV

Besides the specific reactions characteristic of the measured electrode type and the set-up used in measuring it, CV is known for being heavily influenced by the test parameters chosen. Three key parameters in CV will be discussed: the potential window, the number of cycles performed, and the potential sweep rate.

SWEEPING POTENTIAL WINDOW

The potential window is the range of voltage values across which the electrode will be swept back and forth. When testing for neural interfaces, the objective is to find the optimum performance while remaining safe for the body and its tissues. When the voltage reaches the necessary potential to initiate water hydrolysis, as water in tissue breaks down and reactive species are liberated, it is almost certain that non-reversible damage is happening [9]. That is why it is common practice to set the limits of the CV window to those within the window of water hydrolysis for each type of electrode. The specificity of this process implies that each type of electrode should be tested to figure out its water window values [10] -later discussed in this section. Reference values can indeed be found in the literature for different materials. Still, the moment surface modifications are introduced, or the manufacturing process prevents the electrode from being ideal, the water window will be different. To determine the water window, it is possible to run a CV test well outside of the window and then study the resulting curve. As the potential of the test reaches the V_r necessary for water hydrolysis, the faradaic reaction will begin, greatly increasing the current response. As the reactant (H_2O) is widely available, kinetics do not limit the reaction, and the observed peak is expected to be very large in comparison to those of other chemical species [10]. This can be observed in the voltammogram obtained. The test should also be ideally split into two separate runs, wherein in each test only one side of the water window is tested, as can be seen in Figure 10. As the purpose of the experiment is to provoke non-reversible reactions at the electrode´s surface, only one boundary may be tested at a time. By the time the second boundary would be tested in the same run, the electrode´s surface would have been modified in a non-reversible way leading to an output different from other electrodes that have only been subjected to reversible reactions. Additionally, it is for this same reason the test may only require one cycle. Any subsequent cycles would not provide representative data. Thus, the water window for testing and future tissue stimulation is then determined as the potential values from the first cycle of each boundary test before any faradaic behaviour is observed [68].

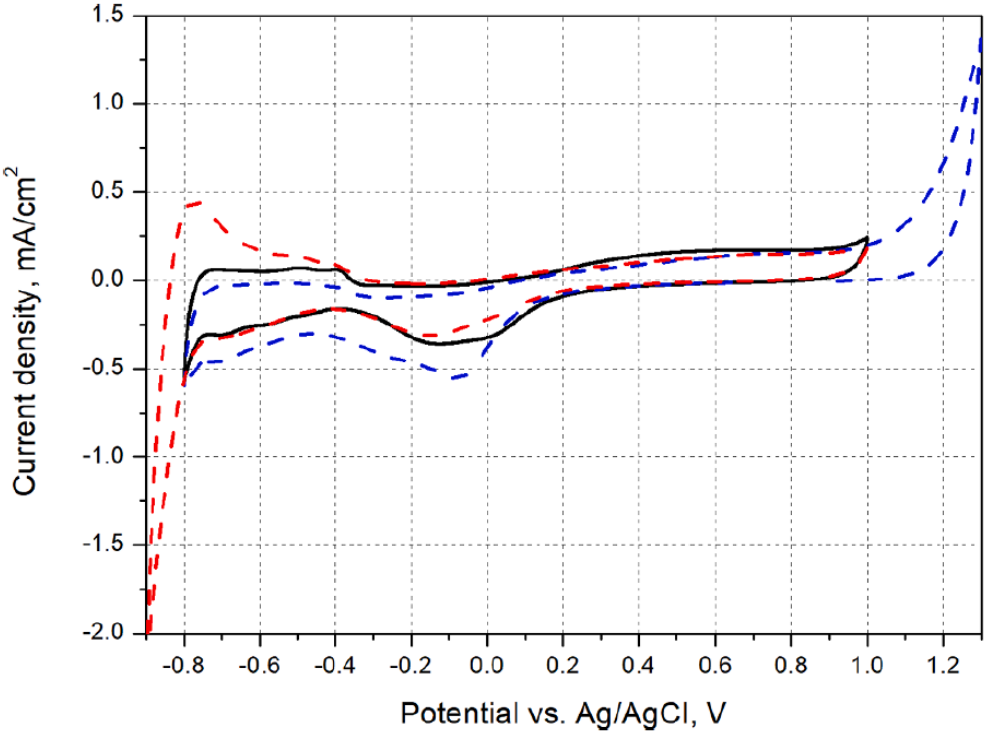

Figure 10: CV obtained for a Pt electrode at 100mV/s in PBS. The black line shows a test run within the water window, while the dashed blue line extends its range into the anodic direction, and the dashed red line extends its range into the cathodic direction. Adapted from [68]

NUMBER OF CYCLES

The number of cycles a CV test will have is a parameter that may seem trivial at first, but it should be tailored to each electrode type and test. When the CV test begins, not all of the electrode's surface features may be activated, resulting in a changing output through its cycles. This phenomenon can result in the output current lacking features (such as peaks from faradaic exchanges), showing a diminished response and charge storage capacity; or the total opposite, with reactions appearing only in the first cycles thus giving a false impression on the electrode's performance if they were used for the final characterization [69]. Figure 11 shows how a ZnO film has very different voltammograms between cycles one and twenty. The longer the exposure of the WE to an input voltage, the higher the chance that it will reach its steady-state response. This matters because, under clinical use, the prolonged stimulation and use of the electrode will drive its performance to a state close to its steady state. Yet, based on the properties of the electrode, it may reach such a state after a different number of cycles [29]. This is relevant because to characterize electrode properties (the presence of EC reactions, amount of charge stored), it should be done with the steady-state response. It is easy to determine when such a state is reached, as the response will stop drifting cycle after cycle as illustrated in Figure 12. This behaviour also implies that it is heavily recommended that the cycle used for data retrieval is one of the latest ones possible [10]. As long as no non-reversible reactions were happening (again, it is critical to first select an appropriate water window), later cycles display an electrode performance closer to its steady state. Moreover, choosing an appropriate number of cycles can also be done based on the purpose of the CV test. By choosing a small number of cycles, it is possible to study how fast a certain electrode falls into its steady-state response; while an optimum number of cycles would be meant to study the CV response of the electrode [29]. Understanding how fast an electrode reaches its steady state can be very useful for research purposes, as not only time can be saved, but excessive electrochemical stress due to additional cycles can be avoided. Alternatively, long-term tests where the electrode goes through more voltammetry cycles than needed to reach the steady state (e.g.: >1000 cycles) are also used to electrochemically stress the electrode to then study how prolonged performance affects it, akin to other ageing tests [9]. But as repeating cycles introduce stress, they may damage the electrode's integrity, affecting its performance and shifting its steady-state response away from what it was before the test.

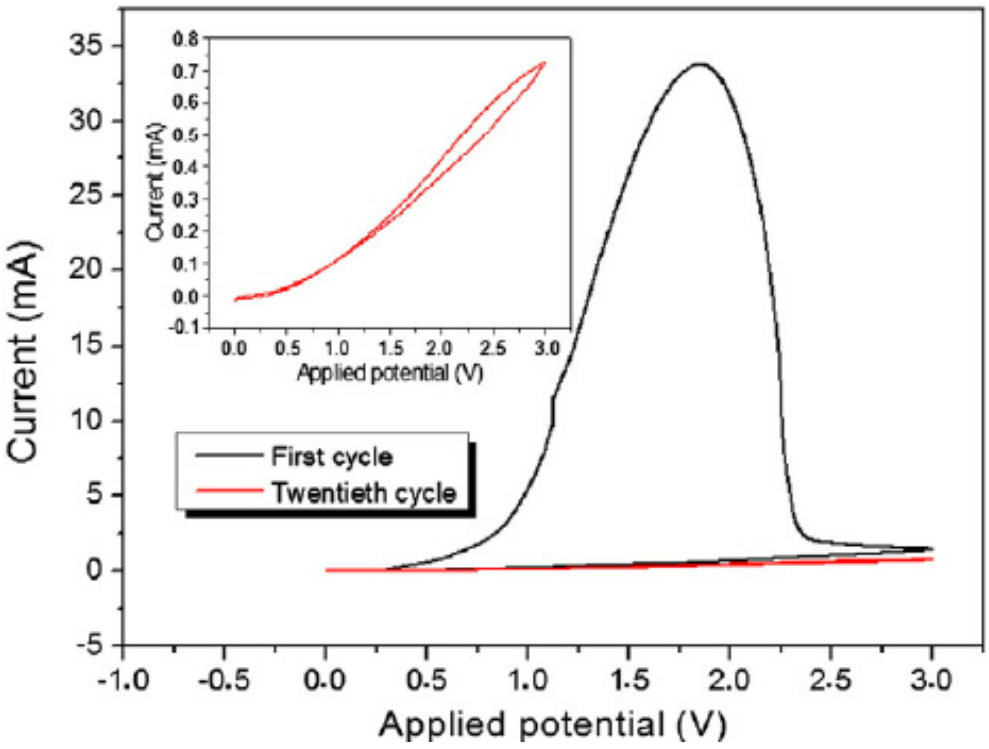

Figure 11: CV obtained for a ZnO film in K_2SO_4 (0.5 M) at 20mV/s. The voltammetry curve for the first obtained cycle is plotted in black, while for the twentieth cycle, it is plotted in red. Adapted from [69]

SWEEP RATE

Sweep rate is probably the parameter with the biggest impact on the measured response. It is directly proportional to the capacitive current response ($\delta v/\delta t$ in Equation 11) and it determines what features of the electrode's surface are recruited when testing for CV. Slower rates allow for finer structures to participate in the charge exchange process [9]- for instance, the grooves of jagged structures or smaller pores in a 3D porous interface. On the other hand, high rates will only recruit features that are more directly exposed to the reactant - such as the tip of a jagged structure, or the external layer of a 3D porous interface. This phenomenon can show changes in the performance of an electrode's CV of up to 2 orders of magnitude [9]. It is thus very relevant when it comes to comparing CV results, as the benefits in charge storage of fine structures can only appear at slower rates. Yet, these structures may only also play a role during stimulation to living tissue if the stimulation parameters also allow for their recruitment, such as a slow AC wave stimulation profile [10]. Only a few applications can benefit from this profile, such as EEG stimulation of slower cortical activity like Delta, Theta, and Alpha waves (Values can be found in Table 1) [70], and some specific Vagus Nerve applications [71]. That is why, to find some common ground, most efforts to review CV as an electrode characterization method report using average values from 50mV/s to 100mV/s [68]. It is encouraged that different sweep rates are used in testing and consequently reported to study the performance of the electrode as different surface features are recruited.

It is now clear why parameters in CV can have such a big impact on the final measurement: these three core parameters are all linked with each other at very fundamental electrochemical levels. If a reaction occurs, how big of a current response it can generate, and how much of the electrode participates in said reaction are all conditioned by the aforementioned parameters. Therefore there should be an effort to standardize the parameters to be able to compare results. Yet, they would still differ based on electrode material (different water windows), their surface modifications (different appropriate scan rates, different water windows), or the purpose behind the test (all parameters can change accordingly). Hence, when reading results from the literature, it is key to be aware of the test parameters they followed and their differential effect on the results measured.

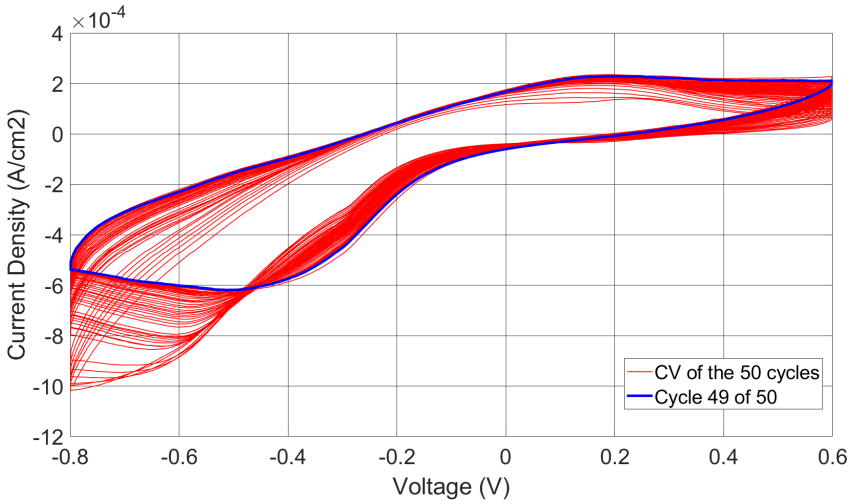

Figure 12: Full CV measurement for an Au electrode immersed in PBS, scanned at 50mV/s. The red line shows the whole 50 cycles, while the blue line remarks the second to last cycle, chosen for further analysis.

3.4 ADDITIONAL USES OF CV

CV has been used in additional experiments to reveal its full potential as an EC characterization tool. These efforts have revealed further properties of the test that have allowed us to understand additional uses of CV while also contextualizing its limitations.

ELECTROCHEMICAL STRESSING

CV, in contrast to VTs and especially EIS, is a technique that can apply a lot of stress to the electrode, as it demands continuous operation across the chosen safety window. Moreover, this stress grows proportionally with the number of cycles involved in the test. Such is the case that CV tests can be designed with this phenomenon in mind, and exploit it to test the reliability of manufactured electrodes before and after prolonged use [9]. Although it is not a substitute for long-term ageing tests, it can also provide information on the evolution of the electrode as it undergoes continuous operation [72, 73]. How well can it endure a certain operation window, and for how many cycles before it starts to show signs of stress (wear, warping, surface damages, surface depositions, changes in colour or finish), are aspects that can be tested for failure by prolonging a CV test. It is also worth mentioning its counter-effect: if the desire is to preserve an electrode as much as possible throughout testing, it should be a priority to determine the minimum number of cycles to reach the steady-state response without incurring excessive cycles.

VARYING SWEEP RATE AS A PREDICTOR FOR THE ELECTRODE-TISSUE INTERFACE

Further exploiting the relationship between ageing electrodes and CV, Cogan *et al.* came up with using fast sweeping rate CV tests as predictors for the evolving electrode-tissue interface [9]. When an electrode is implanted, it will always elicit a foreign body response in the host. This will lead to the encapsulation of the electrode with fibrotic tissue, isolating the electrode from its surroundings. As the electrode is encapsulated, it is more difficult for finer structures at the interface to be active during stimulation. Similarly, as the sweep rate is increased, finer structures cannot be recruited for the CV test. Thus, it has been found that running faster sweep rates can provide voltammogram curves similar to those obtained after exposure in vivo. Additionally, when running comparative tests at the same rate, but before and after implantation, different changes in the CV curve can be observed, illustrated in Figure 13. If testing with slow sweeping rates, electrolytes that may have leaked under the insulation layers will participate in the reaction, showing an increased curve area. On the other hand, if testing with fast sweeping rates, as the electrode becomes encapsulated by scar tissue, the main features of the electrode will have increased isolation, decreasing the curve area [9]. These results illustrate the intricate relationship between sweep rate, activation of finer structures, and electrode fibrotic encapsulation caused by the host's foreign-body response.

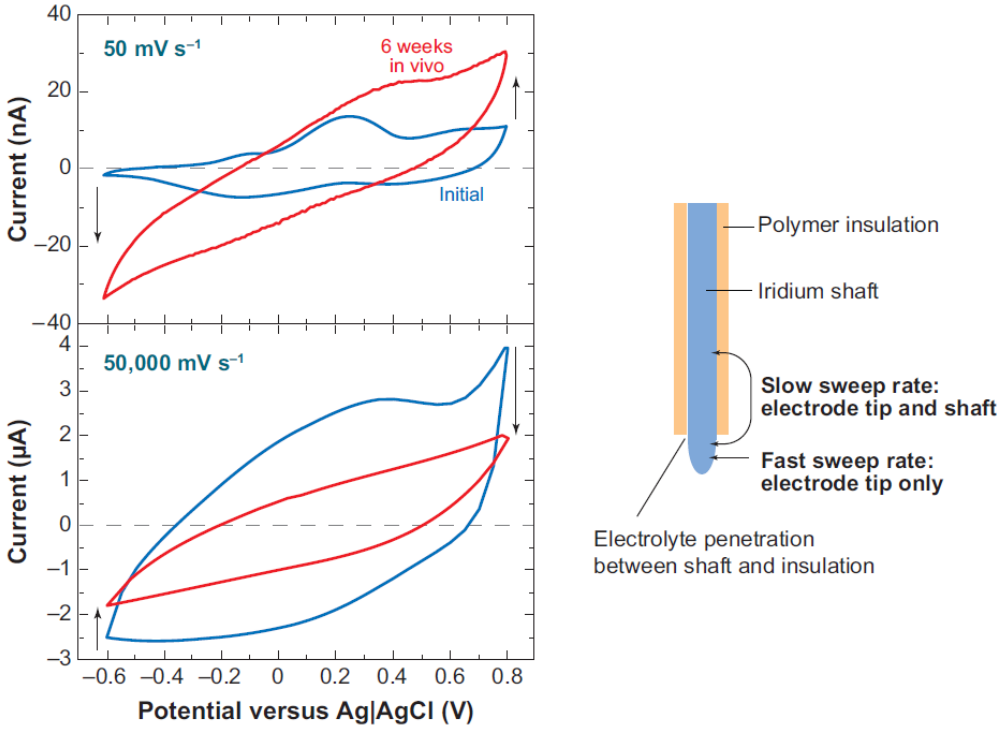

Figure 13: Comparison of CV curves obtained at different scan rates (50mV/s and 50,000mV/s) for an AIROF electrode after being implanted for a day and after 6 weeks in a cat's cortex. Adapted from [9].

3.5 ISSUES WITH CV

CSC AND ITS TRANSLATION TO TISSUE STIMULATION PERFORMANCE

Lastly, there has also been an effort to report that CSC can quickly become a misleading metric because it does not reflect the actual charge used during in vivo stimulation [68]. This occurs mainly because of the foreign body response encapsulation of the electrode and because the stimulation parameters used in vivo may not resemble at all those used in the CV test: it is of no use to test with slow sweep rates if the electrode will stimulate at higher injection rates. Moreover, in the case of intricate 3D interface geometries, it would be rare to have an electrode implanted and achieve a fully activated interface. Differences in medium composition can also play a role in enhancing or inhibiting non-reversible faradaic reactions that may or may not happen in vivo. This is why it is common for CSC estimations to be higher than the actual in vivo measurements that were taken [74].

3.6 CV OF AU ELECTRODES

Looking closer at the behaviour of Au electrodes in CV, there are some common aspects found in the literature that are worth mentioning. The first is the common Water Window versus an Ag|AgCl RE reported for Au electrodes. Each study selects its own window, but most commonly the range is within -0.6V ± 0.2V and 0.6V ±0.2V [9, 75–77]. Commonly, voltammograms of Au exhibit two regions within their water window with Faradaic reactions involved: the adsorption of O_2 occurs at 0.2V, most notably during the anodic sweep; and the adsorption and release of H^+ occurring between the -0.4V and -0.2V range [67]. Their CSC values average 0.53 mC/cm^2 [75–77].

4 VOLTAGE TRANSIENTS

Voltage Transients (VTs) are an EC measurement test where the voltage excursions of an electrode of interest are measured as we stimulate the electrode with a current pulse. VTs are used to determine the amount of charge an electrode can inject while operating within a certain voltage window. The challenge lies in maximizing the electrode's polarization while staying within the water window for safe, optimum electrical stimulation.

4.1 PERFORMING VTS

To perform the test, a 3 electrode setup and a current stimulator are needed. The current stimulator will send pulses over the WE|CE pair, while the output voltage is measured with the WE|RE pair. Pulse amplitude is increased with the test cycles until the maximum potential excursions are reached. These maximum potential excursions have for maximum value those of the water window edges. If the voltage excursion that reaches a water window limit occurs in the cathodic region of operation, it is named maximum cathodic potential excursion or E_{mc}. If the voltage excursion that reaches a water window limit occurs in the anodic region of operation, it is named maximum anodic potential excursion or E_{ma}. The current input that led to these maximum potential excursions is used to define the goal metric of VTs: charge injected per pulse Q_{inj}.

ELECTROCHEMICAL CONTRIBUTORS TO THE VT PULSE PROFILE

There are several independent contributors to the overall output measured voltage, and that play a role in different instances of the simulation pulse. As the pulse is initiated, there will be an immediate voltage response, associated with the resistive behavior of the electrode. This voltage drop is known as the Ohmic Voltage Drop, it is the main contributor to the access voltage (V_{acc}) and is defined as

$$V_{acc} = i_c R_i \tag{12}$$

where i_c is the current amplitude for the pulse, R_i is the resistance of the electrolyte, and V_a is defined as the near-immediate change in voltage at the onset of the pulse, or right after it ends. Following the immediate drop, time-dependent components begin to play a role, driving the electrode's polarization further. This behaviour can be either represented by individual components or simply as the electrode-electrolyte potential shift (ΔE_p), which will determine the maximum potential excursions (E_{mc}, E_{ma}) based on where the interpulse potential (E_{ipp}) was resting before stimulation. Individual components with a time dependency are the activation overpotential η_a, the concentration overpotential η_c, and the shift in the electrode's equilibrium potential ΔE_o). η_a refers to the drop in voltage necessary to maintain the current flow, provided by the redox reactions happening at the interface. η_c refers to the voltage drop caused by the chemical species concentration gradient that appears once redox reactions begin to occur: as it is an interface process, concentration values for each species change as they are closer or further away from the interface [9]. Putting everything together, the voltage transient can be defined as

$$\Delta V = i_c R_i + \eta_a + \eta_c + \Delta E_o \tag{13}$$

It is important to note that it is the result of time-dependent terms and others that are not, giving the voltage transient its characteristic profile. Yet, not all terms have the same time dependence: η_a and ΔE_o are the only contributors to the electrode-electrolyte interface polarization change over time, while η_c will not change throughout a pulse due to reaction kinetics and general quick pulse duration [9]. A voltage transient for a biphasic, cathodic-first pulse is illustrated in Figure 14. To analyze the actual charge injected in a cycle (Q_{inj}), ΔE_p is also considered to be the difference between the total voltage excursion, ΔV, and the access voltage V_{acc}. As such, E_{mc} could be determined following the equation

$$E_{mc} = E_{ipp} + \Delta E_{pc} = E_{ipp} + (\Delta V_c - V_{acc}) \tag{14}$$

$$E_{ma} = E_{ipp} + \Delta E_{pa} = E_{ipp} + (\Delta V_a - V_{acc}) \tag{15}$$

E_{ma} would be calculated in the same way, but using the ΔV of the anodic pulse instead.

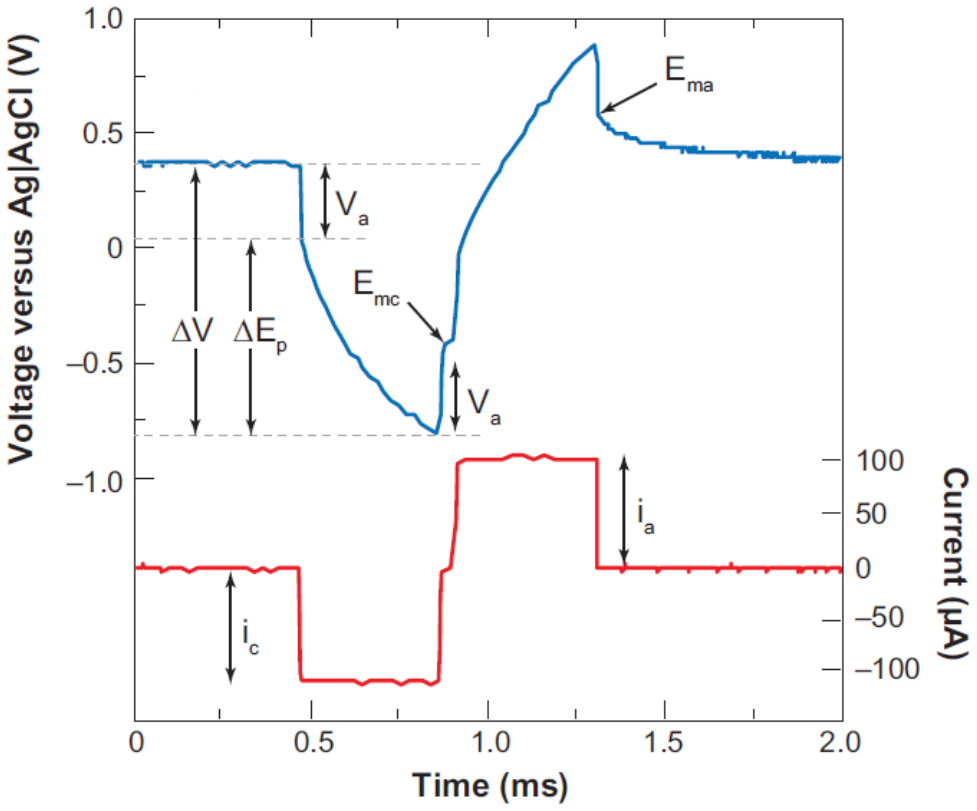

Figure 14: VT response of an AIROF electrode for a biphasic symmetric cathodic-first current pulse. Adapted from [9].

CHARGE BALANCED PULSES

In the context of neural stimulation, one of the main concerns with stimulation pulses is that they remain charge-balanced. This means that any processes caused by the charge injected in the first phase, are reversed by the second pulse or some other mechanism. Avoiding doing so may result in species accumulating pulse after pulse, making the electrode's VT drift and even causing damage to both tissue and electrode. The key to ensuring charge balancing is to avoid faradaic processes which may require different activation conditions in the second phase to be reversed, or may simply cause damage [78]. As faradaic processes depend on the chemical species present, they are conditioned by the electrode-electrolyte composition. Yet, the faradaic process of water hydrolysis (Equations 16 and 17) is common to all electrode types stimulating biological tissue and is known to cause irreversible damage in both tissue and electrode [10].

$$2H_2O \rightarrow O_2 + 4H^+ + 4e^- \tag{16}$$

$$2H_2O + 2e^- \rightarrow H_2 + 2OH^- \tag{17}$$

This is why, the voltages at which these reactions occur are generally considered as the maximum thresholds for safe charge injection. Hence, it is common practice to determine the maximum amount of safely injected charge (Q_{inj}) by increasing the current pulse amplitude until ΔE_p reaches the water window for that electrode. By normalizing the maximum safely injected charge with the electrode's area, we can define the electrode's Charge Injection Capacity (CIC), which is the maximum safely injectable charge per unit area.

MODES OF STIMULATION

Besides the previously mentioned biphasic pulse, there are other possible monophasic waveforms used in charge injection, capable of doing so in a charge-balanced manner. As monophasic waveforms cannot rely on a second phase to reverse the charge injected, researchers rely on other methods such as shorting to the return electrode, allowing the WE's potential to fall back to the RE's unchanged potential during quick pulsing [79, 80]; using capacitor-coupled pulsing, discharging the capacitor in the opposite direction [9]; or using

Table 4: Table containing stimulation parameters for stimulating certain specific neurons, cochlear auditory nerve stimulation, vagus nerve stimulation (VNS), and deep brain stimulation (DBS). STN stands for the Subthalamic Nucleus brain region. Data presented from Thompson *et al.*, 2021 is selected as the most common parameters used in the literature reported by the review article. All VNS and DBS protocols except those indicated, are in humans. Adapted from [84, 85, 87–93]

Neural Tissue under Pulse Stimulation	Duration (µs)	Frequency (Hz)	Author
Reticulospinal cell bodies of Rat	200	100	Hentall *et al.*, 1984
Midbrain of Rat	100	300	Yeomans *et al.*, 1982
Pyramidal Tract Bodies of Cat	200	NA	Stoney *et al.*, 1968
Pyramidal Tract Axons of Cat	200-300	NA	Shinoda *et al.*, 1976
Cochlear auditory nerve in Cat	25-50	33	Xu *et al.*, 1997
VNS in Animal Models	100	30	Thompson *et al.*, 2021
VNS for Epilepsy	500	30	Thompson *et al.*, 2021
VNS for Depression	500	30	Thompson *et al.*, 2021
VNS for Neuroplasticity and Rehabilitation	100	30	Thompson *et al.*, 2021
Transcutaneous auricular VNS	250	25	Thompson *et al.*, 2021
STN DBS for Movement Disorders	60	130	Koeglsperger *et al.*, 2019
DBS for Tremor Suppression	100	45-100	Kloster *et al.*, 2016
Subthalamic Nucleus DBS for Dystonia	100	130	Kloster *et al.*, 2016

biased monophasic waveforms, which requires a small net DC charge during the interpulse period to inject charge and restore the interpulse potential [81]. Still, biphasic stimulation seems to be the most extended technique to ensure optimum charge-balancing and it is thus preferred by researchers for both electrode characterization with voltage transients, or their following use in tissue stimulation. Additional considerations, such as coupling a capacitor to avoid net DC charge flow or implementing actively performing charge balancing with complementary circuits, are also implemented in biphasic pulsing to ensure a safe operation during stimulation.

4.2 KEY PARAMETERS IN VTS

To maximize the charge injected during a biphasic stimulation pulse, it is possible to tune several of the parameters defining the waveform: pulse duration, interpulse delay, frequency of stimulation, cathodic or anodic first, and pulse asymmetry.

PULSE DURATION

Pulse duration is directly proportional to the amount of charge transferred across the electrode-electrolyte interface. As ΔE_p is time-dependent, more time will equal to more charge injected. This implies that, due to the Chronaxie-Rheobase of neuron excitation, shorter pulse duration stimuli will require higher currents to deliver the same charge [10]. By using a longer pulse duration, nerve excitation can be reached with lower currents/voltages, at the expense of spending more time under the faradaic charge transfer state, increasing the chance of irreversible reactions taking place [82, 83]. It has become a standard during VT characterization to use a pulse duration of 200 µs, as it is usually the same time scale for stimulation protocols [10]. However it is worth noting that different electrode stimulation scenarios require different stimulation pulse duration, such as cochlear implant electrodes requiring on average pulses of 25 to 50 µs [84]. The most important factor regarding pulse duration protocol is that pulse duration should not exceed the chronaxie of the stimulated tissue. The necessary pulse duration values to activate different neural tissue types can be found in Table 4 [85, 86]

INTERPULSE DELAY

Incorporating an interpulse delay is a common practice for VTs, as it allows the potential excursion to fall back to a resting state in between pulses. As no current is delivered to the electrode, the Ohmic resistance component becomes null, and the actual potential of the electrode after the pulse can be read. It can be used to determine the access voltage Va, or the E_{mc}/E_{ma} to determine the final CIC of the electrode [9]. Most commonly, interpulse delays are set around 20µs.

FREQUENCY OF STIMULATION

The frequency of stimulation becomes relevant as a parameter in VTs because it must not lead to a new pulse before the electrode's potential is once again at the E_{ipp}. Most electrodes will require some time after the second phase to stabilize back to their interpulse potential, so the waveform frequency shall allow for this to prevent issues such as drifting outside of the potential window due to charge accumulation over time [9].

POLARITY OF THE FIRST PULSE

Regarding the polarity of the first pulse, VTs can be performed cathodic-first or anodic-first. It is more common to observe cathodic-first tests for two reasons: it is under cathodic behaviour that electrodes actually inject charge into the tissue, while in the anodic region, charge flows back into the electrode; and most stimulation protocols follow as well a cathodic-first approach. Still, some stimulation protocols actually require an anodic-first biphasic stimulation waveform [94–96]. Electrodes designed for such applications should be tested accordingly.

PULSE ASYMMETRY

Finally, one of the key parameters that can have a significant effect on the final CIC is pulse symmetry. Cogan *et al.* [32] showed how, by using asymmetric biphasic pulses, meaning a short, high-current first pulse, followed by a long, low-current second pulse, one could maximize the electrode's injected charge within their potential safety window. This is true because electrodes will usually reach one end of their water window extremes under symmetric pulsing, and by using asymmetric pulses it is possible to minimize the positive polarization of the electrode. In the case of cathodic-first protocols, this allows having a higher positive electrode bias, while a higher negative bias is also achieved in anodic-first protocols [9]. Although different electrode materials may find their optimal performance at different asymmetry ratios, ratios spanning from 1:4 to 1:16 seem to maximize CIC under experimental conditions [9, 31, 32, 97, 98].

4.3 REPORTING OF VT DATA

Voltage Transient results are mostly reported in literature through the maximum CIC obtained for an electrode. Sometimes, the maximum Q_{inj} is also reported separately. These results usually come with the corresponding plot of their VT, but what is not a widely spread practice is sharing values or methods for determining VT components, such as V_a, the water window used, or the offset voltage (V_{off}) of the electrode [10]. Although it is true that for characterization purposes, these values are secondary to the amount of charge injected, they are important for transparency and ensuring adequate testing. Additional parameters, such as those involved in the waveform's profile, are often shared.

4.4 ISSUES WITH VTS

Still, despite VTs being a necessary test for characterizing the stimulation capabilities of electrodes, it present many issues preventing research teams from carrying them out properly. These mainly concern the difficulty in acquiring adequate stimulators, calculating precisely V_a, and performing VT in vitro to determine CIC under living tissue conditions.

EQUIPMENT

The first challenge a team of researchers may face is acquiring a current stimulator capable of performing VT tests. The requirements of tuning the waveform throughout the test, performing with low noise levels for high impedance electrodes, and avoiding unnecessary corrections such as shorting in between pulses turn out to make current stimulators for electrode characterization more scarce than they should be. Current market applications shift to either traditional RF devices, requiring different magnitudes of scale and resolution; or current stimulators devised for living-tissue and neuron stimulation, which include built-in safety measures like shorting between pulses making the test electrode not behave as intended [99]. This means few "ready-to-go" solutions can perform VT tests in the market, much less if we look for a dedicated solution. Hence, it is common to find that when discussing the methods and materials discussed, research teams resort to self-built printed circuit boards (PCBs) to run VT tests. This situation is further evidenced by the fact that, as a response to the situation, there has been an effort by many groups to publish schematics of their current stimulator platforms designed for VT specifically [100]. There are even a few Open Source projects, as the need for a tailored solution for electrode characterization of VTs becomes a challenge common to the whole field [101]. Although by no means are these current stimulator PCBs complex, they still pose the first obstacle that needs

to be surpassed to run a VT test.

DETERMINING V_A

Determining V_a accurately remains a hot topic of debate. Access voltage is the near-immediate voltage shift as the current pulse is initiated or ends. It is directly related to the non-time-dependent terms such as the Ohmic resistance of the electrode, making it a constant potential contributor throughout the pulse. Thus, by determining its constant contribution, it can be subtracted from the transient, leaving only the changes in driving voltage over the pulse, which shall not exceed the safety window [10]. This is why, V_a is necessary to be able to accurately identify the amount of charge injected over time throughout the current pulse [9]. Still, factors such as stray-capacitance and current-pulse rising times play a role in V_a, making it difficult to identify it straightforwardly. Determining V_a is usually done through offline signal analysis (sometimes directly on an oscilloscope, sometimes through code), and there are two main methods to do so. The first way tries to determine V_a at the onset of the current pulse: in a cathodic-first biphasic pulse, the current onset leads to the immediate voltage drop that would be V_a (Equation 12). Alternatively, V_a / V_{mc} can also be measured right after the first pulse, as only interface potentials will remain when the current is 0 and there is no contribution from the Ohmic resistance. Still, both of these methods require having a sufficient temporal resolution to identify V_a accurately, while also relying either on manual identification or software detection [99]. On the other hand, it has been seen that for some electrodes like AIROF electrodes, V_a may differ in value when compared between the beginning of the pulse and at the end of it, especially for higher current amplitudes, as seen in Figure 15. Further recommendations on improved methods have been published, but there is still no consensus on the best method for identifying V_a [10].

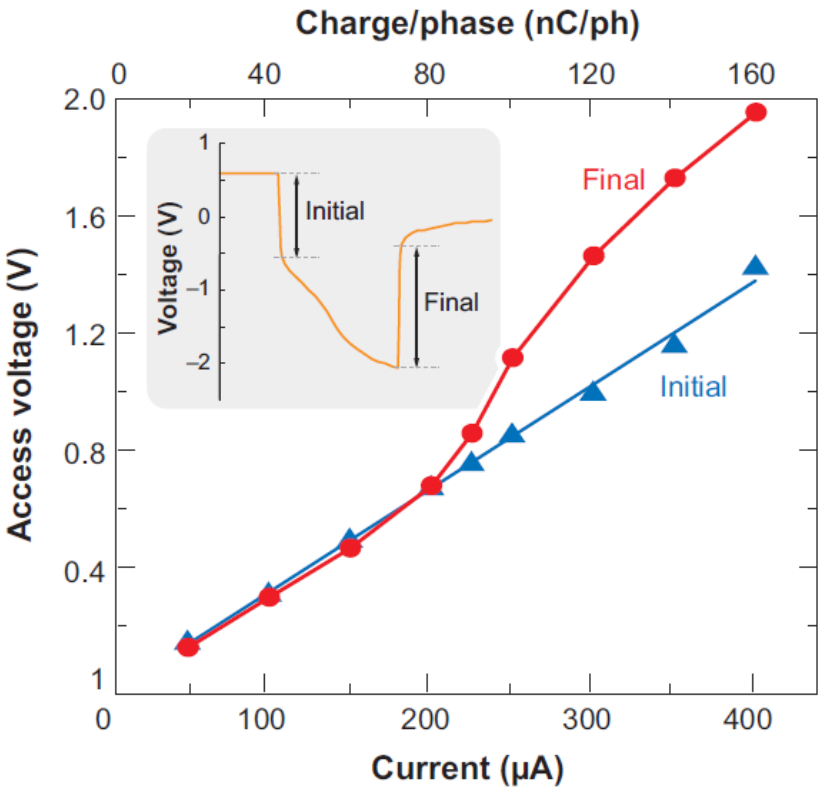

Figure 15: Comparison of V_a values in an AIROF's electrode VT measurement as current-pulse amplitude increases. Adapted from [9].

PERFORMING VTS IN VIVO

As the purpose of running VT experiments is to determine the stimulation capabilities of an electrode, there has always been a keen interest in studying both how the in vitro results translate to in vivo performance and how, if possible, could a VT test be performed directly in vivo. In general terms, due to the increase in diversity of chemical species, their limited availability, the inhomogeneity and anisotropy of the in vivo environment, and the adsorption of molecules to the electrode's surface, stimulation becomes more difficult in vivo than in

vitro. Results from Hu *et al.* seem to indicate that, while operating within the safety window determined in vitro, in vivo tissue would receive approximately four times less charge than measured in PBS [102]. Additionally, it seems that ΔE_p grows twice as large when in vivo [97]. Cogan *et al.* theorized that this may be due to the lack of available species in the medium to sustain the rate of reversible reactions, leading to the recruitment of new chemical species through irreversible reactions. There have been efforts to run VT tests with electrodes implanted in vivo, to accurately determine the safety thresholds on site. Special precautions need to be taken, as the risk of inducing damage through irreversible reactions is inherent to trying to find the maximum safe current-pulse amplitude. Commonly, the maximum Q_{inj} is determined in vitro, then evaluated again in vivo, only to find that it decreased [103]. Efforts revolve around incorporating adaptive algorithms that can not only safely determine the maximum Q_{inj} upon implantation, but also through time as the electrode is isolated as a consequence of the hosts' foreign body response [29, 45].

SETUP AND DESIGN FACTORS

VTs are affected by factors such as environmental temperature and electrode size. Of course, these parameters play a role in the previously mentioned characterization tests (EIS, CV), but they can heavily influence VT and CIC measurements. Cogan *et al.* estimated the temperature contribution to Q_{inj} to increase by nearly 20% when comparing in vitro results at 20°C against at 37°C. They attributed this effect to an observed decrease of the R_i through V_a. Electrode size also seems to play a critical role in CIC. It is known that the charge will distribute in a non-uniform manner across an electrode's surface, accumulating mostly on edges and avoiding the central areas of the surface or thicker segments of 3D-interface electrodes. As the general area decreases, the ratio of edge features to the overall surface increases, leading to a stronger influence of said features. Moreover, charge accumulating on the surface is necessary to inject said charge. This is why out of the three discussed ECM tests, VTs present such a strong effect with smaller electrodes [9]. Additionally, as CIC (mC/cm^{-2}) is a metric normalized by unit area, values for smaller electrodes benefit from this normalization. Figure 16 shows the quick increase in CIC of a SIROF electrode as electrode area is decreased.

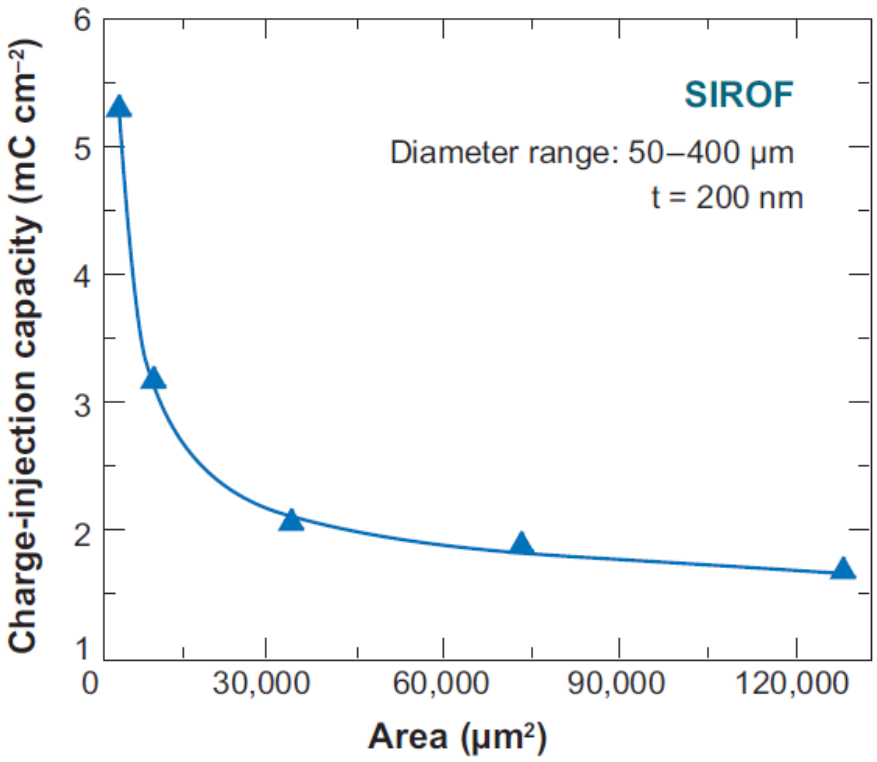

Figure 16: Study of the evolution of CIC of a SIROF electrode as the electrode area changes. Adapted from [9].

Table 5: Table collecting reported charge injection capacity values from the literature for Au electrodes. Adapted from [30, 37, 76, 77]

Electrode Description	CIC (mC/cm^2)	Author
Bare Au	0.4	Du *et al.*, 2015
80 µm diameter bare Au	0.2	Ganji *et al.*, 2017
Bare Au	0.5	Won *et al.*, 2018
Nanoporous Au	0.98	Kim *et al.*, 2015
Au nanoparticles on bare Au	2.56	Won *et al.*, 2018

4.5 VTs OF AU ELECTRODES

Reported tests of Voltage Transients under standard stimulation parameters for Au-based electrodes set their average CIC around 0.35 mC/cm^2 [30, 76, 77]. To improve its performance, it has also been studied how modifying the surface of these Au electrodes can increment their CIC, setting the average for them at 1.75 mC/cm^2 [30, 37]. All the values for these electrodes may be found in Table 5.

5 COMBINING TEST RESULTS FOR ADVANCED CHARACTERIZATION

Characterization of electrodes has been performed for decades following the previously explained EC tests. These tests yield isolated metrics that all reference back in one way or another to the same electrode, so recent research has looked into new ways that these metrics can be related to further our understanding of the electrode. Two examples of these combinations are using CSC and CIC as a ratio of one another to determine the performance of a stimulating electrode, and doing better estimations of CIC through the study of the electrode's impedance in EIS.

5.1 CSC/CIC RATIO

As both Cyclic Voltammetry and Voltage Transients are EC tests characterizing the simulation capabilities of an electrode, researchers have tried to find the relationship that these tests have with one another. Ganji *et al.* introduced a ratio between the CIC and CSC as one possible measure of this relationship [77]. By evaluating the relationship of the charge stored at the electrode's interface against how much of it can be safely injected, they were able to quantify the performance of the electrode under stimulation. To study this, they also evaluated the absolute power (P) consumed for a voltage transient biphasic pulse following

$$P = V * I \tag{18}$$

where V symbolizes the voltage output achieved and I the pulse's current amplitude. Results indicate a direct relationship between electrodes exhibiting higher CIC/CSC ratios (those with a better ability to convert the stored charge into injected charge) and those same electrodes having a better power/cycle relationship. This compound metric creates a new way of characterizing stimulating electrodes, especially for implants. Evaluating electrodes through their CIC/CSC ratio may indicate how an electrode that has huge CSC values will be a worse option over time than one with less storage capacity [77]. As researchers in literature often do not perform all characterization tests, or fall into quick comparisons of solely CIC or CSC values, it is difficult to accurately understand and predict the performance of the electrode. Hence, incorporating the CIC/CSC ratio as a common metric not only requires teams to perform complete characterization of the electrodes, but it enables more insightful comparisons that may relate to better implant electrodes'.

5.2 STUDYING ELECTRODE IMPEDANCE FROM BOTH RECORDING AND STIMULATION TESTS

Another compound metric that still has to be further explored is the relationship between electrode impedance, obtained through EIS, and its charge injection capabilities. Although EIS measures the electrode's impedance when recording signals from the medium, and Voltage Transients study the electrode's stimulating capabilities, they are both studying the same electrode's ability to transform signals from the electrical to the chemical domain and vice-versa. Studies like that of Lempka *et al.* have studied the evolution of EIS impedance after in vitro implantation, showing a steady increase caused due to the host's foreign body response [45]. Similarly, it

has been shown that the potential needed to inject in vivo the same charge as the Q_{inj} measured in vitro needs to be between 2 to 4 times as high [97, 102], and it does get worse over time as fibrotic tissue encapsulates the electrode. It would be very useful, especially in the context of electrodes used for both recording and stimulation, to look further into the relationship between the evolution of electrode-electrolyte impedance and its capacity to stimulate tissue. Even if measured through tests operating the electrode in opposite directions, they both refer to the same interface, and it can be modelled to fit its impedance behaviour. The isolated trends have been studied in the cited literature, and the relationship between lower impedance and a higher capability to inject charge safely has also been proven [104], but the exact evolution, model, and evolution of this model under in vivo conditions has yet to be tested. In the context of in vivo implantable electrodes, this would open the door to adaptable devices, capable of tuning their stimulation parameters to their environment (foreign body response), ensuring adequate neuron activation. Currently, to determine whether the maximum charge is injected, it may be necessary to run in vivo VTs, which can be harmful to the electrode and its surrounding tissue. By replacing this periodic test with EIS measurements instead of Voltage Transients, less harm is done to the patient, and electrode longevity is increased.

6 ISSUES IN STANDARDIZING ELECTROCHEMICAL CHARACTERIZATION OF ELECTRODES FOR NEURAL STIMULATION

Throughout the literature researched for this review, one additional issue became clear: there is a lack of consistency in how researchers carry out these experiments and in how they report their results. Tests are not carried out in the same way between two different teams, and full results may not even be shared properly. This all makes comparing electrode performance to reach a scientific consensus of what works best a very complex task. This is true to the point that there have even been efforts by other research teams to put out literature establishing standardized practices, recommended protocols, and discussing to which values should certain parameters adhere to [9, 10, 20]. Despite papers like these, it seems the issue is still going to be a part of the electrode EC characterization field, and two independent reasons will be presented: the dependence on specific hardware, and the complexity of parameter choice underlining electrochemical performance.

It is obvious that experiments require hardware equipment, and this should not necessarily be an impediment for research teams to carry out similar experiments. Yet, when it comes to electrode characterization, the need for highly precise galvanostats and potentiostats usually clashes with managing resources within the research team. If a machine is available to carry out a test, it will most likely be employed with little regard to whether it fulfils all the parameter criteria: not all instruments can reach the same ranges, or be as precise when delivering small current/voltage inputs. If the EIS is only able to be carried out from 10Hz onward, or a CV test may only have a minimum scan rate of 200mV/s, or the current stimulator is incapable of delivering asymmetric pulses, teams lacking resources may be willing to go forward. As some of these tests are used in fields different from electrode characterization, machines available may not have been designed with the appropriate ranges in mind, hindering the testing ability of the teams. Coupled with the fact that tests like Voltage Transients are commonly performed with PCBs designed in-house [99, 100], it is clear that there is a great degree of variability in the hardware that is used in electrode characterization. Efforts like creating open-source platforms for set-up instruments are appreciated, and as characterizing electrodes for Neural Interfaces becomes more urgent, better solutions for characterization enter the market.

While the previous issue may have a clear solution, dealing with adequate parameter selection and result reporting across the literature is more complex. It has been evidenced in this review that not only do EC tests contain a large number of tunable parameters, but they can greatly influence the results obtained [10, 29]. More so, one cannot simply extrapolate others' results with certain parameter settings to the parameter value of choice - e.g.: determining the equivalent CSC of an electrode at 50mV/s when it was obtained at 100mV/s. Relationships are not linear and depend on the precise electrochemistry happening at the electrode's interface. And as explained, many times even the figures of merit are not good enough to reflect the electrode's full behaviour. It is incredibly challenging to find reports of similar electrodes, tested in similar conditions, from two independent teams. Even simple things like the medium used in vitro, its concentration, and its preparation will change vastly. On top of all of this, the intricate relationship between parameters and how they should be tuned based on the purpose of the test makes it very easy for teams lacking expertise in characterization to have bad methods. For instance, CV tests may be carried out for only a few cycles, without allowing the electrode to reach its steady state. Literature with incomplete descriptions of testing methods can be easily found. Because characterization is only one more area to report on when developing a novel electrode, it can often be rushed or tweaked to fit expectations. All of this combined is at the core of why electrode charac-

terization remains an unstandardized field: it is easy to hide or miscommunicate the actual performance and potential clinical use of an electrode type behind sub-optimal figures of merit, wrong testing parameters, and incomplete testing. Characterization is only truly useful when it can provide readers with information that is comparable to the rest of the field and translatable to real-life use.

Providing a solution to this issue is beyond the point of this review. But it is worth bringing up that it has been recognized and the whole community is trying to create standardized testing guidelines that are accessible and useful. Boehler *et al.* summarize their whole review with info-graphics containing all the essential steps and parameter selection needed to carry out electrode characterization from beginning to end (Figure 17)[10]. It is to the benefit of the whole field that more and more groups follow standard guidelines for both testing and reporting results.

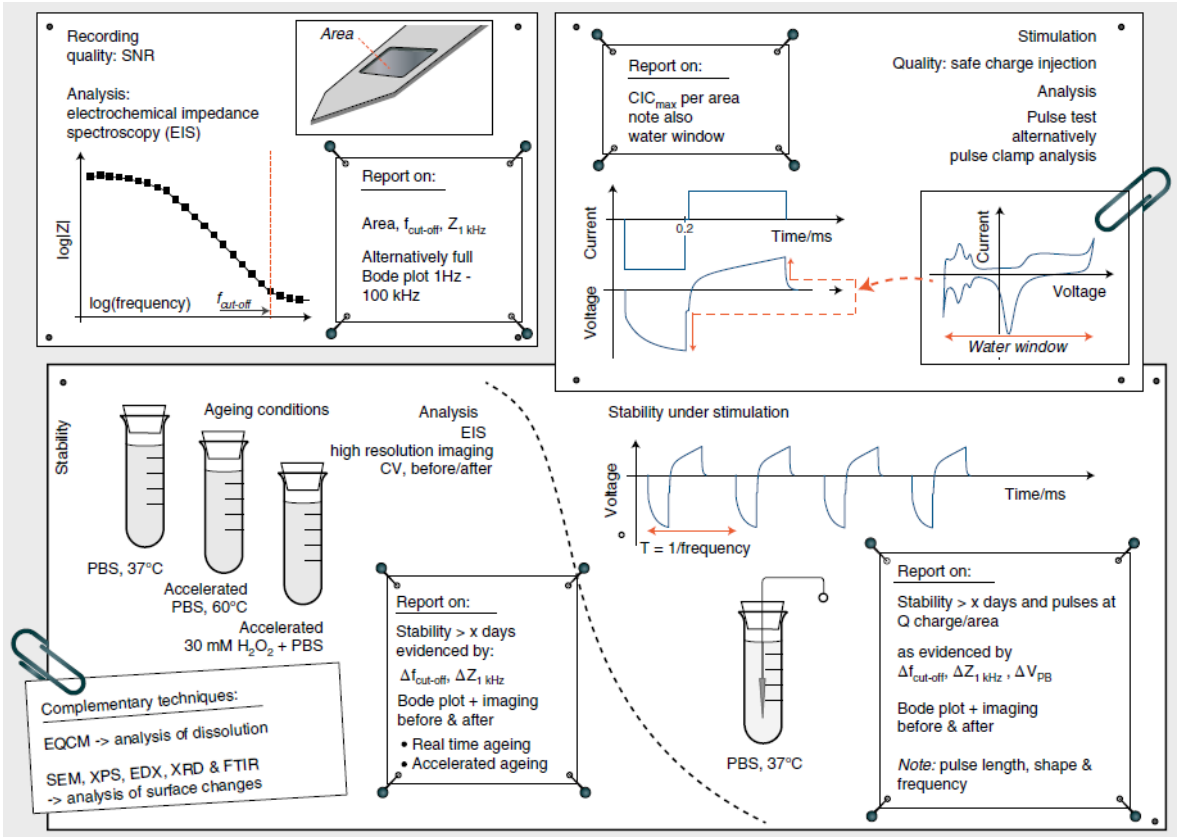

Figure 17: Info-graphic illustrating how to carry out good practices when characterizing both recording and stimulating electrodes. Additional tests are also indicated in the lower section. Adapted from [10].

BIBLIOGRAPHY

[1] C. Ding, Y. Wu, *et al.*, "Global, regional, and national burden and attributable risk factors of neurological disorders: The global burden of disease study 1990–2019," *Frontiers in Public Health*, 2022.

[2] J. Dumurgier and C. Tzourio, "Epidemiology of neurological diseases in older adults," *Revue Neurologique*, 2022.

[3] P. Ortinski and K. J. Meador, "Cognitive side effects of antiepileptic drugs," *Eplisepsy Behaviour 5*, 2003.

[4] R. Makins and A. Ballinger, "Gastrointestinal side effects of drugs," *Expert Opinion on Drug Safety*, 2003.

[5] I. L. Michael Kuhn *et al.*, "The sider database of drugs and side effects," *Nucleic Acids Research*, 2015.

[6] S. Reardon, "Electroceuticals spark interest," *Nature*, 2014.

[7] S. Mishra, "Electroceuticals in medicine – the brave new future," *Indian Heart Journal*, 2017.

[8] A. Majid, *Electroceuticals - Advances in Electrostimulation Therapies*. Springer International Publishing, 2017.

[9] S. F. Cogan, "Neural stimulation and recording electrodes," *Annual Review Biomedical Engineering*, 2008.

[10] C. Boehler *et al.*, "Tutorial: guidelines for standardized performance tests for electrodes intended for neural interfaces and bioelectronics," *Nature Protocols*, 2022.

[11] G. Yao *et al.*, "Flexible bioelectronics for physiological signals sensing and disease treatment," *Journal of Materiomics*, 2020.

[12] FocusedUltrasoundFoundation, "State of the field report 2022," 2022.

[13] J. P. Donoghue, "Connecting cortex to machines: recent advances in brain interfaces," *Nature Neuroscience*, 2002.

[14] B. P. Bean, "The action potential in mammalian central neurons," *Nature Reviews Neuroscience*, 2017.

[15] I. Chen *et al.*, "Neuroanatomy, neuron action potential," *StatPearls*, 2019.

[16] V. Giagka, "Bioelectricity lecture notes," 2022.

[17] M. Zhang *et al.*, "Electronic neural interfaces," *Nature Electronics*, 2020.

[18] V. S. Polikov *et al.*, "Response of brain tissue to chronically implanted neural electrodes," *Journal of Neuroscience Methods*, 2005.

[19] W. Serdjin, V. Giagka, *et al.*, "Active implantable biomedical devices lecture notes," 2022.

[20] G. Schiavone *et al.*, "Guidelines to study and develop soft electrode systems for neural stimulation," *Neuron*, 2020.

[21] T. D. Y. Kozai, "The history and horizons of microscale neural interfaces," *Micromachines*, 2018.

[22] Neuronexus, "A Brief history of Electrode Technology," May 2021.

[23] J. L. C. Jr. and H. S. White, "Electrochemical characterization of electrodes with submicrometer dimensions," *Analytical Chemistry*, 2000.

[24] T. Hepel and J. Osteryoung, "Electrochemical characterization of electrodes with submicrometer dimensions," *Journal of the Electrochemical Society*, 1986.

[25] J. Niedziolka *et al.*, "Characterisation of gold electrodes modified with methyltrimethoxysilane and (3-mercaptopropyl) trimethoxysilane sol–gel processed films," *Journal of Electroanalytical Chemistry*, 2005.

[26] M. Kullapere *et al.*, "Surface modification of gold electrodes with anthraquinone diazonium cations," *Electrochemistry Communications*, 2009.

[27] E. M. Pinto *et al.*, "Electrochemical and surface characterization of carbon-film-coated piezoelectric quartz crystals," *Applied Surface Science*, 2009.

[28] C. E. Larson and E. Meng, "A review for the peripheral nerve interface designer," *Journal of Neuroscience Methods*, 2020.

[29] N. Elgrishi *et al.*, "A practical beginner's guide to cyclic voltammetry," *Journal of Chemical Education*, 2018.

[30] S. M. Won *et al.*, "Recent advances in materials, devices, and systems for neural interfaces," *Advanced Materials*, 2018.

[31] S. F. Cogan *et al.*, "The influence of electrolyte composition on the in vitro charge-injection limits of activated iridium oxide (airof) stimulation electrodes," *Journal of Neural Engineering*, 2007.

[32] S. F. Cogan *et al.*, "Potential-biased, asymmetric waveforms for charge-injection with activated iridium oxide (airof) neural stimulation electrodes," *IEEE*, 2006.

[33] B. Fan, B. Wolfrum, *et al.*, "Impedance scaling for gold and platinum microelectrodes," *Journal of Neural Engineering*, 2021.

[34] W. Franks *et al.*, "Impedance characterization and modeling of electrodes for biomedical applications," *IEEE Transactions on Biomedical Engineering*, 2005.

[35] V. Woods, "Long-term recording reliability of liquid crystal polymer μecog arrays," *Journal of Neural Engineering*, 2018.

[36] Y. Lu *et al.*, "Flexible neural electrode array based-on porous graphene for cortical microstimulation and sensing," *Scientific Reports*, 2016.

[37] Y. H. Kim *et al.*, "In vitro extracellular recording and stimulation performance of nanoporous gold-modified multi-electrode arrays," *Journal of Neural Engineering*, 2015.

[38] G. H. Kim *et al.*, "Cnt-au nanocomposite deposition on gold microelectrodes for improved neural recordings," *Sensors and Actuators B: Chemical*, 2017.

[39] M. E. Orazem, "University of Florida Lecture: Electrochemical Impedance Spectroscopy," 2018.

[40] C. M. Brett, "Electrochemical impedance spectroscopy in the characterisation and application of modified electrodes for electrochemical sensors and biosensors," *Molecules*, 2022.

[41] G. D. Dario Delgado, "Forum Discussion: What is the difference between Ohm and Ohm cm 2 In electrochemical Impedance (EIS) analysis of raw data?," 2015.

[42] B.-A. Mei *et al.*, "Physical interpretations of nyquist plots for edlc electrodes and devices," *Journal of Physical Chemistry*, 2018.

[43] F. Ciucci, "Modeling electrochemical impedance spectroscopy," *Current Opinion in Electrochemistry*, 2019.

[44] T. K. Zoltán Lukács, "A generalized model of the equivalent circuits in the electrochemical impedance spectroscopy," *Electrochimica Acta*, 2020.

[45] S. F. Lempka *et al.*, "In vivo impedance spectroscopy of deep brain stimulation electrodes," *Journal of Neural Engineering*, 2009.

[46] A. Lasia, *Modern Aspects of Electrochemistry n32*, ch. Electrochemical Impedance Spectroscopy and its Applications, p. 435. 2002.

[47] M. J. Barsoukov E, *Impedance Spectroscopy Theory, Experiment, and Applications, 2nd Edition.* Wiley-Interscience, 2005.

[48] D. D. Macdonald, "Reflections on the history of electrochemical impedance spectroscopy," *Electrochimica Acta*, 2006.

[49] K. Krukiewicz, "Electrochemical impedance spectroscopy as a versatile tool for the characterization of neural tissue: A mini review," *Electrochemistry Communications*, 2020.

[50] D. M. Simon *et al.*, "Design and demonstration of an intracortical probe technology with tunable modulus," *Society for Biomaterials*, 2016.

[51] M. M. Straka *et al.*, "Characterizing longitudinal changes in the impedance spectra of in-vivo peripheral nerve electrodes," *Micromachines*, 2018.

[52] ZurichInstruments, "Hands-on Electrochemical Impedance Spectroscopy (EIS) | Zurich Instruments Webinar," July 2022.

[53] G. Buzsáki, *Rhythms of the Brain*. Oxford University Press, 2006.

[54] P. Berens *et al.*, "Feature selectivity of the gamma-band of the local field potential in primate primary visual cortex," *Frontiers in Neuroscience*, 2008.

[55] C.-C. Huang *et al.*, "Front-end amplifier of low-noise and tunable bw/gain for portable biomedical signal acquisition," *International Symposium on Circuits and Systems*, 2008.

[56] K. D. Harris *et al.*, "Improving data quality in neuronal population recordings," *Nature Neuroscience*, 2016.

[57] J. P. Neto *et al.*, "Does impedance matter when recording spikes with polytrodes?," *Frontiers in Neuroscience*, 2018.

[58] E. Seker *et al.*, "The fabrication of low-impedance nanoporous gold multiple-electrode arrays for neural electrophysiology studies," *Nanotechnology*, 2010.

[59] M. Gryszel *et al.*, "High-capacitance nanoporous noble metal thin films via reduction of sputtered metal oxides," *Advanced Material Interfaces*, 2022.

[60] X. Cui and D. C. Martin, "Fuzzy gold electrodes for lowering impedance and improving adhesion with electrodeposited conducting polymer films," *Sensors and Actuators A*, 2002.

[61] H.-B. Zhou, G. Li, X.-N. Sun, Z.-H. Zhu, Q.-H. Jin, J.-L. Zhao, and Q.-S. Ren, "Integration of au nanorods with flexible thin-film microelectrode arrays for improved neural interfaces," *Journal of Microelectromechanical Systems*, 2009.

[62] Z. C *et al.*, "Implantable electrode array with platinum black coating for brain stimulation in fish," *Microsystem Technologies*, 2015.

[63] D. M. Simon, H. Charkhkar, *et al.*, "Design and demonstration of an intracortical probe technology with tunable modulus," *Society for Biomaterials*, 2016.

[64] S. Chen, W. Pei, *et al.*, "Pedot/mwcnt composite film coated microelectrode arrays for neural interface improvement," *Sensors and Actuators A*, 2013.

[65] W. Lee, D. Kim, *et al.*, "Transparent, conformable, active multielectrode array using organic electrochemical transistors," *PNAS*, 2017.

[66] A. Weremfo *et al.*, "Investigating the interfacial properties of electrochemically roughened platinum electrodes for neural stimulation," *American Chemical Society*, 2015.

[67] J. P. Hoare, "A cyclic voltammetric study of the gold-oxygen system," *The Electrochemical Society*, 1984.

[68] K. K. Justyna Lipus, "Challenges and limitations of using charge storage capacity to assess capacitance of biomedical electrodes," *Measurement*, 2022.

[69] A. Achour *et al.*, "Nanostructuration and band gap emission enhancement of zno film via electrochemical anodization," *Thin Solid Films*, 2014.

[70] M. B. Davide Reato, Asif Rahman and L. C. Parra, "Effects of weak transcranial alternating current stimulation on brain activity—a review of known mechanisms from animal studies," *Frontiers in Human Neuroscience*, 2013.

[71] A. Sukasem *et al.*, "The effects of low-and high-frequency non-invasive transcutaneous auricular vagal nerve stimulation (tavns) on gastric slow waves evaluated using in vivo high-resolution mapping in porcine," *Neurogastroenterology and Motility*, 2020.

[72] R. Sharma and S. M. Andersen, "Quantification on degradation mechanisms of polymer electrolyte membrane fuel cell catalyst layers during an accelerated stress test," *ACS Catalysis*, 2018.

[73] R. Chattot *et al.*, "Beware of cyclic voltammetry! measurement artifact in accelerated stress test of fuel cell cathode revealed by operando x-ray diffraction," *Journal of Power Sources*, 2023.

[74] E. M. Hudak *et al.*, "Electron transfer processes occurring on platinum neural stimulating electrodes: calculated charge-storage capacities are inaccessible during applied stimulation," *Journal of Neural Engineering*, 2017.

[75] Z. He *et al.*, "Fabrication of iridium oxide neural electrodes at the wafer level," *Science China - Technology Science*, 2016.

[76] Z. J. Du *et al.*, "Poly(3,4-ethylenedioxythiophene)-ionic liquid coating improves neural recording and stimulation functionality of meas," *Royal Society of Chemistry*, 2015.

[77] M. Ganji *et al.*, "Scaling effects on the electrochemical stimulation performance of au, pt, and pedot:pss electrocorticography arrays," *Advanced Functional Materials*, 2017.

[78] S. Brummer and M. Turner, "Electrical stimulation of the nervous system: The principle of safe charge injection with noble metal electrodes," *Bioelectrochemistry and Bioenergetics*, 1975.

[79] N. Donaldson and P. Donaldson, "When are actively balanced biphasic ('lilly') stimulating pulses necessary in a neurological prosthesis? i," *Medical and Biological Engineering and Computing*, 1986.

[80] N. Donaldson and P. Donaldson, "When are actively balanced biphasic ('lilly') stimulating pulses necessary in a neurological prosthesis? ii," *Medical and Biological Engineering and Computing*, 1986.

[81] X. Beebe and T. Rose, "Charge injection limits of activated iridium oxide electrodes with 0.2 ms pulses in bicarbonate buffered saline (neurological stimulation application)," *IEEE Transactions on Biomedical Engineering*, 1988.

[82] T. Rose and L. Robblee, "Electrical stimulation with pt electrodes. viii. electrochemically safe charge injection limits with 0.2 ms pulses (neuronal application)," *IEEE*, 1990.

[83] I. C. Stefan *et al.*, "Theoretical analysis of the pulse-clamp method as applied to neural stimulating electrodes," *Journal of the Electrochemical Society*, 2001.

[84] J. Xu *et al.*, "Chronic electrical stimulation of the auditory nerve at high stimulus rates: a physiological and histopathological study," *Hearing Research*, 1997.

[85] E. J. Tehovnik, "Electrical stimulation of neural tissue to evoke behavioral responses," *Journal of Neuroscience Methods*, 1995.

[86] J. B. Ranck, "Which elements are excited in electrical stimulation of mammalian central nervous system: A review," *Brain Research*, 1975.

[87] S. Stoney, W. Thompson, and H. Asanuma, "Excitation of pyramidal tract cells by intracortical microstimulation: Effective extent of stimulating current," *Journal of Neurophisiology*, 1968.

[88] Y. Shinoda, A. Arnold, and H. Asanuma, "Spinal branching of corticospinal axons in the cat," *Experimental Brain Research*, 1976.

[89] I. D. Hentall *et al.*, "Relations among threshold, spike height, electrode distance, conduction velocity in electrical certain medullospinal neurons," *Journal of Neurophisiology*, 1984.

[90] J. S. Yeomans, R. Pearce, and D. Wen, "Mapping midbrain sites for circling using current-frequency trade off data," *Phisiology and Behaviour*, 1982.

[91] S. L. Thompson *et al.*, "A review of parameter settings for invasive and non-invasive vagus nerve stimulation (vns) applied in neurological and psychiatric disorders," *Frontiers in Neurscience*, 2021.

[92] T. Koeglsperger *et al.*, "Deep brain stimulation programming for movement disorders: Current concepts and evidence-based strategies," *Frontiers in Neuroscience*, 2019.

[93] D. Klooster *et al.*, "Technical aspects of neurostimulation: Focus on equipment, electric field modeling, and stimulation protocols," *Neuroscience and Biobehavioral Reviews*, 2016.

[94] D. N. Anderson *et al.*, "Anodic stimulation misunderstood: preferential activation of fiber orientations with anodic waveforms in deep brain stimulation," *Journal of Neural Engineering*, 2019.

[95] C. C. McIntyre and W. M. Grill, "Extracellular stimulation of central neurons: Influence of stimulus waveform and frequency on neuronal output," *Journal of Neurophisiology*, 2002.

[96] E. J. Tehovnik and W. M. Slocum, "Depth-dependent detection of microampere currents delivered to monkey v1," *European Journal of Neuroscience*, 2009.

[97] S. Cogan, "In vitro and in vivo differences in the charge-injection and electrochemical properties of iridium oxide electrodes," *IEEE TRANSACTIONS ON BIOMEDICAL ENGINEERING*, 2006.

[98] J. K. Andreas Weltin, "Electrochemical methods for neural interface electrodes," *Journal of Neural Engineering*, 2021.

[99] A. Cisnal, J.-C. Fraile, *et al.*, "A measurement setup and automated calculation method to determine the charge injection capacity of implantable microelectrodes," *Sensors*.

[100] S. Mottaghi *et al.*, "Modular current stimulation system for pre-clinical studies," *Frontiers in Neuroscience*, 2020.

[101] J. S. Nathan Cermak, Matthew A. Wilson and J. P. Newman, "Stimjim: open source hardware for precise electrical stimulation," *bioRxiv*, 2019.

[102] Z. Hu *et al.*, "In vitro and in vivo charge capacity of airof microelectrodes.," *IEEE TRANSACTIONS ON BIOMEDICAL ENGINEERING*, 2006.

[103] R. T. Leung *et al.*, "In vivo and in vitro comparison of the charge injection capacity of platinum macroelectrodes," *IEEE TRANSACTIONS ON BIOMEDICAL ENGINEERING*, 2014.

[104] A. S. Pranti *et al.*, "Pedot: Pss coating on gold microelectrodes with excellent stability and high charge injection capacity for chronic neural interfaces," *Sensors and Actuators B: Chemical*, 2018.

B Appendix: Code

All code files, can be accessed in the following DOI: https://doi.org/10.34894/HK1GND

Code block B.1 - Matlab Code used to plot EIS data from the ModuLab XM+ as both Bode and Nyquist plots, averaging several signals and plotting their average EIS too (as bode plots). The code also includes data from researched literature to compare the electrode´s performance. Finally, it also determines and prints the corresponding metrics: Z @ 1 kHz, and f_{cutoff} for both the single data entries and the averaged-out entries.

Code Block B.1: EIS plotting.m - Analyzing and plotting EIS data

Code block B.2 - Matlab Code adapted from smusall, that creates a shaded area corresponding to the standard deviation of an averaged curve.

Code Block B.2: stdshadelog.m - Shading of standard deviation of a curve

Code block B.3 - Matlab Code used to plot CV data from the ModuLab XM+, and with logic implemented to show determined cycles within the whole voltammogram. Using the function CV_cycle_variation.m, it can determine when the CV is at a stable cycle and uses said cycle for the computation of metrics such as CSC and CSC_{cath}. It exports the whole data matrix as an Excel file for more accessible storage.

Code Block B.3: CV Plotting.m - Analyze and plot CV data

Code block B.4 - Matlab Code used to determine when a cycle in a CV measurement is approaching stability. It uses both numeric criteria to assess the relative difference between consecutive maxima and minima, in addition to a logic piece that checks whether the CV curve is approaching a point where the overall trend (increasing/decreasing current density cycle after cycle) reverses.

Code Block B.4: CV_cycle_variation.m - Detect the stable cycle in a CV scan according to a set of criteria

Code block B.5 - Python code used to operate the AFG from the Tektronix MDO34 oscilloscope, which is then connected to our VCCS PCB to send biphasic current pulses over the electrode pair. Pulse parameters can be tweaked in code, and the prompts guide the user when deciding whether to export and save the data file or not.

Code Block B.5: VT Acquisition.py - Operate the Tektronix MDO34 Oscilloscope while connected to the VCCS PCB to perform VTs

Code block B.6 - Matlab code used to plot VT data extracted from the Tektronix MDO34 Oscilloscope. Time data is plotted, and using the headers in the data file, it calculates the CIC metric.

Code Block B.6: VT Plotting.m - Analyze and plot VT data

Code block B.7 - Matlab code used to plot the noise spectrum power density used in the noise characterisation of the samples. It imports data from the instrument's noise measurements too, to determine the final noise sample contribution. Additionally, thanks to the function noisemeasure.m, it also computes other noise-related metrics, such as V_{RMS}.

Code Block B.7: Noise Characterization Plotting.m - Analyze and plot Noise characterization data

Code block B.8 - Matlab function of H. Zhivomirov, capable of outputting the PSD of a time signal. He includes additional code to perform signal weighting (A and C weights), but these steps are meant for auditory purposes. The code is adapted to the needs of electrode characterization.

Code Block B.8: noisemeasure.m - Function by H. Zhivomirov to compute the PSD of a time signal

Code block B.9 - Matlab code used to create the transfer function for the Test Cell model used for calibration of the Modulab XM+, to further check that the LT Spice model simulation was done correctly.

Code Block B.9: TestCellModel.m - Recreate the transfer function of the Test Cell model

C Appendix: Characterization Platform Infrastructure

Figure C.1: Status of the Electrode Characterization setup before the work done in this thesis.

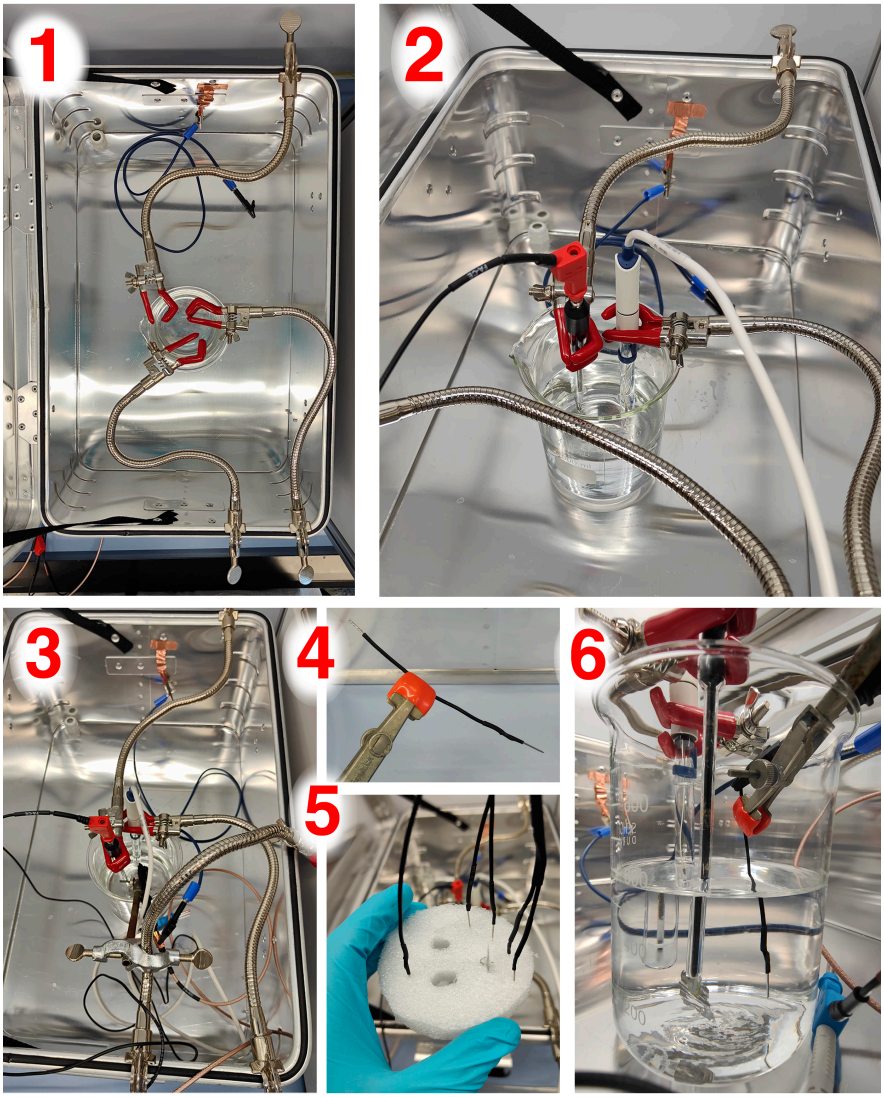

Figure C.1: Images of the previous setup used to characterize electrode samples at TBE. In numerical order: **1** - To hold the electrodes, metal grippers need to be fixed by screwing to the sides of a metal crate (limiting its capabilities as a Faraday cage). They are difficult to place in the same position between tests. **2** - The RE and CE being held in place. **3** - Top view of the three electrodes being held over the PBS beaker. It can quickly become complex and tedious to sort and fix clamps, electrodes and cabling. **4** - Holding the WE can be particularly challenging for thin, wire-like electrodes. **5** - An alternative method was using a cut-out foam piece to hold samples in place, similar in concept to the later 3-electrode holder that was designed in this thesis, **6** - Close-up shot of the three electrodes immersed in PBS. Having them in an optimal and repeatable position was not feasible due to the difficulty of setting the clamps with the required precision. Regardless, setting up could take up to 75 minutes.

Figure C.2 and C.3: Electrode Characterization setup equipment common to all tests

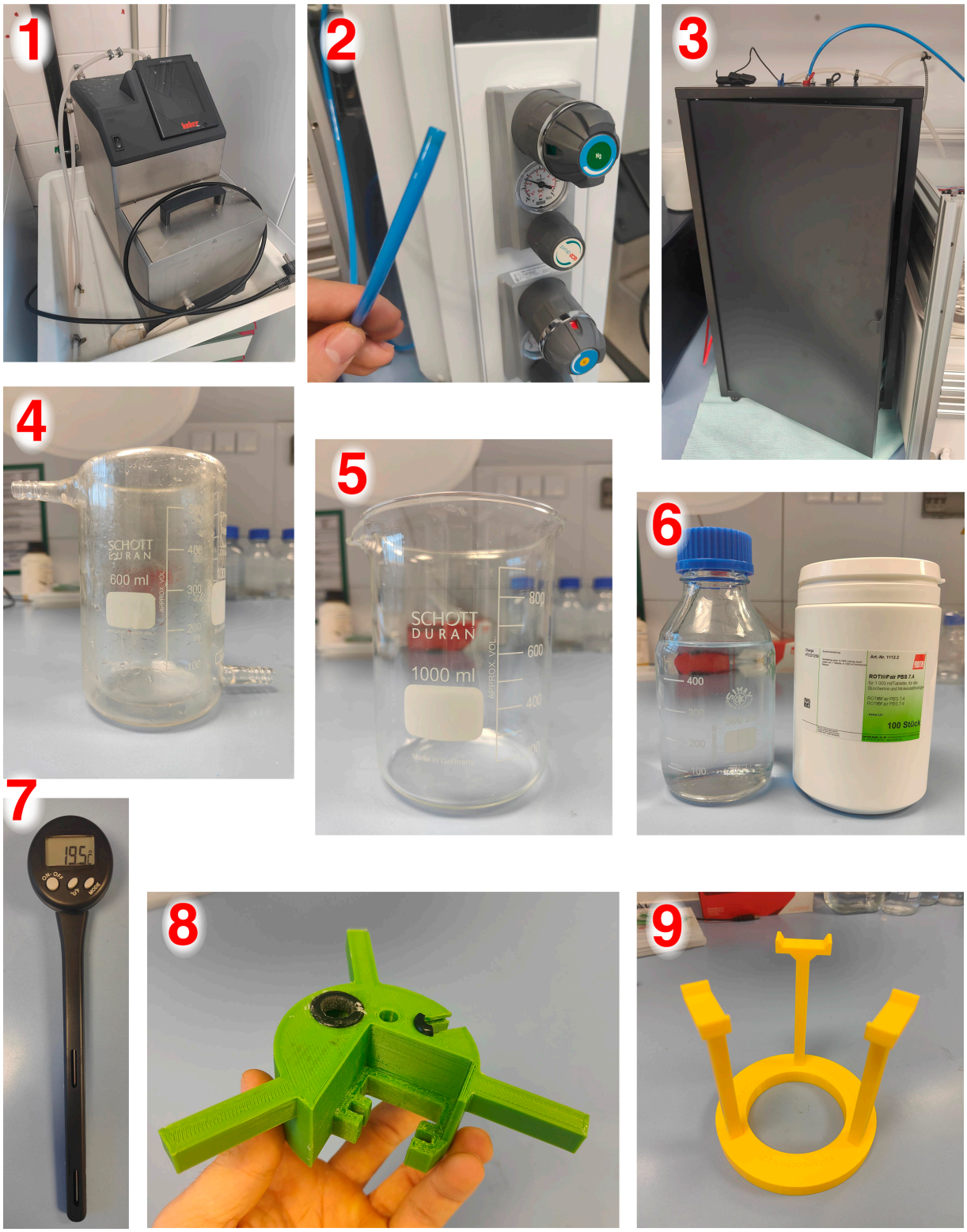

Figure C.2: Equipment items needed for all types of Electrode Characterization Testing 1. In numerical order:**1** - Thermostat, **2** - N_2 Gas Probe, **3** - Faraday Cage, **4** - Double Glass Walled Beaker, **5** - 1L Glass Beaker, **6** - PBS Solution, **7** - Thermometer, **8** - 3-Electrode Holder, **9** - 3-Electrode Holder Support

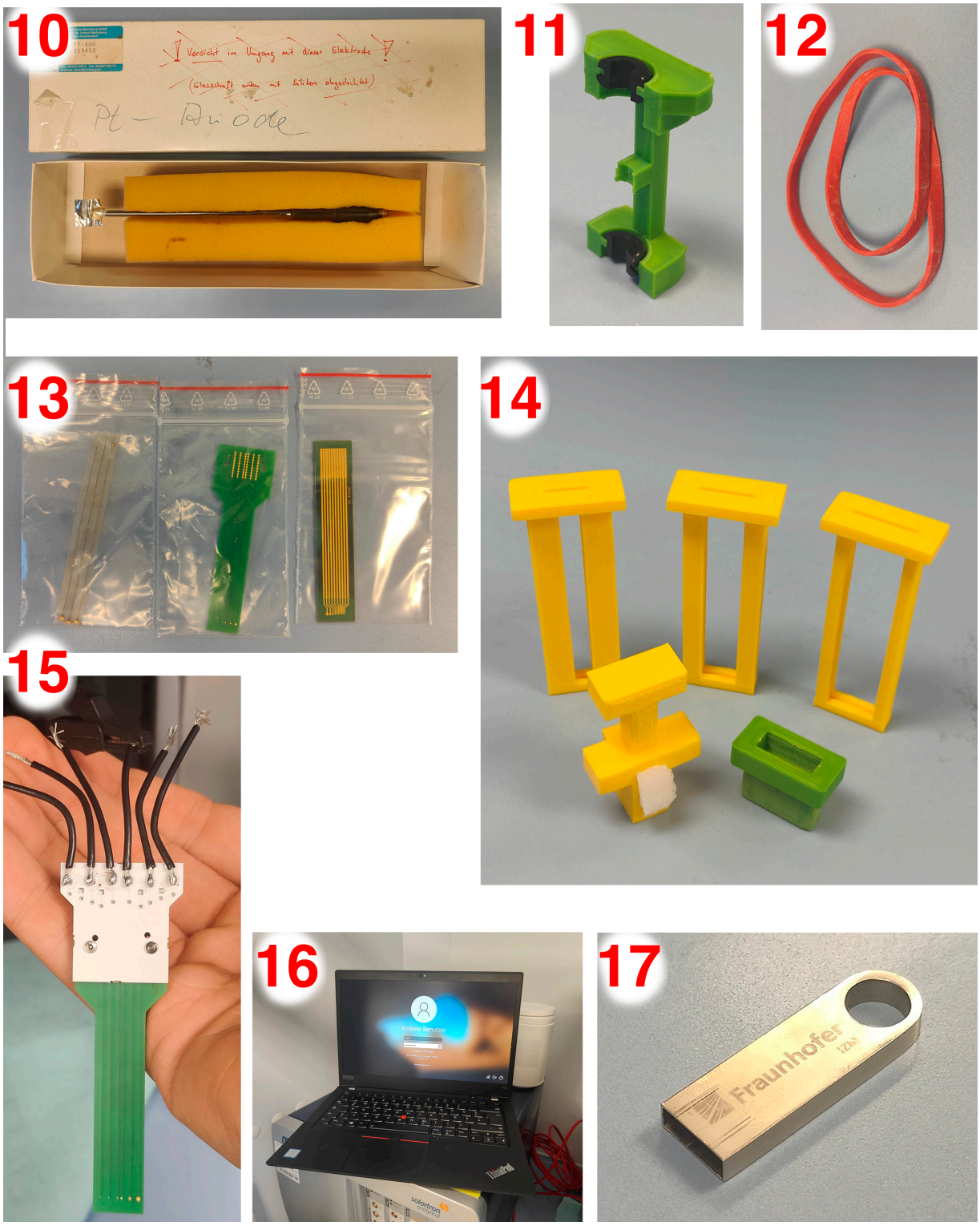

Figure C.3: Equipment needed for all types of Electrode Characterization Testing 2. In numerical order: **10** - Pt flag foil large return electrode (CE), **11** - CE Lock, **12** - Rubber Band, **13** - WE Samples, **14** - WE Sample Holder, **15** - WE Connector, **16** - Working Laptop NB-SIIT086, **17** - USB Thumbstick Drive

Figure C.4: Setup specific elements used in EIS & CV tests

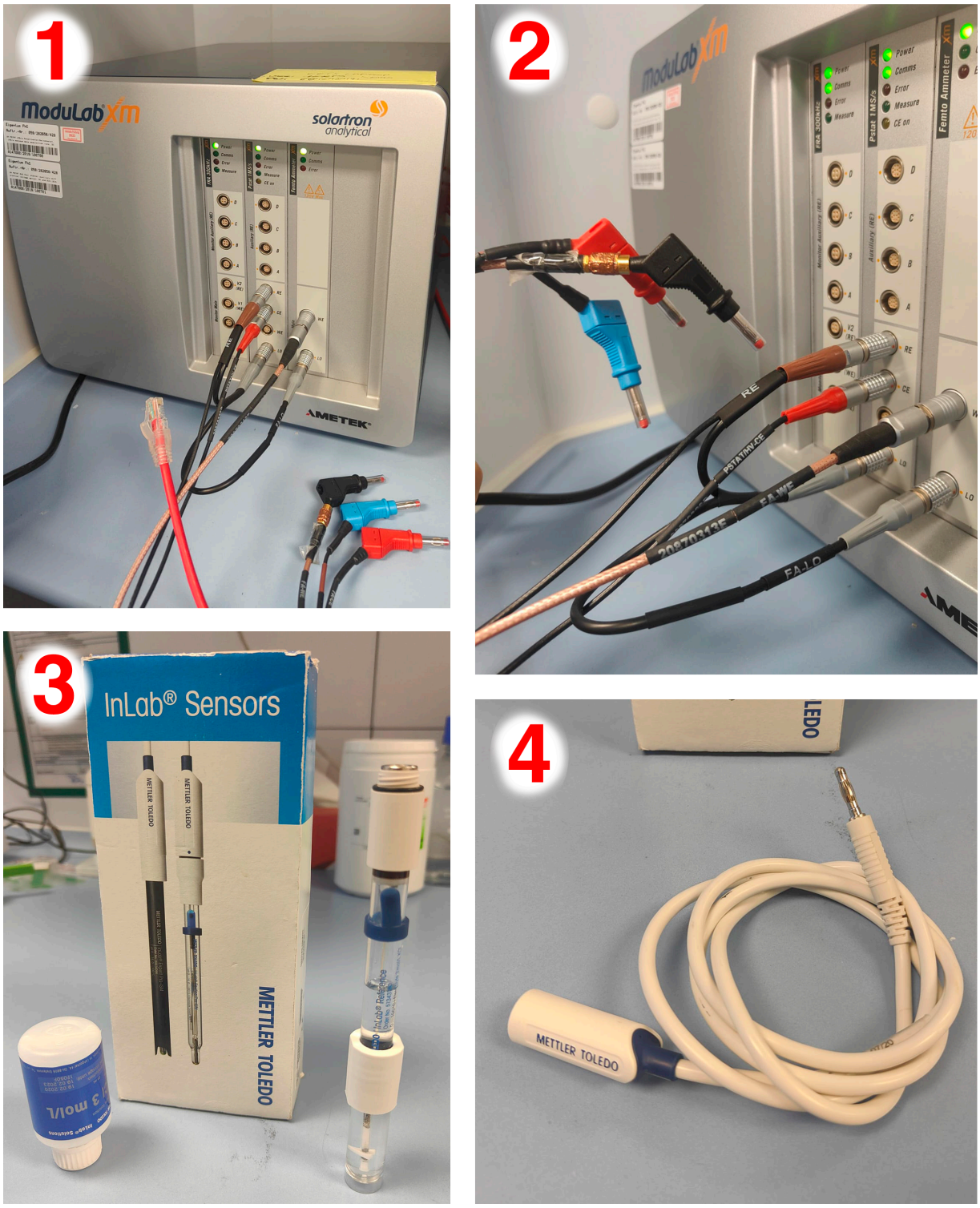

Figure C.4: Equipment for EIS and CV testing. In numerical order: **1** - Modulab XM Solartron Analytical, **2** - FA Module Cabling, **3** - Mettler Toledo Glassy Cargon Ag|AgCl RE, **4** - RE connector banana cable

Figure C.5: Test Cell circuit (Physical and LT Spice model) to be used for adequate calibration of the Modulab XM+.

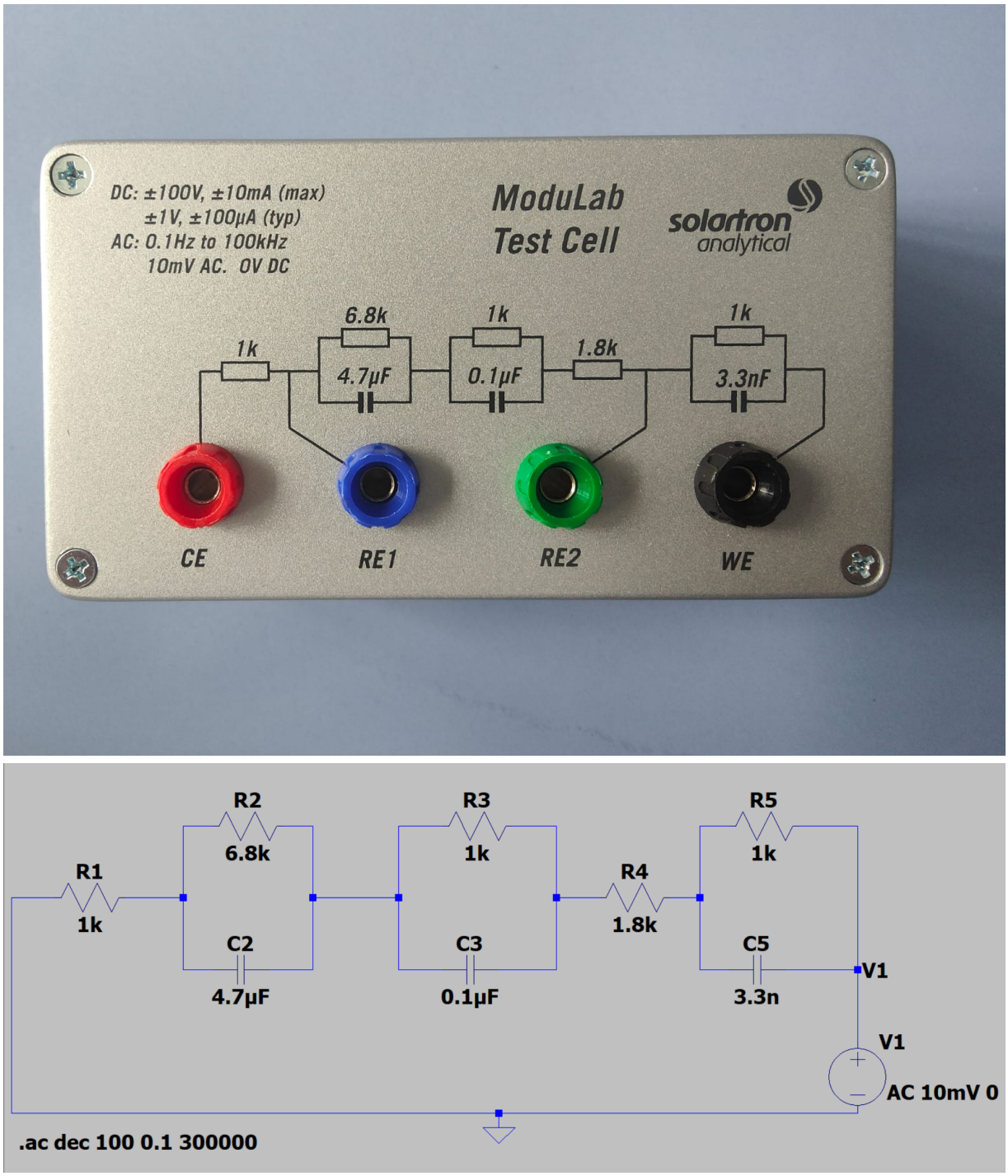

Figure C.5: Test Cell circuit used for calibration of the Modulab XM+. **Top:** Image of the physical test cell that came with the Modulab XM+ to ensure adequate calibration of the instrument.**Bottom:** Circuit modelled in LT Spice after the test cell to have a theoretical output response to compare the calibration measurements to.

Figures C.6 and C.7: Setup specific elements used in VT tests

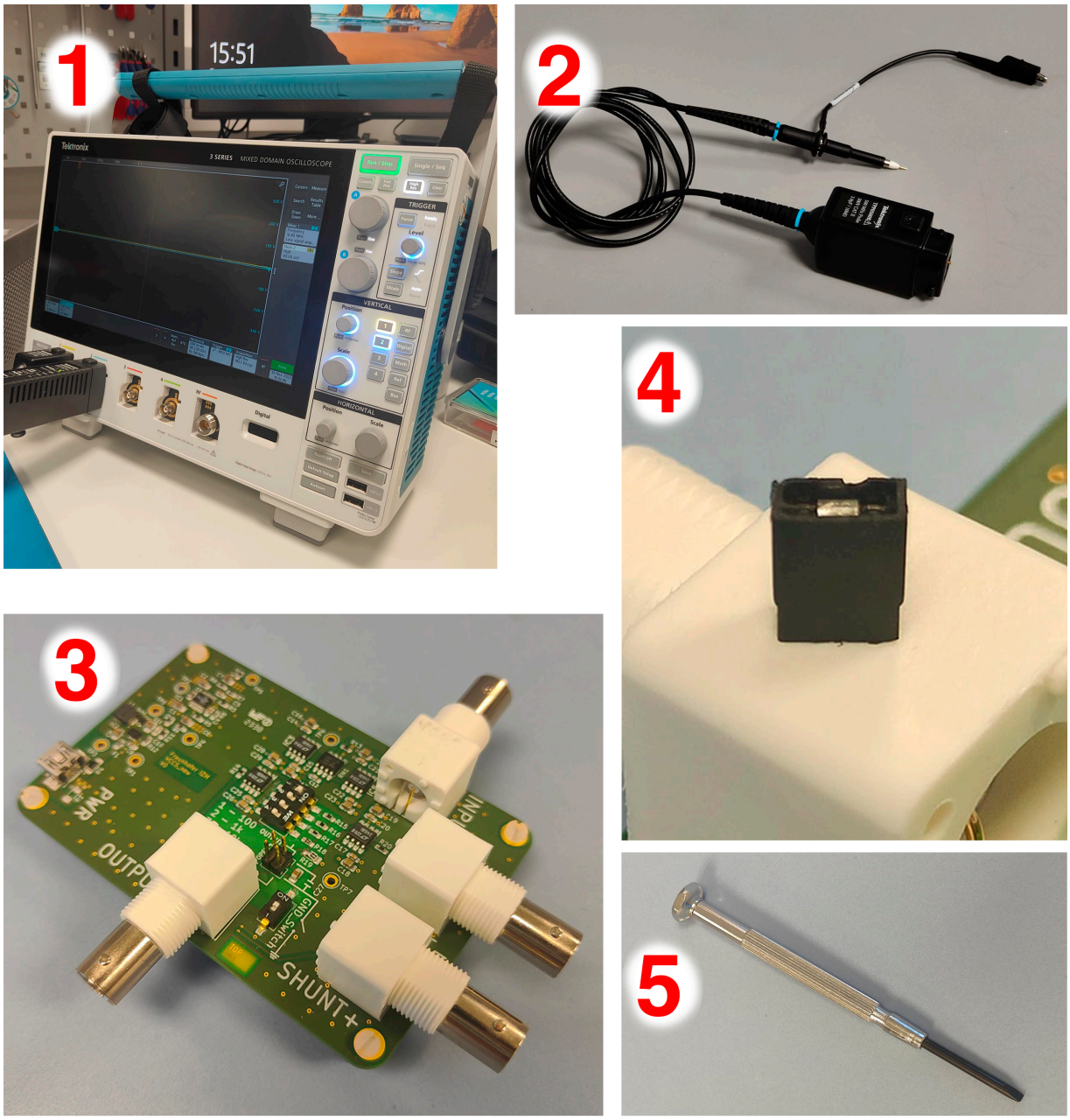

Figure C.6: Equipment for VT Testing 1. In numerical order: **1** - Tektronix MDO34 Oscilloscope, **2** - 1 MDO34 CH Probe, **3** - VCCS PCB, **4** - 1 PCB jumper, **5** - Tool to manipulate PCB switches

Figure C.7: Equipment for VT Testing 2. In numerical order: **6** - 3 BNC cables, **7** - 1 BNC cable signal Y-splitter, **8** - 1 BNC to Banana +,- adapter, **9** - 1 Banana to Hook cable, **10** - 1 Banana to Banana cable, **11** - 1 MINI USB to USB cable

Figures C.8 and C.9: Equipment and procedure used in the 3-step Noise Characterization

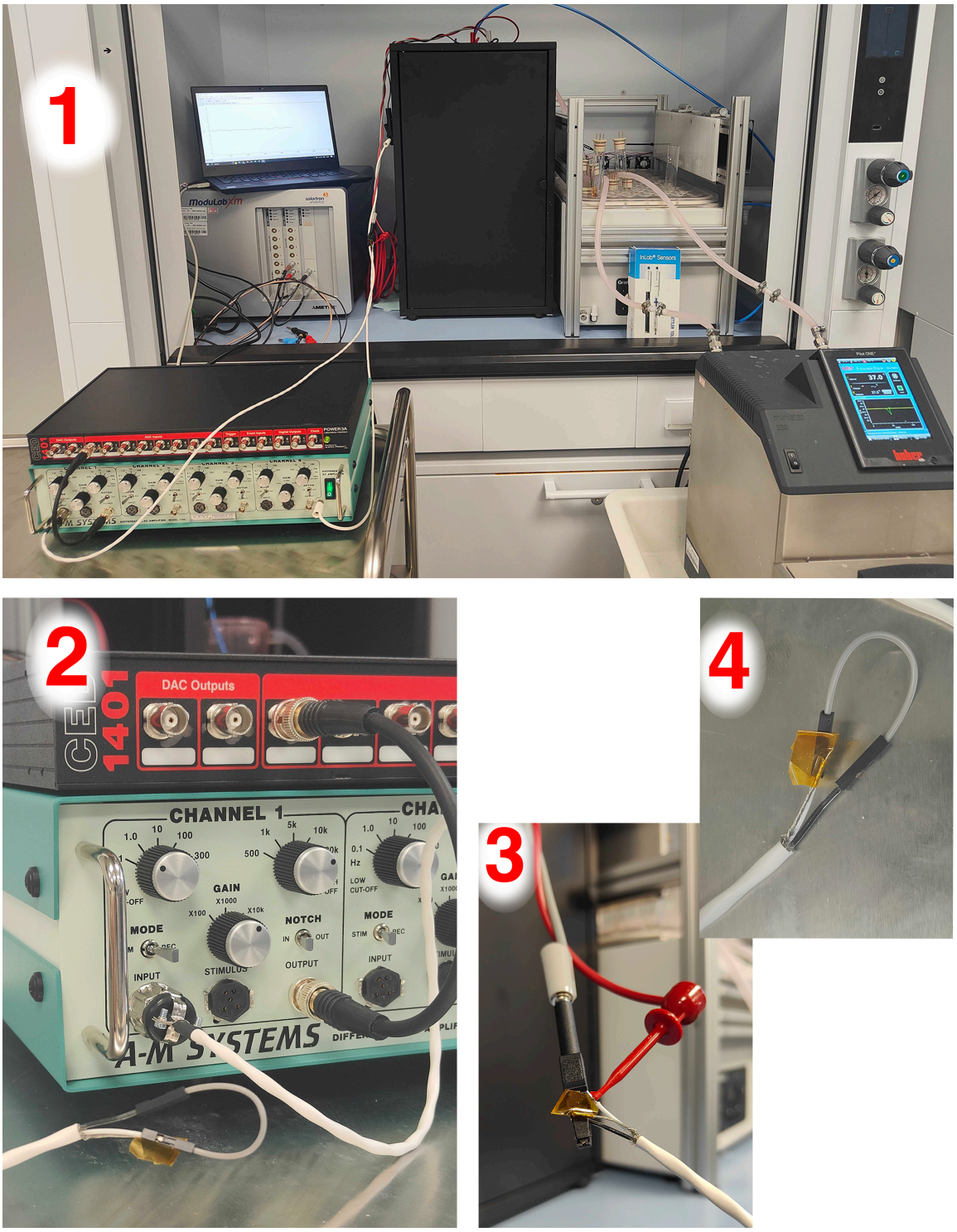

Figure C.8: Equipment and setup for Noise Characterization 1. In numerical order: **1** - General View of the Noise Characterization Setup, **2** - Close up of the setup of the Amplifier, connected via a BNC cable to the ADC, and recording the signal at the input, **3** - Cabling connections when connecting the input cable to the cage for Noise Characterization steps 2 and 3 of the 3-step Noise Characterization, **4** - Short circuit of the input signal of the amplifier to record the internal noise of the instrument, used in step 1 of the 3-step noise characterization.

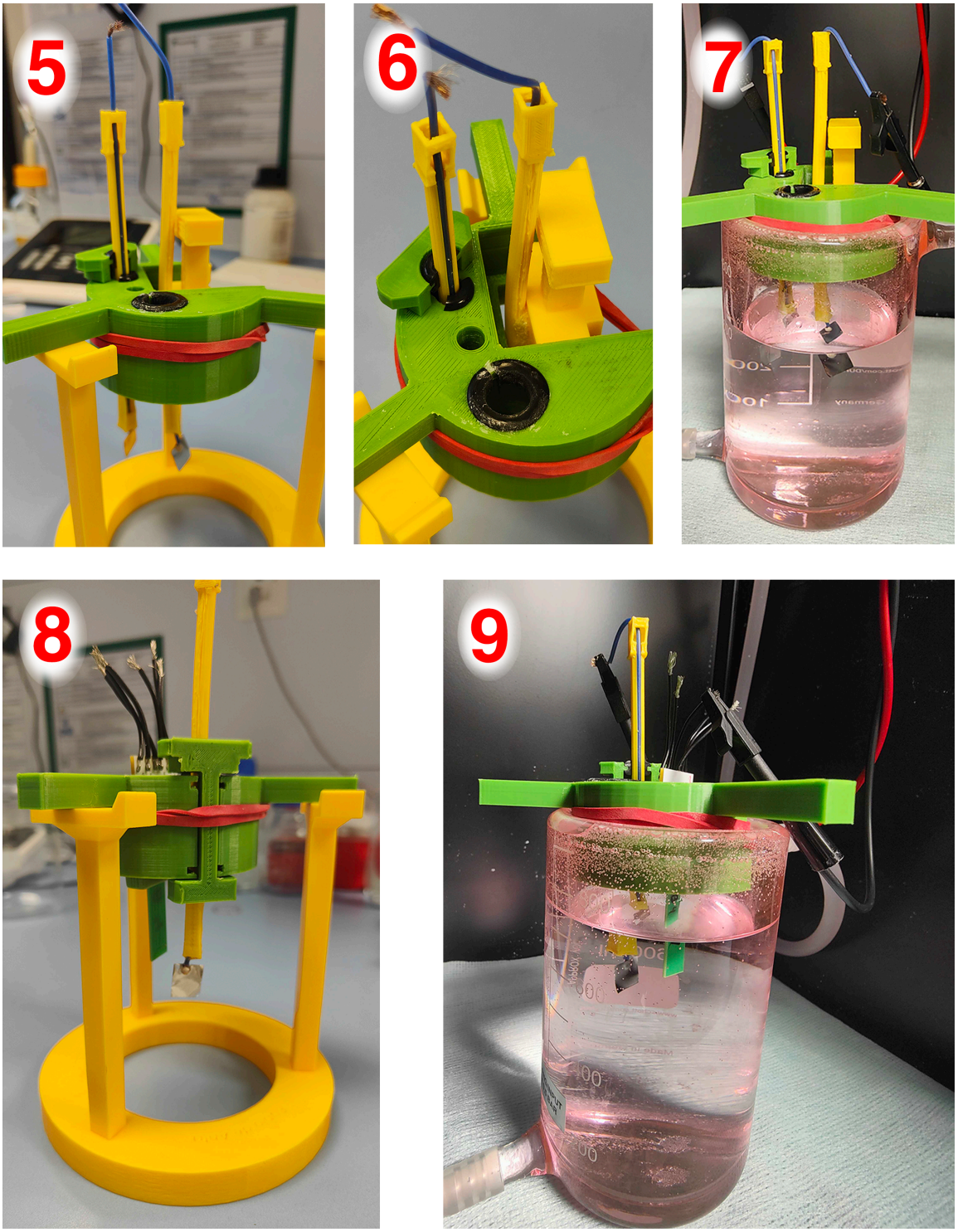

Figure C.9: Equipment and setup for Noise Characterization 2. In numerical order: **5** - 3-Electrode Holder holding two Pt foil large return electrodes, **6** - Close up of the 3-electrode holder holding the Pt foil large return electrodes, using the universal electrode holder, **7** - Setup for the measurement of the noise between the two Pt foil large return electrodes, **8** - 3-electrode Holder holding a Pt foil large return electrode and a working electrode sample, **9** - Setup for the measurement of the noise of the different opening sizes of the Working electrode.

Figure C.10: Manufacturing the Pt foil large return electrodes for Noise Characterization

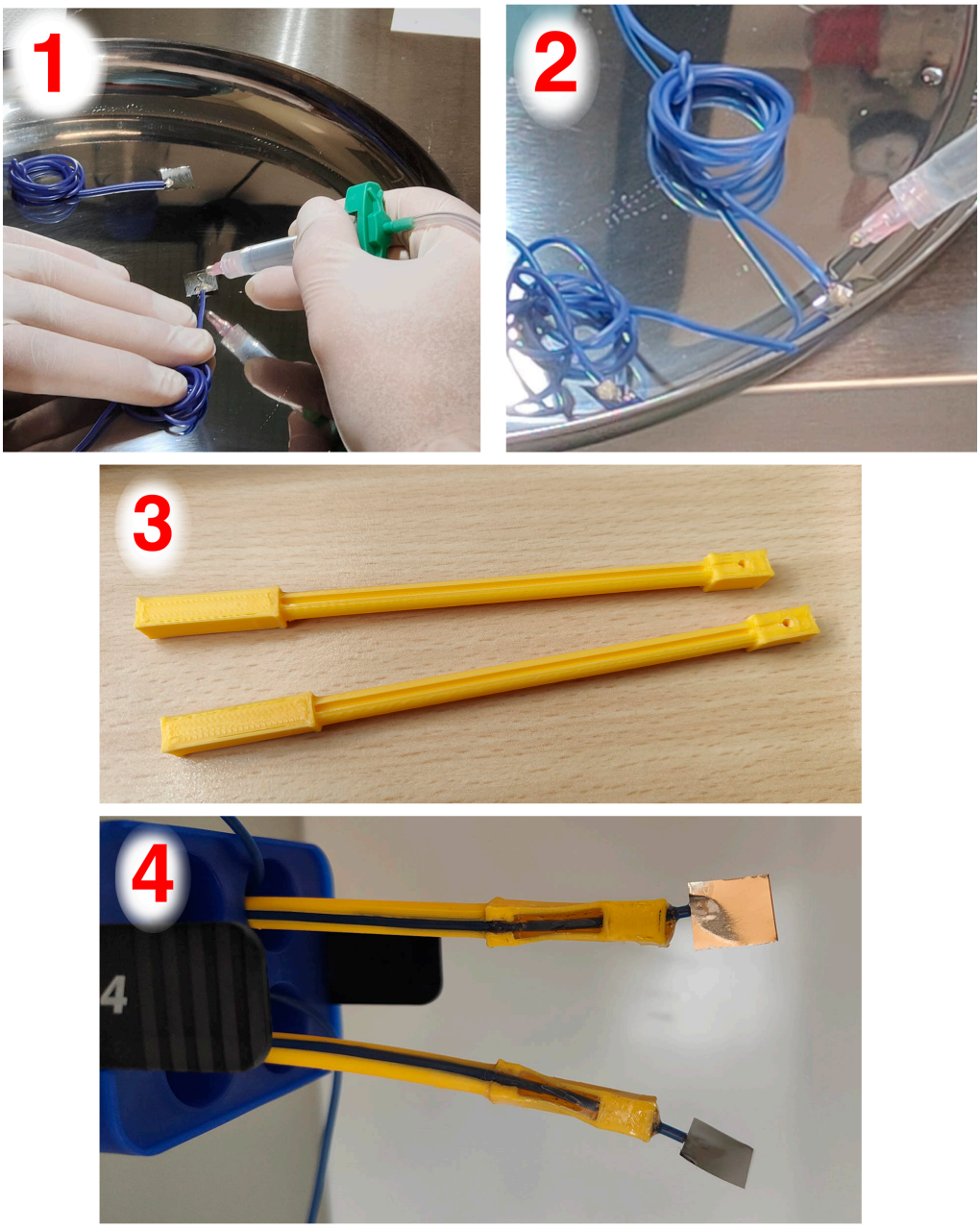

Figure C.10: Procedure of manufacturing the Pt foil large return electrodes for Noise Characterization. In numerical order: **1** - The Pt foil needs to be attached to the electrical wire. This is done by using conductive glue to attach the wire to one side of the foil, **2** - To ensure only the Pt foil is contributing to the electrochemical measurement, the conductive glue joint is isolated by covering it with silicone, **3** - A custom body for the electrode was designed and printed. It features a carving throughout its body to hold the electrical wire while keeping its form, **4** - After assembly, the whole electrode is cured by placing it in the oven. Due to a miscalculation of the applied heat, the plastic body warped. They are still usable and can still be held with the electrode holder.

Figure C.11: Solidworks screenshots and drawing schematics of the 3-Electrode Holder

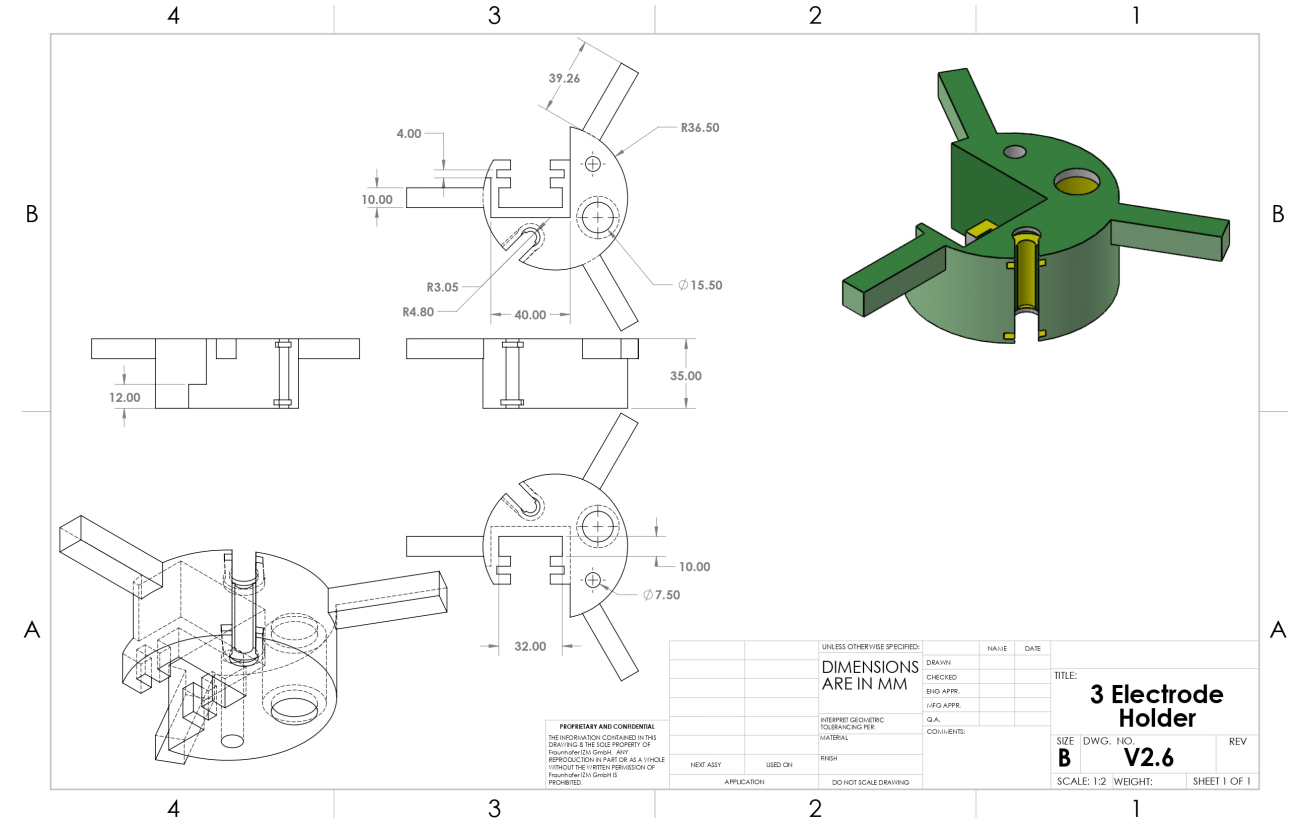

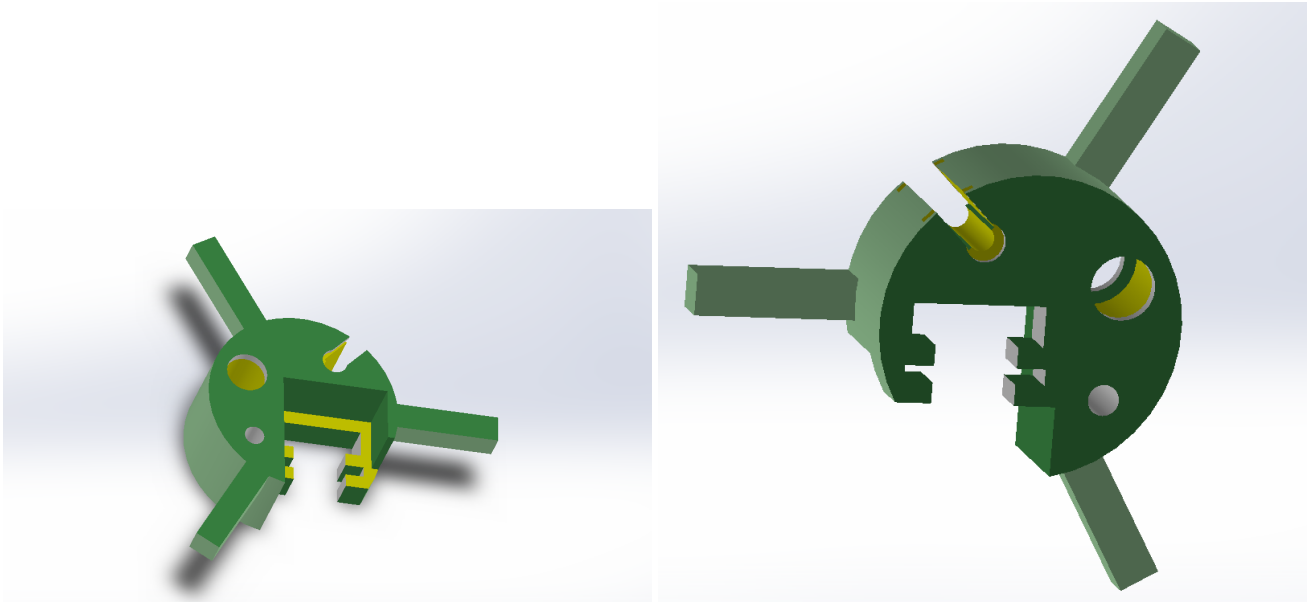

Figure C.11: Solidworks screenshots and drawing schematics of the 3-Electrode Holder. From top to bottom, left to right: **Top** - 3-Electrode Holder drawing schematic, **Bottom Left** - 3-Electrode Holder Screenshot showing the top isometric view, **Bottom Right** - 3-Electrode Holder Screenshot showing the bottom isometric view.

Figures C.12 and C.13: Solidworks screenshots and drawing schematics of the 3-Electrode Holder loading support.

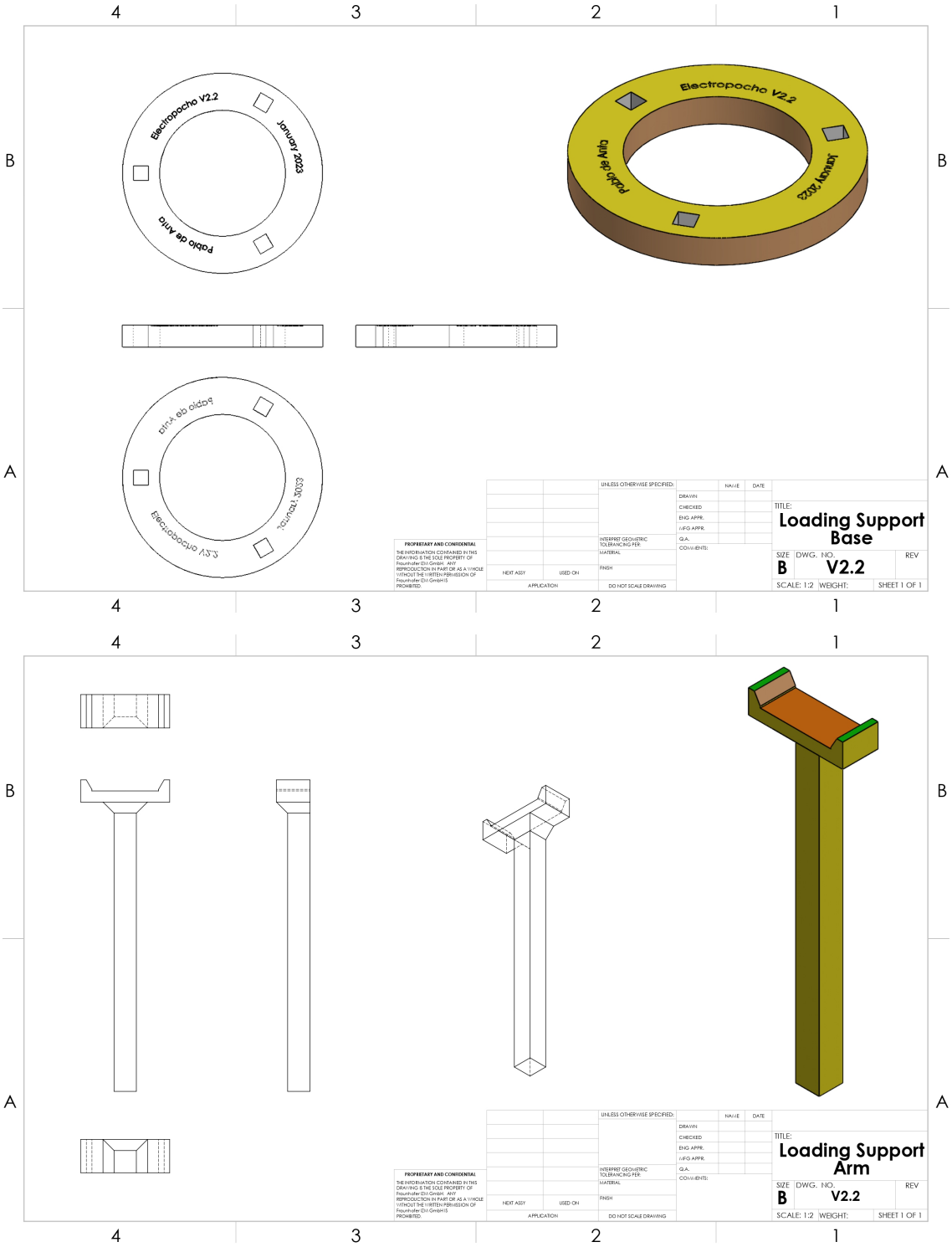

Figure C.12: Solidworks drawing schematics of the 3-Electrode Holder Loading Support Components. From top to bottom: **Top** - Loading Support Base, **Bottom** - Loading Support Arm (3 are needed)

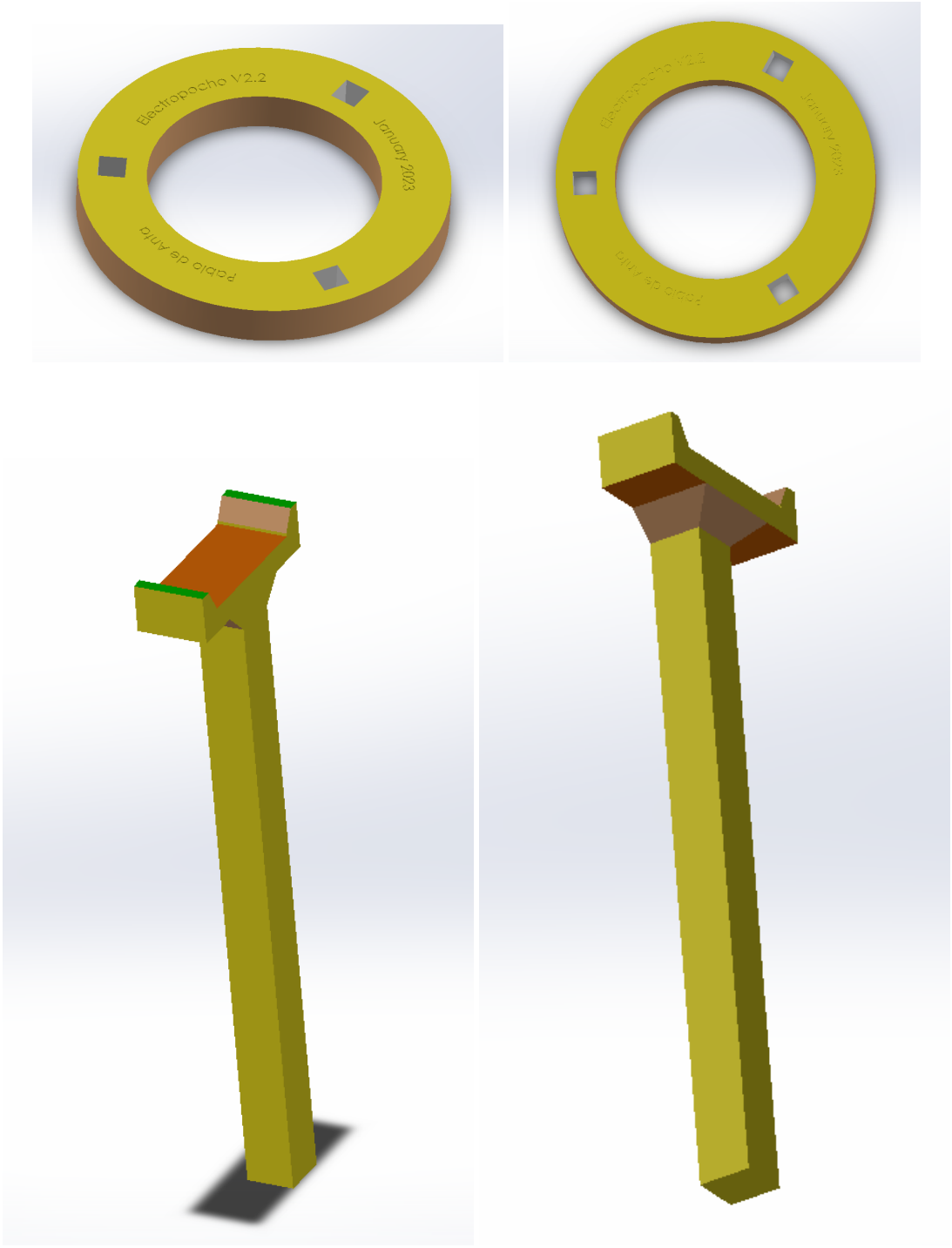

Figure C.13: Solidworks screenshots of the 3-Electrode Holder Loading Support Components. From top to bottom, left to right: **Top Left** - Isometric View of Loading Support Base, **Top Left** - Top View of Loading Support Base, **Bottom Left** - Isometric view showing interior face of Loading Support Arm, **Bottom Right** - Isometric view showing exterior face of Loading Support Arm.

Figure C.14: Solidworks screenshots and drawing schematics of the CE Lock

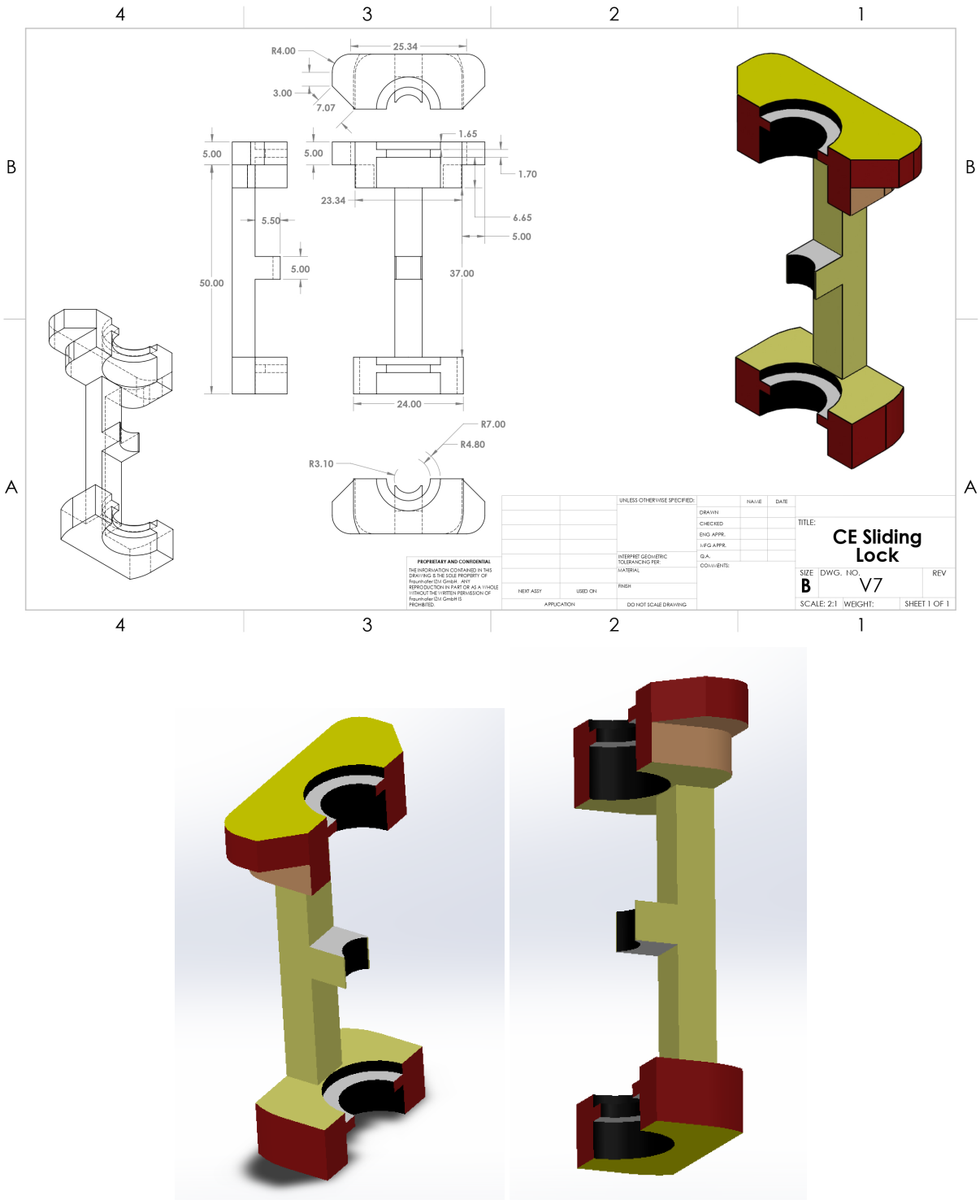

Figure C.14: Solidworks screenshots and drawing schematics of the CE Lock. From top to bottom, left to right: **Top** - CE Lock Drawing Schematic, **Bottom Left** - CE Lock screenshot showing top-left isometric view, **Bottom Right** - CE Lock screenshot showing bottom-right isometric view.

Figure C.15: Pictures of the 3-Electrode Holder assembled with the corresponding rubber rings to softly grip the electrodes without damaging them.

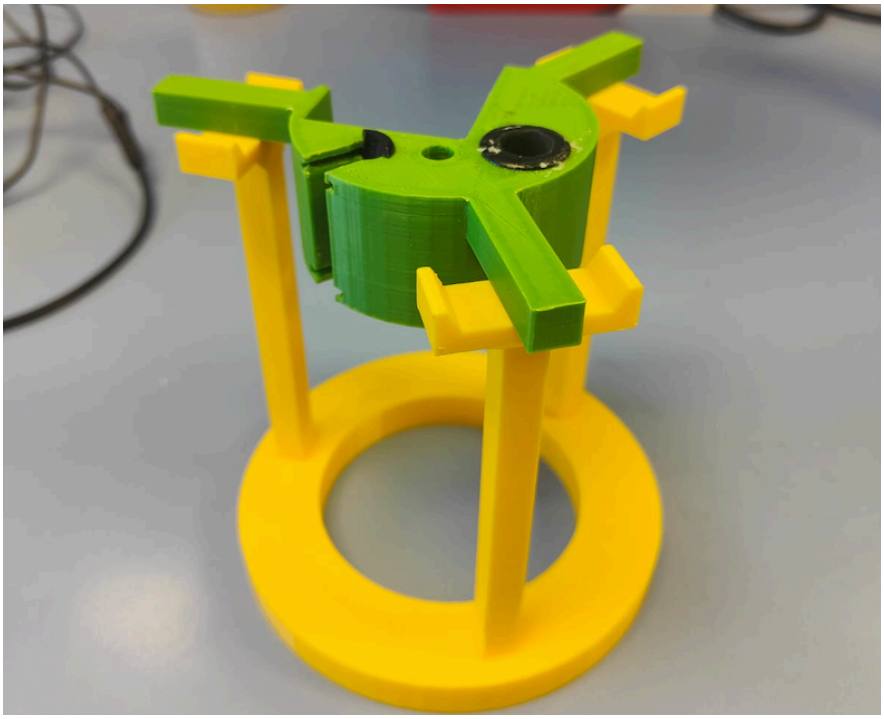

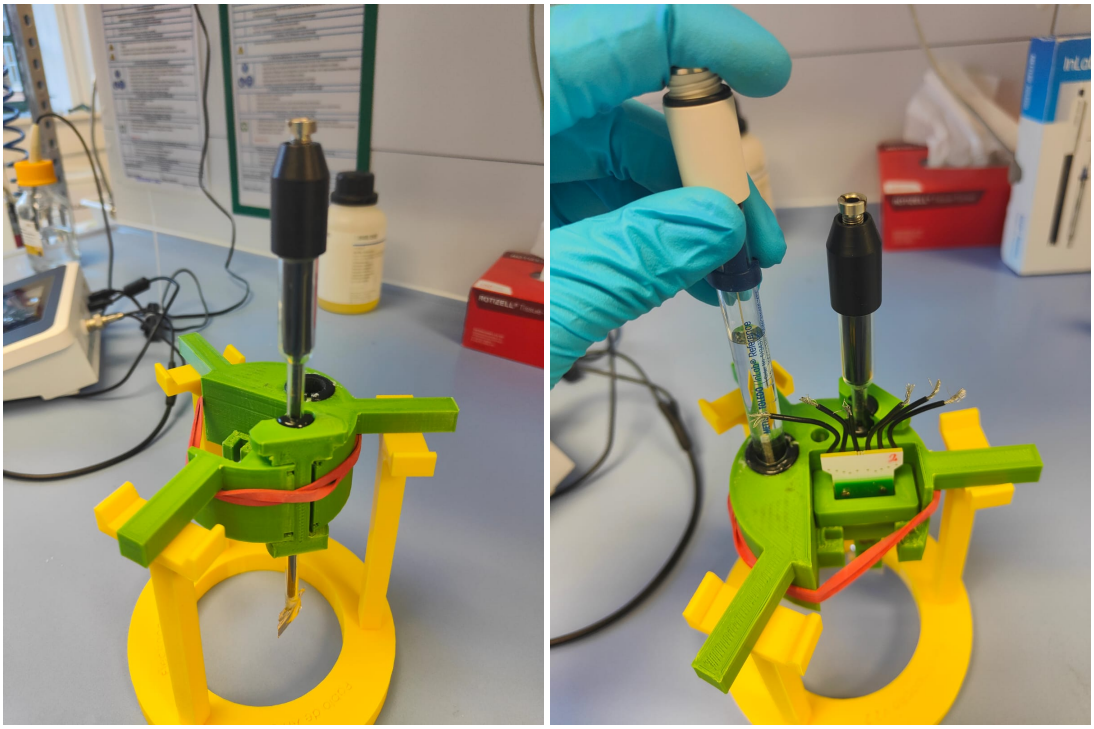

Figure C.15: Images of the final assembly of the 3-Electrode Holder with rubber rings, softly gripping the electrodes. From top to bottom, left to right: **Top** - 3-Electrode Holder with rubber rings, supported by the loading support, **Bottom Left** - Rubber rings on both the 3-Electrode holder and the CE Lock hold in place the CE, **Bottom Right** - The RE can be directly slid in through the rubber ring, holding it at whichever preferred height.

Figure C.16: Solidworks screenshots and drawing schematics of the Large-Sized Flexible Electrode holder for electrodes ranging from 20 mm to 25 mm in width.

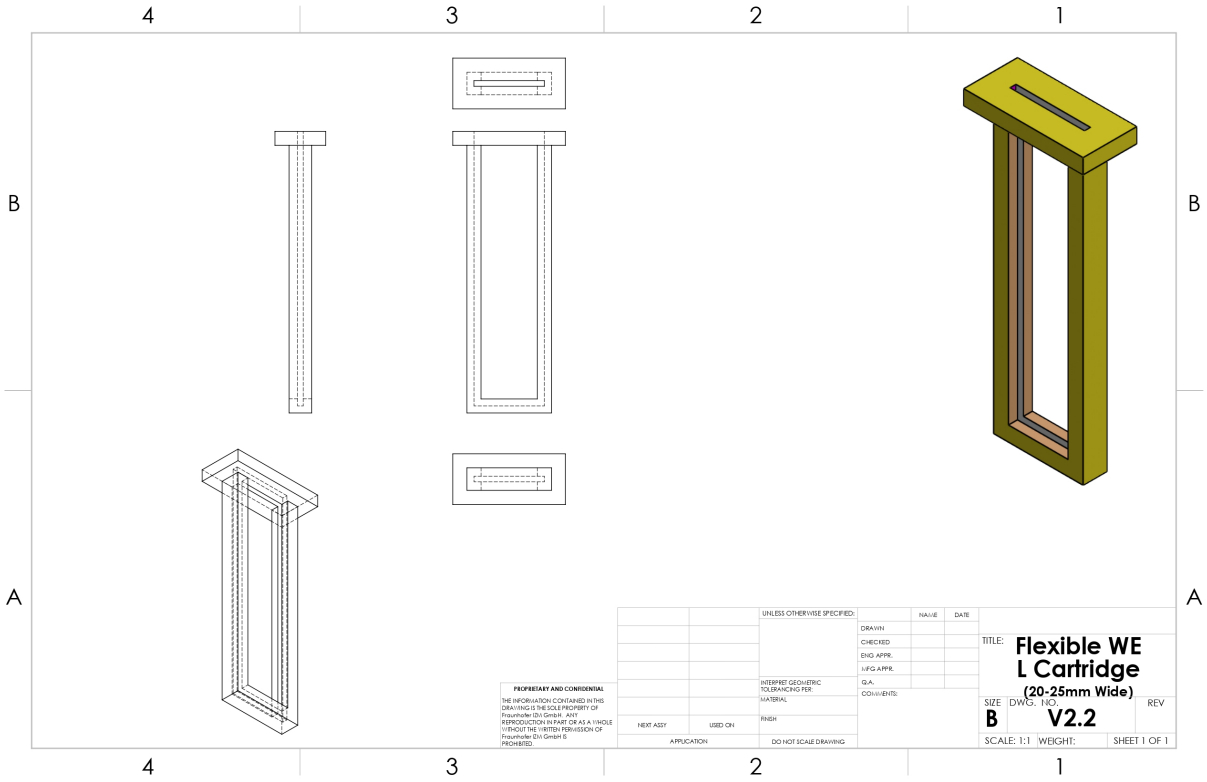

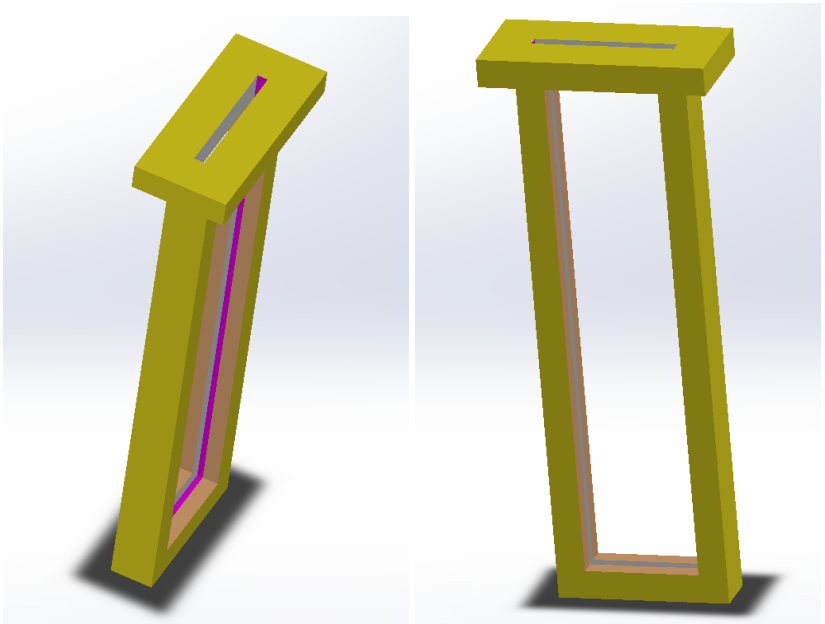

Figure C.16: Solidworks screenshots and drawing schematics of the Large-Sized Flexible Electrode Holder. From top to bottom, left to right: **Top** - Large-Sized Flexible Electrode holder Drawing Schematic, **Bottom Left** - Large-Sized Flexible Electrode holder screenshot showing top-left isometric view, **Bottom Right** - Large-Sized Flexible Electrode holder screenshot showing front view.

Figure C.17: Solidworks screenshots and drawing schematics of the Medium-Sized Flexible Electrode holder for electrodes ranging from 15 mm to 21 mm in width.

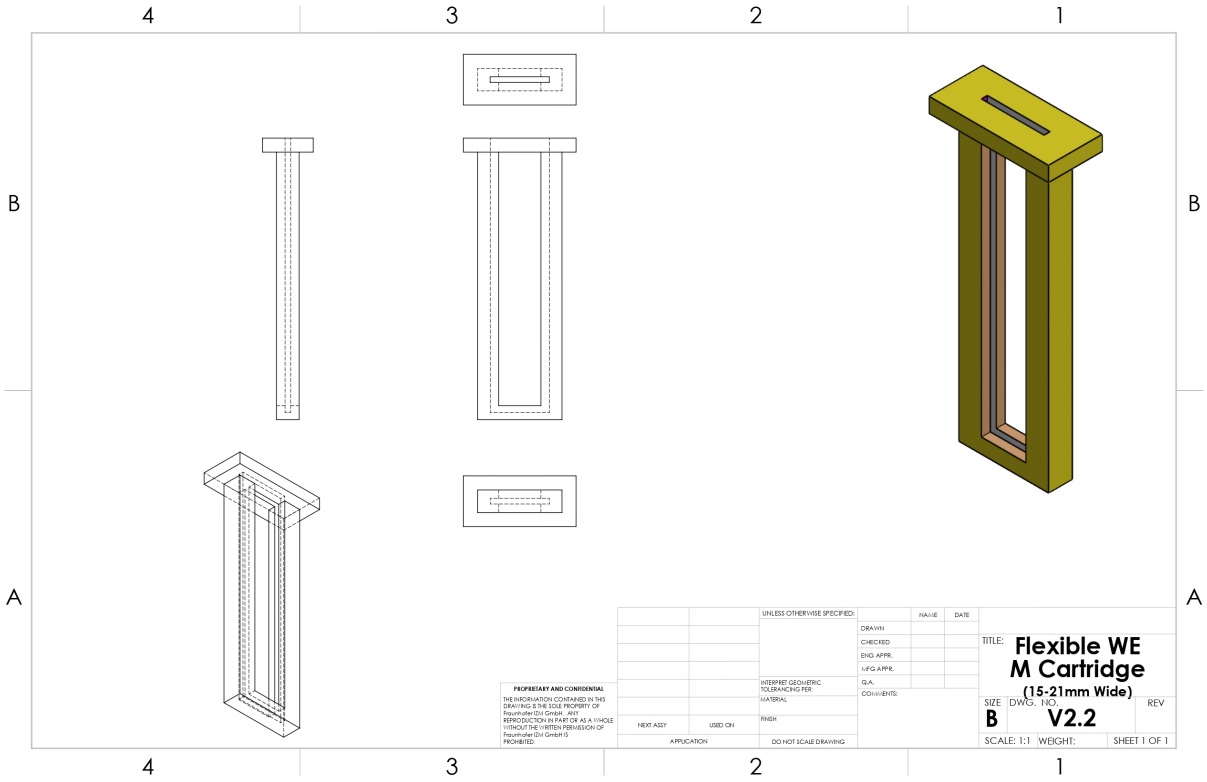

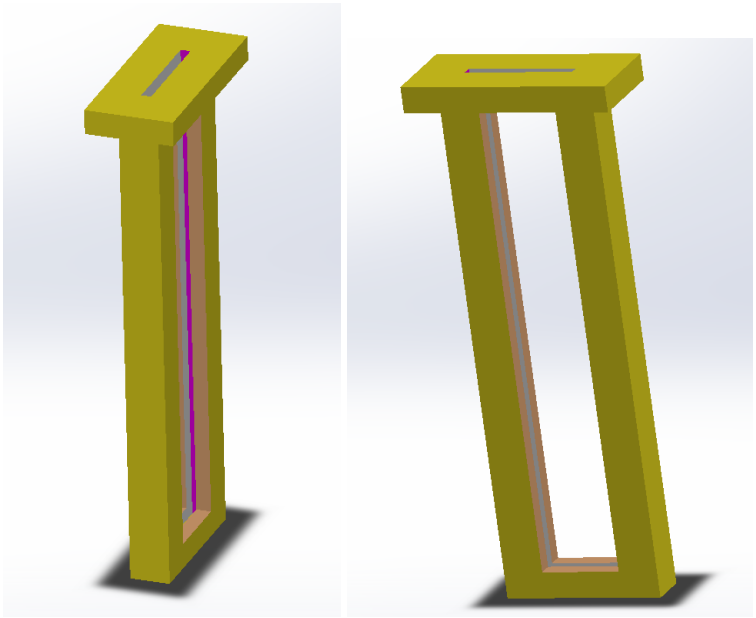

Figure C.17: Solidworks screenshots and drawing schematics of the Medium-Sized Flexible Electrode Holder. From top to bottom, left to right: **Top** - Medium-Sized Flexible Electrode holder Drawing Schematic, **Bottom Left** - Medium-Sized Flexible Electrode holder screenshot showing top-left isometric view, **Bottom Right** - Medium-Sized Flexible Electrode holder screenshot showing front view.

Figure C.18: Solidworks screenshots and drawing schematics of the Small-Sized Flexible Electrode holder for electrodes ranging from 8 mm to 16 mm in width.

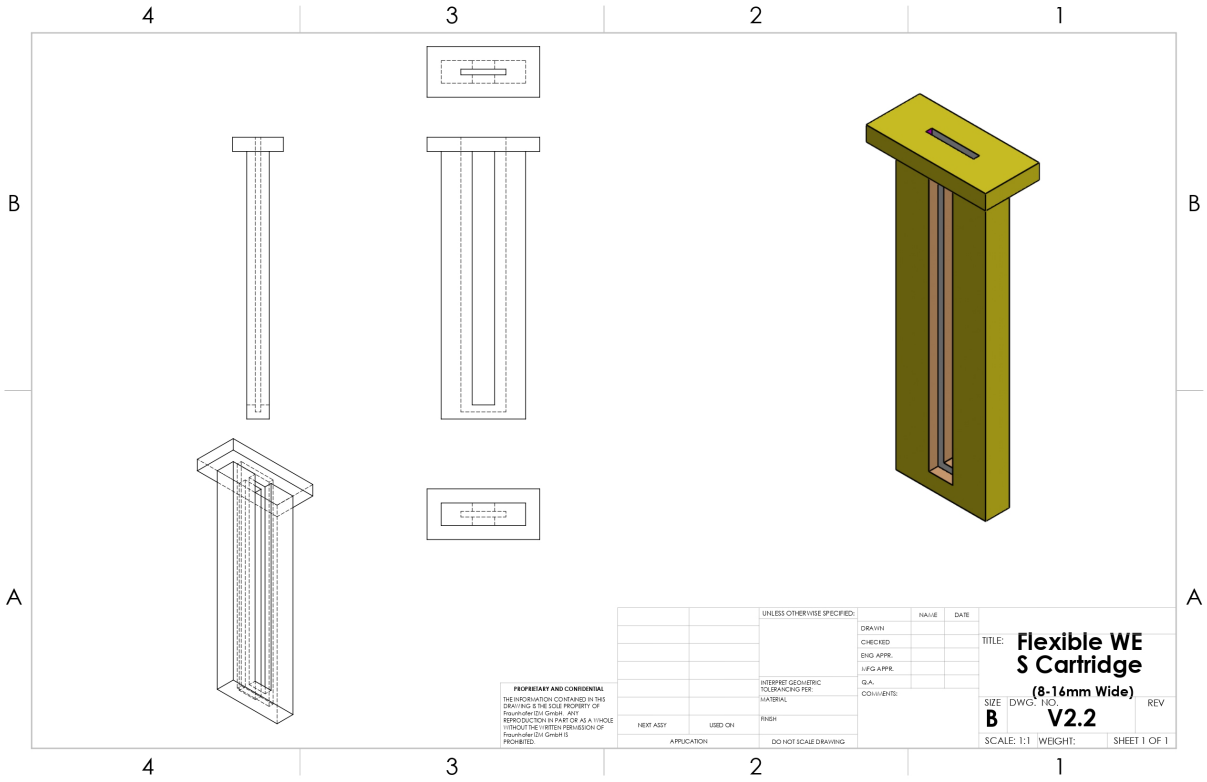

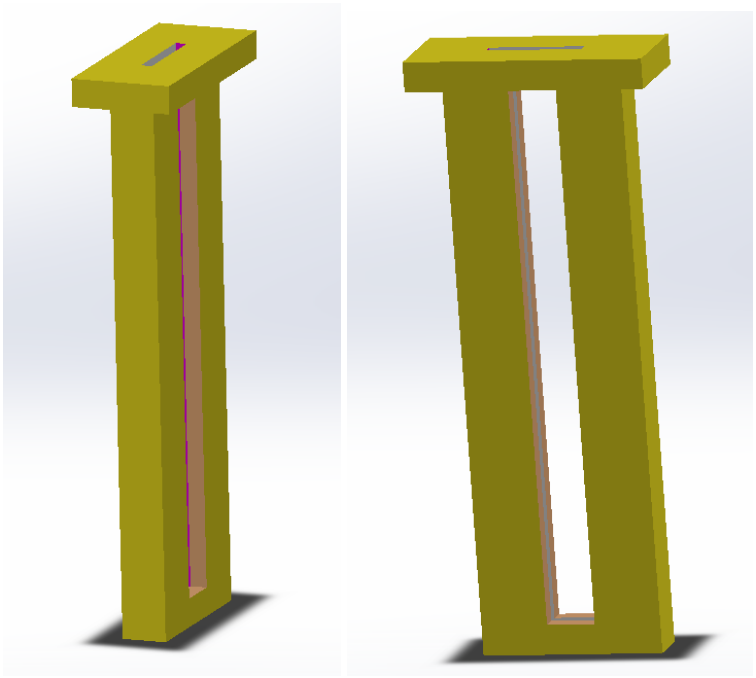

Figure C.18: Solidworks screenshots and drawing schematics of the Small-Sized Flexible Electrode Holder. From top to bottom, left to right: **Top** - Small-Sized Flexible Electrode holder Drawing Schematic, **Bottom Left** - Small-Sized Flexible Electrode holder screenshot showing top-left isometric view, **Bottom Right** - Small-Sized Flexible Electrode holder screenshot showing front view.

Figure C.19: Solidworks screenshots and drawing schematics of the PCB Electrode Holder

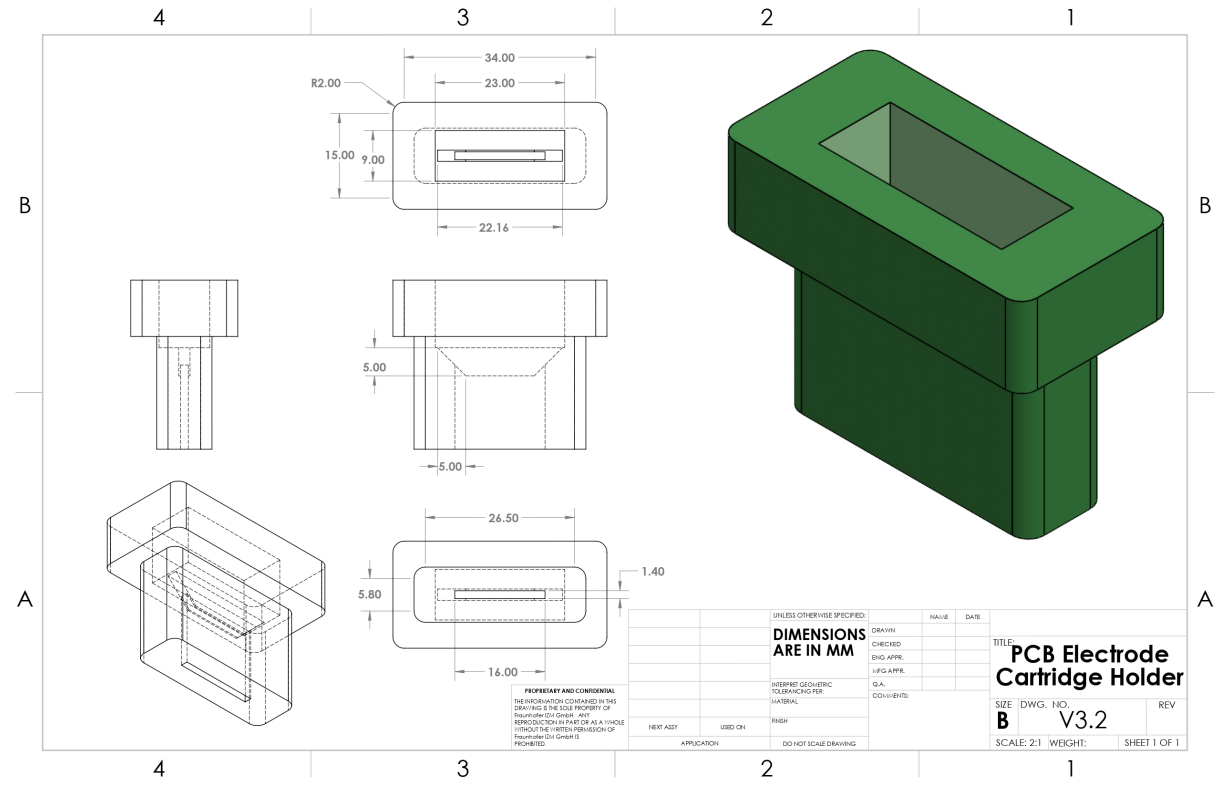

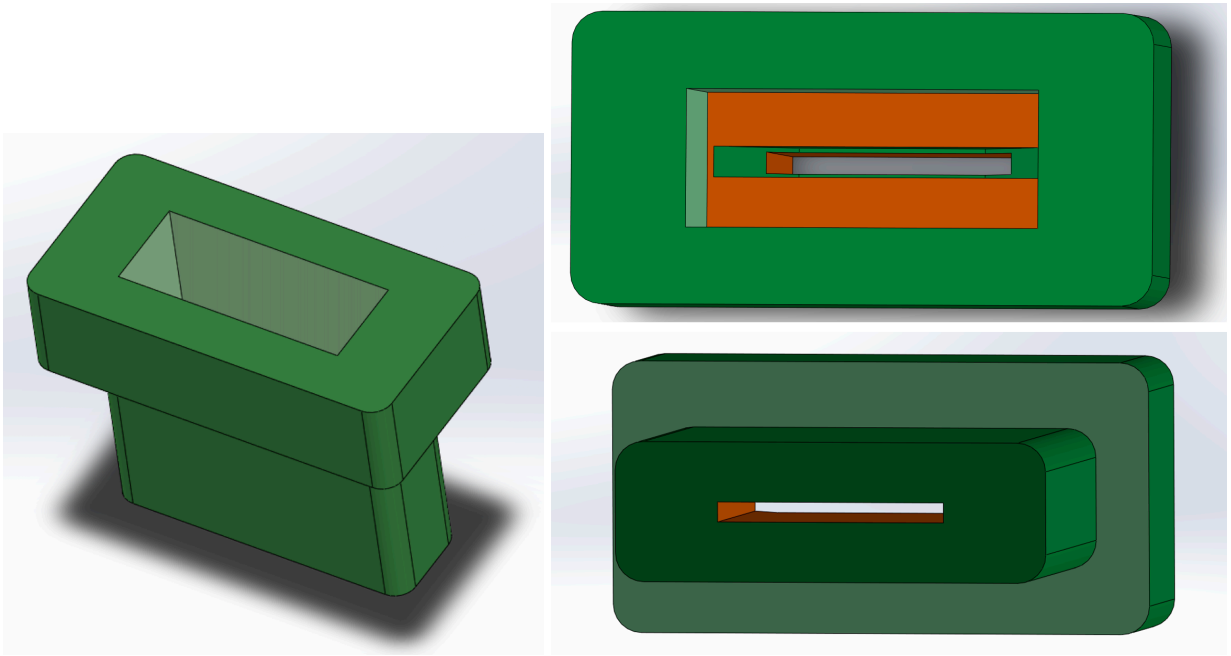

Figure C.19: Solidworks screenshots and drawing schematics of the PCB Electrode Holder. From top to bottom, left to right: **Top** - PCB Electrode Holder Drawing Schematic, **Bottom Left** - PCB Electrode Holder screenshot showing top-right isometric view, **Center Right** - PCB Electrode Holder screenshot showing top view, **Bottom Right** - PCB Electrode Holder screenshot showing bottom view.

Figure C.20: Solidworks screenshots and drawing schematics of the Universal Electrode Holder

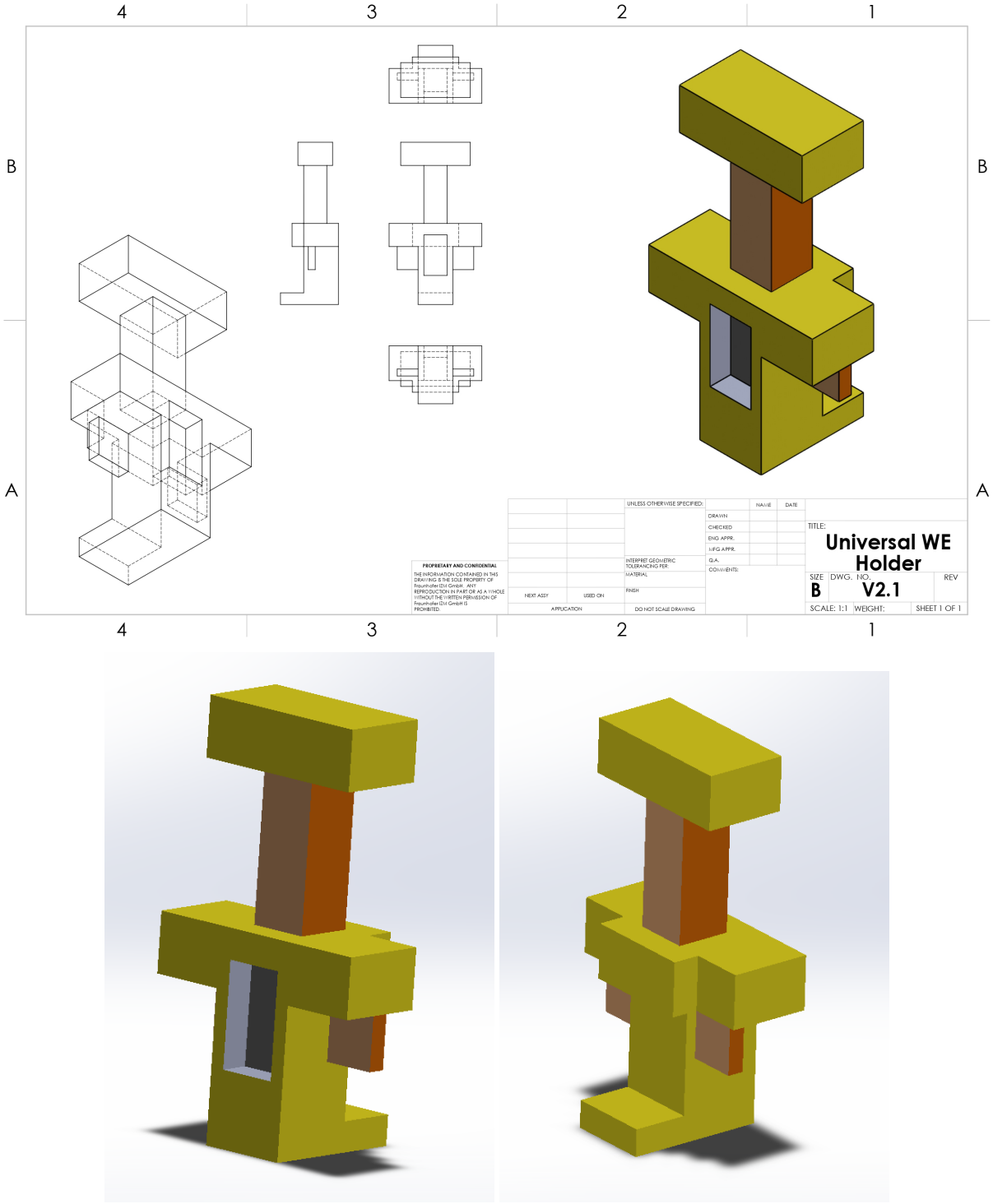

Figure C.20: Solidworks screenshots and drawing schematics of the Universal Electrode Holder. From top to bottom, left to right: **Top** - Universal Electrode Holder Drawing Schematic, **Bottom Left** - Universal Electrode Holder screenshot showing the front-right isometric view, **Bottom Right** - Universal Electrode Holder screenshot showing the back-left view.

Figure C.21: Solidworks screenshots and drawing schematics of the Parylene Electrode Holder´s base.

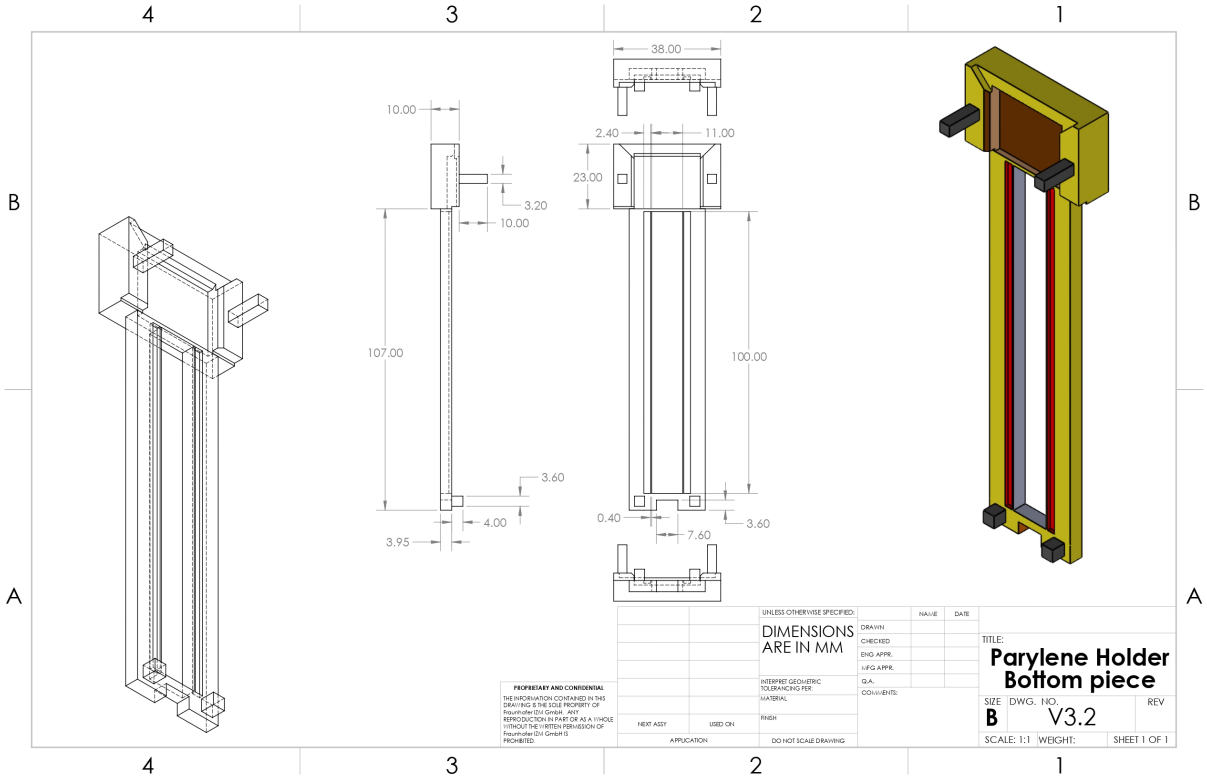

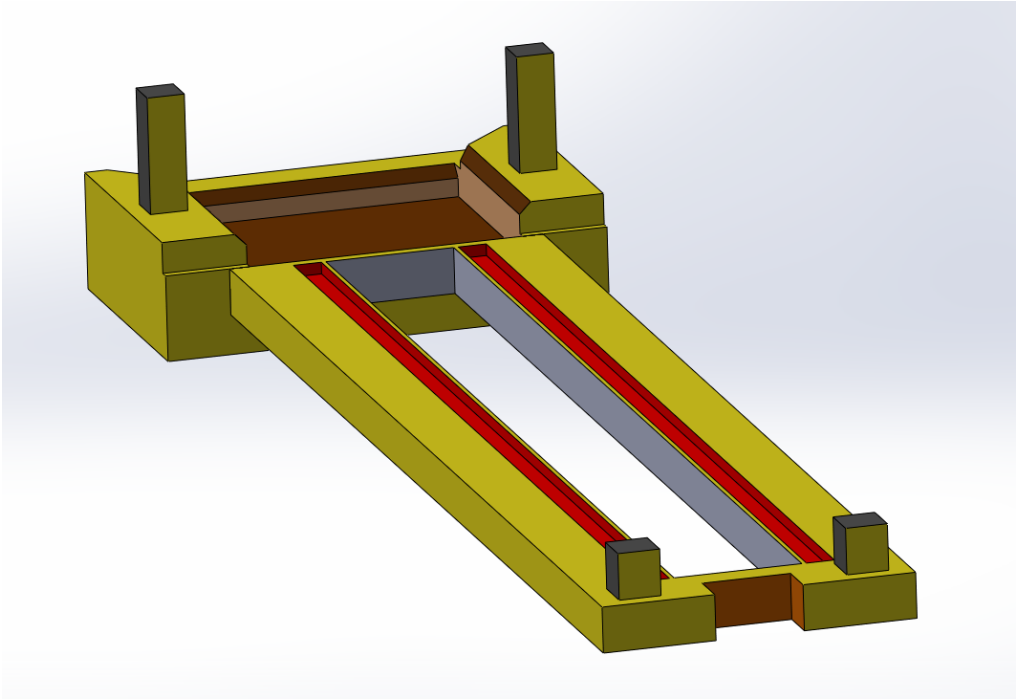

Figure C.21: Solidworks screenshots and drawing schematics of the Parylene Electrode Holder´s base. From top to bottom: **Top** - Parylene Electrode Holder´s base Drawing Schematic, **Bottom** - Parylene Electrode Holder´s base screenshot showing the front-left isometric view.

Figure C.22: Solidworks screenshots and drawing schematics of the Parylene Electrode Holder´s top.

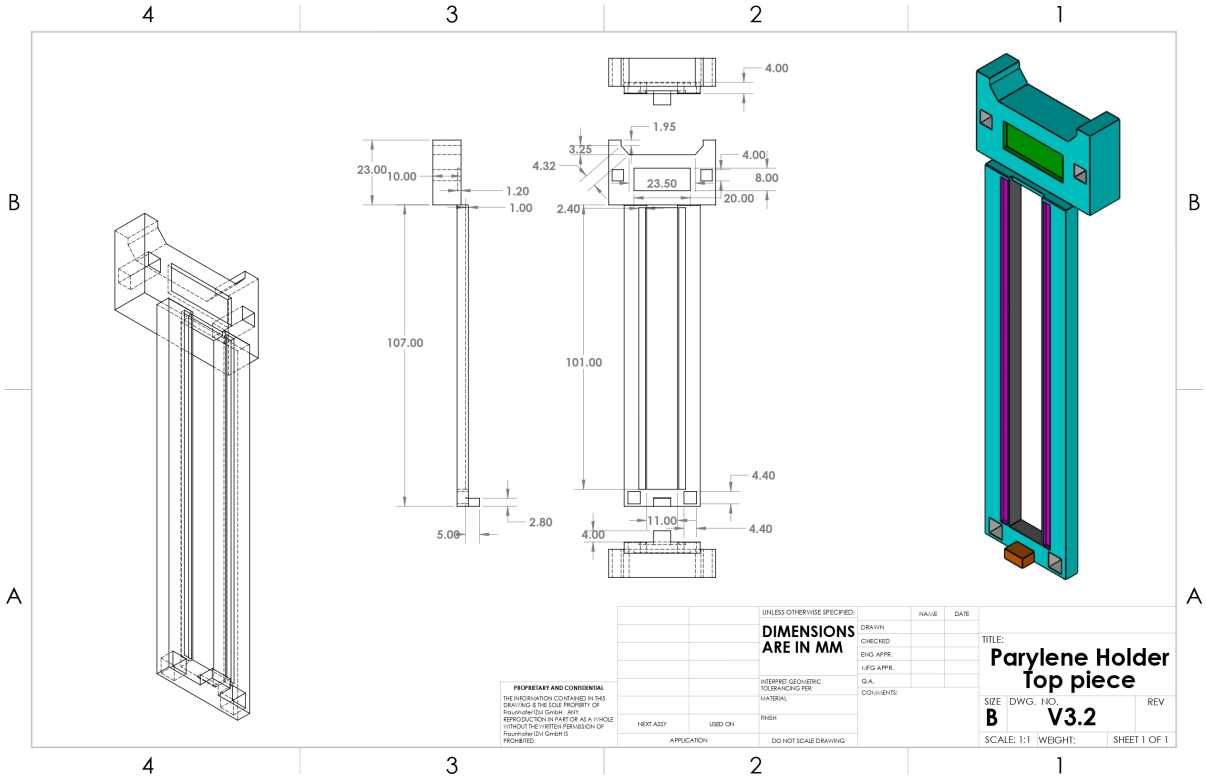

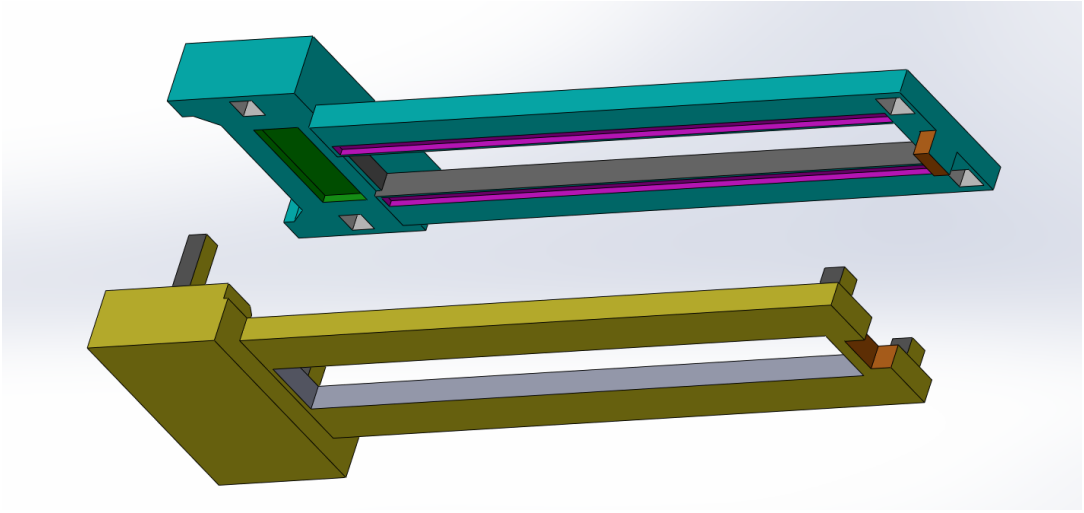

Figure C.22: Solidworks screenshots and drawing schematics of the Parylene Electrode Holder´s top. From top to bottom: **Top** - Parylene Electrode Holder´s top Drawing schematic, **Bottom** - Parylene Electrode Holder´s top screenshot showing how the top piece should be aligned to the bottom piece.

Figure C.23: Solidworks screenshots and drawing schematics of the Parylene Electrode Holder´s support.

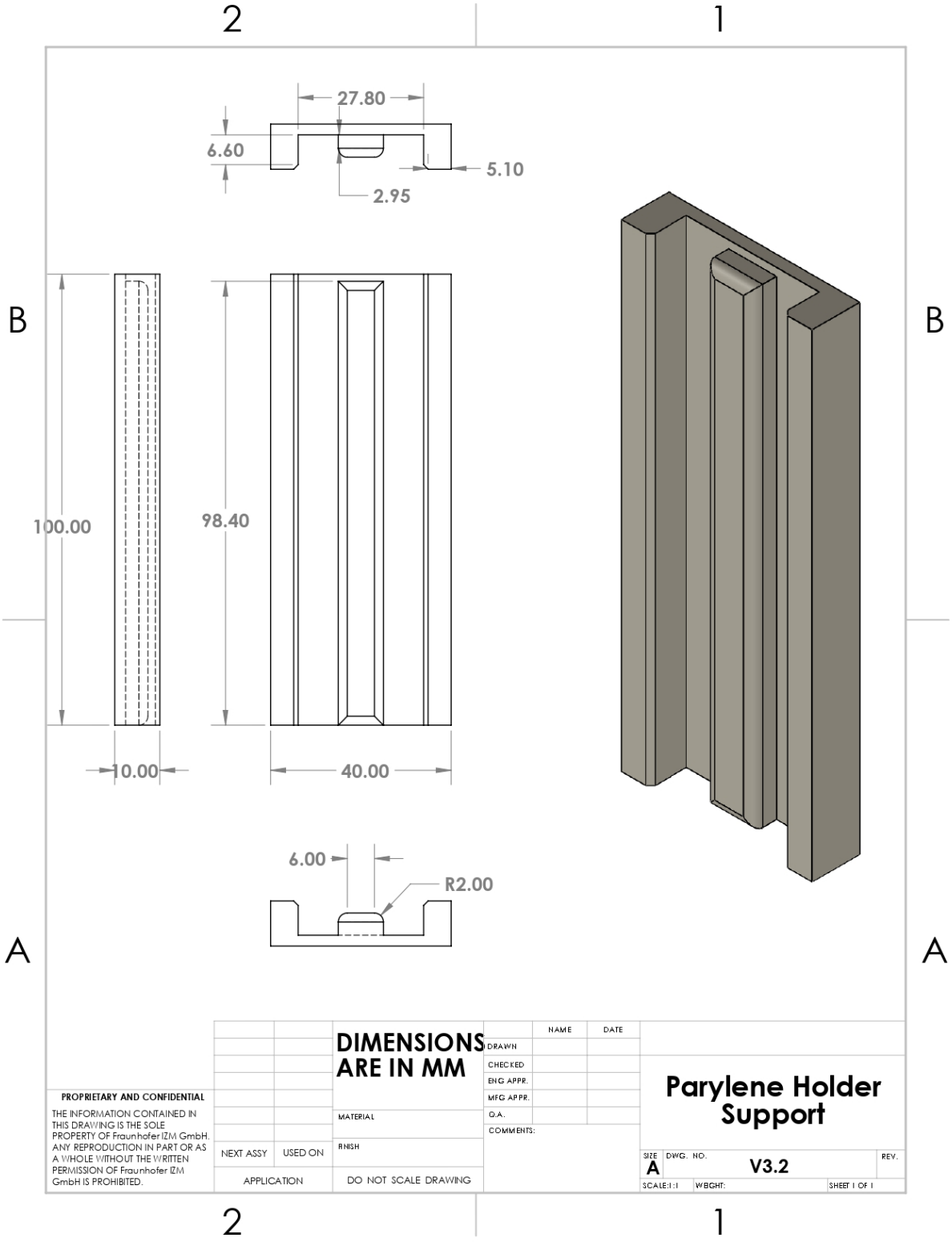

Figure C.23: Solidworks screenshots and drawing schematics of the Parylene Electrode Holder´s support.

Figure C.24 and C.25: Solidworks screenshots and drawing schematics of the Parylene Electrode Holder´s Assembly.

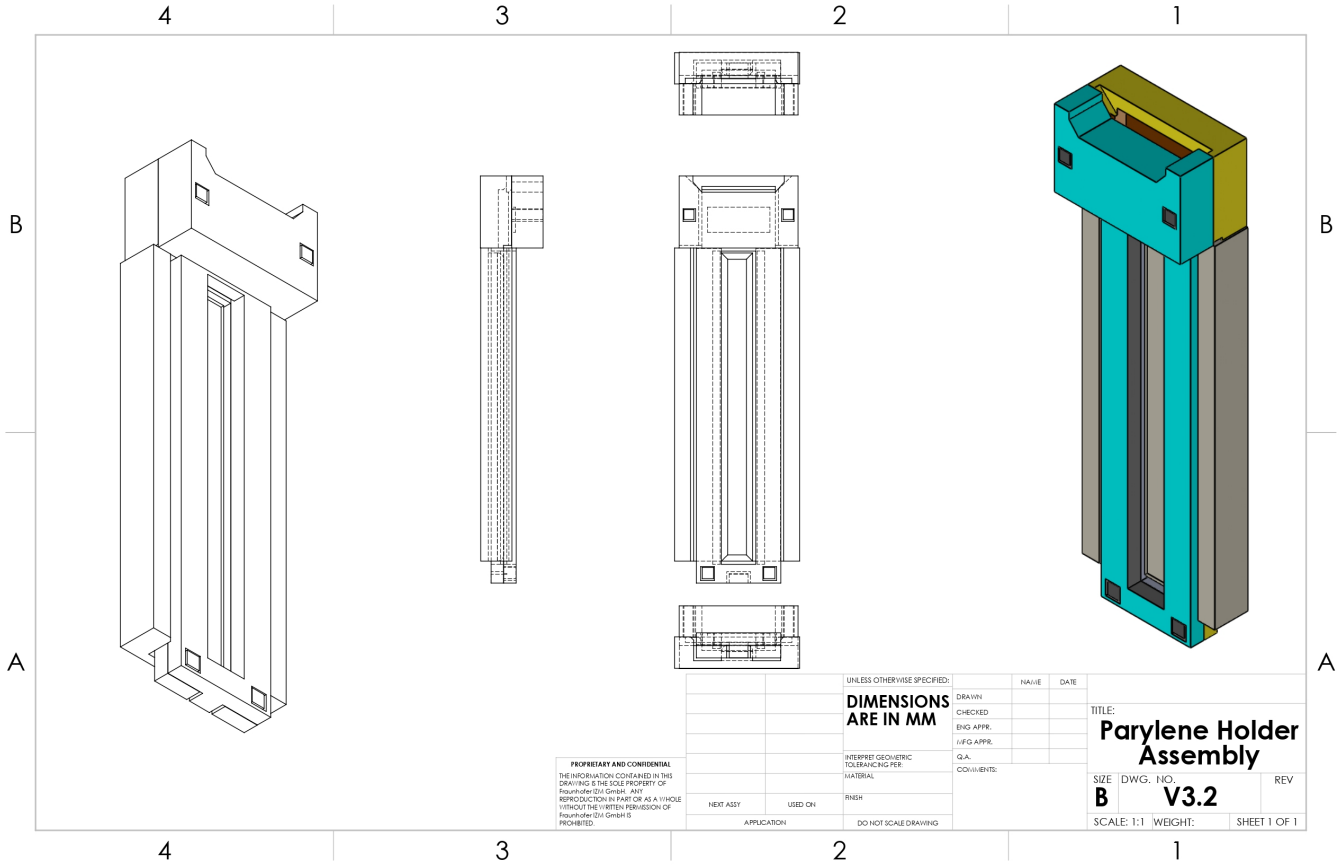

Figure C.24: Solidworks drawing schematics of the Parylene Electrode Holder´s Assembly.

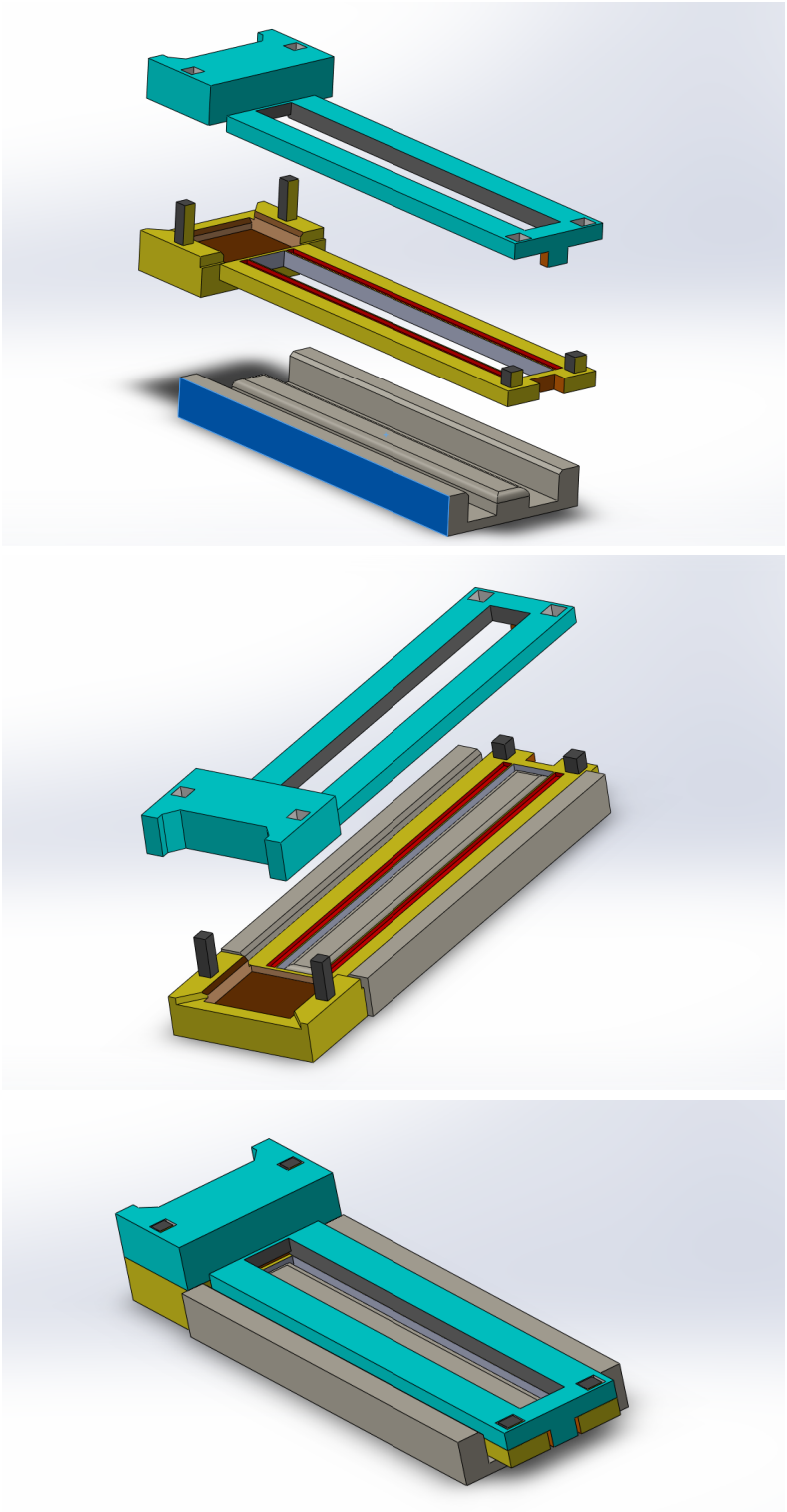

Figure C.25: Solidworks screenshots of the Parylene Electrode Holder´s Assembly. From top to bottom: **Top** - 3 Pieces of the Parylene Electrode Holder aligned, **Center** - The Parylene Electrode Holder should be used by first placing the base piece over the support piece, allowing for the Parylene electrode to be placed without falling through the opening of the base piece. Then the top piece may be placed to fix both sample and top and base pieces, **Bottom** - Once fully assembled, but not taken out of the support, the holder should look like in the screenshot.

Figures C.26 and C.27: Solidworks screenshots and drawing schematics of the Pt foil large return electrode´s body.

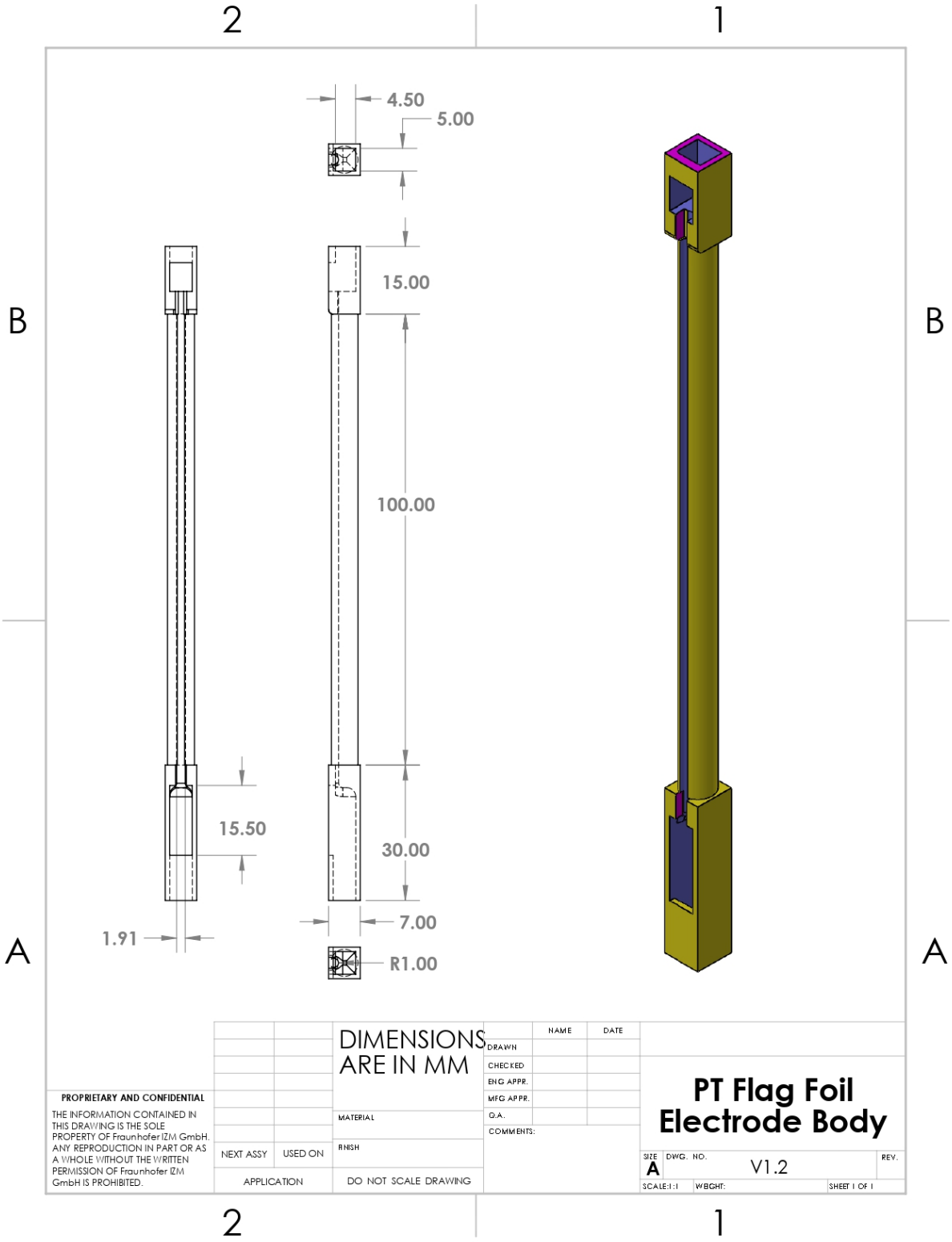

Figure C.26: Solidworks drawing schematics of the Pt foil large return electrode´s body.

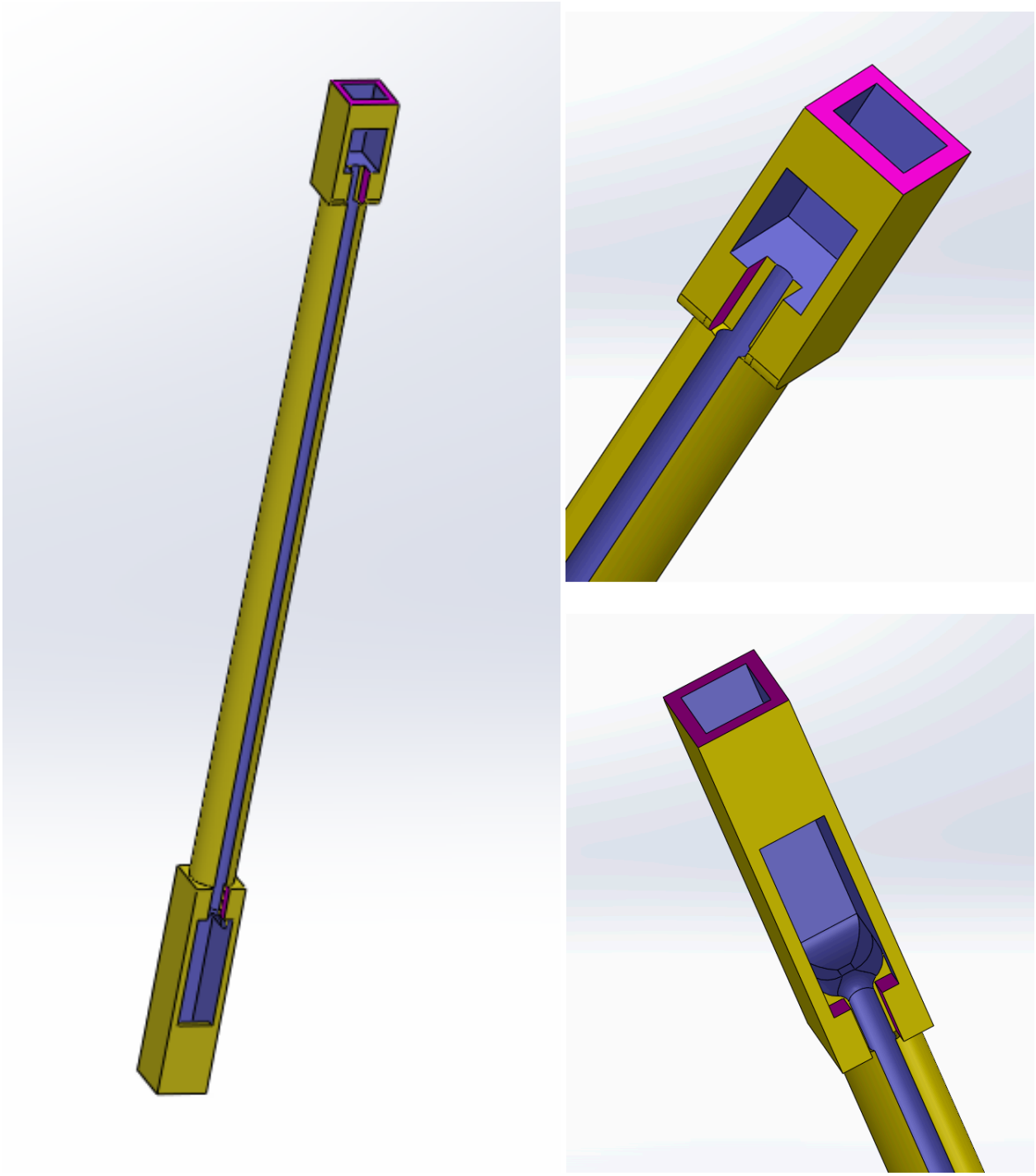

Figure C.27: Solidworks screenshots of the Pt foil large return electrode´s body. From top to bottom, left to right: **Left** - Pt foil large return electrode´s body screenshot showing the full piece, highlighting the groove across it intended for the electrical wire to be kept inside the piece, **Top right** - Pt foil large return electrode´s body screenshot of the opening intended to hold the wire to connect to the setup, **Bottom right** - Pt foil large return electrode´s body screenshot of the opening intended to host the reactive Pt foil end.

Figure C.28 and C.29: Samtec connector build technical sheet and images of the connector adapted to use the Samtec with the electrode samples and the setup

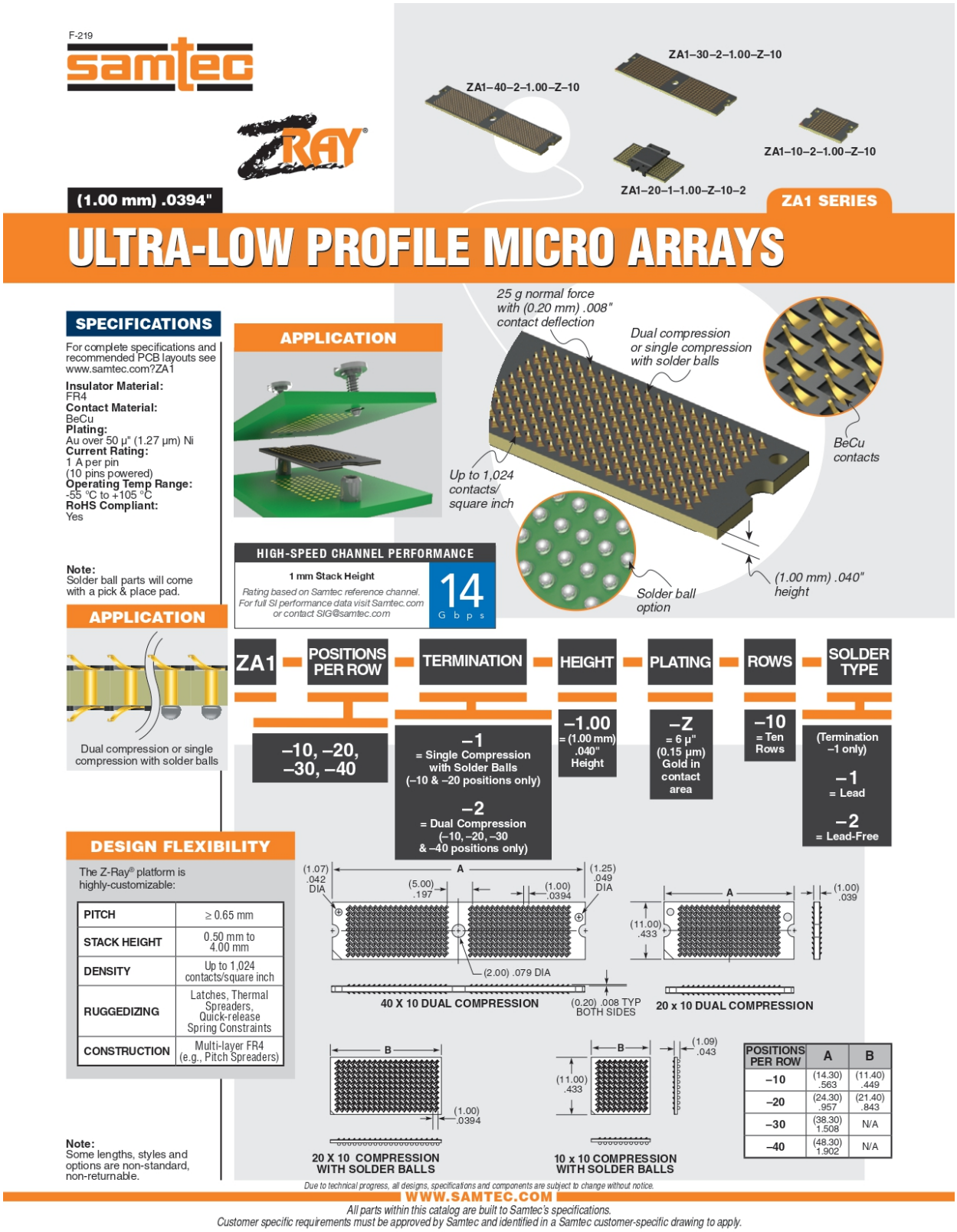

Figure C.28: Technical product sheet for the Samtec Connector

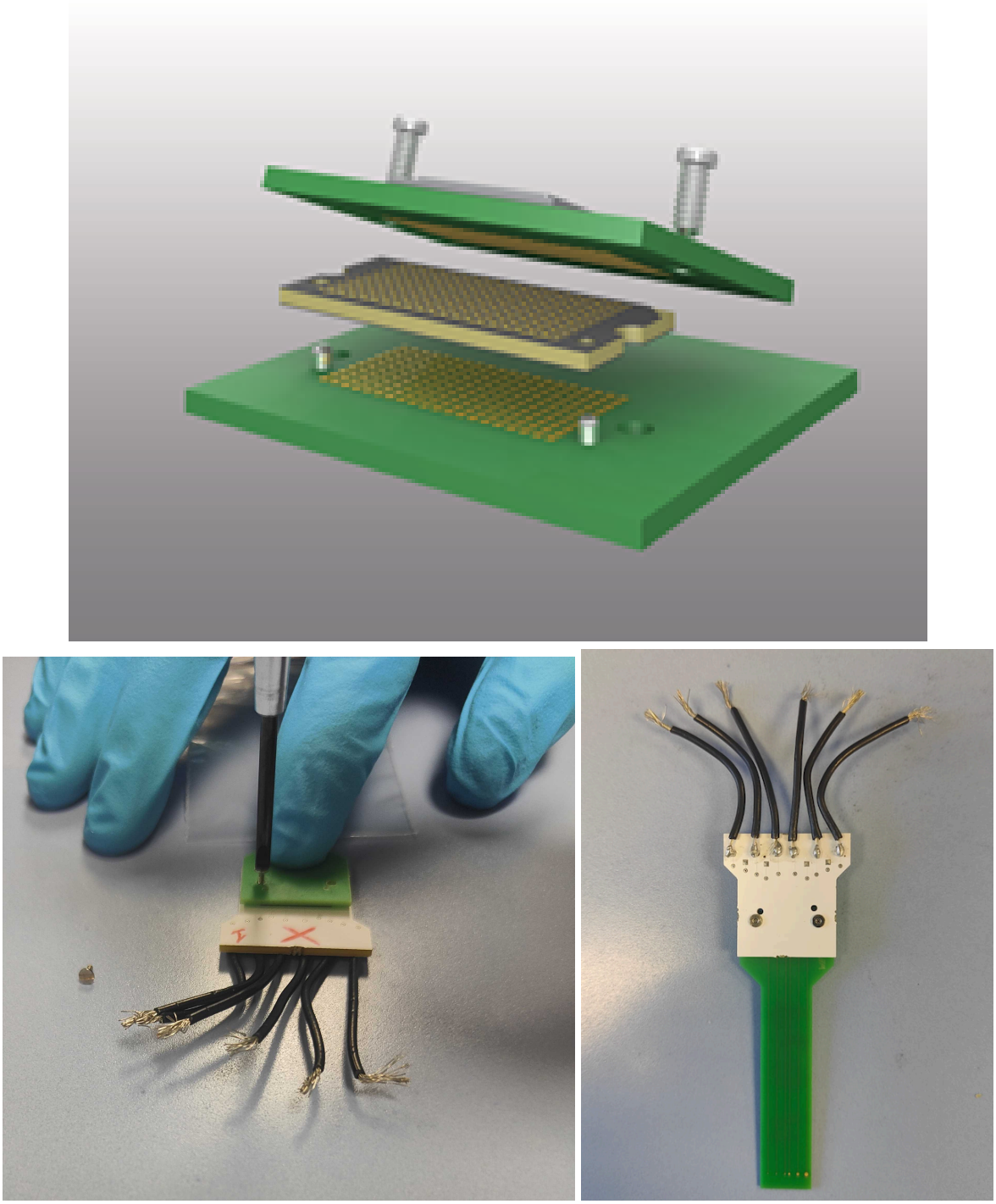

Figure C.29: Diagrams and pictures regarding the assembly of the Samtec connector to the sample electrodes: **Top** - Diagram showing how the Samtec is to be used: sandwiched between the sample electrode and another board where connections can be permanently wired, **Bottom Left** - Process of fixing the sample to the Samtec board and the connections with a pair of screws, **Bottom right** - Image of a sample electrode with the Samtec and wiring fixed to be tested on.

Figures C.30 and C.31: VCCS PCB Schematics

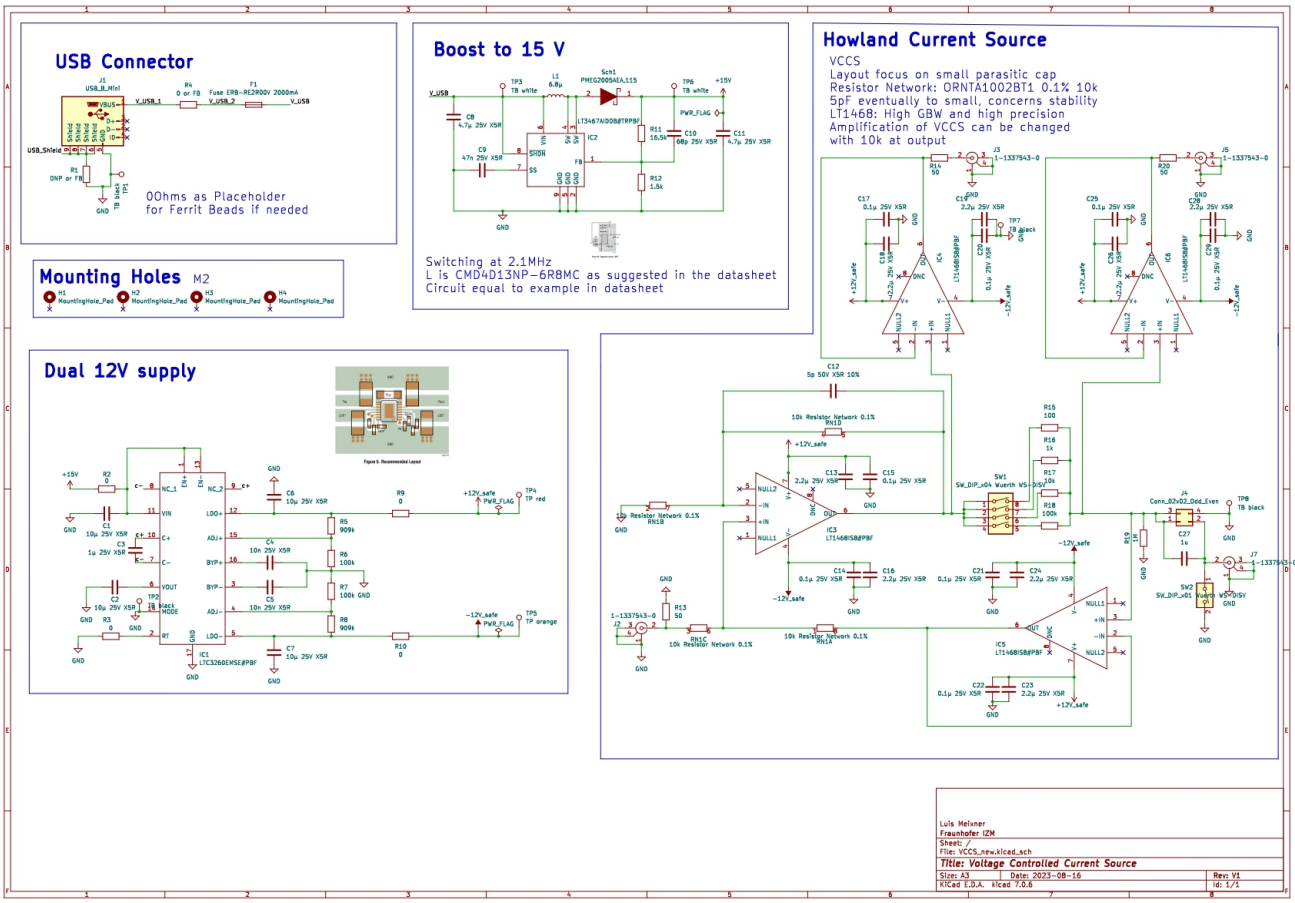

Figure C.30: General Schematic for the VCCS PCB

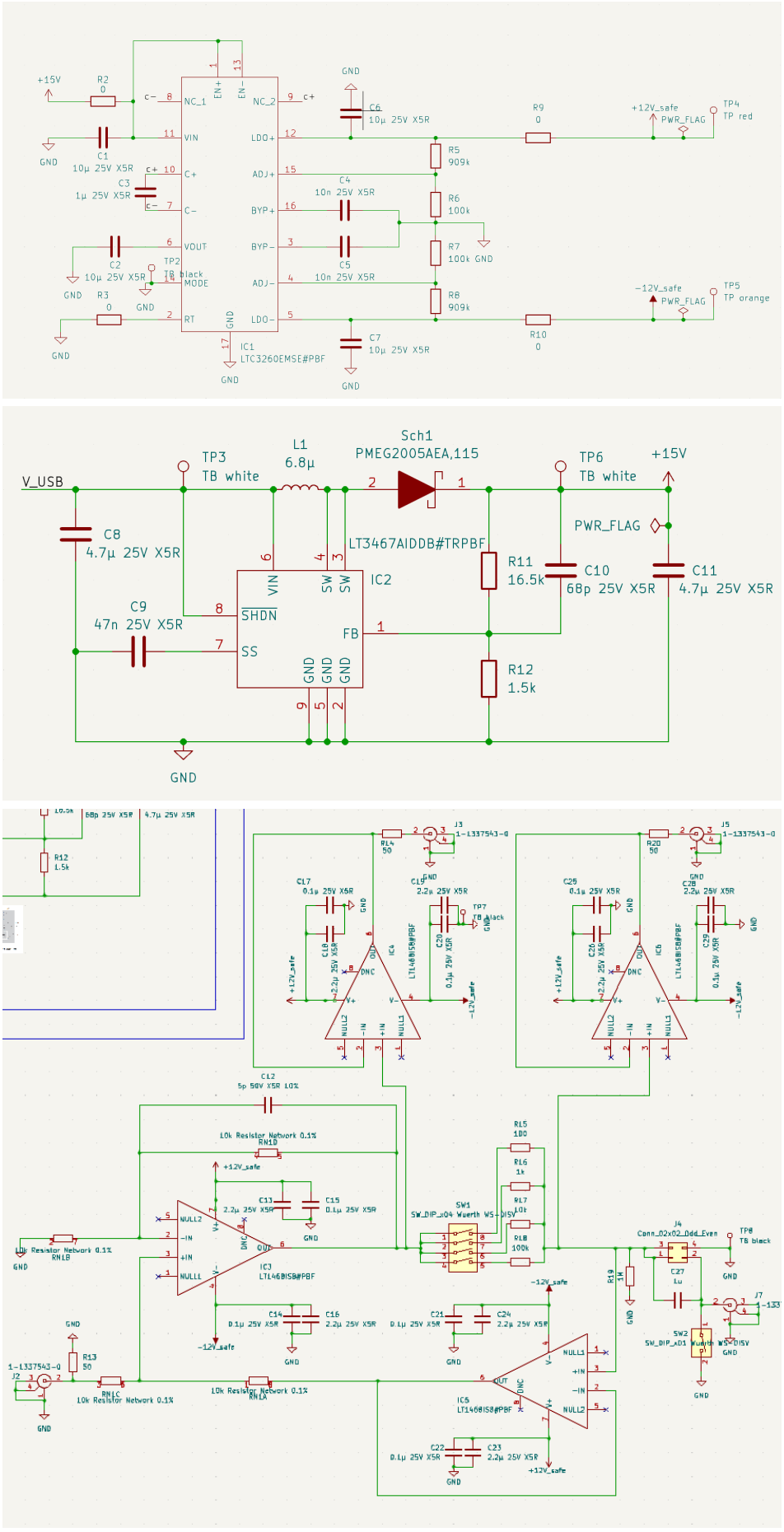

Figure C.31: Close-up of the schematics of individual circuitry blocks used in the VCCS PCB. From top to bottom: **Top** - 12 V supply circuitry schematic, **Middle** - Boosting to 15 V circuitry schematic, **Bottom** - Howland Current Source circuitry schematic.

D Appendix: Electrode Characterization Supplementary Data

Figure D.1: Screenshots from the Gerber file design that was sent to Würth Elektronik to manufacture the sample electrodes.

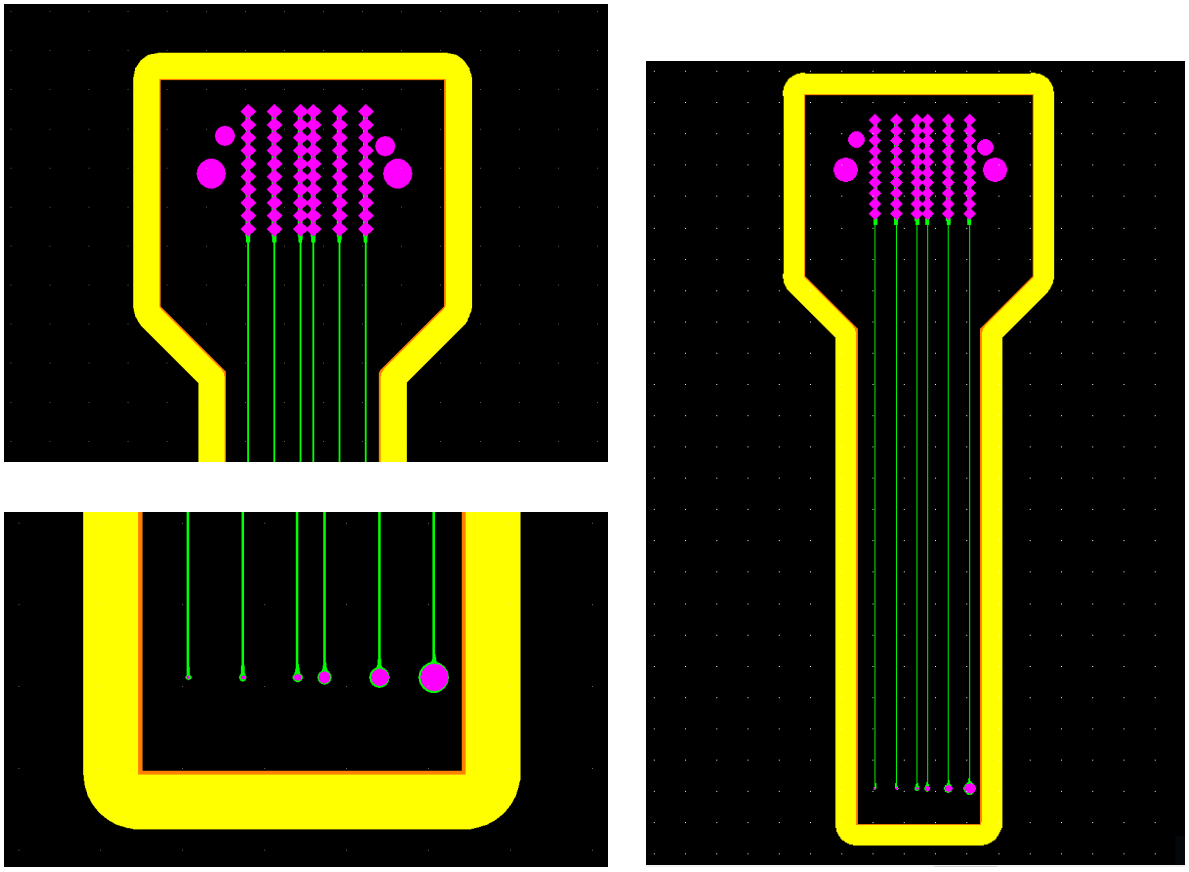

Figure D.1: Screenshots for the Gerber file used in producing the sample electrode. From top to bottom, left to right: **Top Left:** Schematic for the connection section of the sample. It was designed to work with the Samtec connector and its fixing screws. **Right:** Overall schematic for a single sample. **Bottom Left:** Schematic for the section containing the openings of the electrodes. The theoretical opening size progression would be, from left to right: 200 µm, 270 µm, 370 µm, 500 µm, 670 µm, 900 µm

Table D.1: Table with statistics for the measured electrode openings. Row 1 ”Theoretical Diameter” indicates the intended diameter size of the opening when designing the samples. Row 2 ”Usable Samples” shows how many of the 15 ordered samples were viable to measure and use. Rows 3 and 4, ”Average Diameter (µm)” & ”Standard Deviation (µm)” contain the statistics obtained after measuring each opening under the optical microscope.

Theoretical Diameter (µm	Usable Samples	Average Size (µm)	Standard Deviation (µm)
200	13	157,00	5,52
270	15	211,00	7,17
370	15	310,47	5,91
500	14	441,71	5,77
675	15	615,40	9,26
900	15	843,07	7,89

Table D.1: Table containing the statistics of measured dimensions for the electrode openings.

Figure D.2: Optical Microscopy images used in surface characterization of the samples and measurement of their opening diameter.

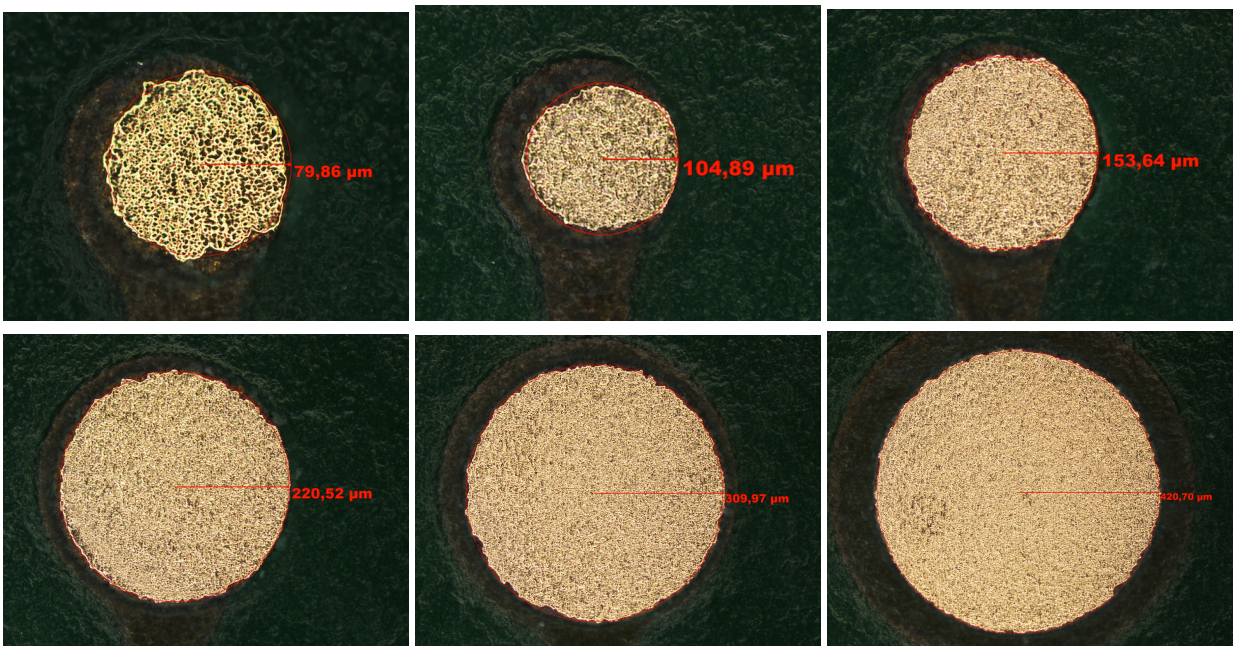

Figure D.2: Optical Microscopy images of sample electrodes using Dark Field lighting. Measurement is of the radius of the circumference in µm. From top to bottom, left to right: **Top Left:** 200 µm opening, measured radius: 79.86 µm. **Top Center** 270 µm opening, measured radius: 104.89 µm. **Top Right:** 370 µm opening, measured radius: 153.64 µm. **Bottom Left:** 500 µm opening, measured radius: 220.52 µm. **Bottom Center** 670 µm opening, measured radius: 309.97 µm. **Bottom Right** 900 µm opening, measured radius: 420,70 µm.

Figure D.3, D.4 & D.5: Interferometry imagery performed on samples both before and after electrochemical testing. Optical microscope images of the same samples are also provided for comparison.

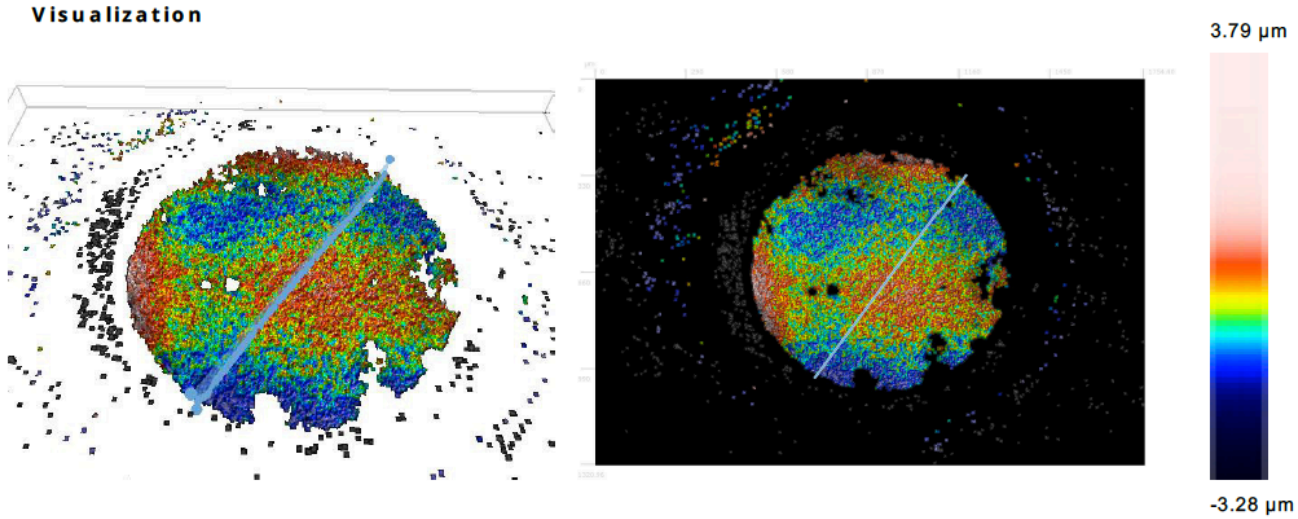

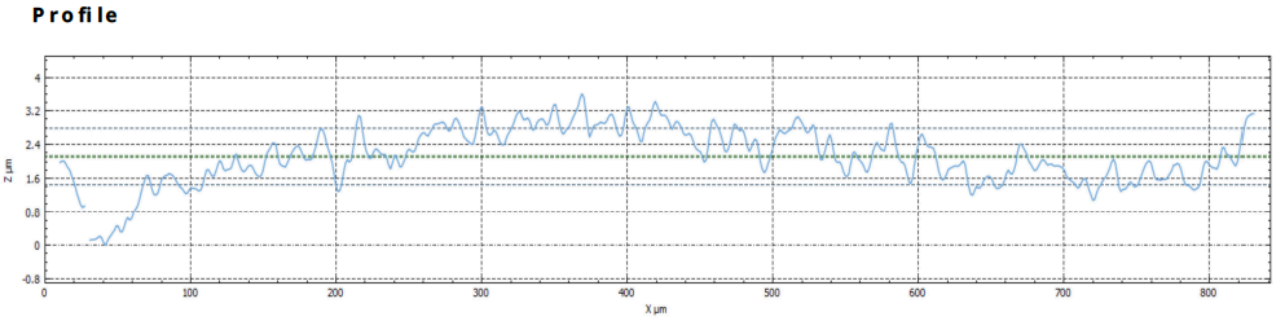

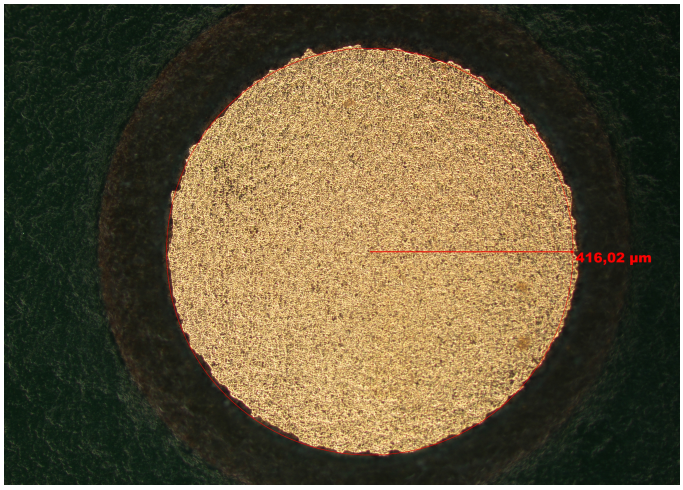

Figure D.3: Top: Interferometry image example of a sample electrode. Image obtained with the MIRAU x10 SR lens. Although the surface presents warping, surface roughness features have dimensions < 1 µm in height and ≈ 10 µm across. **Bottom:** Optical Microscope Image of the same electrode for reference.

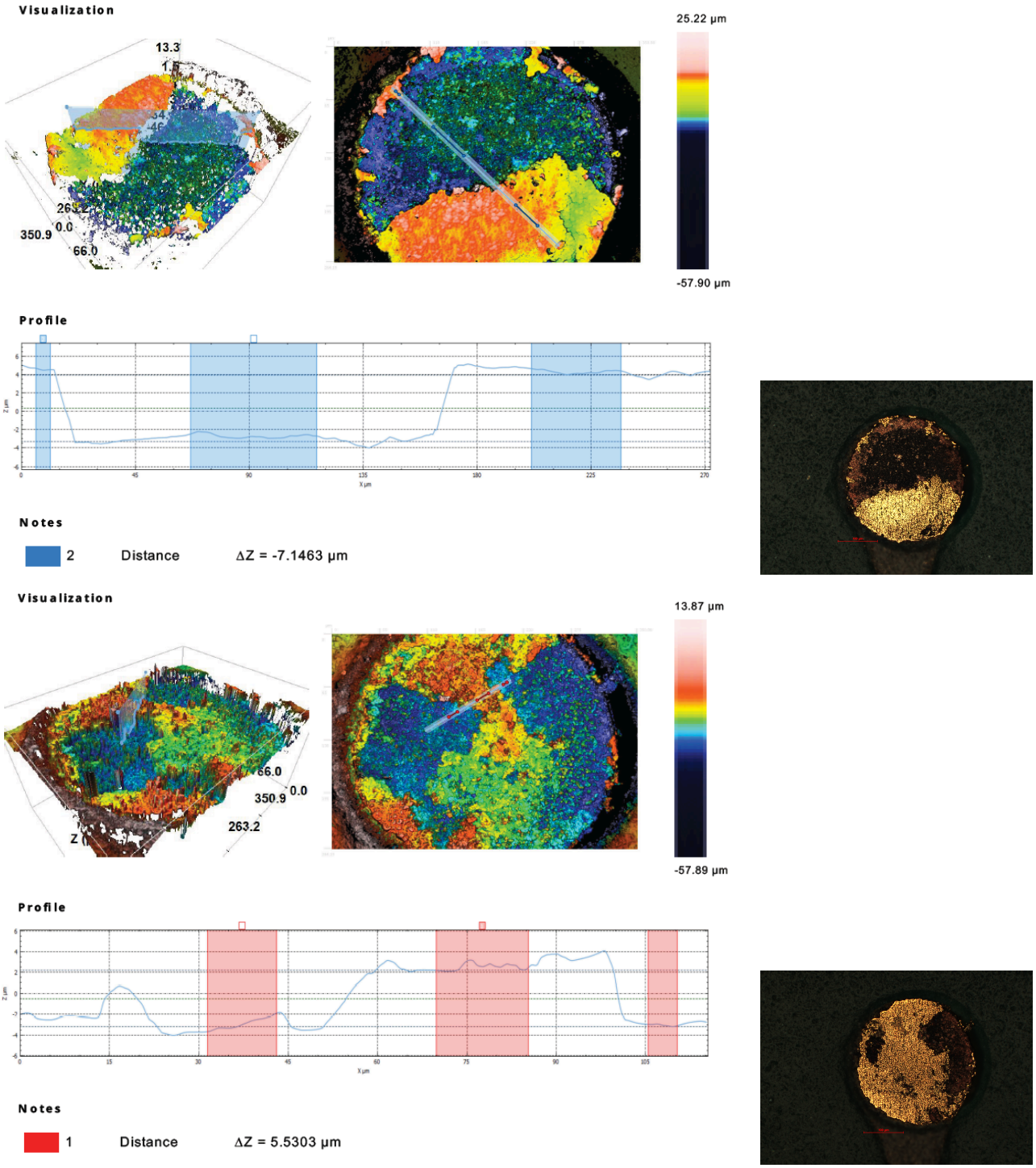

Figure D.4: Examples of topography imaging of samples presenting surface damage after testing. **Top Left:** Confocal microscopy image of PCB9-370µm. Image obtained with the EPI x50 0.9 lens. **Top Right:** Optical Microscope Image of PCB9-370µm for reference. **Bottom Left:** Interferometry image of PCB11-370µm. Image obtained with the MIRAU x50 SR lens. **Bottom Right:** Optical Microscope Image of PCB11-370µm for reference.

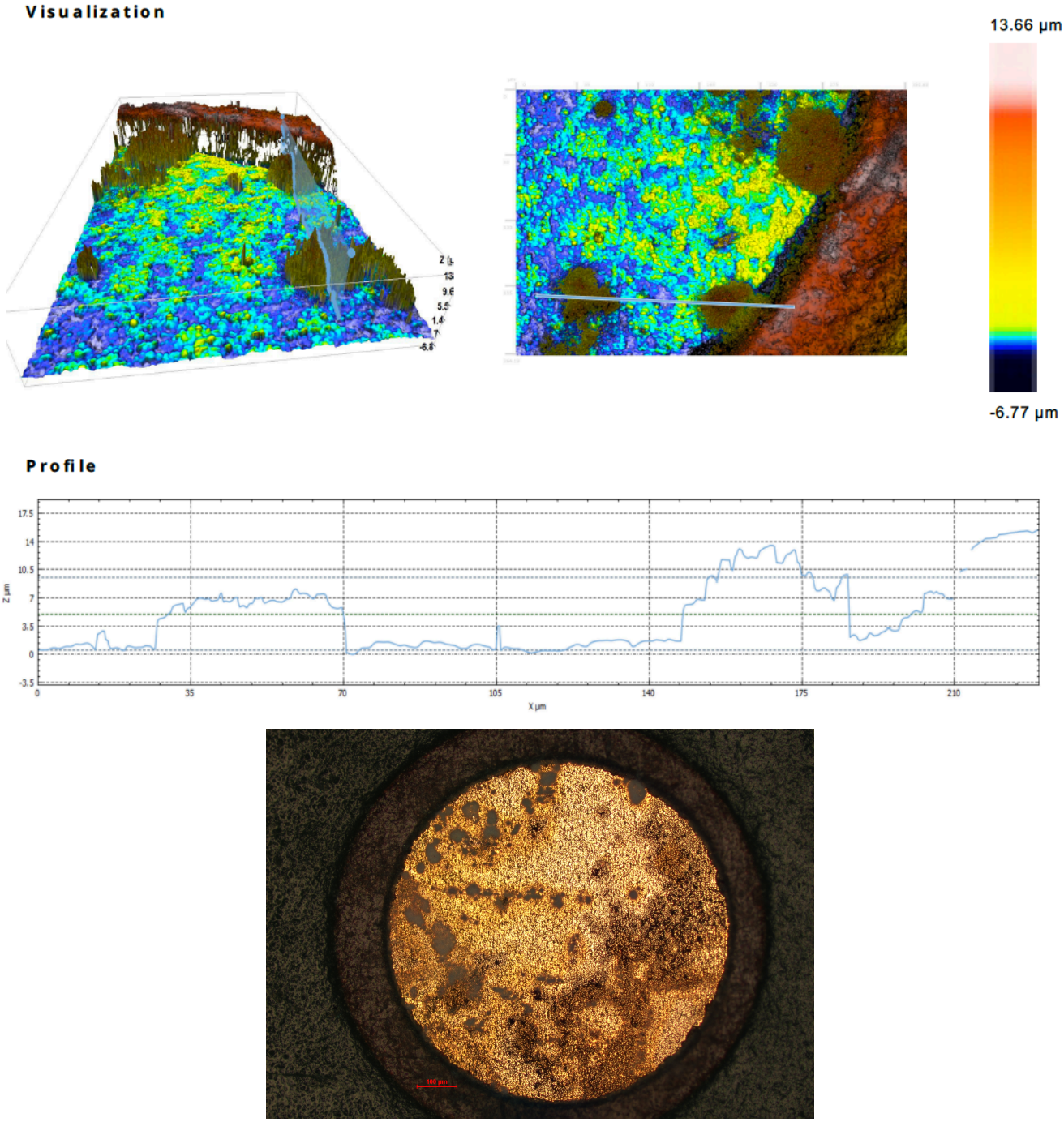

Figure D.5: Top: Interferometry images of a sample electrode presenting deposited residues after testing. Image obtained with the MIRAU x50 SR lens. Residue thickness averages ≈ 7 µm. **Bottom:** Optical Microscope Image of the same electrode for reference.

Figure D.6: Bode plot of the average EIS measured at every size opening category. $|Z|$ and θ are separated for further clarity. Averages are the result of 5 different sample measurements per size category. The shading around the curve represents the calculated standard deviation between the measurements. A dashed line is placed at the 45° threshold in the Phase Angle plot.

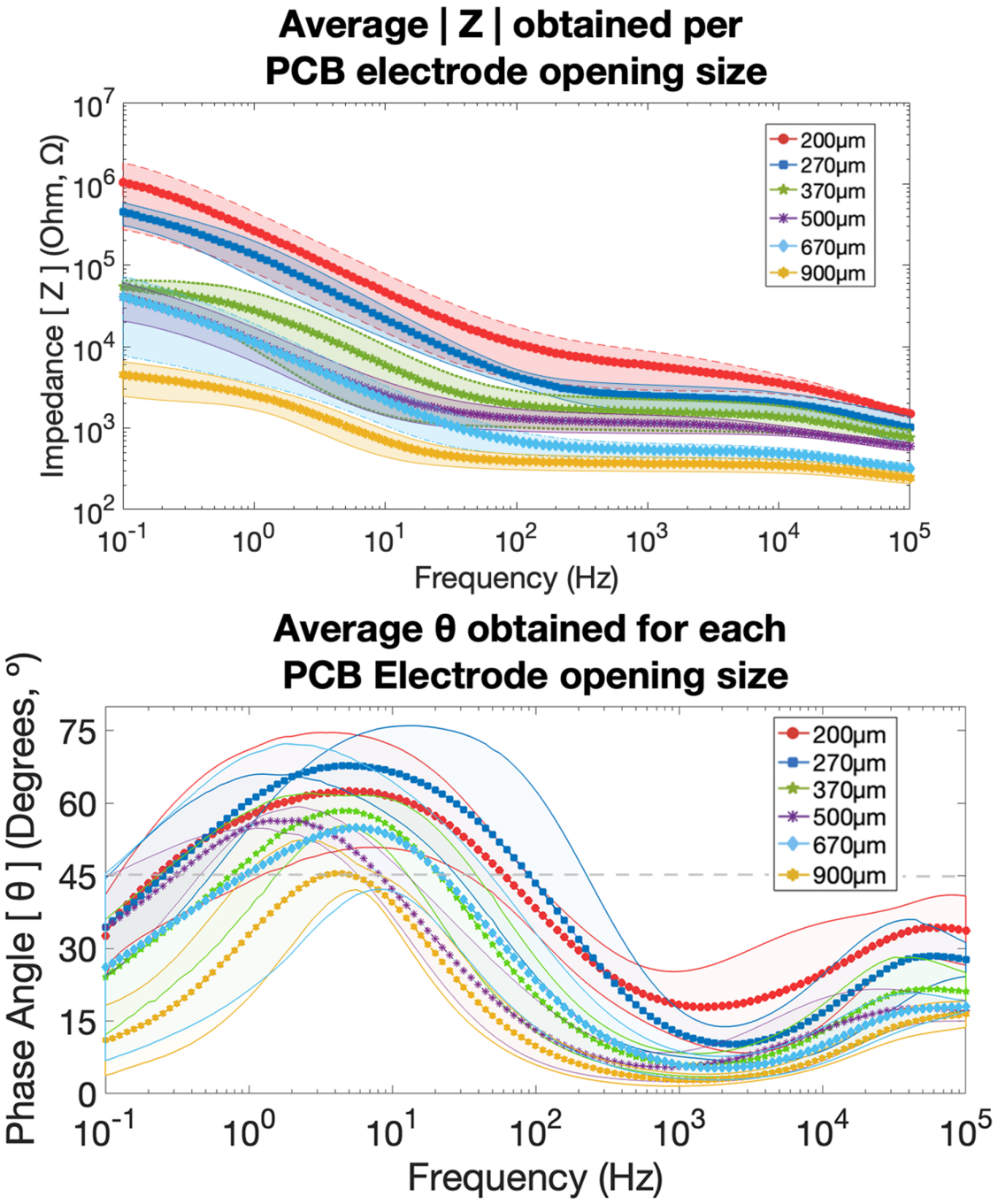

Figure D.6: Top: $|Z|$ average curves for the six opening size categories. The shaded area around each curve represents the standard deviation calculated from averaging measurement data from 5 samples. **Bottom:** θ average curves for the six opening size categories. The shaded area around each curve represents the standard deviation calculated from averaging measurement data from 5 samples

Figure D.7: Bode plots of the average EIS measured at each opening size electrode. $|Z|$ is plotted in a continuous, bold line, while θ is plotted in a discontinuous, circle-marked line.

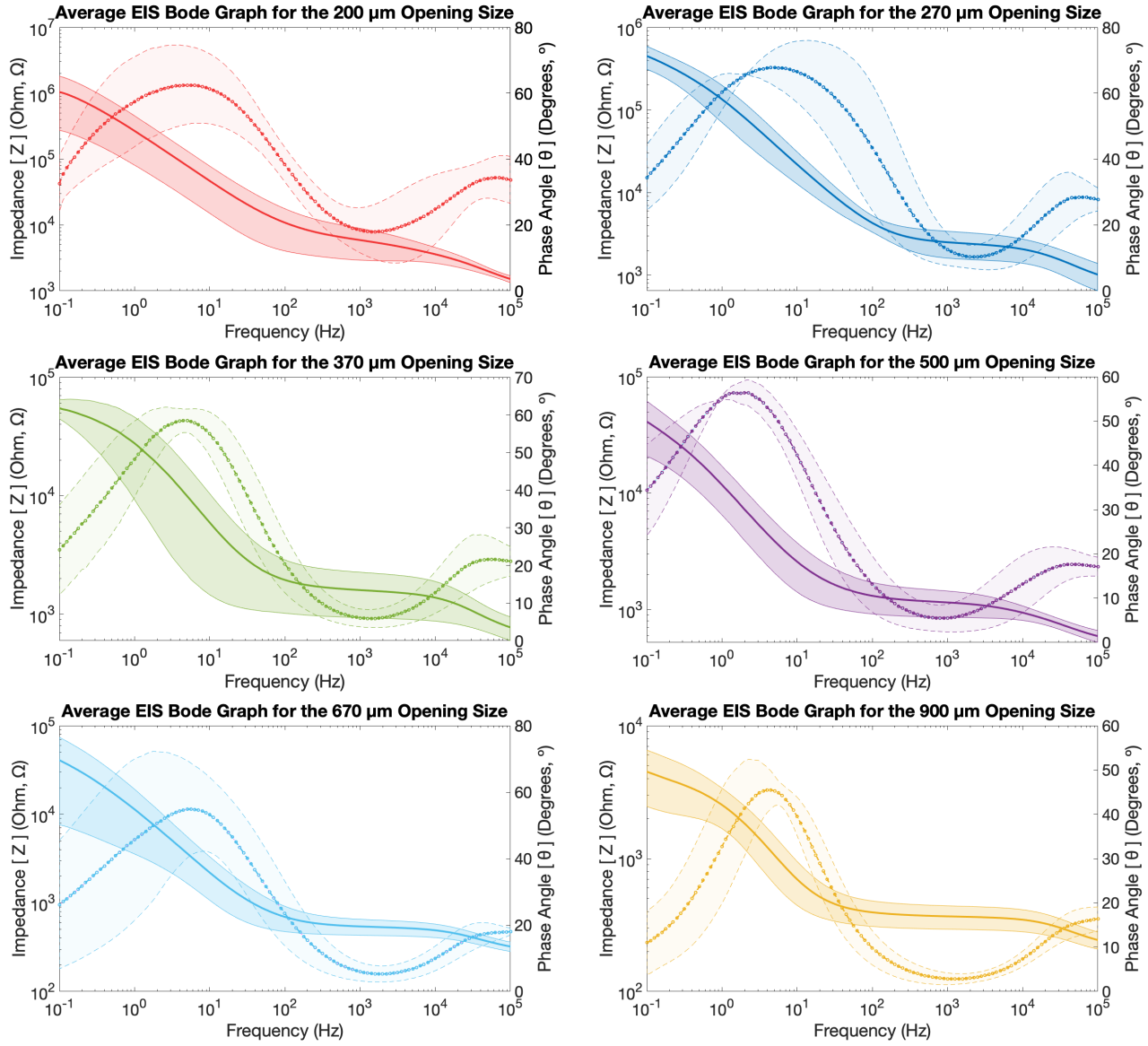

Figure D.7: Bode plots of the average EIS measured at each electrode´s opening. From top to bottom, left to right: **Top Left** Bode plot from 200 µm opening size category. **Top Right** Bode plot from 270 µm opening size category. **Center Left** Bode plot from 370 µm opening size category. **Center Right** Bode plot from 500 µm opening size category. **Bottom Left** Bode plot from 670 µm opening size category. **Bottom Right** Bode plot from 900 µm opening size category.

Figures D.8, D.9 & D.10: Figures containing individual sample data measurements. Figure D.8 shows Bode plots for 3 sample EIS measurements. Figure D.9 shows CV scan plots for 3 sample measurements, with their stable cycle highlighted in dark red. The Stable cycle number and CSC value can be found in the legends. Figure D.10 shows plots for 3 sample VT measurements, plotting both the input current biphasic pulse and the output voltage transient.

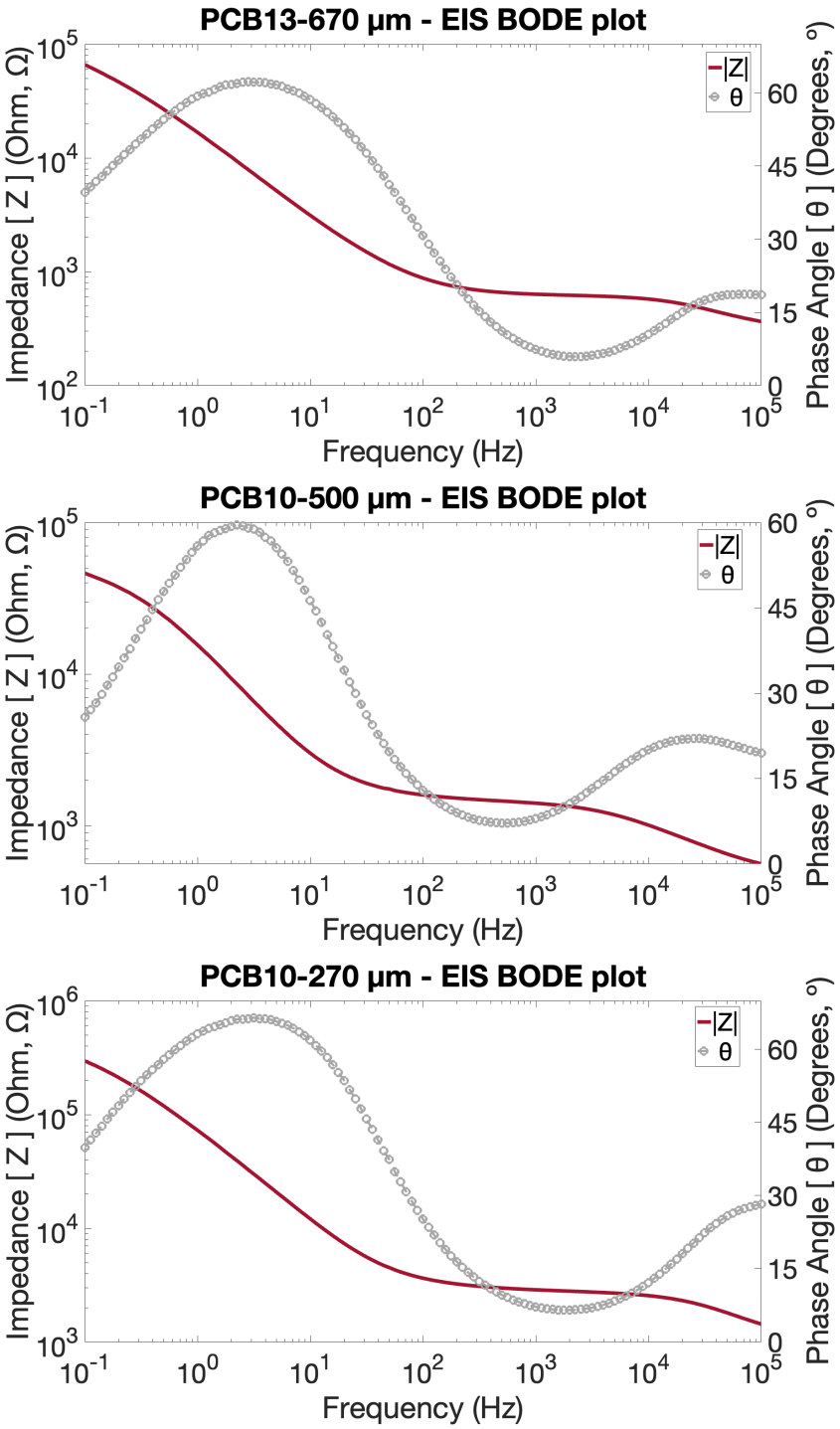

Figure D.8: A solid red line represents $|Z|$ and θ is represented by a grey dashed line with circular markers. **Top:** Bode plot of the EIS measurement of sample PCB13-670 µm. **Center:** Bode plot of the EIS measurement of sample PCB10-500 µm. **Bottom:** Bode plot of the EIS measurement of sample PCB10-270 µm.

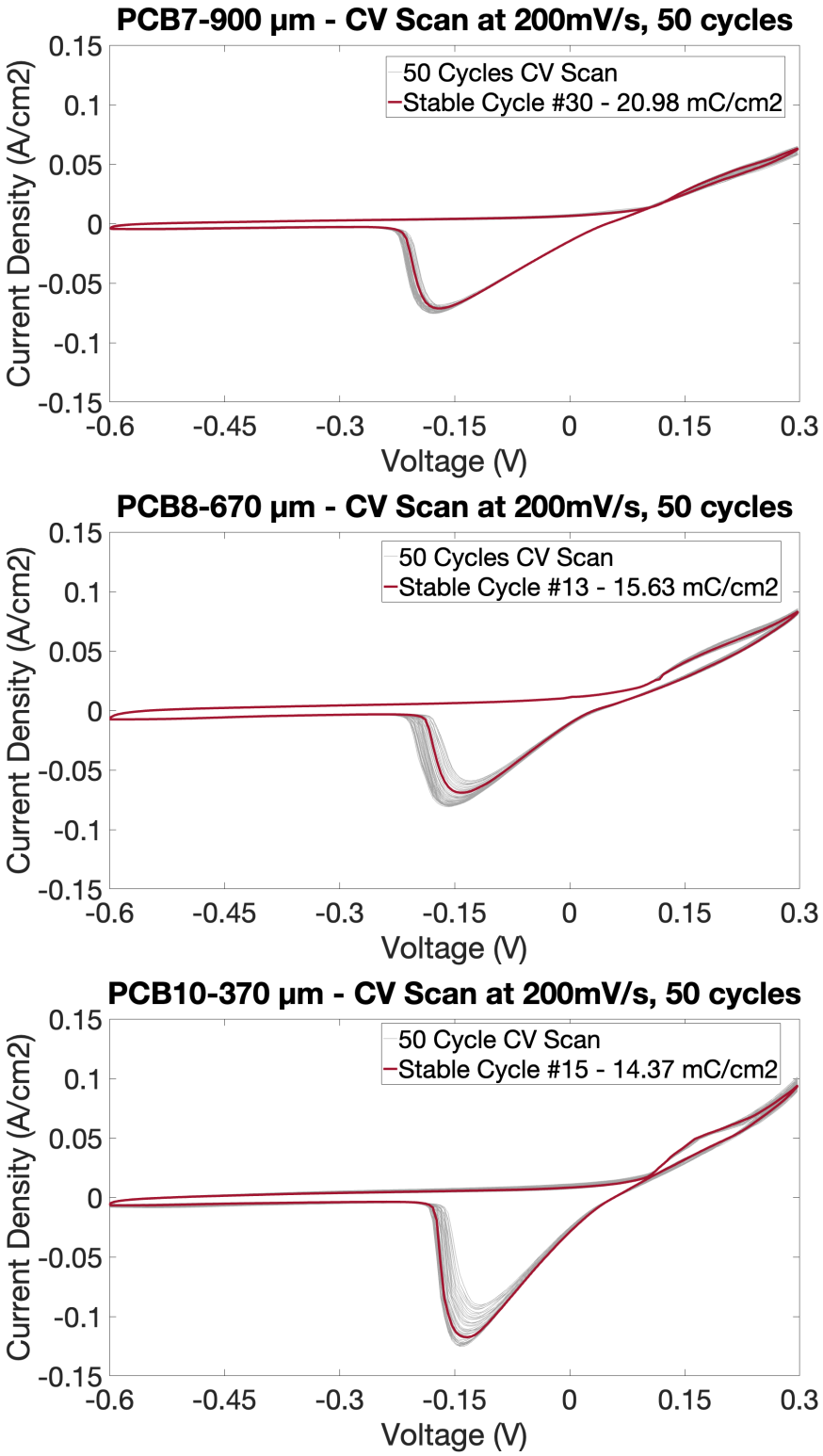

Figure D.9: Solid red lines indicate the stable cycle, while grey lines show the whole voltammetry scan. Information on which cycle achieved stability, and the CSC of such cycle can be found in the respective legends. **Top:** CV Scan at 200 mV/s of sample PCB7-900 µm. **Center:** CV Scan at 200 mV/s of sample PCB8-670 µm. **Bottom:** CV Scan at 200 mV/s of sample PCB10-370 µm.

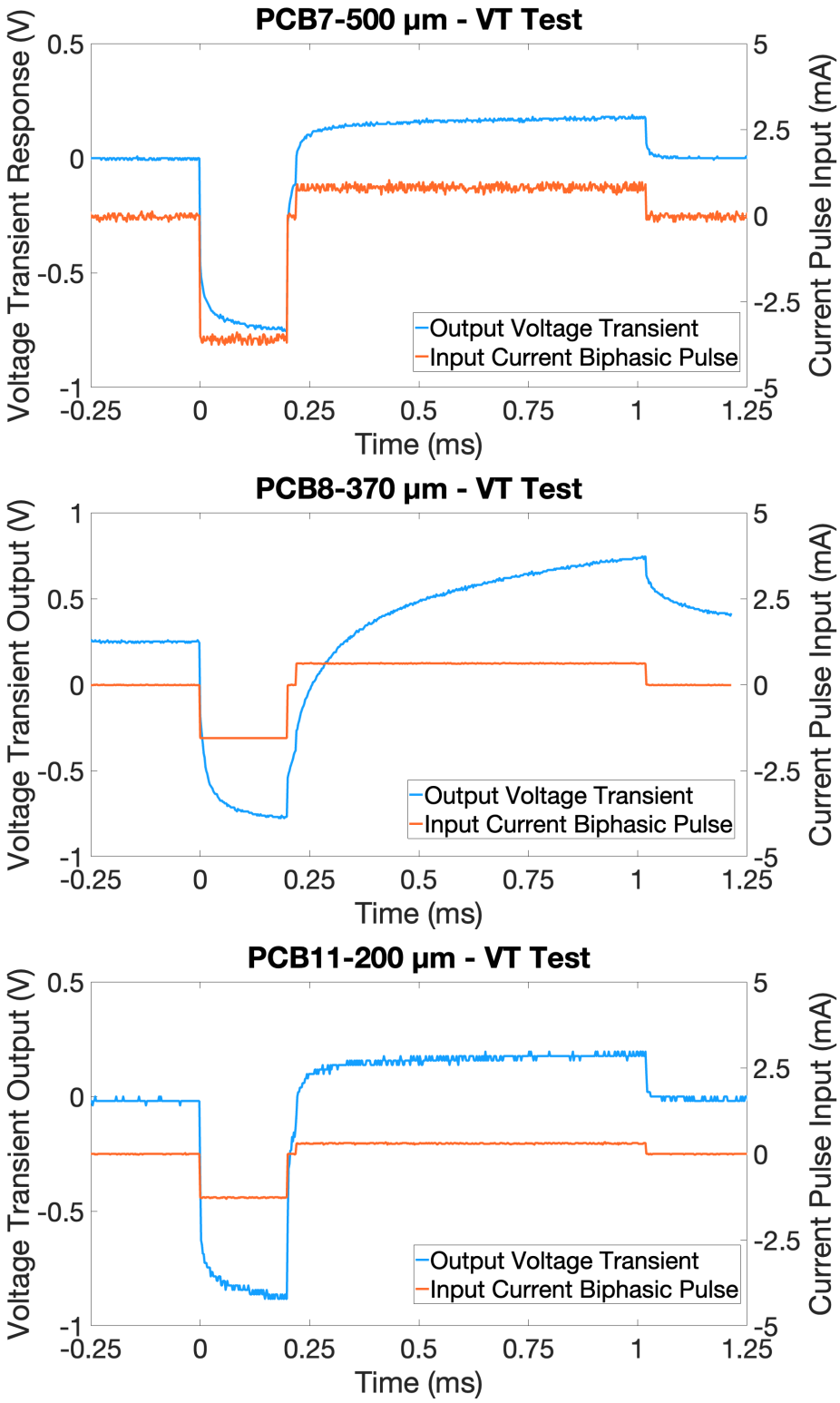

Figure D.10: The orange curve (right vertical axis) plots the input current biphasic pulse, while the blue curve (left vertical axis) plots the output voltage transient **Top:** Voltage transient measurement for sample PCB7-500 µm. **Center:** Voltage transient measurement for sample PCB8-370 µm. **Bottom:** Voltage transient measurement for sample PCB11-200 µm.

Table D.2: Table containing all main electrochemical characterization metrics, averaged out by electrode opening size category. The number between brackets near the Size category indicates the amount of samples for that category measured. Each measurement unit can be found between brackets in the metrics column next to the test reported.

Table D.2: Table summarizing all main electrochemical measurements, averaged by opening size category.

Metrics	Size Averages					
	900 µm (7)	670 µm (7)	500 µm (7)	370 µm (7)	270 µm (7)	200 µm (6)
CIC (mC/cm^2))	0,15	0,20	0,37	0,53	0,84	1,19
CSC-500 (mC/cm^2)	17,70	17,58	27,65	41,19	48,77	25,12
CSC_{cath}-500 (mC/cm^2)	11,04	10,66	16,86	26,24	31,25	14,75
ISR @ 500	0,01	0,02	0,01	0,03	0,03	0,14
CSC-200 (mC/cm^2)	11,80	13,34	19,24	32,08	25,65	15,72
CSC_{cath}-200 (mC/cm^2)	8,96	9,48	14,34	23,25	17,07	10,35
ISR @ 200	0,01	0,02	0,02	0,02	0,05	0,21
CSC-50 (mC/cm^2)	5,92	5,34	7,83	17,08	12,79	6,22
CSC_{cath}-50 (mC/cm^2)	4,40	3,94	5,76	12,16	9,18	4,10
ISR @ 50	0,04	0,07	0,08	0,10	0,12	0,32
Z @ 1 KHz (Ω)	541,34	889,33	1706,07	2506,69	5057,43	15208,40
No f_{cutoff} (# of samples)	3	1	0	0	0	0
Low f_{cutoff} (Hz)	0,96	0,49	0,64	0,80	0,32	0,63
High f_{cutoff} (Hz)	82,83	457,15	5700,76	4083,46	5578,71	20217,12

Figure D.11: Microscopy images used to assess the surface damage incurred after performing mock CV measurements at different negative bounds. Tests were run at 50 mV/s for 15 cycles. The positive bound was set to +0.3 V in all tests. Tests performed started at -0.3 V and increased the negative bound by -0.1 V at each test. As the surface presented significant damage at -0.8 V, the test ended there. After closer examination, and to ensure the survivability of the samples while keeping the most extensive window possible, the negative bound was set to -0.6 V.

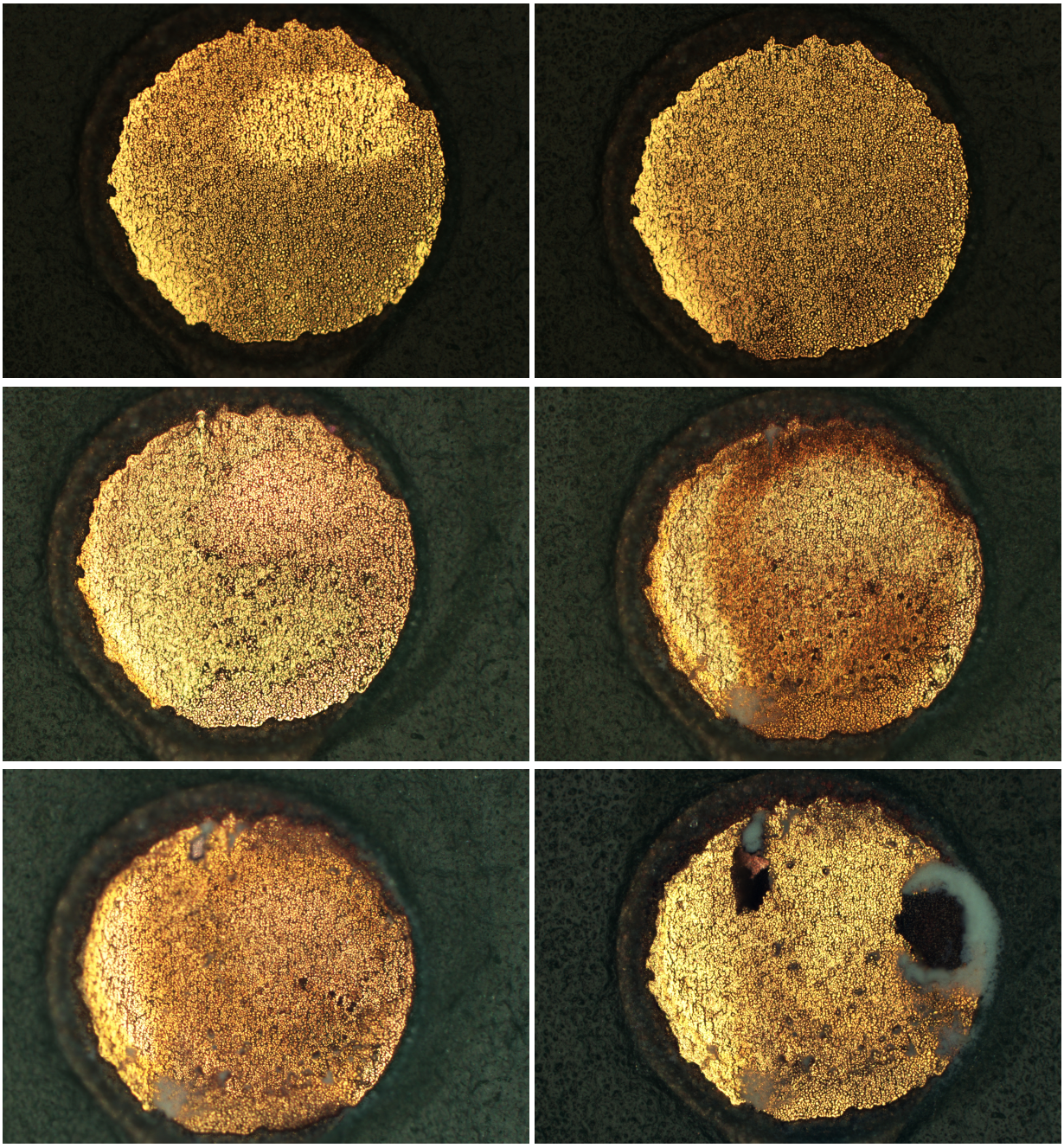

Figure D.11: Microscopy images of sample electrode PCB2-500µm, after undergoing CV stressing at different voltage windows. Tests were performed at 50 mV/s for 15 cycles. From top to bottom, left to right: **Top Left** Surface state after testing from -0.3 V to +0.3 V. **Top Right** Surface state after testing from -0.4 V to +0.3 V. **Center Left** Surface state after testing from -0.5 V to +0.3 V. **Center Right** Surface state after testing from -0.6 V to +0.3 V. **Bottom Left** Surface state after testing from -0.7 V to +0.3 V. **Bottom Right** Surface state after testing from -0.8 V to +0.3 V.

Figure D.12 and Equations D.1 to D.4: Methods followed to build equivalent circuit models from Nyquist plot data. To build basic models, 4 elements were identified in the Nyquist plots.

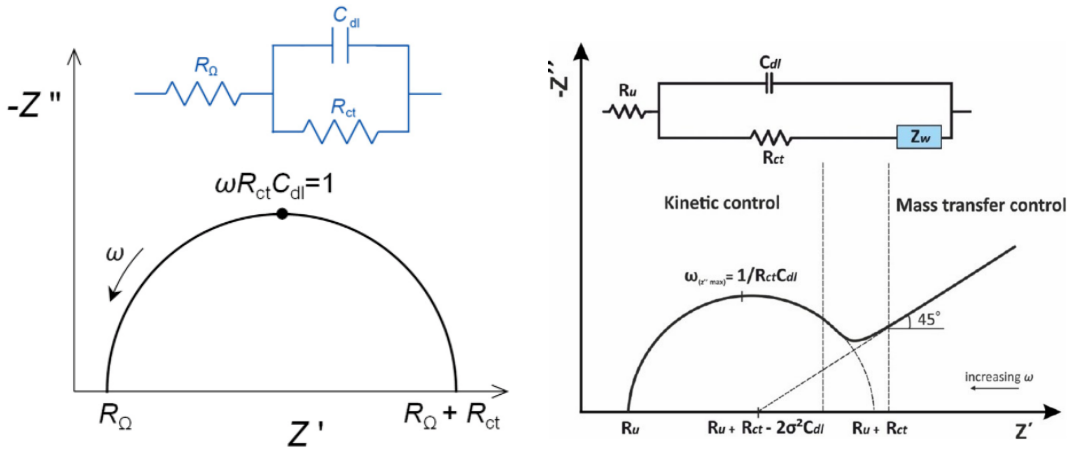

Figure D.12: Diagrams showing how the different equivalent circuit components can be extracted from an EIS Nyquist plot. **Left** Simple single layer electrode modelled with R_Ω,R_{ct} and C_{dl} components. Extracted from Bret *et al.* 2022 [45]. **Right** Standard Nyquist plot with Warburg Impedance effect, modelling a Randles circuit. By finding the intersection of the slope with the ReZ axis σ can be determined. Extracted from Lazanas *et al.* 2023 [16].

- **Cell Resistance (R_Ω, also R_{u}):** The electrochemical resistance imposed by the medium in which the experiment takes place. It can be extracted by evaluating Z at the highest frequency along the ReZ axis.
- **Electron Transfer Resistance (R_{ct}, also R_{t}):** Determined by the electrochemical kinematics of the reacting species, R_{ct} models the resistance experienced by ions exchanged in a faradaic process. R_{ct} is identified in the Nyquist plot as it appears as local minima in the curve. Previous resistor values must be accounted for and subtracted from the value of ReZ at the minimum.

$$ReZ = R_\Omega + R_{\text{ct}} \tag{D.1}$$

- **Double-layer capacitance (C_{dl}):** Determined by the electrochemical kinematics of the reacting species, C_{dl} models the impedance experienced by ions exchanged in a capacitive process. By observing the curve points with ImZ maxima, the frequency (ω, in radians per second) at which maximum capacitance occurs can be extracted. From there, C_{dl} is calculated as such:

$$C_{\text{dl}} = \frac{1}{j\omega Z} \tag{D.2}$$

- **Warburg Effect Impedance (Z_{W}):** This component attempts to model the difficulty for redox species to be transported to the surface of the electrode, given a semi-infinite linear diffusion process. It is frequency-dependent and behaves similarly to a resistor and capacitor in series. That is why it is often modelled with the value of σ:

$$Z_{\text{W}} = R_{\text{W}} + C_{\text{W}} = [\sigma\omega^{-\frac{1}{2}} - j(\sigma\omega^{-\frac{1}{2}})] \tag{D.3}$$

  To obtain σ and model Z_{W}, the characteristic low-frequency 45° slope of the Nyquist plot must be identified. The intersecting point of this slope with the ReZ axis is necessary to calculate σ:

$$Z = R_\Omega + R_{\text{ct}} - 2\sigma^2 C_{\text{dl}} \tag{D.4}$$

These four components are the most commonly used to build circuit models, usually to make the Randles circuit (Figure D.12). Additional components such as inductors (L) or constant phase elements (Z_{CPE}) can also be used in models. As extracting values for them can be challenging, curve-fitting software has been designed to build accurate inductor and Z_{CPE} models. However, this study was left out as modelling was not automated.

In the case of measurements taken without the entire bandwidth necessary to show all the necessary features, it is possible to estimate the theoretical "ideal" value of R_{ct}. Given that an ideal behaviour would produce a semi-circular plot, R_{ct} can be estimated by taking the distance in the ReZ axis between R_Ω and C_{dl} as the radius of that semi-circumference. This is also useful for determining R_{ct} in samples with Z_{W}, as shown in Figure D.12.

Figures D.13, D.14 & D.15: Equivalent Circuit models built from EIS data as Nyquist plots. In D.14 & D.15, Nyquist plots can be seen to illustrate what plotted data looked like. Further information on how to build the equivalent circuit models from the Nyquist data can be found in the previous Appendix section (figure D.12), which closely follows the indications proposed in Lazanas *et al.* 2023 review, among others [16, 53, 54, 55, 45].

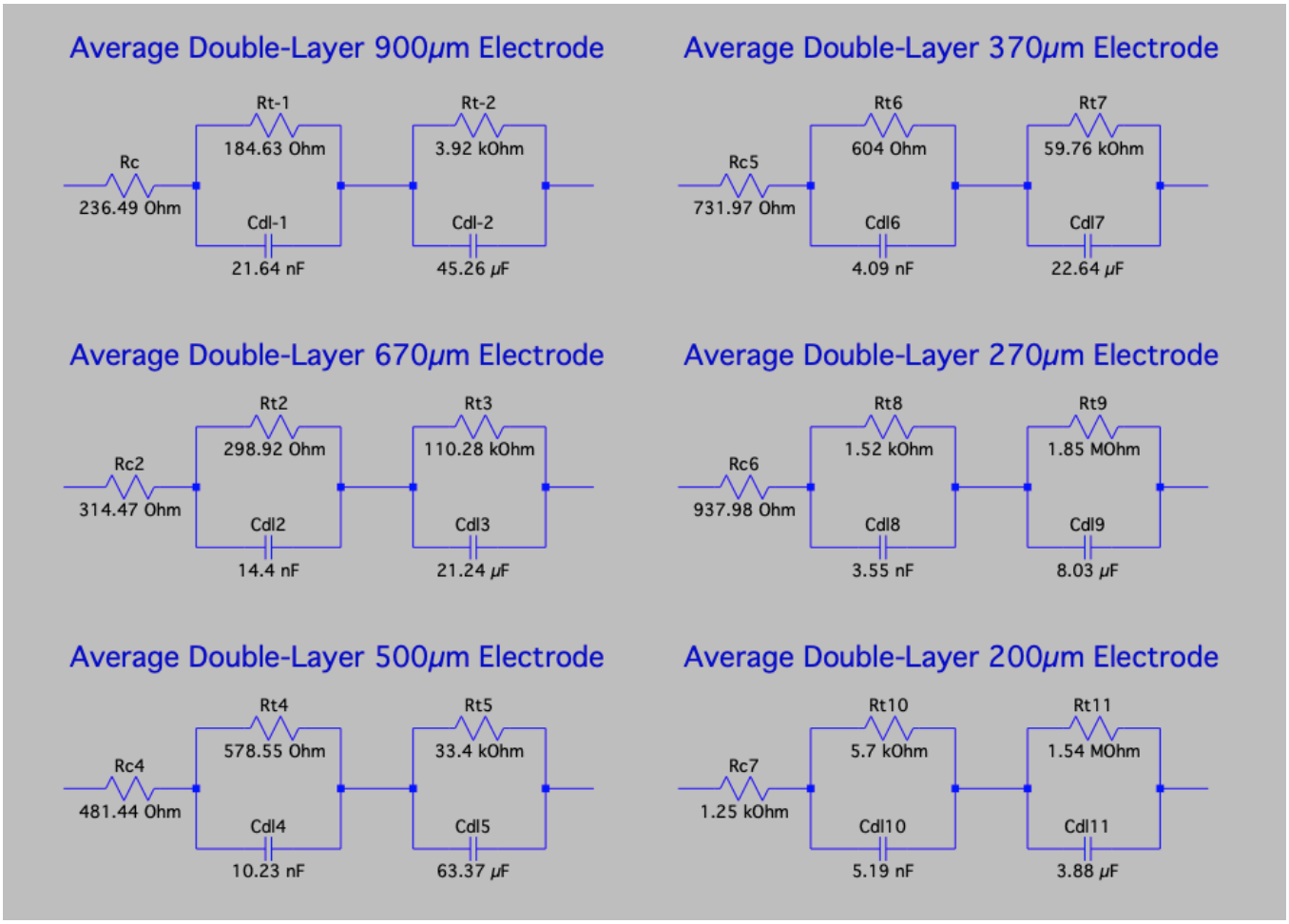

Figure D.13: Equivalent Circuit Model of the average double layer circuit model at each size opening. Following the individual model data, circuit components were averaged over the three models per size category available.

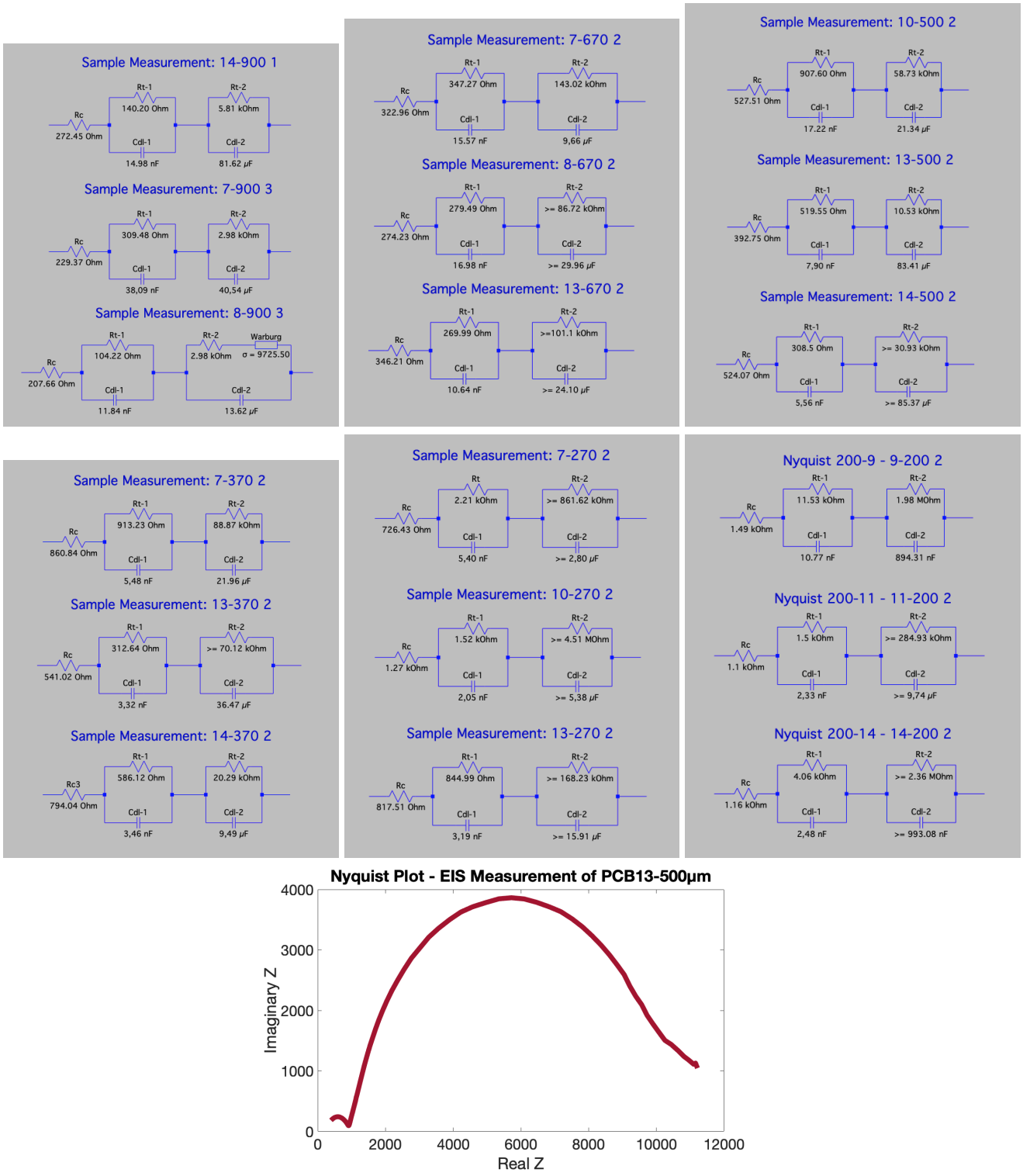

Figure D.14: Circuit models built from EIS Nyquist data. When R_{ct} or C_{dl} are preceded by ">=", it is to indicate that the current value is only an estimate due to the bandwidth of the EIS not being wide enough. From top to bottom, left to right: **Top Left** 900 µm opening model circuits. **Top Center** 670 µm opening model circuits. **Top Right** 500 µm opening model circuits. **Bottom Left** 370 µm opening model circuits. **Bottom Center** 270 µm opening model circuits.**Bottom Right** 200 µm opening model circuits.

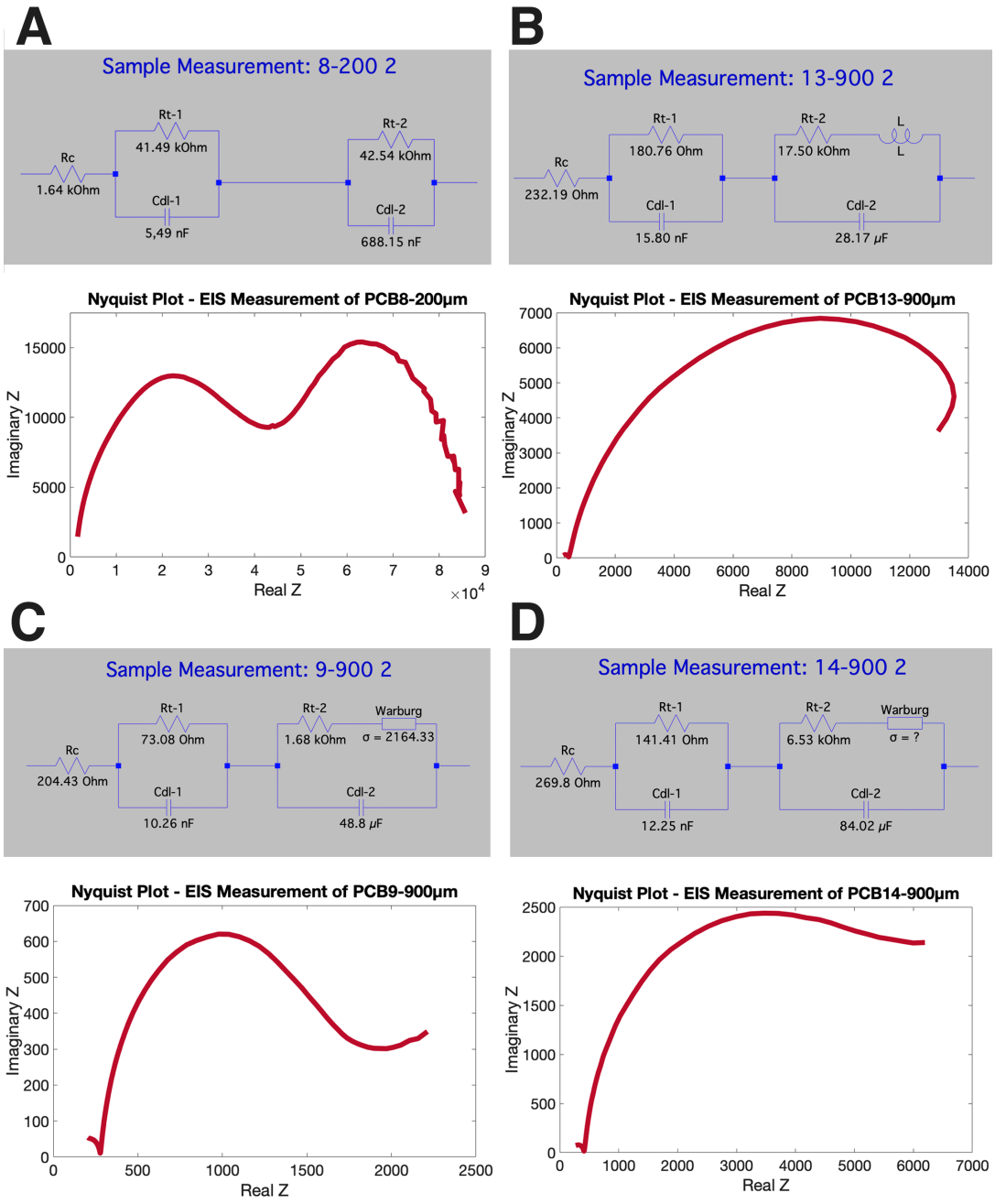

Figure D.15: Circuit models built from EIS Nyquist data of samples that presented abnormal EIS readings. Different elements are included in the circuits, such as Warburg impedances and inductors. From top to bottom, left to right: **A** Double-layer circuit formed by two resistive layers, with values for the resistances higher than other equally sized samples and similar between layers. **B** Sample showing inductive behaviour in its low-frequency spectrum. The element is left without quantifying due to the curve not crossing the X-axis, and lacking any curve fitting programme. **C** Sample showing Warburg impedance. The σ coefficient can be estimated from the Nyquist plot as the frequency is low enough to show its characteristic slope. **D** Sample showing Z_{W}. σ cannot be estimated from the Nyquist plot as the frequency is not low enough to show its characteristic slope.

Figures D.16 & D.17: Figures plotting results from CSC data analysis, same as in Figure 4, but using the whole sample population. As the ISR is derived from the computed CSC, it was also affected by the sample selection. Sample selection in the main body was done according to PCB samples showing significant measurement differences due to manufacturing issues introducing variability. These plots present weaker trends, higher variance, and more significant outliers. It is thus more challenging to extract meaningful conclusions from them.

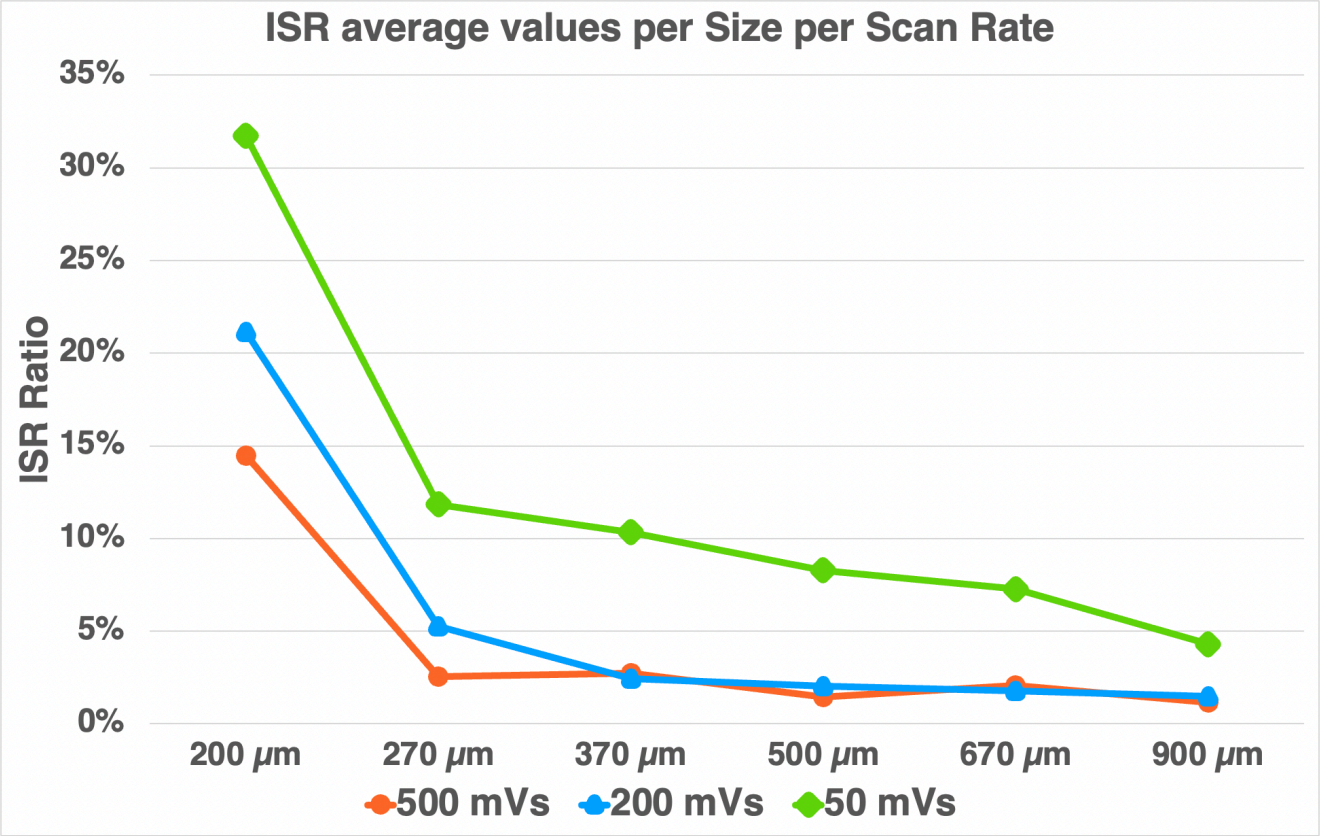

Figure D.16: ISR data analysis was done using the whole sample population. The plot compares the progression of the ISR at the three different scan rates (500, 200, 50 mV/s) across the differently sized electrode openings.

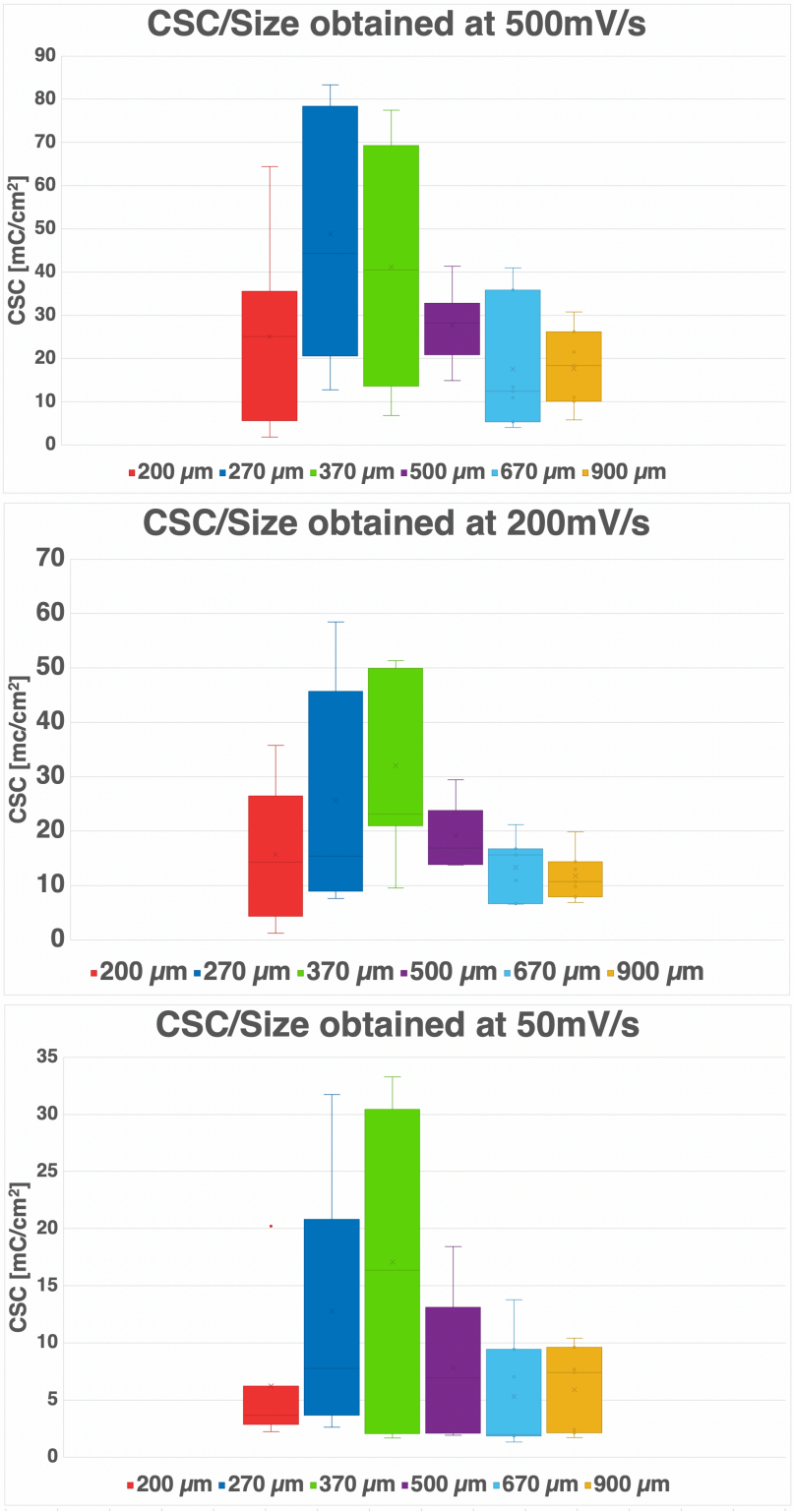

Figure D.17: CSC data analysis plots using the whole sample population. From top to bottom, left to right: **Top** Boxplots of CV data obtained at 500 mV/s. **Center** Boxplots of CV data obtained at 200 mV/s.**Bottom** Boxplots of CV data obtained at 50 mV/s.

Figure D.18: Additional plots resulting from the study of the sample population EIS and CSC results. The top graph plots the average Z @ 1 kHz obtained per size category. The bottom graph plots the obtained average CSC values for each scan rate at every size opening category.

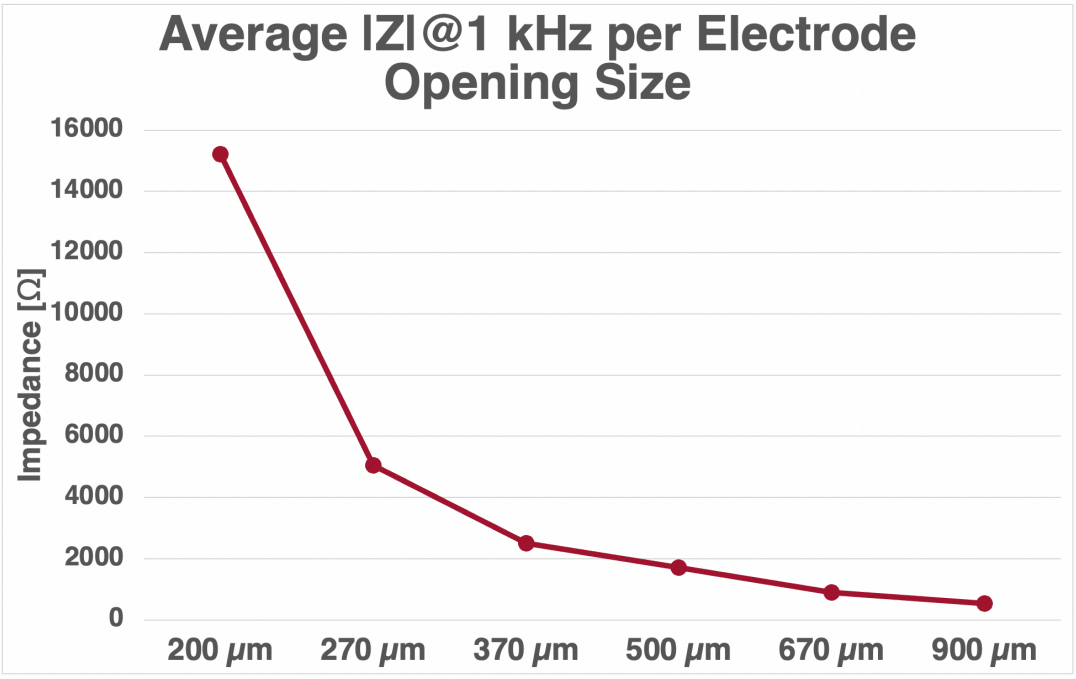

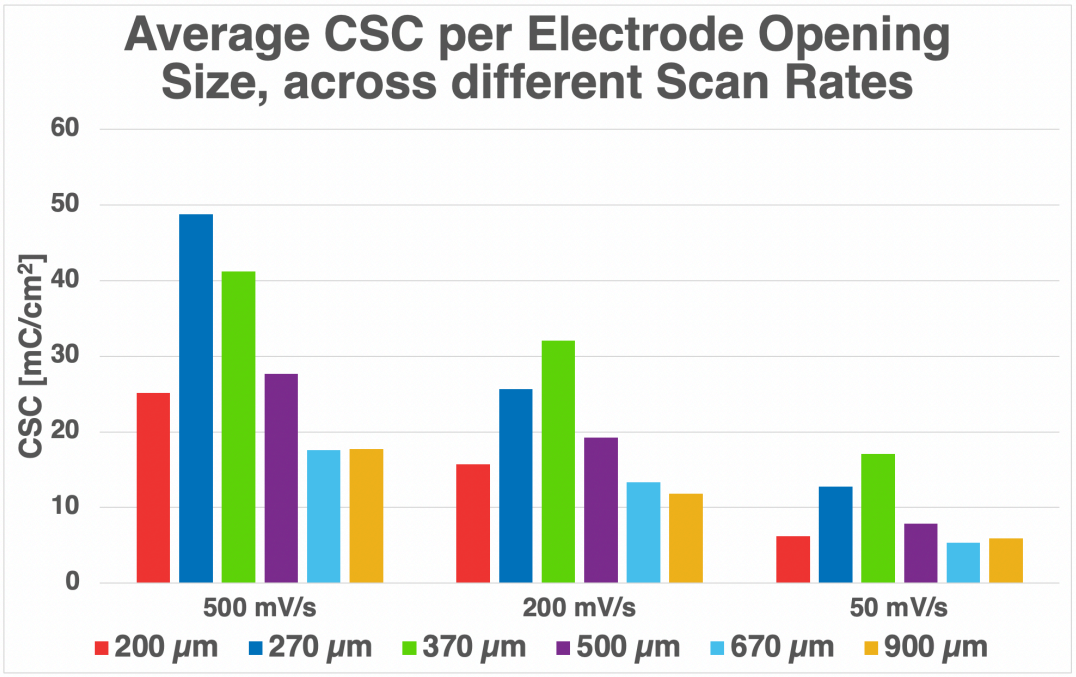

Figure D.18: Additional results from studying the sample population's characterization results across the size opening categories. Averages are of the whole sample population for each size category. From top to bottom: **Top** Average Z @ 1 kHz obtained at each size category. **Bottom** Average CSC values obtained with each scan rate for every size opening category

E Appendix: Electrode Characterization Protocol

Document E.1: Electrode Characterization Protocol written for the TBE team at IZM. It contains:

- Safety information
- Indications to set up the testing platform to perform the three main tests (EIS, CV and VTs)
- Additional information on other related tests, such as WW testing using CV (Noise Characterization was left open to fill up at a later date)
- Indications to dismantle the different setups and clean up.

Figure E.1: Electrode Characterization Protocol written for the TBE team at IZM to ensure current and future electrode characterization practices can be performed in a repeatable, reliable and standardized manner. Continued in next pages.

1 INTRODUCTION

1 SAFETY & RULES

1.1 SAFETY GUIDELINES

General safety guidelines of the CoALab must be followed at all times. Specifics regarding adequate use of the lab, emergency contacts and emergency procedures may be found in the most recent version of the lab´s rule guidebook.

In order to safely manipulate samples, and protect yourself, the following personal safety equipment is necessary:

- **Lab Shoes.** Blue ones are preferred.
- **Lab Coat.** Any standard IZM lab coat suffices
- **Nitril Gloves.** Found on the wall by the lab entrance door, they are important to avoid contaminating samples. Most chemicals used are not harmful, but wearing gloves protects against mildly hazardous substances such as IPA or the thermostat´s heating liquid.

Figure 1.1: Nitril gloves found at the entrance of CoALab

1.2 Characterization Protocol Rules

Follow the following rules for an adequate lab setup.

1. **Read first the whole protocol before attempting any experiment for the first time.**
2. Always follow CoALab rules. This includes turning on the ventilation system when working at the lab.
3. Tests must be performed at adequate conditions (temperature, N2 degassing). This implies allowing the setup to warm up until the desired state is reached.
4. Perform characterization tests **inside** the digestorium. As N2 gas is released, it needs to be extracted safely.

Figure 1.2: TBE´s Digestorium at Coalab

5. Use fresh PBS every day when you start the measurements. If a sample breaks down electrochemically throughout the process, it is imperative to change the PBS medium as it will be contaminated.
6. Follow the wiring guidelines throughout the whole procedure.
7. Before leaving the lab, ensure the equipment has been stored away, and the working space is free and clean.

2 Protocol Workflow

Due to the requirements of electrode characterization tests having both common and specific elements/procedures, this protocol will often divide steps between those that are common to all experiments, as they are part of the basic electrode characterization setup; and the specific guidelines for tests.

3 Required Equipment

The equipment needed to perform each type of test(s) may be found in the Electrode Characterization storage box, the digestorium and some pieces in our Lab 231.

Figure 1.3: Electrode Characterization storage box. It may be found in the metal trolley, or in the storage cabinet of CoALab

2

COMMON PREPARATIONS FOR ALL TESTS

1 EQUIPMENT NEEDED FOR ALL TYPES OF ELECTRODE CHARACTERIZATION TESTING - SEE FIGURES 2.1 AND 2.2

1. **Thermostat** - Huber ministat 270. Tubing sections for heating liquid are also required. An official introduction is required.
2. **N2 Gas probe** - Use the inner outlet of digestorium.
3. **Faraday Cage** - Black metal cabinet. Inner connecting sections (electrical wiring, N2 degassing tube, thermostat´s heating liquid tubes) should be present and connected to their respective ports. Make sure no items are blocking the door to properly access the interior of the cage.
4. **Double-Glass-Walled Beaker** - 600ml capacity. Used for the experiment setup.
5. **1L regular Beaker** - Used in cleaning up.
6. **PBS solution** - CarlRoth Ph 7.4, 0.1M. At least 400ml is needed.
7. **Thermometer** - Any standard thermometer suffices. Make sure it has batteries and works. Many others may be found in Galvanic Lab (Lab 353).
8. **3-Electrode Holder** - 3D printed piece to hold electrodes in place during testing. **Ensure rubber rings are in place.**
9. **3-Electrode Holder Support** - 3D printed support piece, for easier sample and electrode loading.
10. **Pt flag foil large return electrode (CE)** - CE with a large surface to minimize introducing any electrochemical contribution to the sample tests.
11. **CE Lock** - 3D printed piece used to hold in place the CE by holding it in its groove.
12. **Rubber Band** - Used to hold the CE lock in place. If it loosens up with time, replace it. **Ensure rubber rings are in place.**
13. **WE samples** - Samples to be tested

14. **WE sample holder** - 3D printed pieces, custom designed for each type of sample. General design guidelines ensure it fits in the 3-Electrode Holder
15. **WE connector** - Each WE may have a different layout design, but they all should be prepared for the correct electrical connection to the cage setup. The internal cabling of the cage is prepared with banana connectors and crocodile grippers, allowing it to connect to exposed cabling. An interface, such as the Samtec connectors and additional soldered cables, may have to be used.
16. **Working Laptop NB-SIIT086** - Other laptops with adequate software installed could be used, but NB-SIIT086 is intended for this setup and protocol. It is important to also keep it charged with its charger.
17. **USB thumbstick drive** - Necessary to extract files from the computer for later processing.
18. **Matlab software** - Used in all tests for subsequent data processing. It may be run on any machine, not necessarily NB-SIIT086

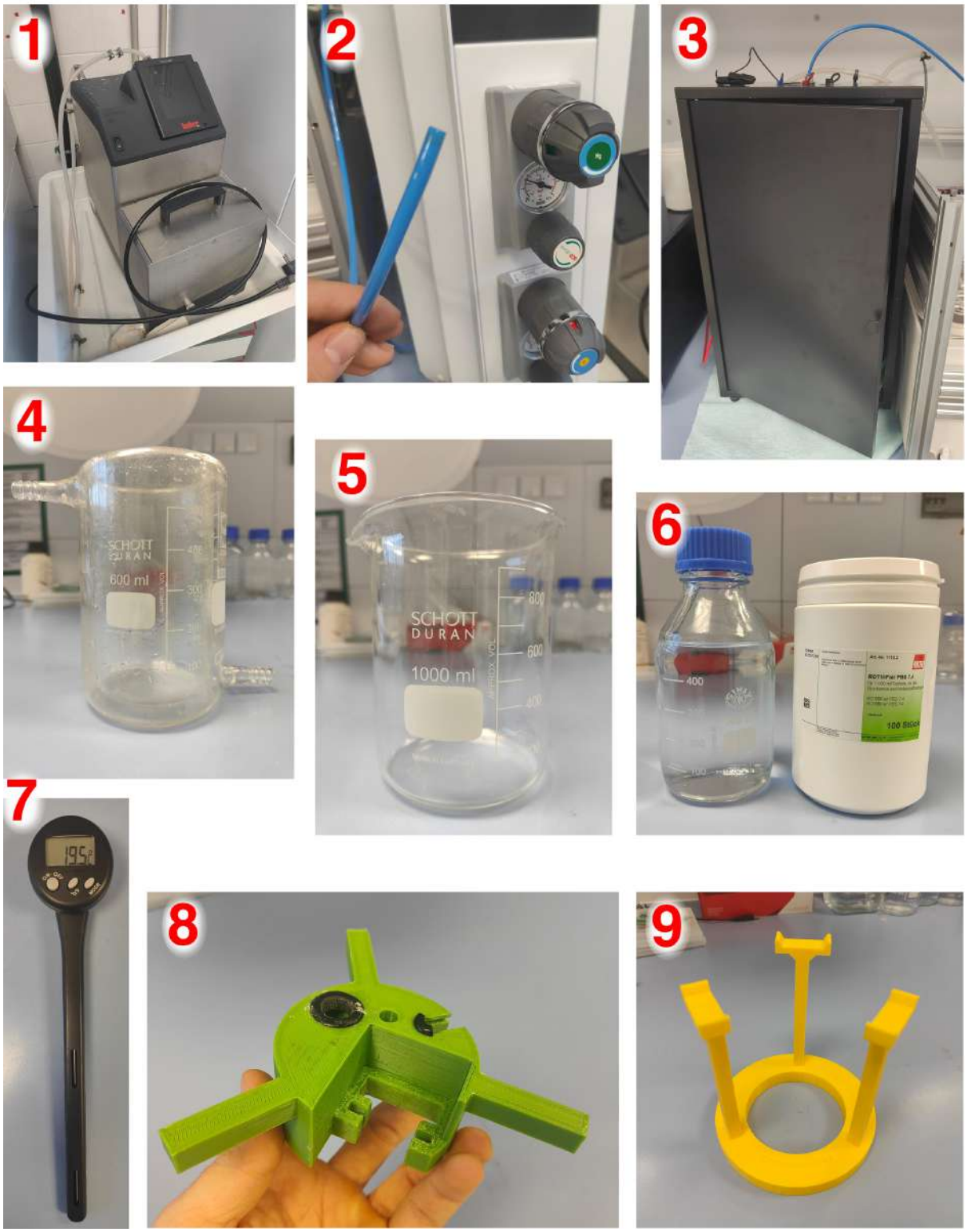

Figure 2.1: Equipment items 1 to 9 specified in the list in Section 3.1 - Equipment needed for all types of Electrode Characterization Testing

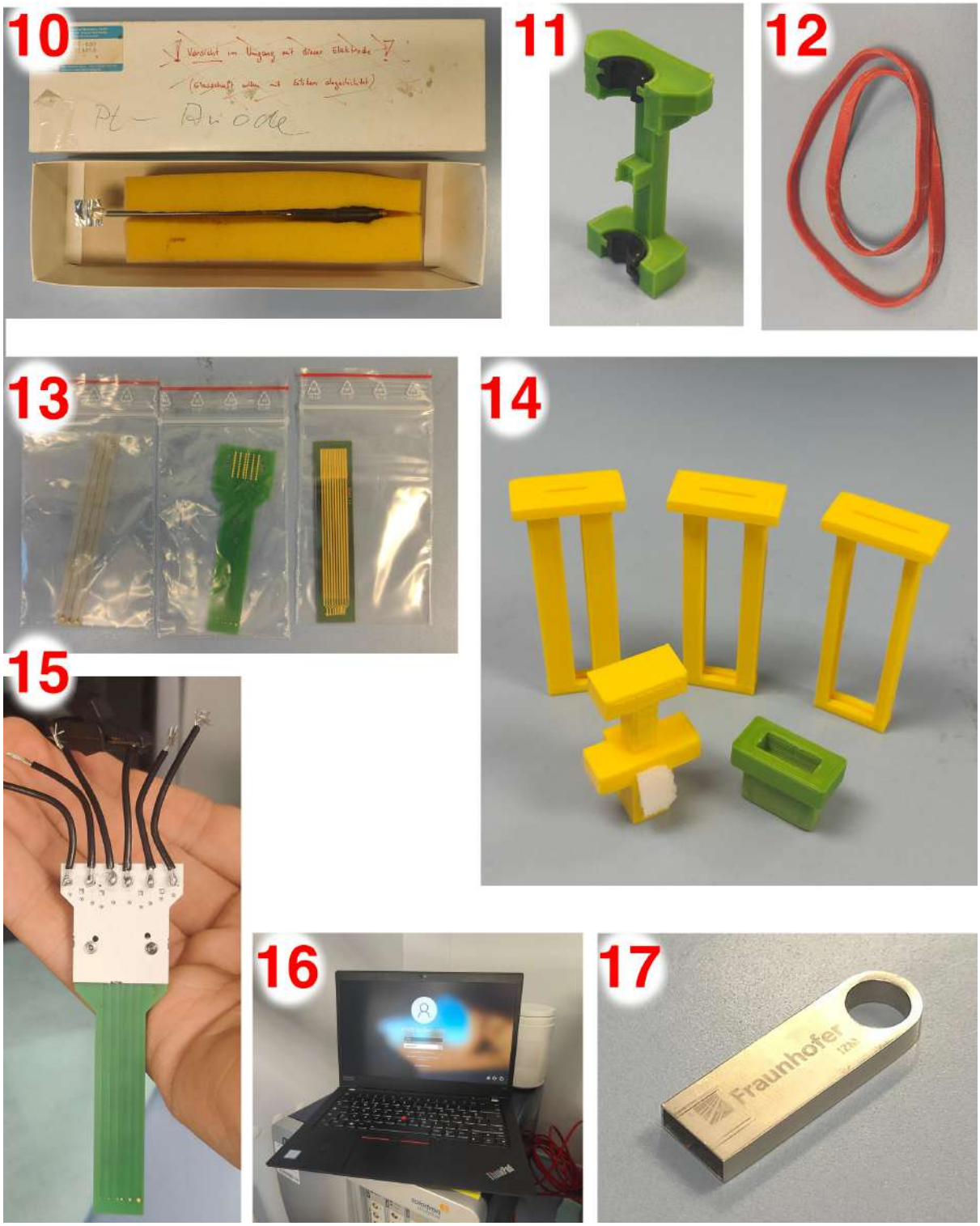

Figure 2.2: Equipment items 10 to 17 specified in the list in Section 3.1 - Equipment needed for all types of Electrode Characterization Testing

2 Setup Preparation

2.1 Cage Preparation

Ensure the rules of the CoALab are followed.

Begin by opening the digestorium. This is done through the panel on the right of the window pane. Slide the icon to the top of the line.

Figure 2.3: Panel showing the window pane is open, as the bar is at the top

We will first set up the temperature with the thermostat and the double-glass-walled beaker, as it takes around 30 minutes to heat up to 37°C.

Bring out the thermostat, and plug it in. Using the thermostat is only possible after having recieved an introduction by the lab manager.

DO NOT START THE THERMOSTAT UNTIL ALL PORTS ARE CONNECTED

At the top, two tubes should be connected. Next to each connection, there should be an icon of an arrow indicating whether liquid flows out of it, or into it.

- Take the tubing with outward flow, and connect it to the cage´s left (facing in front of the Cage, through the door) outer tube
- Then take the cage´s interior section of that left tube and connect it to the lower port of the double glass walled beaker.
- Ensure that outward flow from the thermostat connects to the lower port of the beaker.

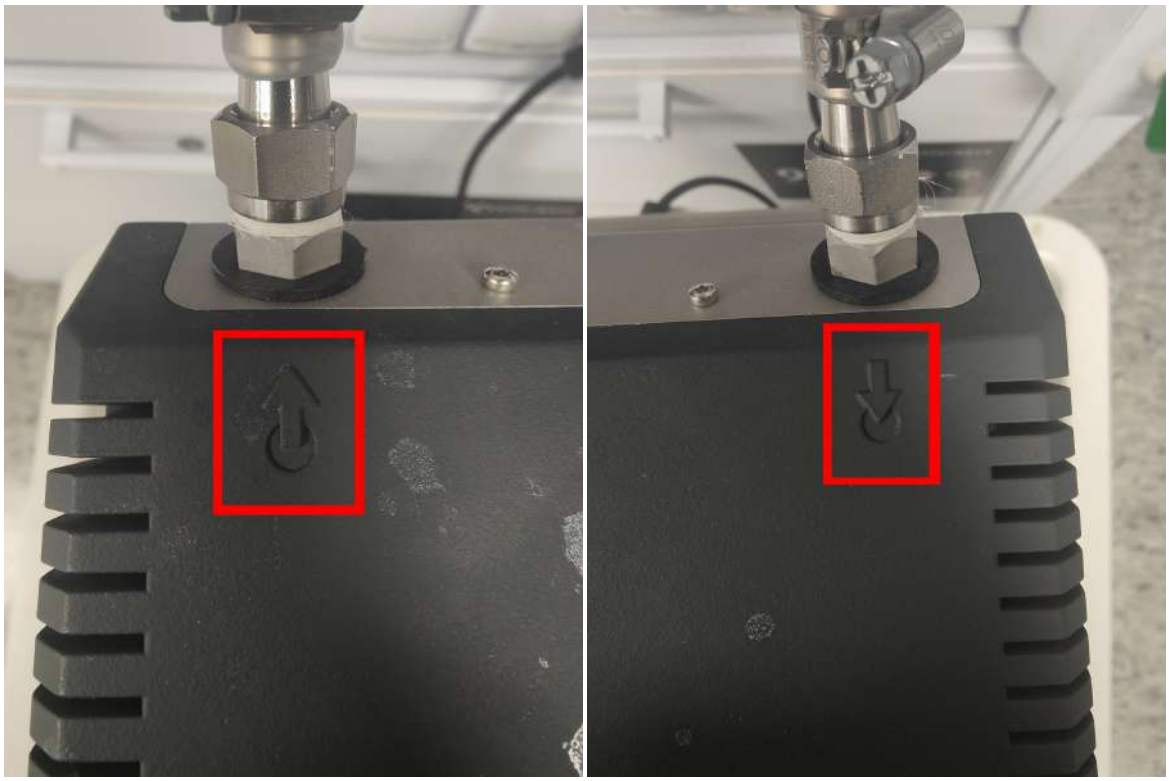

Figure 2.4: Left: Inward flowing Thermostat port | Right: Inward flowing Thermostat port

Repeat the process for the inward flow tube section. Connect to the right side outer tube, and then connect the right inner tube to the beaker´s top port.

Plug in the thermostat and switch it on by using the switch on the left side of the interface. It is normal that it states an error in the display, notifying that maintenance is recommended, shown in Figure 2.6. You may ignore it.

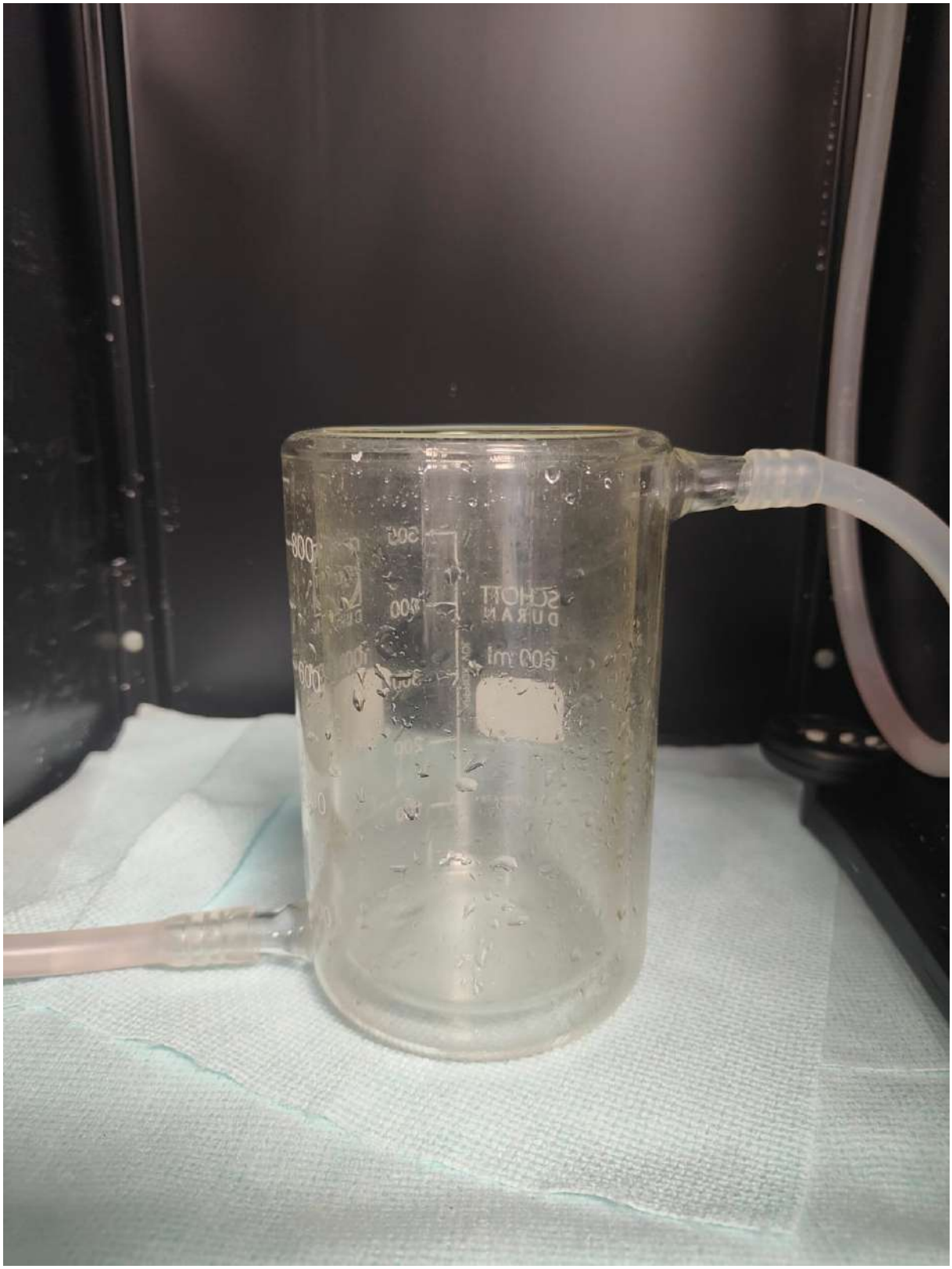

Figure 2.5: Double Glass Walled beaker connected to thermostat probes, with the inflow tubing at the bottom, and the outflow tubing at the top

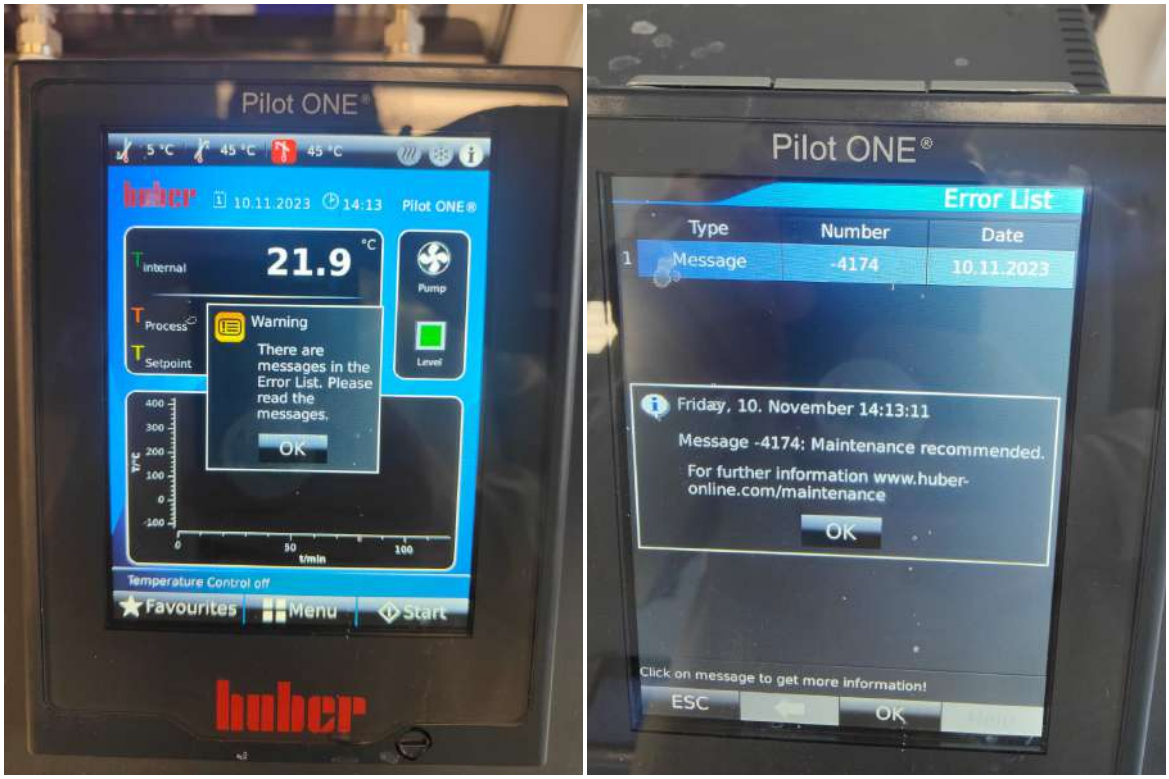

Figure 2.6: It is common for an error message to show when booting up the thermostat. If checked, it shows it is indicating for maintenance.

Check the temperature is set to 37C, with the icon for max temperature set at 45C as in Figure 2.7. If not, to turn it on:

1. **Set Process Temperature:** > Menu > Temperature Control > Setpoint > 37°C
2. **Set Maximum Temperature:** > Menu > Protection Options > Setpoint Limits > Max Setpoint > 45°C

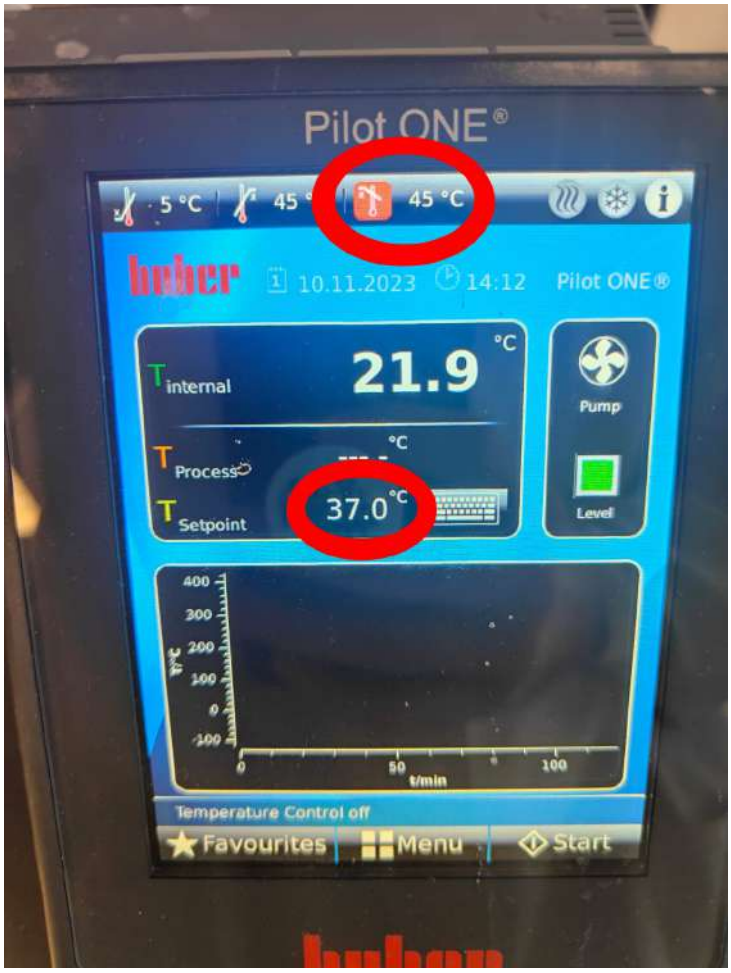

Figure 2.7: Check the safety temperature limit (top row) and the Setpoint T (in yellow, in the centre square). This is how the thermostat screen should look before starting the flow of heating liquid.

Troubleshooting Thermostat

Although an introduction is necessary to operate the thermostat, and should cover these points, here are some common troubleshooting issues while operating the thermostat.

- If the thermostat indicates that the heating liquid level is low (due to spilling or use), locate the container with the pink liquid labeled "Glyfosor N/H20 50/50", shown in Figure 2.8
- If there are any spills, use a paper piece to clean it up. Be thorough, as it is quite oily and can be slippery.
- To avoid skin irritations, always clean with gloves and lab equipment on (section 1.1)

Figure 2.8: Container holding the heating liquid used by the thermostat

With the temperature set and all 4 ports connected, it is safe to start the thermostat. Do so by pressing the start button (bottom right of the screen), then Ok. The heating liquid will flow through the outlet. Please ensure there are no bends through the tubing preventing adequate flow. Once the heating liquid has completed the whole circuit, you may continue.

Add 400-450ml of fresh PBS to the beaker, For more on fresh PBS, check Chapter 6.

Next, take the N2 tubing from the digestorium, and connect it to the cage´s port on its top, as in Figure 2.9. You may take the cage´s inner N2 cable and put it in the beaker. Use the outer (right) gauge for N2 (labelled) and open the flow. The gauge's numbers are not really useful to set a good flow, so instead check visually the stream of bubbles. A continuous flow of N2 is good for medium degassing while it heats up. It can be turned down if it is agitating the surface of the liquid too much, as this will spill into the electrode holder.

You may introduce a thermometer. Wipe it clean before inserting it to get accurate measurements. It usually takes around 35-40 minutes to heat up to 37C. You can use a thermometer to check the temperature.

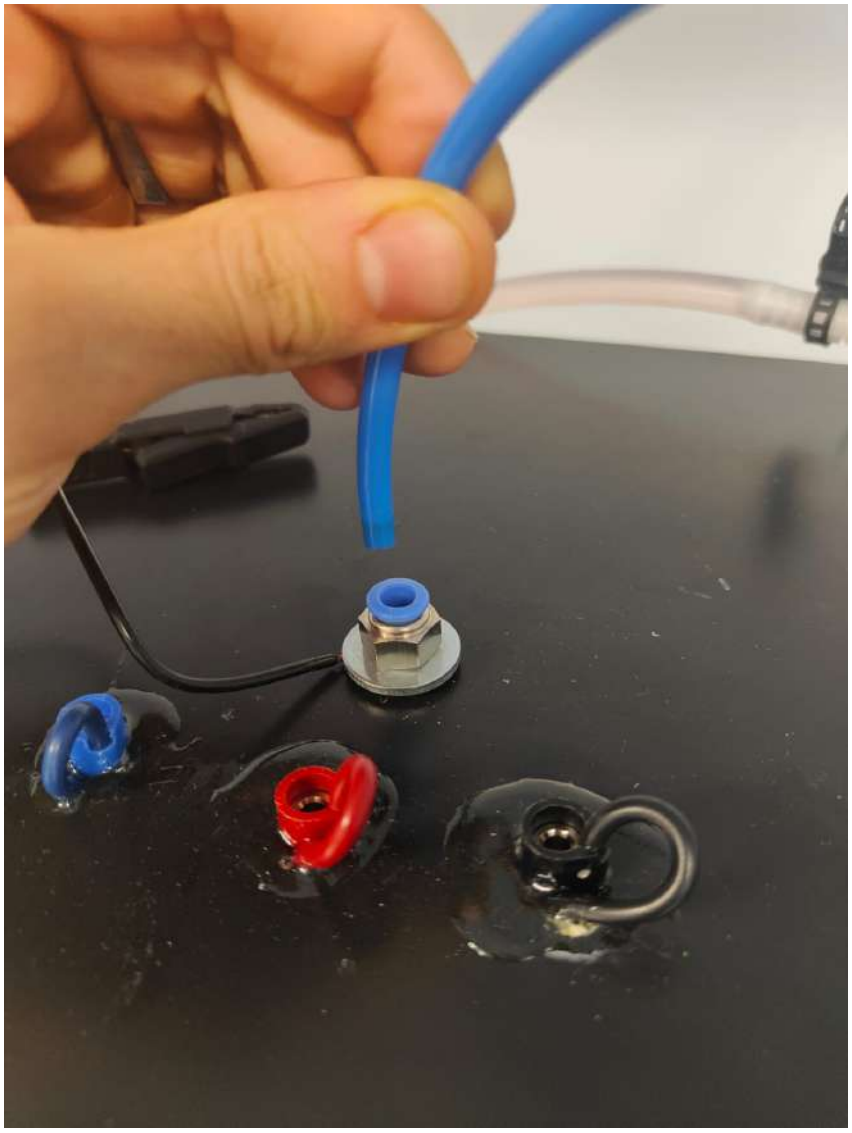

Figure 2.9: Port to connect the N2 probe. Just push it in.

With the thermostat heating up, N2 degassing the medium, and the thermometer reading the beaker's temperature, the basic cage preparation is done. Close the door of the cage.

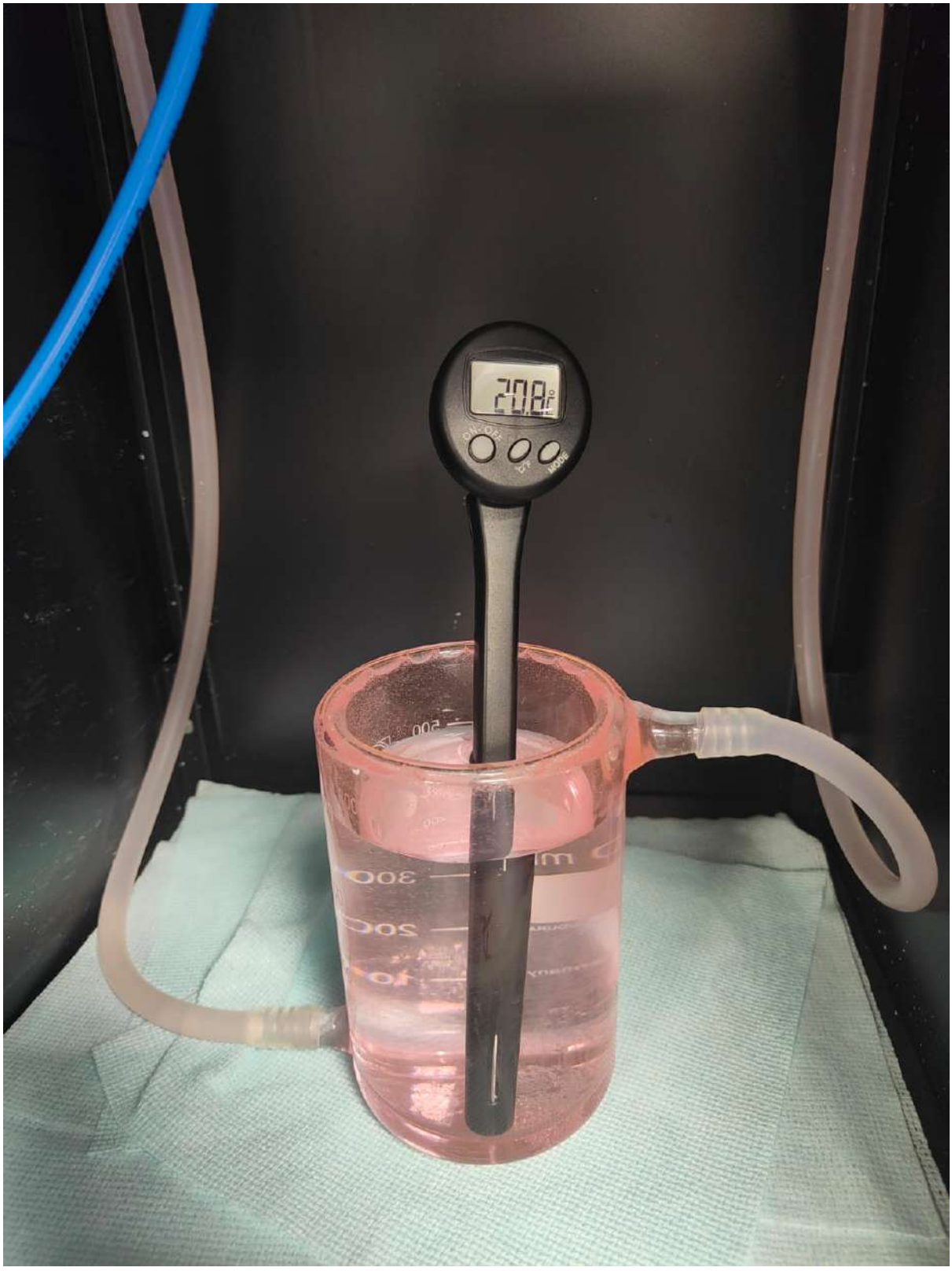

Figure 2.10: Once temperature control, N2 degassing and PBS are ready, the setup must be left to reach optimal testing conditions. A thermometer is useful.

2.2 Computer Preparation

The computer used in this lab is unit NB-SIIT086. It is important that it has enough battery when starting, so make sure to plug it in before starting it. When booting it up, it will first connect to the Fraunhofer network, avoid clicking anything as this may interrupt the decryption.

Log in with these credentials (Do not include quotes ”):

- **User, from the encrypted Fraunhofer booting up screen:** 'berlin\ERTS'
- **User, from the user log in Windows screen:** '.\ ERTS'
- **Password:** ’E@izm2019!’

IMPORTANT: When booting up the computer, until credentials are used to log in, avoid connecting any kind of ethernet cable preventing the computer from connecting via wifi to the Fraunhofer servers.

If still facing issues with the log in, disconnect any cables besides power, restart the laptop and do not click anything until it is ready for the user to input the credentials.

2.3 Electrode Holder Preparation

All the equipment needed to perform the electrode characterization tests may be found in the plastic container box labelled **Electrode Characterization**. It should be stored on the second level of the metal cart placed on the left of the working bench.

To set up the Counter Electrode (CE) and Reference Electrode (RE) is best to use the electrode holder support, shown in figure 2.11. Start by placing the support on the working bench.

Figure 2.11: Place the electrode holder (green) on the workbench with the help of the support (yellow)

Begin by setting up the Pt foil CE. You will need the electrode holder, the Pt foil lock, and the red elastic band found in the box. Follow Figure 2.12 for a better idea

- Begin by looping the red band once around itself. Get this double-loop band and put the CE body through it
- Slide the electrode into the electrode´s holder groove designated for the Pt foil CE electrode. Make sure the electrode is not bent by touching any kind of surface
- While holding the electrode and red band inside the groove of the holder, use the CE lock to keep it in place
- Now use the double-looped red elastic band to wrap around the elec-

trode holder and CE lock. This should hold the plastic pieces together, keeping the Pt foil electrode in place.

- Place again the electrode holder on the support

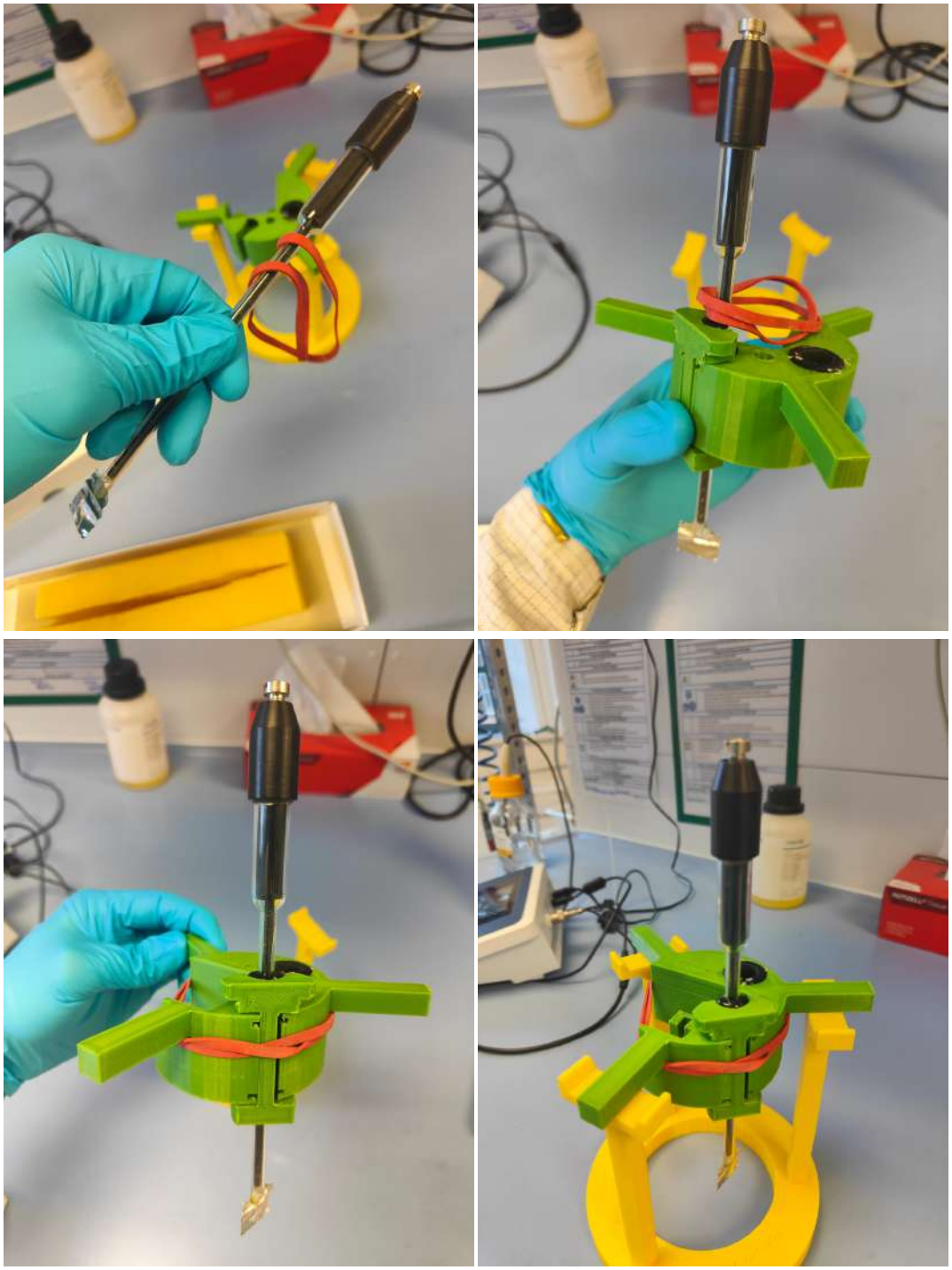

Figure 2.12: Steps to follow for CE locking. Place the double loop band on the CE electrode. Lock it in the support and use the band to hold everything in place.

3 Sample Preparation

Each sample type will have its own electrode holder. Still, the modular design of the electrode holder should allow all sample types to be used.

Ensure first that the sample can be connected electrically. For most cases, this would involve using some version of the Samtec Connector. It may also be necessary to solder wires to the connector in order to be able to connect it to the other connections.

To easily connect the Samtec Connector, follow these steps, with further aid from Figure 2.13:

- Start by covering the electrical contacts of your sample with the Samtec Connector piece (black plastic body with several gold pins). Ensure the screw and pin openings are aligned.
- Then use the other connecting piece, with outward connections such as soldered cables, to sandwich the Samtec connector between this piece and the sample.
- For extra thin and flexible samples, a backpiece to support and properly fix the connector is needed.
- Place first the screwing pieces on the bottom face of the build.
- Put screws in through openings, connected to their screwing piece. Screw them in until they become tight.
- If struggling, remember to hold down the whole build to avoid the screwing pieces from coming loose. Manually place the screw, and then carefully give it a turn with the screwdriver to screw it in place. Follow Figure 2.13 for these steps

For the most common sample types, here are the basic steps to place them in their sample holders.

3.1 Rigid/PCB-like electrodes

Rigid electrodes have no issues of floating and bending upwards. Their holder allows one to slide the sample into a slit, and hold it in place. Be sure to avoid scraping the sensible side of the electrode against the holder´s plastic opening by sliding it against the holder on the side opposite to the sensible one.

Once in place, make sure to clean the sample with DI Water, IPA, and some light pressurized N2.

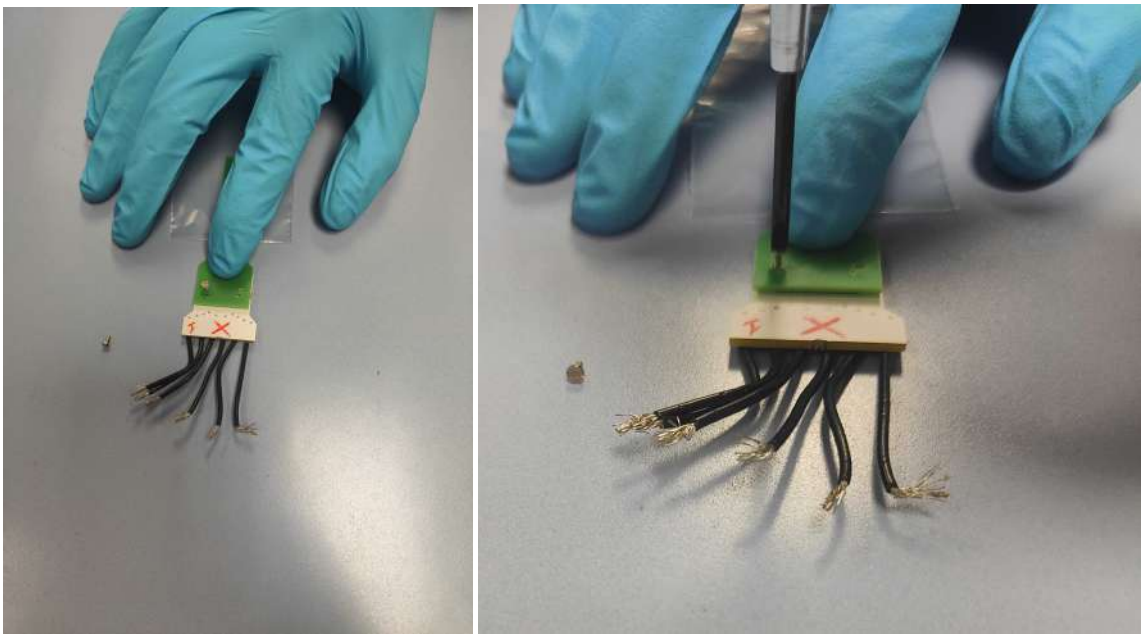

Figure 2.13: To easily place the screws, make sure the whole build is held down, manually place the screws and gently screw them in place with a few turns.

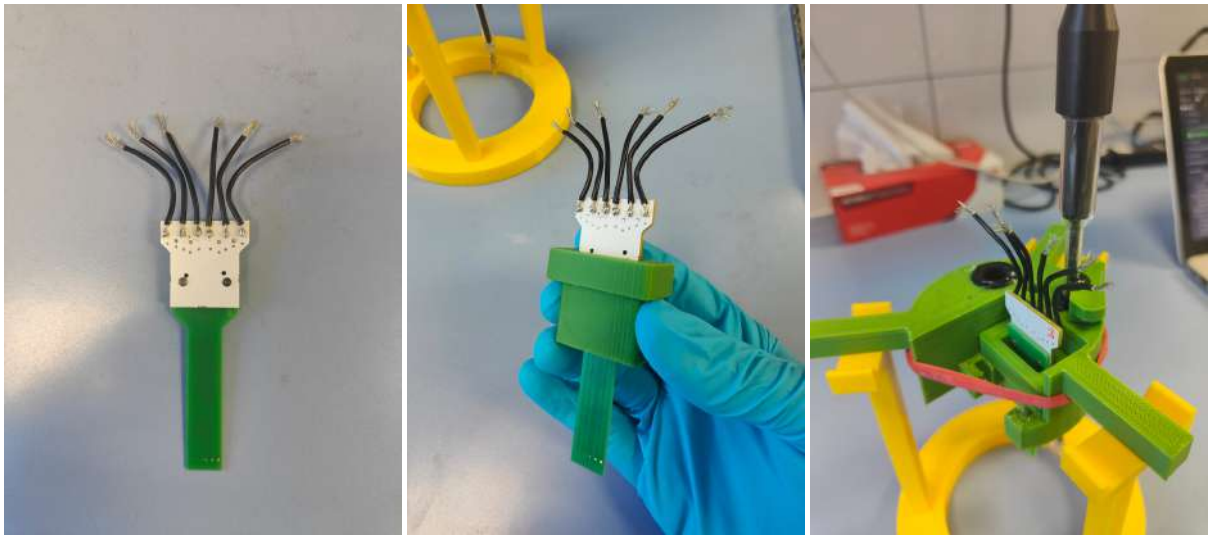

Figure 2.14: Rigid electrodes may be inserted directly on their holder. Then you may place everything in the main electrode holder.

3.2 PARYLENE ELECTRODES

Parylene electrodes can be difficult to manipulate due to their extremely thin thickness. A dedicated electrode holder was designed for parylene electrodes

Ensure first the electrode is fixed to the Samtec connector and the rest of the connector piece. Start by placing the part of the holder capable of housing the connector over the sample support, as shown in the picture.

Place the electrode's connector into the holder, holding the sample elec-

trode out of the way. Then let the sample parylene electrode roll over the sample support. Its edges should fall on top of the silicon edges, ensuring that no hard surface is in contact with the parylene.

Then grab the top piece of the electrode holder, and place it on top of the bottom piece. Pins should align for a tight fit, holding the sample down the opening. You may now manipulate the holder safely.

Although cleaning the sample is good, with parylene's mechanical properties it can be more of a risk than anything else. Clean the electrode with a gentle use of Water and IPA

3.3 Other flexible electrodes

Any other flexible electrode that needs to be held down while tested, may be held using the regular slit-electrode holder pieces. Ensure the one with the right size is used for the sample piece.

The sample should:

- Fit in the top slit
- Be wide enough to be covered by at least one side of the plastic holder's groove
- Be placed so that no sample opening is hidden behind the plastic holder's groove.
- Avoid any bends or misplacement that may damage the sample
- The sample opening should be oriented to face the other instrumentation electrodes.

Once in place, make sure to clean the sample with DI Water, IPA, and some light pressurized air.

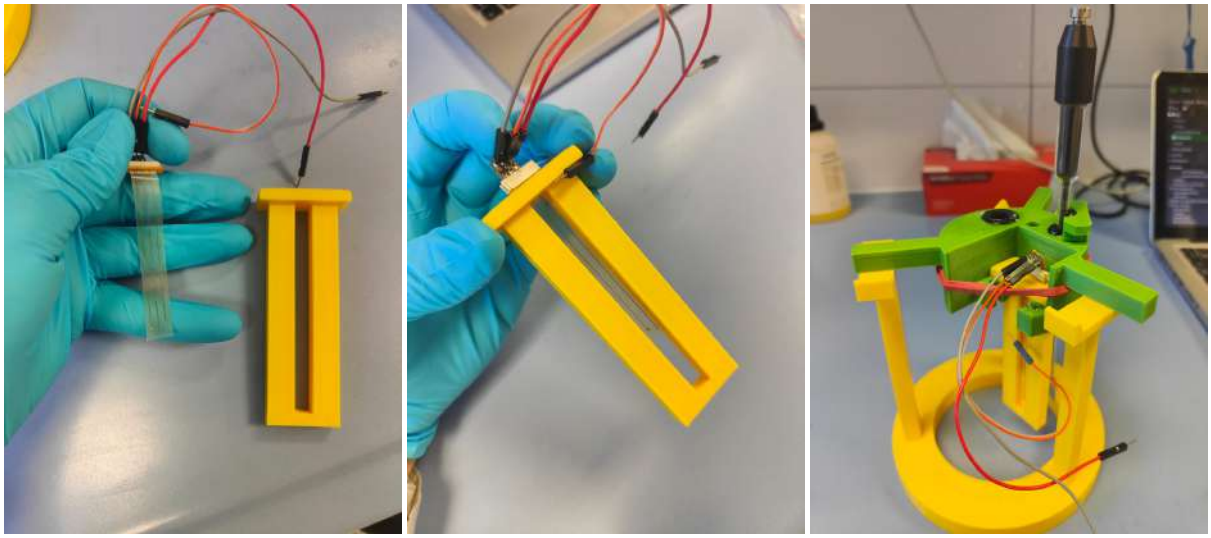

Figure 2.15: To hold other flexible electrodes, make sure the right sized holder is chosen. Slide it in, and check that the electrode is not covered by the holder´s plastic border.

3.4 Universal Electrode Holder

For electrodes not described above, be it mainly because of their geometry, a "universal" holder was designed. Using a foam piece, it can press down on samples to hold them in the electrode holder. It was limitations, such as the sizes of electrode it could fit.

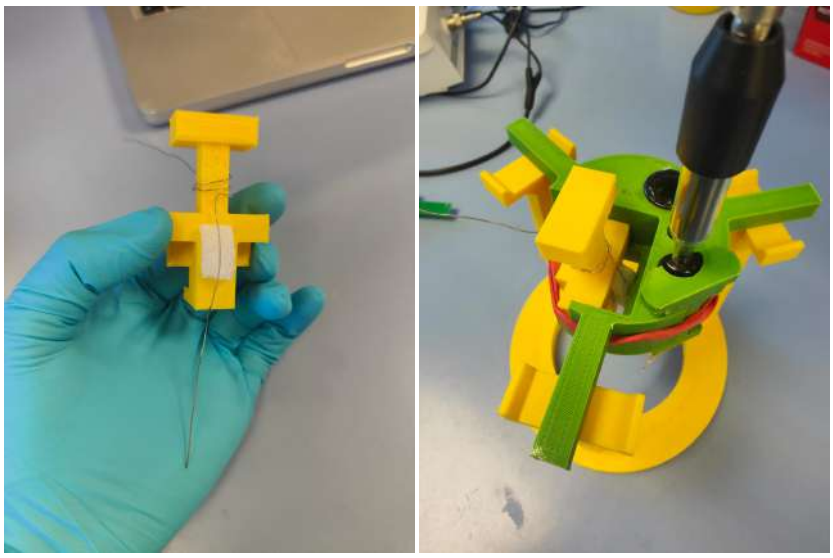

Figure 2.16: Wired electrodes may be looped around the holder directly. It may be necessary to insert both electrode and holder at the same time in other cases.

It works best with wire-like, thin electrodes. Still, it is not a perfect solution and if the sample type is to be tested thoroughly, it may be best to design a new sample holder.

Once in place, make sure to clean the sample with DI Water, IPA, and

some light pressurized N2.

IF AN ELECTRODE DOES NOT FIT ANY OF THESE HOLDERS, A NEW HOLDER MAY HAVE TO BE DESIGNED. YOU MAY FIND THE SOLDIWORKS FILES FOR ALL THESE HOLDERS IN TBE's OWNCLOUD. MAKE SURE FINAL DIMENSIONS FIT THE ELECTRODE HOLDER'S OPENING FOR THE SAMPLE ELECTRODE.

3

PROTOCOL FOR EIS & CV

1 EQUIPMENT FOR EIS AND CV TESTING - SEE FIGURE 3.1

1. **Modulab XM Solartron Analytical** - Besides the main instrument, a cable for power is necessary, and the proprietary red cable with an ethernet connection for data transfer must be used.
2. **FA Module Cabling** - As each XM module requires different cabling, in our experiments we will need the WE,CE and RE cables. Note that the RE cable connector to the Modulab XM also is connected to another cable used to connect both LO ports.
3. **Mettler Toledo Glassy Cargon Ag|AgCl RE** - Glassy carbon electrode used as RE in several tests. It should be found and stored in its box, with a vial of additional storage solution. It must always be held in a vertical position.
4. **RE connector banana cable** - Cable required to electrically connect the RE. There are a few, but we will use the one whose connector is a banana type connector.
5. **XM Studio ECS** - Software program used to control, design and run experiments with the Modulab XM. Already installed in computer NB-SIIT086

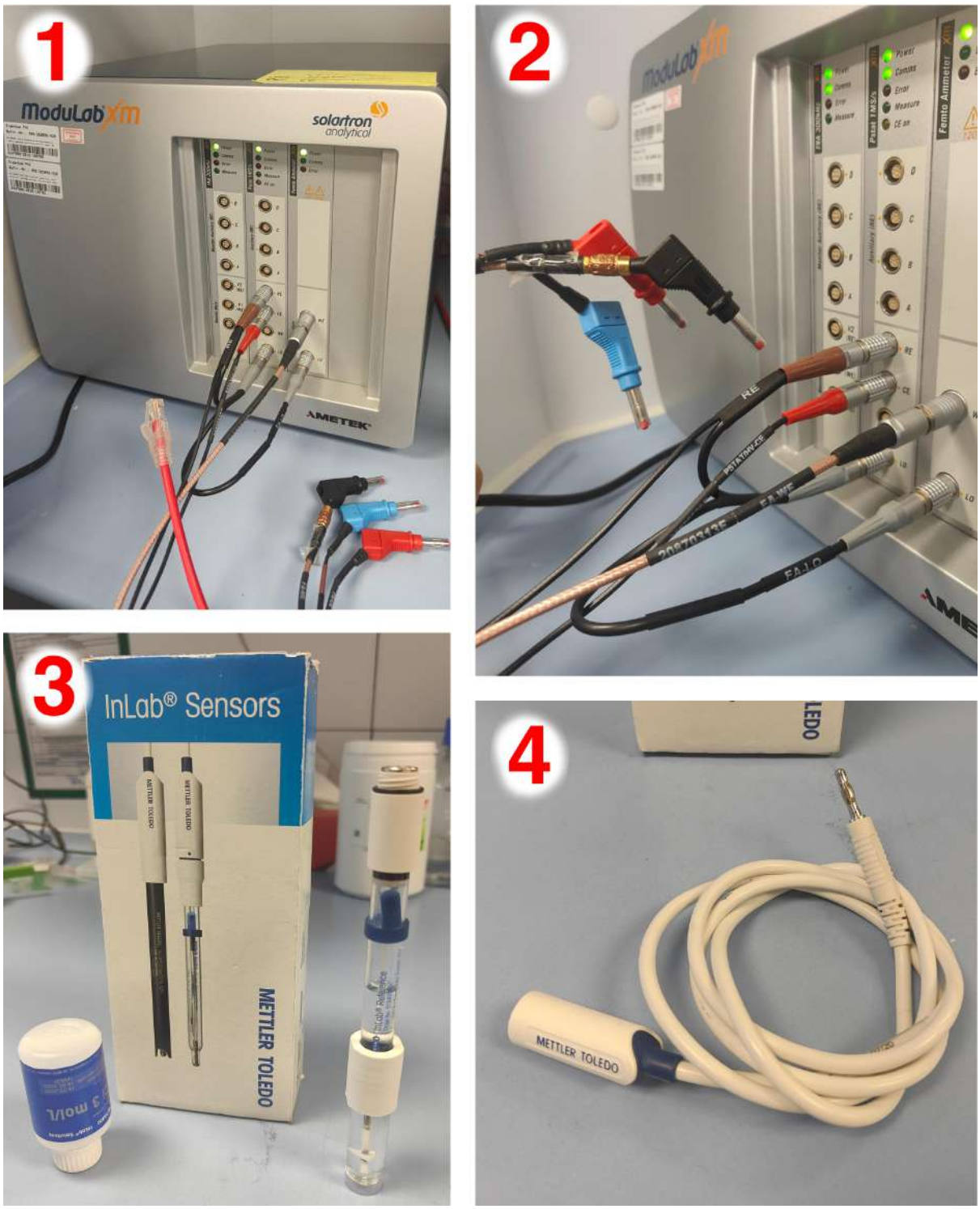

Figure 3.1: Equipment items 1 to 4 specified in the list in Section 3.1 - Equipment for EIS and CV testing

2 Setup Preparation

2.1 Cage Preparation

The cable connections at the Modulab instrument, when using the FA module, should look like in the following picture.

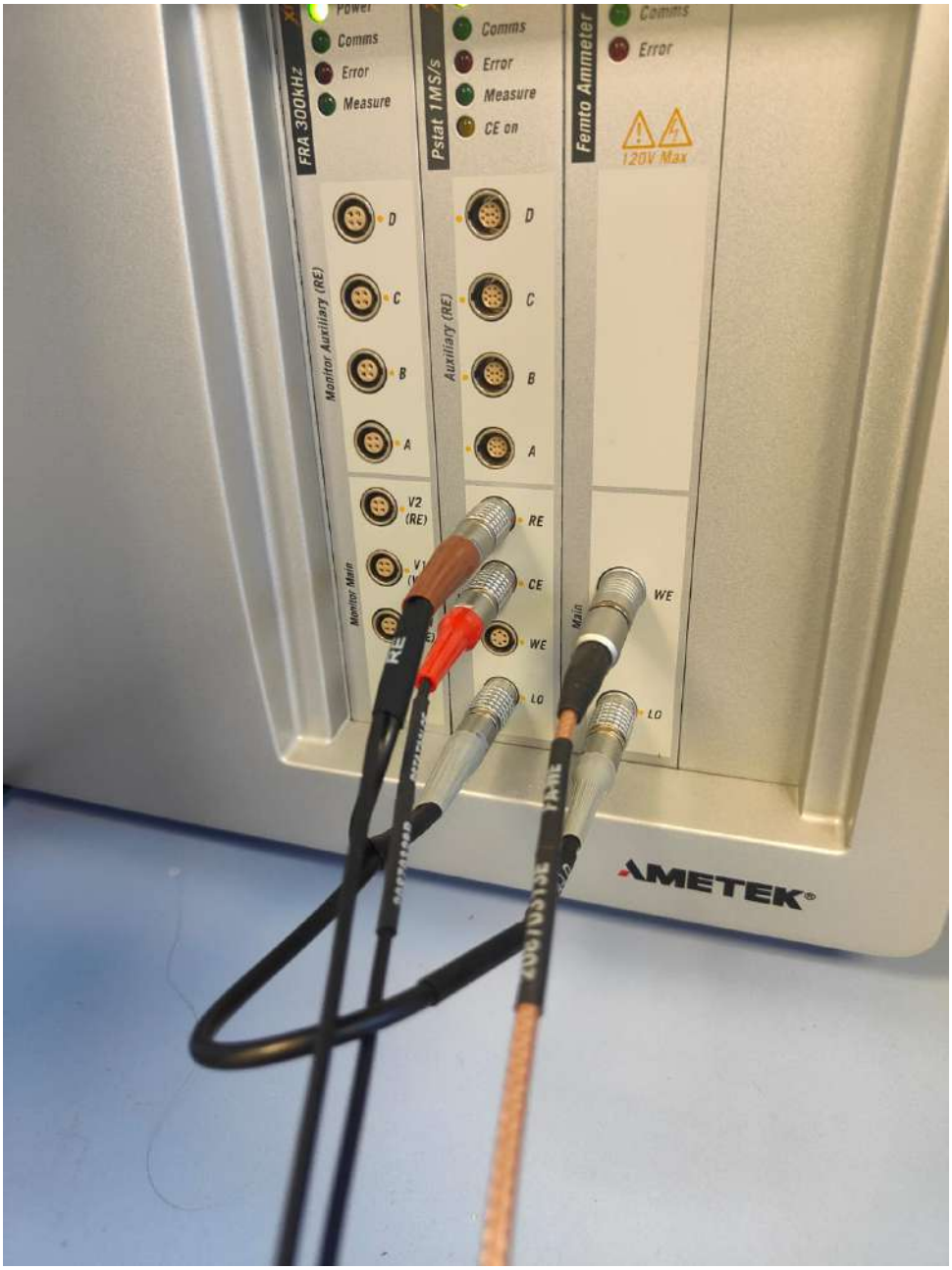

Figure 3.2: Cabling required for usage of the Modulab with the FA module.

An additional diagram of the correct cabling may be found in the desktop program, showed in Figure 3.3.

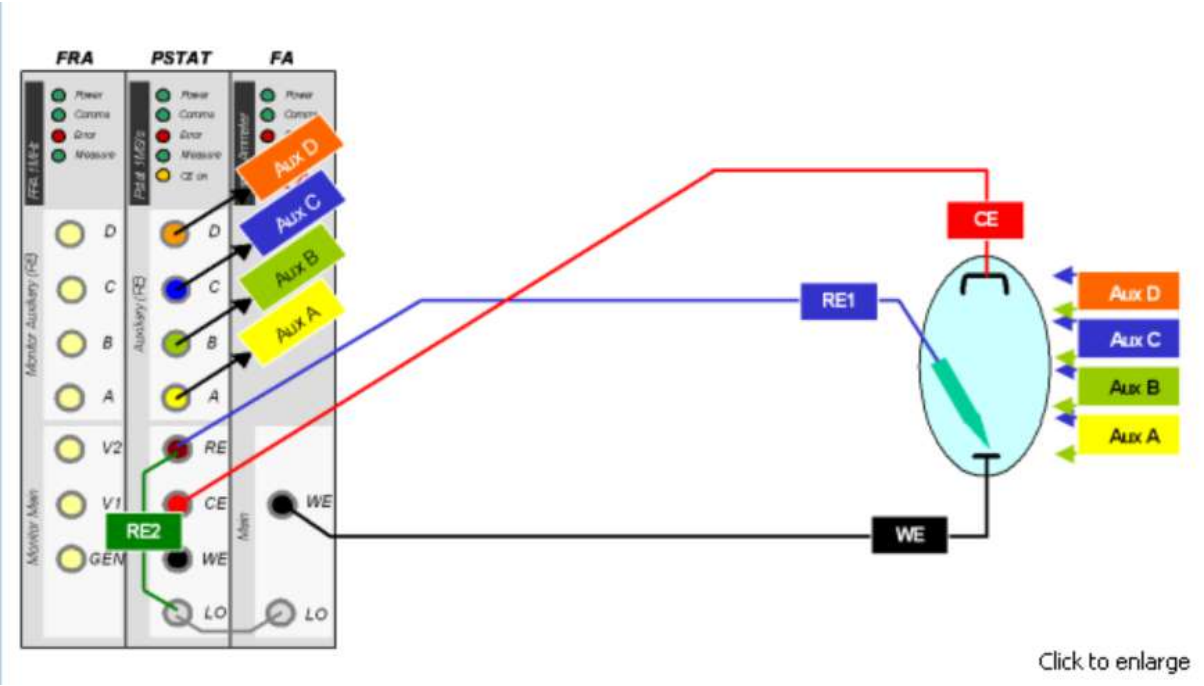

Figure 3.3: Cabling diagram for the correct use of the FA Module showed in the Modulab ECS software.

When using the Modulab instrument, cable connections need to be connected at their corresponding Faraday Cage ports.

They are colour-coded, so ensure that the right cable is at the right connector. Follow Figure 3.4

- The blue connector for the RE connects to the blue port.
- The red connector for the CE connects to the red port.
- The black connector for the WE connects to the black port.
- The black connector for the WE has a piece of copper tape near its end, used as a grounding connection. **Use the grippers connected to the cage to clamp the copper tape, effectively grounding the connection to the cage.**

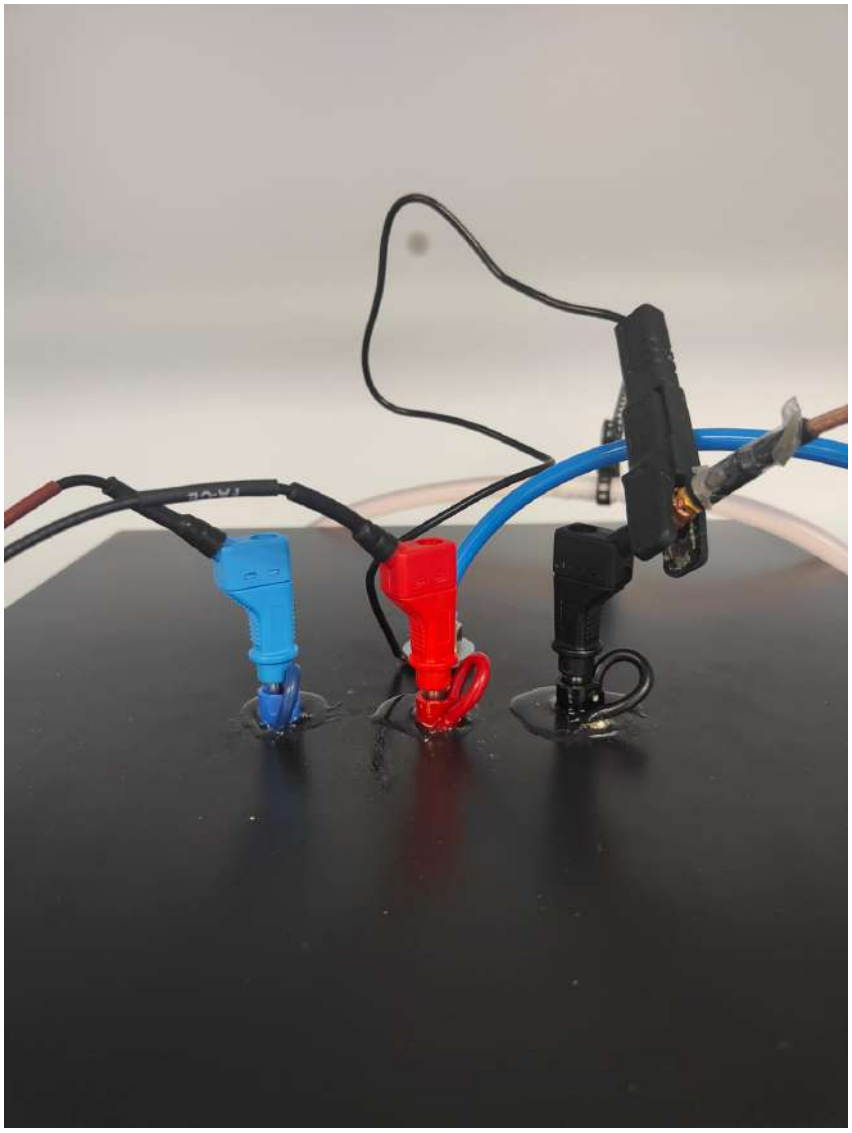

Figure 3.4: Cable connections at the Faraday cage interface. This configuration is only correct if the other connections (Modulab, Electrodes in Cage) are kept according to the Protocol.

2.2 Electrode Holder Preparation

Next, you may set up the glassy carbon RE (Figure 3.5. It should be stored in its box, which must remain in a vertical position at all times.

The RE electrode is protected by a plastic vial on the reactive end. To remove it, turn it in an anticlockwise direction (looking at the RE from the top, where the electrical connection is). Its grip should loosen, although you may still feel some underpressure. You may now slide out the RE. Rinse it with DI water.

Be careful, as the PBS solution is kept inside the plastic vial. Store the opened plastic vial somewhere where it may not be knocked over.

Figure 3.5: Glassy Carbon Ag|AgCl RE´s box from Metler Toledo. Remove the protective cap, and make sure to keep it upright to avoid spilling the storage solution.

Slide the RE electrode through the circular opening with a black rubber ring in the electrode holder, as in Figure 3.6. Do so gently to avoid breaking the tube. It should slide with a bit of resistance, but nevertheless easily.

Both the RE and CE electrodes should be kept at the same height, making sure they will be immersed in the PBS.

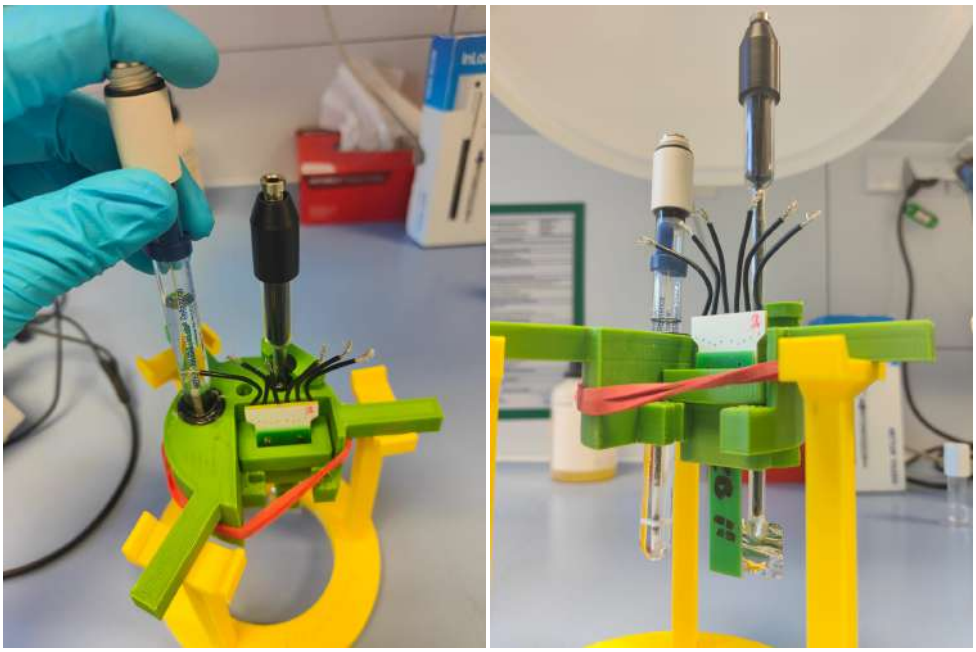

Figure 3.6: Inserting the RE electrode into its opening in the Electrode Holder. The active elements should be at the same level for optimum positioning

Lastly, we shall connect the RE with its wire. The white connector wire should be found in the equipment box. It needs to be screwed on the top side connector of the RE. One may first connect the wire, then rotate/turn the RE

electrode to make sure the cable is not falling over the electrode holder.

With the RE & CE fixed in position, you may now take the electrode holder and place it in the beaker. First, remove the thermometer and the N2 tube from the beaker. When placing the holder, make sure that the rectangular opening area to hold the Working Electrode (WE) is kept facing you, as in the right picture in figure 3.7

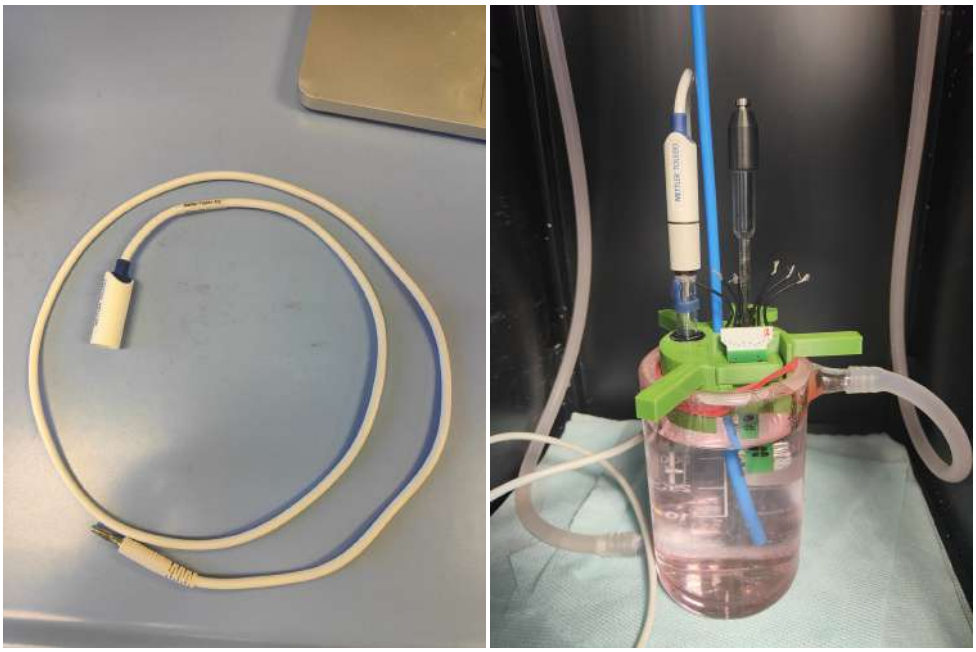

Figure 3.7: (Left) Cable used to electrically connect the RE. Screw it before placing the electrode holder in the beaker for better positioning.(Right) Electrodes and N2 probe fixed in place over the beaker.

After the electrode holder is placed over the beaker, take the N2 tube from within the cage, and slide it through the opening in the holder. Now, all 3 electrodes and N2 probe should be immersed in PBS

Make sure to connect the electrical wires from inside the cage to the electrodes. If following the pictures and cabling diagrams, further showed in Figure 3.8:

- The blue wire may be connected to the RE's white cable.
- The red wire shall be connected to the CE's banana port
- The black wire shall be connected to the sample electrode. It may be needed to attach some crocodile grippers to connect directly to exposed wires.
- Close the Cage's door.

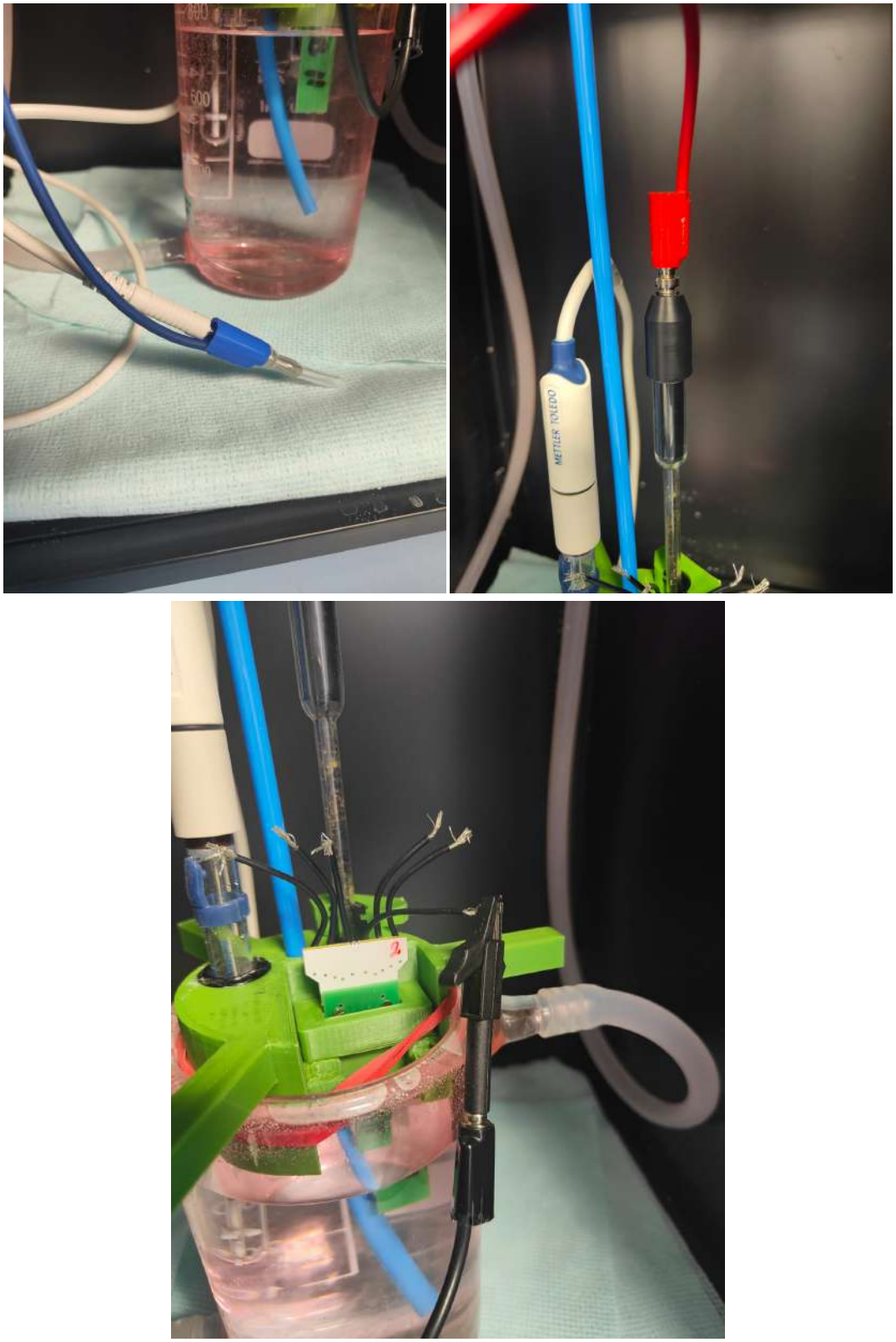

Figure 3.8: Correct cable connections within the cage for the protocol. The blue cable carries the signal of the RE. The red cable carries the signal of the CE. The black cable carries the signal of the WE.

2.3 Computer & Modulab XM Preparation

Make sure to plug in the power cable from the Modulab XM. Then, its power switch may be flipped. It is located at the back part of the instrument, near its left side, below the fan. Figure 3.9 shows the back of the Modulab XM, serving as further reference to find the switch. You may also now connect the red data cable to the computer.

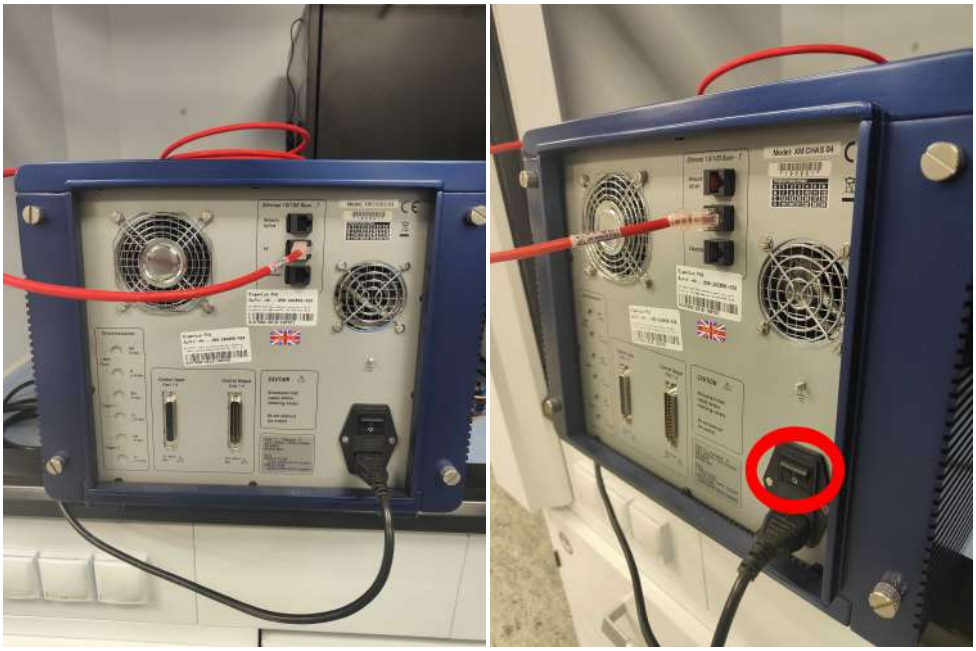

Figure 3.9: Backside of the Modulab XM. Notice the power switch is located at the bottom right corner in the pictures, meaning that when reached from the front, it will be at the bottom left corner

The Modulab XM needs some time to boot up effectively. The LED lights in the front interface indicate this. Please do not operate the setup until LEDs show as in Figure 3.10. The top row of LEDs labelled Power should be constantly on, with the second row of LEDs labelled Comms should be blinking.

Figure 3.10: LEDs indicating a correct standby status of the Modulab XM after booting up. The second row, with labels "Comms" should be blinking.

If LEDs for Error remain lit up, or other LEDs such as the Power LEDs are blinking, the Modulab XM did not boot up correctly. Reach out for the switch, turn it off, give it 10 seconds to cool off, and turn it back on. Eventually, it should boot up correctly.

Figure 3.11: Different status of the Modulab XM, while which it should not be operated. They may show during boot up, or after booting up if this step was unsuccessful, or if the system freezes/bugs out during an experiment.

Click on the Modulab XM ECS desktop icon to open the Modulab software. This will be how experiments will be programmed and sent over to the three-electrode setup.

Figure 3.12: Icon of the program XM-Studio ECS, used to operate the Modulab XM. It is found on the desktop of the computer

Then navigate to the experiment folder. As of Dec 2023, EIS & CV experiments may be found in the following folder directory (screenshot in Figure 3.13).

- **> Modulab XM > Additional Tests > Potentiostatic Impedance Test**
- **> Modulab XM > Additional Tests > Cyclic Voltammetry**

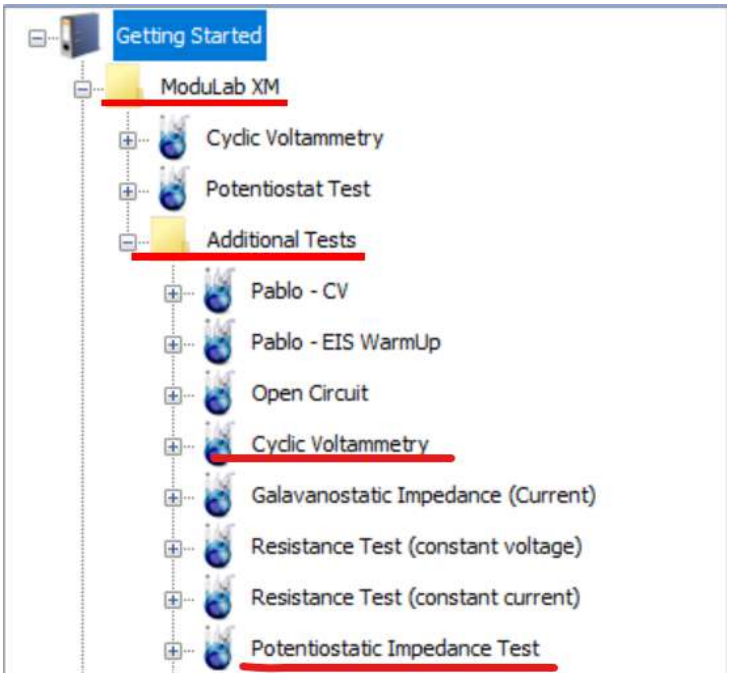

Figure 3.13: Folder path leading to the experiments set up in XM-Studio. Other experiments may be found, and one may design its own experiments too. For more info, check the user guide.

The following diagram summarizes the whole setup configuration for performing experiments with the Modulab instrument.

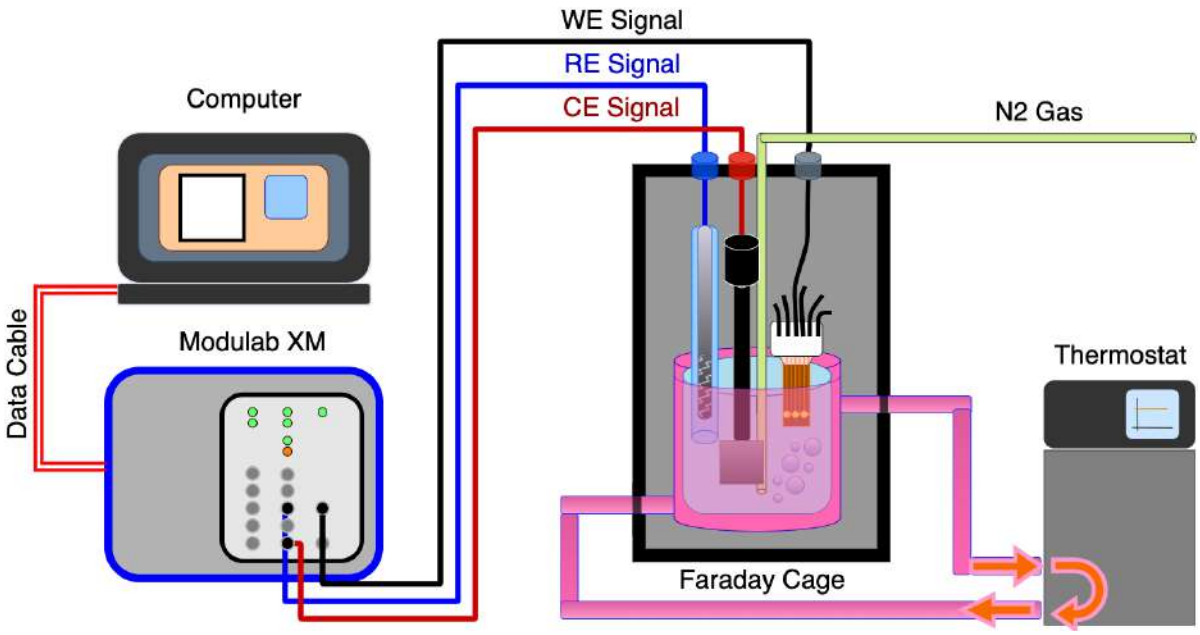

Figure 3.14: Schematic of the experiment setup with the Modulab Xm

3 Electrode Characterization EIS & CV

To navigate the Modulab XM ECS program and understand all parameter choices, please refer to the Modulab XM ECS software user guide.

When conducting tests, several parameters can be tuned. While some may be test-dependent, others should not be modified unless specifically aiming to do so. This is the case for most of the settings found on the Setup page (Hardware Requirements, Cell Setup, Potentiostat Experiment Setup, and Safety Limits). Some of the critical parameters that should be only changed when aiming to do so are:

- **Setup/Hardware Requirements/Grounding** Should be kept at Internal
- **Setup/Hardware Requirements/Potentiostat Configuration** Pstat + Femto Ammeter should be selected.
- **Potentiostatic Impedance/Scan Setup/DC Level** Keep it at 0V vs Reference (only for EIS)

3.1 EIS

To conduct an EIS Test, first of all, turn OFF the N2 gauge. The test is quick, and N2 bubbles may introduce noise, specially at low frequencies.

Several parameters may be considered, reached by following:

> Modulab XM > Additional Tests > Potentiostatic Impedance Test > Setup > 1: Potentiostatic Impedance > Impedance Setup

Additional parameters may be accessed by ticking the "Advanced" checkbox. Check Figure 3.15 for further aid.

- **Start frequency.** Frequency where the sweep is initiated. Maximum value is 300kHz. The recommended value is 100kHz.
- **End frequency.** Frequency where the sweep is ended. Minimum and recommended value is 0.1 Hz.
- **RMS Voltage.** Alternating Voltage is used in the measurement of impedance. 10mV RMS is recommended and standard practice across the literature.
- **Points per decade.** Sample points per log decade are taken. Recommendation: 10 - 25 is good.
- **Cycles of integration.** How many sample points of impedance are measured at each frequency value. As we may later plot averages of several EIS, choosing 1 cycle will yield the fastest test.

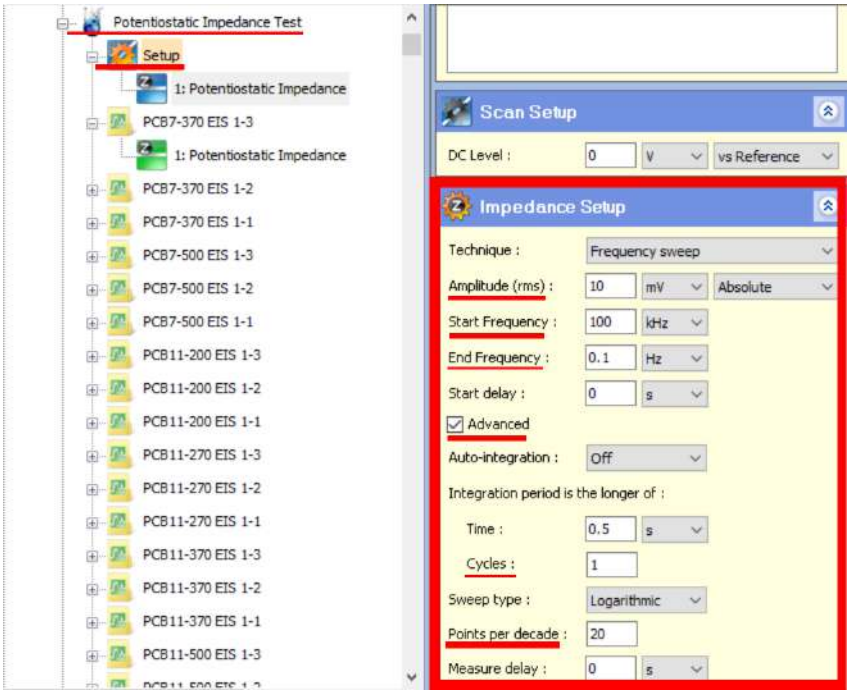

Figure 3.15: Window where most EIS parameters are commonly defined.

Parameters that should **NOT** be modified:

- **Start delay.** Upon previous research, when introducing a delay different from 0, the chances of the machine freezing at the start of the experiment and having to restart the whole instrument are high. This happens because it is not able to communicate with the CE, evidenced by its LED not turning on.

To run an experiment, under the Start Experiment (**> Modulab XM > Additional Tests > Potentiostatic Impedance Test**) page, choose the name for the data file and click run. Figure 3.16 is a screenshot of the page.

When viewing past EIS measurements, you may want to display information using the "Bode ($|Z|$, θ)" plot graph style.

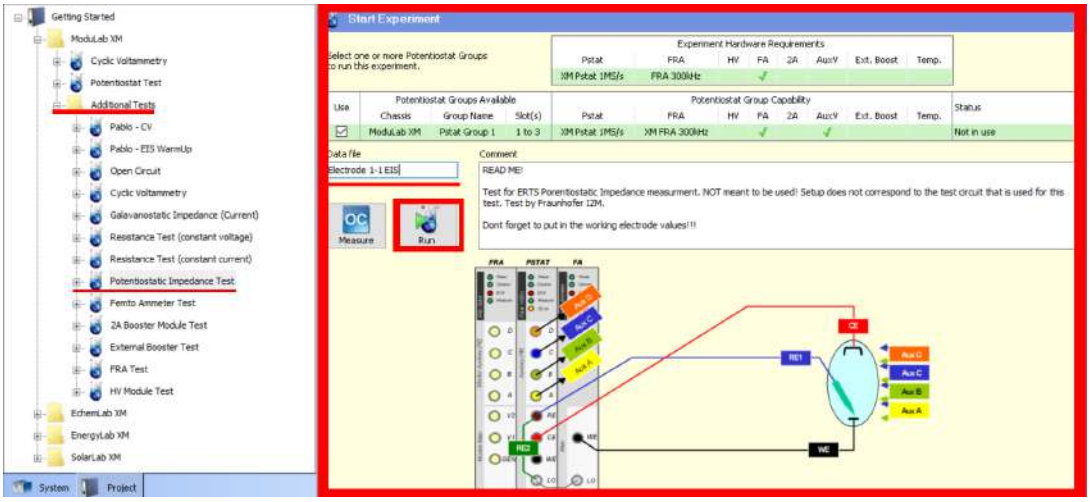

Figure 3.16: Choose an appropriate name for the file, and click Run to perform the EIS experiment.

3.2 CV

To conduct a CV Test

- Turn on the N2 gas flow. These tests are long, and not prone to noise interference by the bubbling
- If you will leave the lab while the test is running, leave a note with all the information necessary.

Several parameters may be considered, reached by following:

> Modulab XM > Additional Tests > Cyclic Voltammetry > Setup > 1: Cyclic Voltammetry > Scan Setup

Check Figure 3.17 for further aid.

- **Starting Voltage.** Voltage where the CV is initiated. Should be one of the Water Window bounds (WW)
- **Ending Voltage.** Voltage where the CV is ended. Should be the other one of the Water Window bounds (WW)
- **Cycle Count.** Number of cycles performed. Should be thought out for each experiment. Note that high cycle counts exert higher electrochemical stress on the sample. They also make the experiment last longer.
- **Scan Rate.** Scan rate greatly influences the CV obtained. For more on that, check the literature (Cogan et al 2008, Boehler et al 2020)[1, 2]. Additionally, the literature review by P. de Anta may also be read.

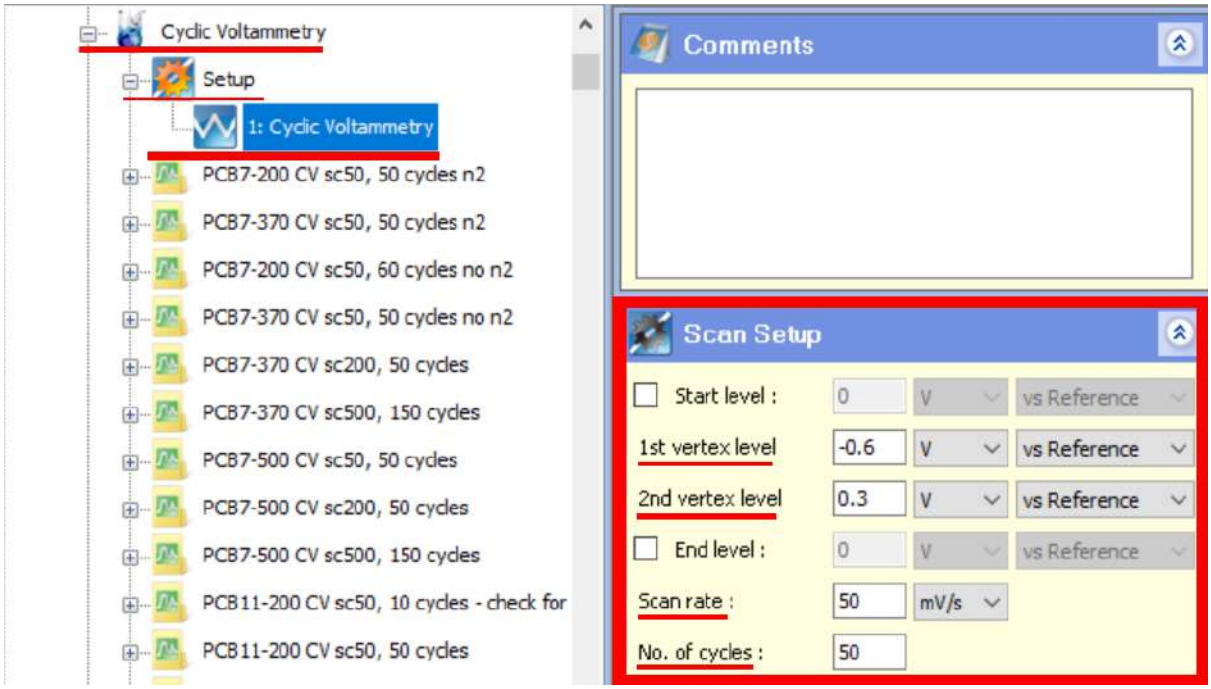

Figure 3.17: Window where most CV parameters are commonly defined.

To run an experiment, under the Start Experiment (**> Modulab XM > Additional Tests > Cyclic Voltammetry Test**) page, choose the name for the data file and click run. Figure 3.18 is a screenshot of the page.

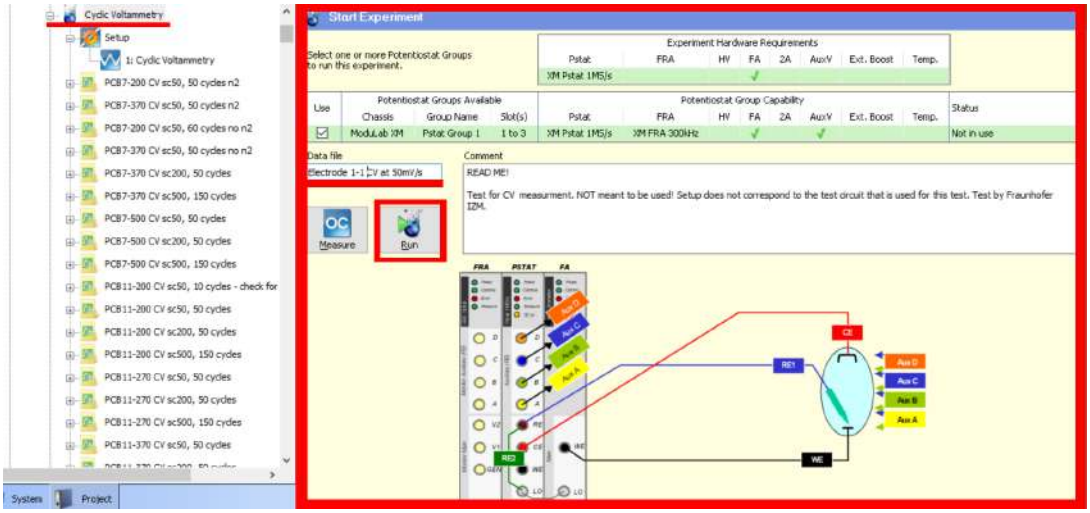

Figure 3.18: Choose an appropriate name for the file, and click Run to perform the CV experiment.

When viewing past CV measurements, you may want to display information using the "I vs E" plot graph style.

4 Clean Up for EIS & CV

Clean-up specific to the Modulab XM implies disconnecting the electrical cables from the cage's ports, and proper storage of the RE.

Disconnect the three electrical cables from the cage's port. Unless strictly necessary, there is no need to disconnect them from the Modulab XM's port interface. They may be kept in a tidy manner while connected to the instrument.

The Modulab XM may now be turned off using the power switch located at the left of its backside. The data ethernet cable may also be disconnected from the computer, and the power cable at the outlet may also be disconnected and stored.

To remove the RE, start by disconnecting the inner electrical blue cable from the white connector cable belonging to the RE. You may also unscrew this white connector cable from the RE.

As with any other experiment clean-up, follow up by disconnecting electrical connections and removing the N2 tube from the electrode holder.

To safely take out the RE from the electrode holder, it may be best first to remove the electrode holder from the beaker and place it in its loading support, back at the working bench.

Gently pull the RE out of the electrode holder. While pulling, look at the tube near the rubber ring. The moment you are able to see the white plastic triangle at the tip of the RE, the electrode is nearly out, shown in Figure 3.19. Slow down at this moment to avoid damaging the electrode when it abruptly comes out.

Rinse the RE with DI water and make sure to properly dry it with some light pressurized N2.

The RE electrode needs to be stored back in its plastic vial containing PBS solution. Slide the RE into the vial. If the solution does not rise until the top plastic screw ring, a refill may be needed. More solutions may be found in the RE's storage box.

With the RE protected by the plastic vial, you may now store it in its box. It is important the RE is always kept in an upward, vertical position.

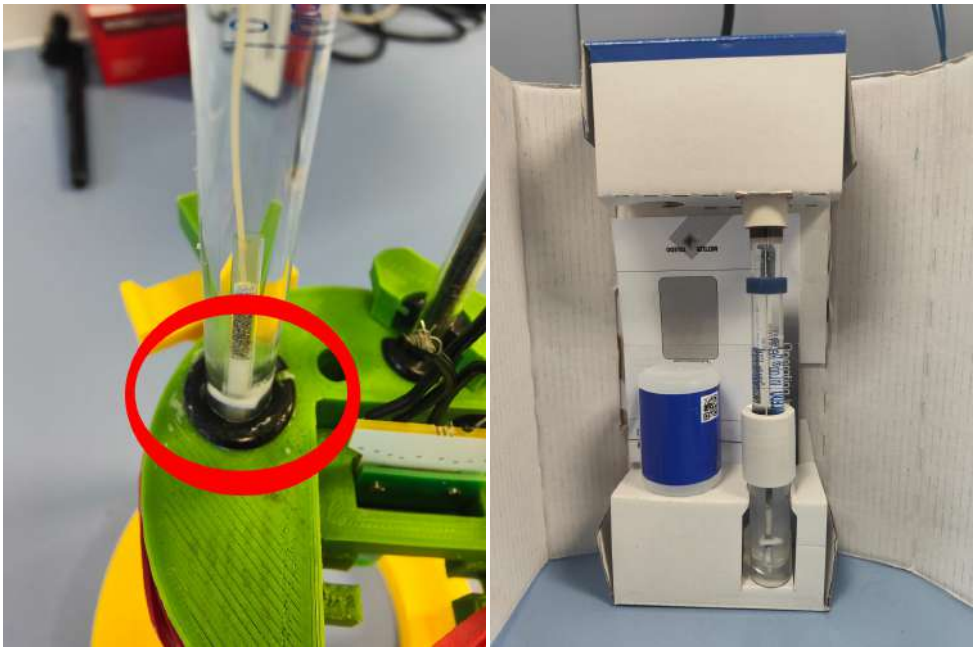

Figure 3.19: While pulling out the Re, when the white plastic triangle becomes visible, the electrode is soon to be released. Be careful to not damage it when the grip loosens.

If you are to continue your experiments, you may keep the WE and CE placed in the electrode holder.

If you are finished with all the experiments, continue with Chapter 7: Clean Up - General

5 Data Retrieval & Processing

In order to perform analysis on the data from EIS and CV measurements, we first need to extract the experiments into workable files. To do this, follow these steps, and check Figure 3.20:

1. Begin by clicking the experiment's name (shown in 3.20). You must do this for every experiment of interest.
2. Click the button under the Graph menu labelled "Export All". An Excel file with the experiment data shall pop up.
3. Once all experiments are exported, you may close all Excel tabs by right-clicking on the program and choosing "Close All"
4. Head to the computer directory of the Solartron. The Modulab XM "Additional Experiments" folder is pinned in Quick Access.
5. In the folder named after each experiment type, .csv files with the exported tables may be found. Copy them to an external USB drive

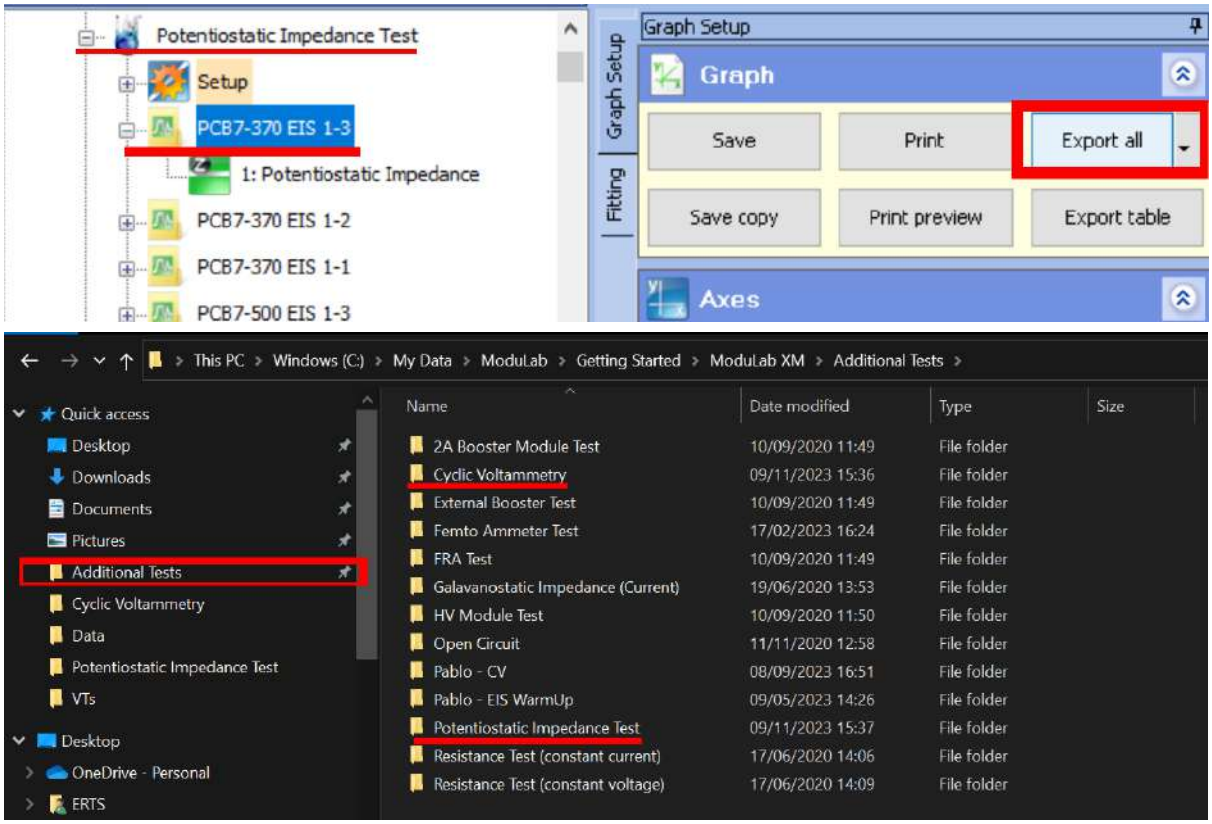

Figure 3.20: To export all the test data into a .csv file, click the "Export All" icon in the test file. Then navigate to the computer´s file directory, easily through the pinned element "Additional Tests", and extract the files of interest.

Using the Matlab code designed for each respective test, you may import the file, specify data about the sample (Opening diameter, CV cycle count) and obtain plots and other metrics of interest.

4

PROTOCOL FOR VTS

1 EQUIPMENT FOR VT TESTING - SEE FIGURES 4.1 AND 4.2

1. **Tektronix MDO34 Oscilloscope** - Other oscilloscopes lack the functionality to use the arbitrary function generator (AFG) or to be controlled with the computer. The MDO34 should come with a power cable to power it up, and a USB to USB-A cable for data communication with the laptop
2. **1 MDO34 CH Probe** - Several of these probes may be found in the bag attached to the MD034. For correct labelling, as it will be used in CH2, choose the light-blue probe.
3. **VCCS PCB** - In this protocol, testing is done with the V0 of this PCB, but any future versions could replace it. This also applies to any future versions having a different list of required materials.
4. **1 PCB jumper** - To be stored and found on the jumper pins of the PCB.
5. **Tool to manipulate PCB switches** - Any kind of thin, long tool works such as a flat-head screwdriver. Be careful when using metallic tools as they may easily damage the PCB´s circuitry. If there are other materials available, choose an insulating one.
6. **3 BNC cables** - May be found in lab 231. Although 2 require a rather short length (connections from the Oscilloscope to the PCB), one should be long enough to take the signal from the PCB to the Faraday Cage.
7. **1 BNC cable signal Y-splitter** - Testing shows T-splitters tend to introduce more noise than Y-splitters, so preferably use the latter. Found in lab 231.
8. **1 BNC to Banana +,- adapter** - Found in lab 231. You may need an additional piece to connect both male BNC connectors, such as an additional splitter.
9. **1 Banana to Hook cable** - Found in lab 231
10. **1 Banana to Banana cable** - Found in lab 231

11. **1 MINI USB to USB cable** - Currently we do not have our own cable, but one can be found and is usually free to use on the VWR pHenomenal device, located on top of the workbench in front of the digestorium.
12. **Python programming executable (Visual Studio Code)** - Software programming language in which the script to control the MDO34 has been written in. Additional software packages such as Visual Studio Code may be useful when testing. Both may be found installed on laptop NB-SIIT086.

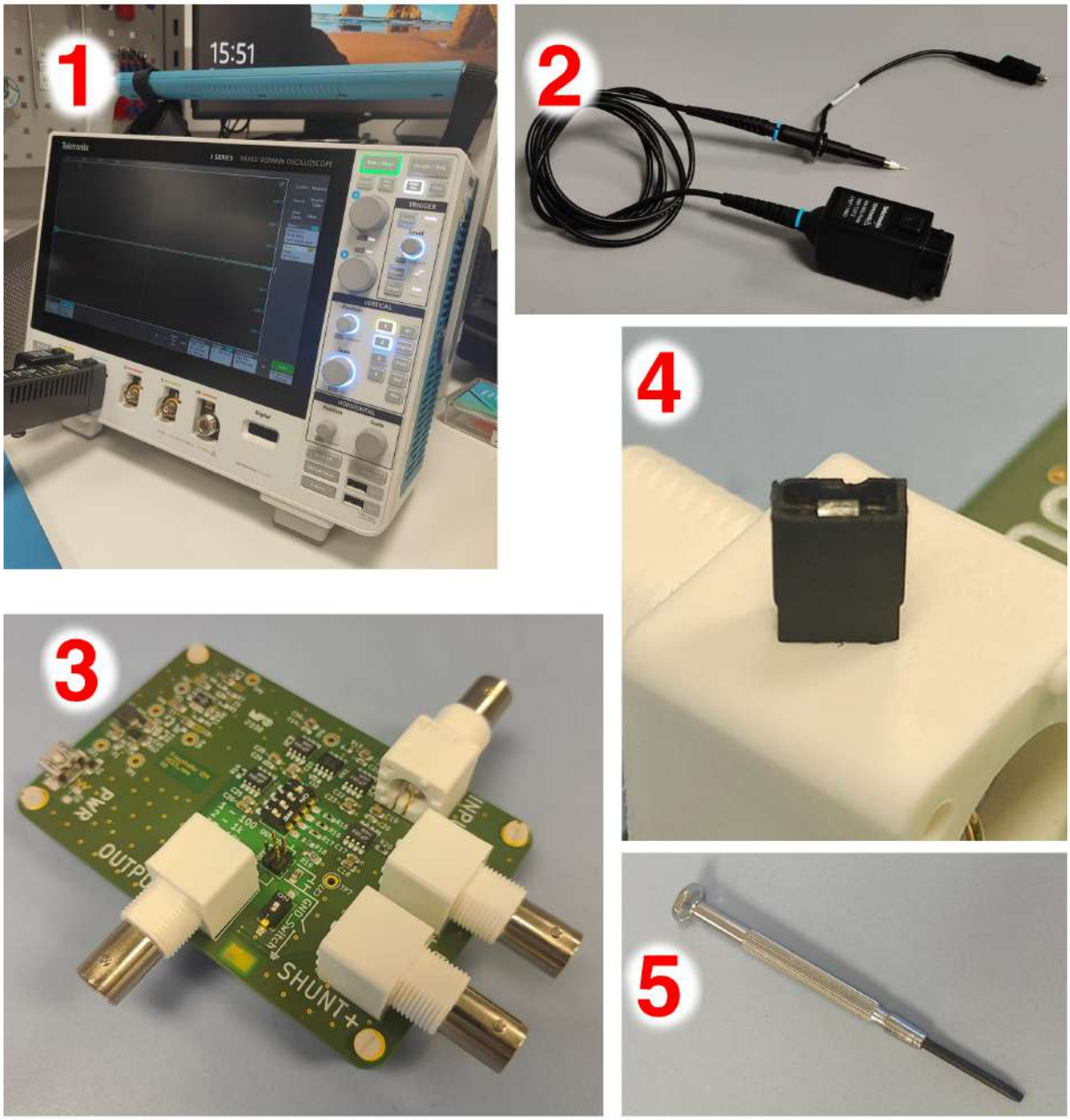

Figure 4.1: Equipment items 1 to 5 specified in the list in Section 3.3 - Equipment for VT Testing

Figure 4.2: Equipment items 6 to 11 specified in the list in Section 4.1 - Equipment for VT Testing

2 Setup Preparation

2.1 VCCS PCB, Oscilloscope and Cage Preparation

To perform VTs, a dedicated Voltage-controlled Current Source (VCCS) PCB and the Tektronix MDO34 Oscilloscope are needed, shown in Figure 4.3

IMPORTANT: This protocol is written with the VCCS PCB V0 in mind, picture in Figure 4.4. Any further versions may differ slightly in build, but the overall setup should be similar. If in doubt, check with the responsible person for the latest PCB.

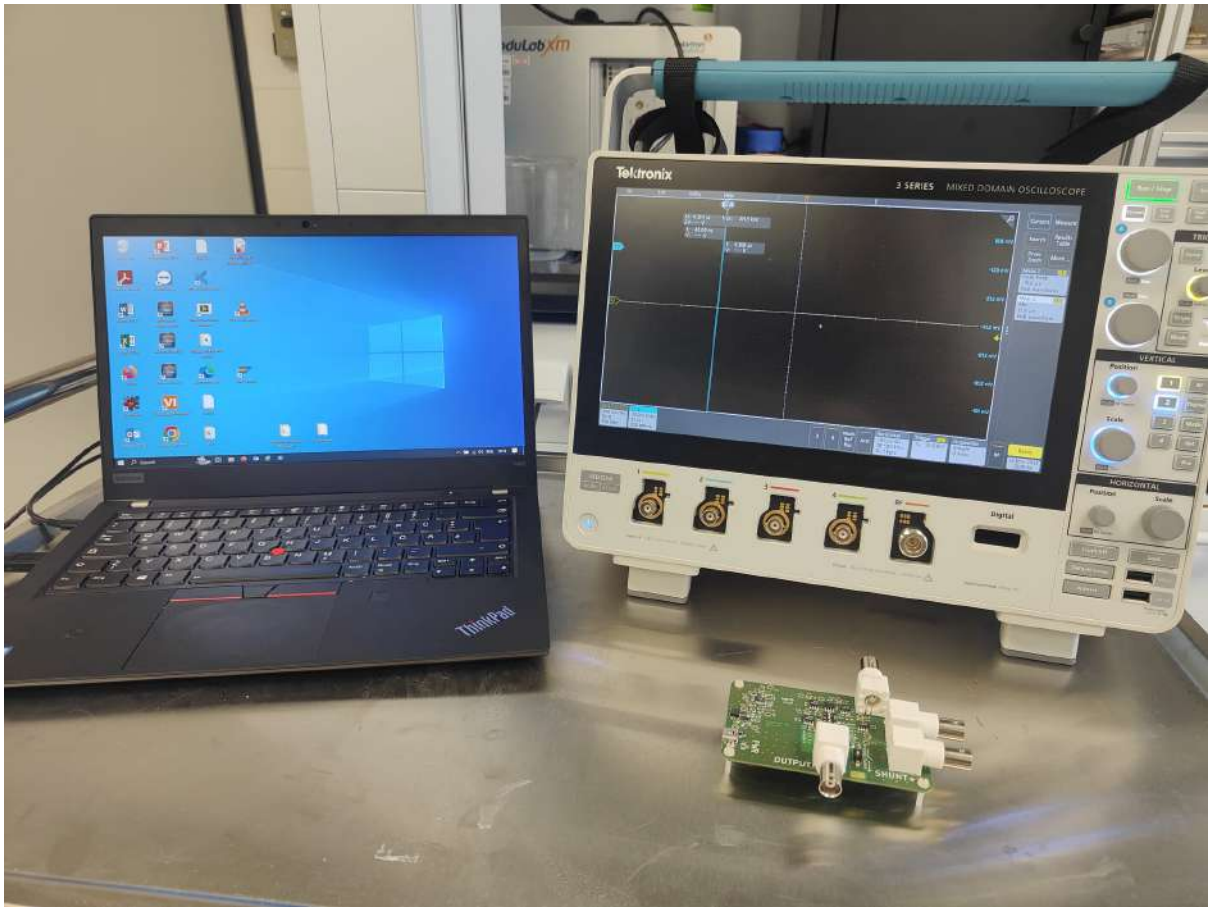

Figure 4.3: Main pieces of equipment required to perform VT tests. Cables not shown.

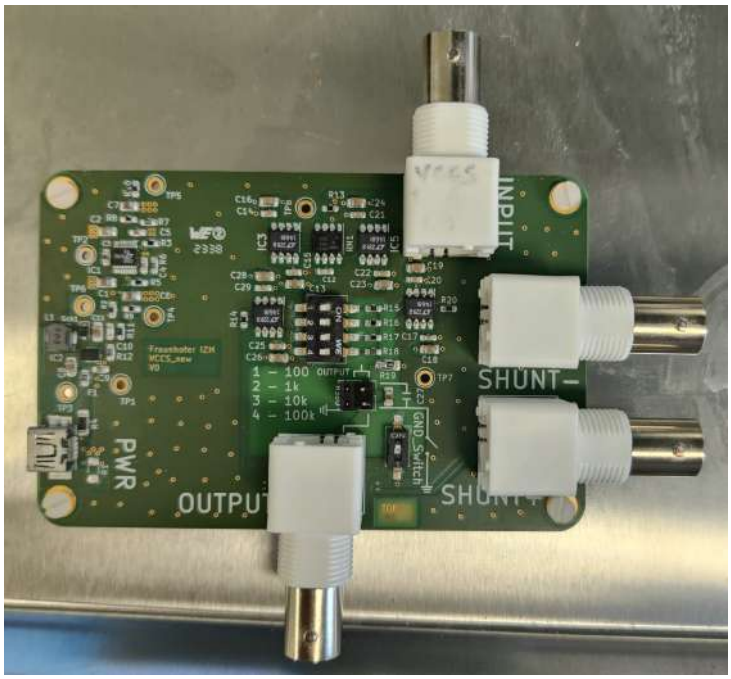

Figure 4.4: The VCCS PCB V0 is the custom-built board used in the setup described in this protocol. Any other future versions could have a different setup and testing procedure.

Start by setting up the Tektronix MDO34 Oscilloscope. Place it close to the setup area, as constant manipulation is needed and shorter cables are preferred.

- Plug it in with the power cable and turn it on.
- Use the USB-A port at the back to connect it via USB cable to the laptop.
- Use a BNC cable to connect to the AFG Out port at the back - this cable will be connected at the input of our PCB.
- Plug one of the oscilloscope measurement probes into CH2.

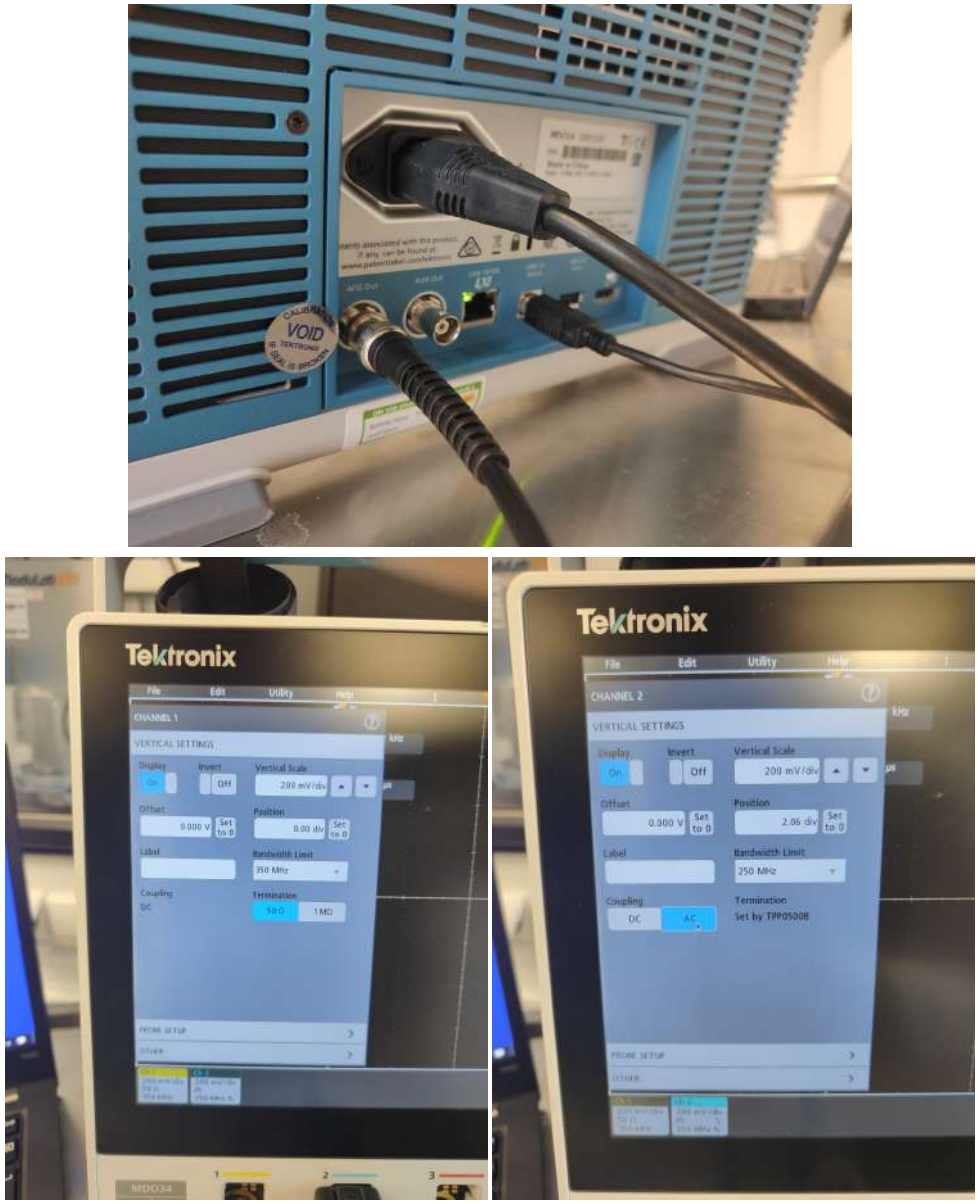

Figure 4.5: Setting up the Oscilloscope requires to plug in the necessary cables at the back of the oscilloscope, and connect and set CH1 and CH2

Other important considerations regarding the oscilloscope are

- In CH1, input Impedance should be set to 50 Ω
- In CH2, make sure coupling is set to AC.
- Set trigger at t=0.
- If the pulse sent is too small, it may be necessary to move up and down the trigger.
- If at any moment the pulse wants to be stopped, the quickest and safest way is to turn off the AFG from the oscilloscope itself.

With the oscilloscope set up, it should look like this:

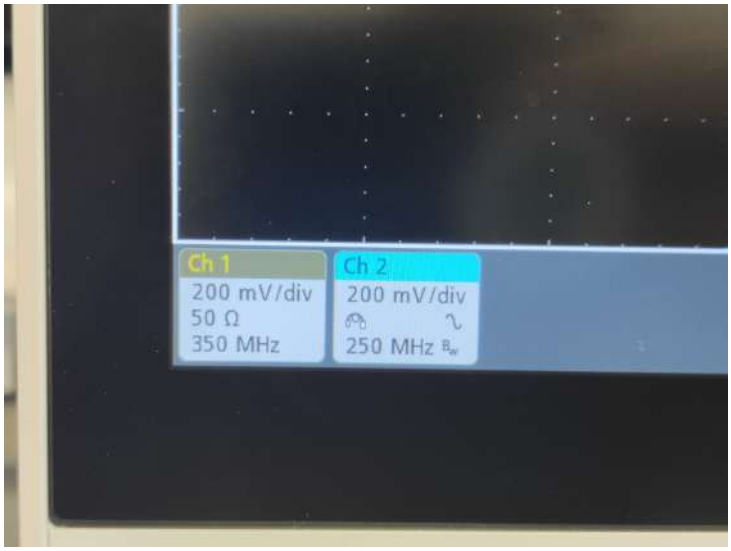

Figure 4.6: Icons for CH1 and CH2 when correct settings for input impedance and AC coupling in Ch2 are chosen.

To set up the VCCS PCB (check Figure 4.7 for references of the BNC splitter connections):

- Start setting up the PCB by ensuring a BNC Y-splitter is connected at the PCB´s input port, by connection 3.
- On one side (connection 2), connect the BNC cable from the AFG Out in the oscilloscope.
- On the other side (connection 1) of the splitter, connect another BNC cable which will then be connected to CH1 in the oscilloscope.
- At the Output port, connect another BNC cable
- To power up the PCB, a mini USB cable is needed. Plug the larger side of the USB cable into the laptop too.

IMPORTANT: BNC splitters are prone to introduce noise and disturbances in your signal. After testing and taking pictures for this protocol, it seems the Y-splitter works better than the T-splitter (Picture 4.7). Try to use this one whenever possible.

Figure 4.7: Left: T-splitter - AVOID if possible. Right: Y-splitter - BETTER option

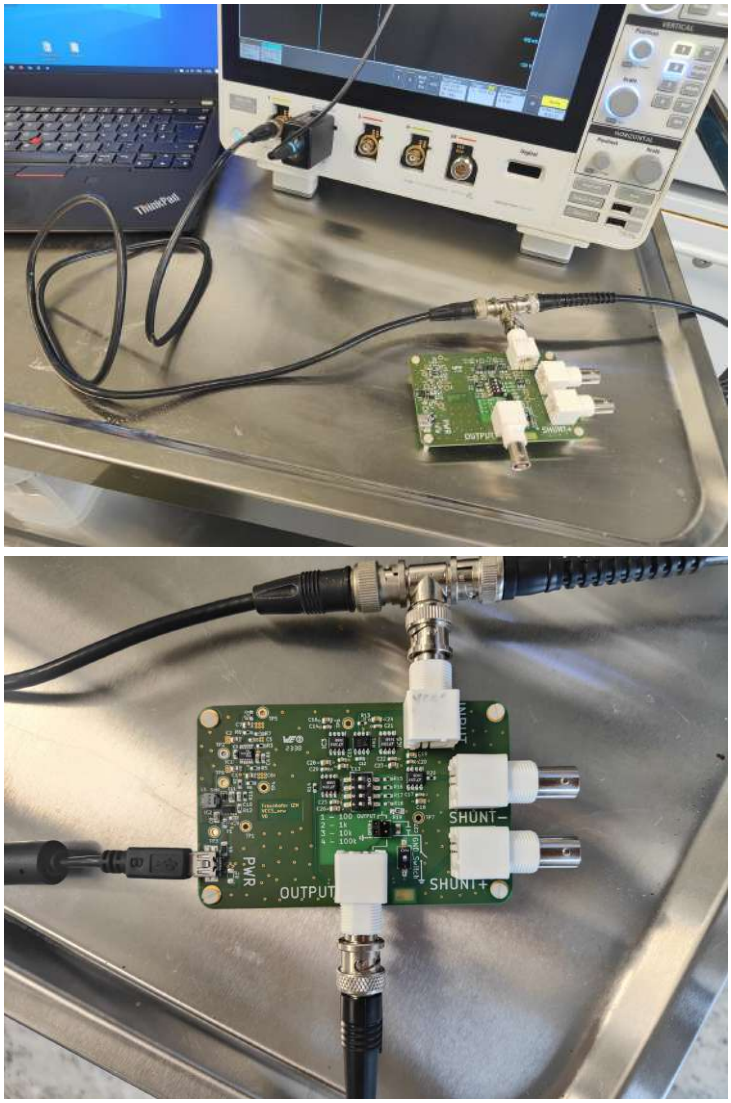

Figure 4.8: Use the BNC signal splitter to drive the AFG signal to both the PCB´s input port, and the oscilloscope´s CH1. Connect the power USB cable, and the output BNC cable.

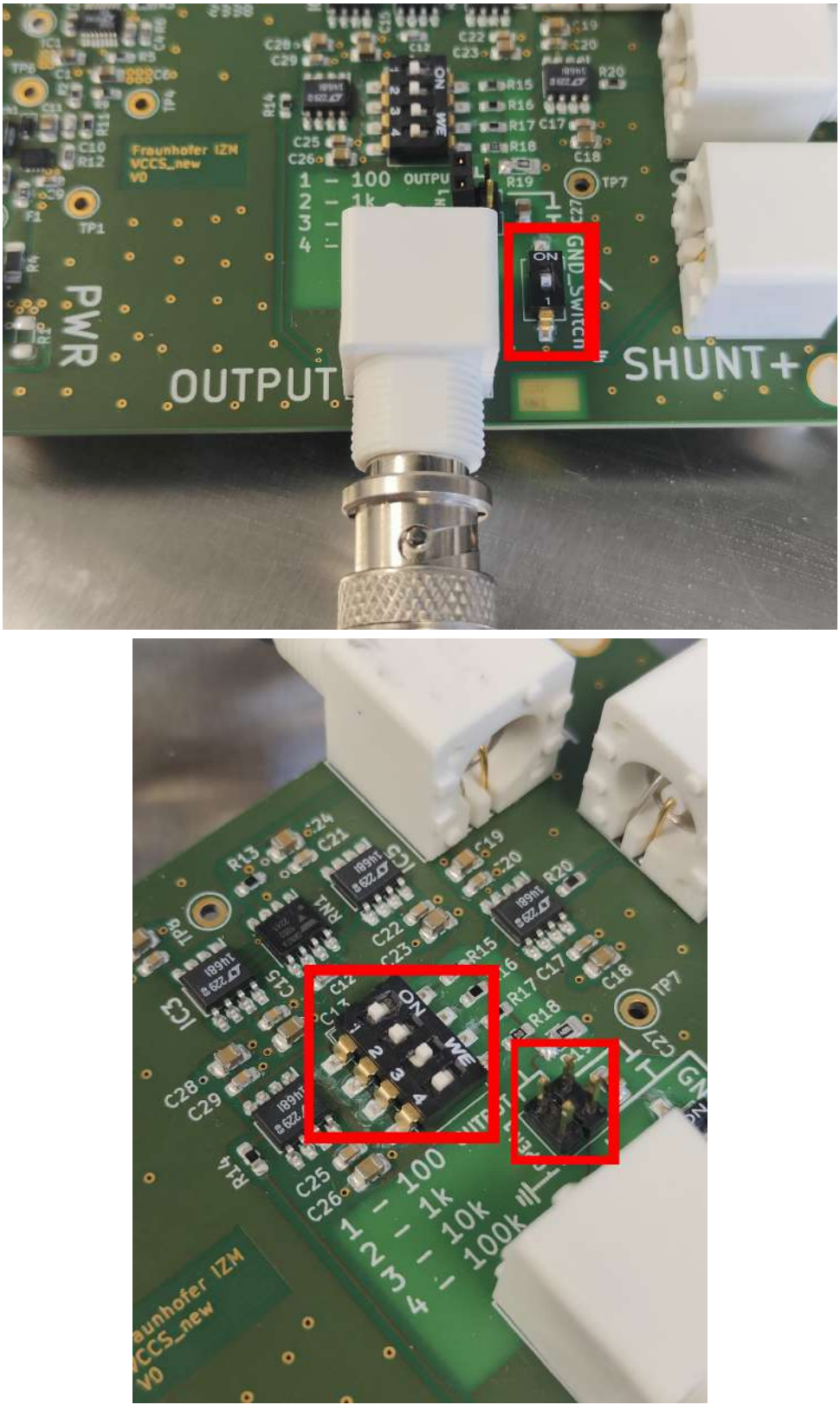

Figure 4.9: Correct switch configuration for initial testing with the board. The Output switch is off, and a high resistance (R3) is chosen for the first test. No jumpers are connected.

There are some other considerations regarding the PCB and its switches:

- Start the board by ensuring that the switch near the output is open. Turn it ON, then grounding the Output.
- When performing VTs on a sample for the first time, it is wise to start with higher resistances to avoid damaging the sample. A reminder [R1: 100 Ω , R2: 1000 Ω , R3: 10000 Ω , R4: 100000 Ω. Switch on the resistance of choice before running a test.
- **If you are using R1, it is necessary to place the jumper on the two right-side pins.** For more on this, visit the subsection 'Modifying the PCB configuration'
- If not using R1, ensure there is no jumper connecting the left or right pins.

With the PCB set-up, it should look like Figure 4.10:

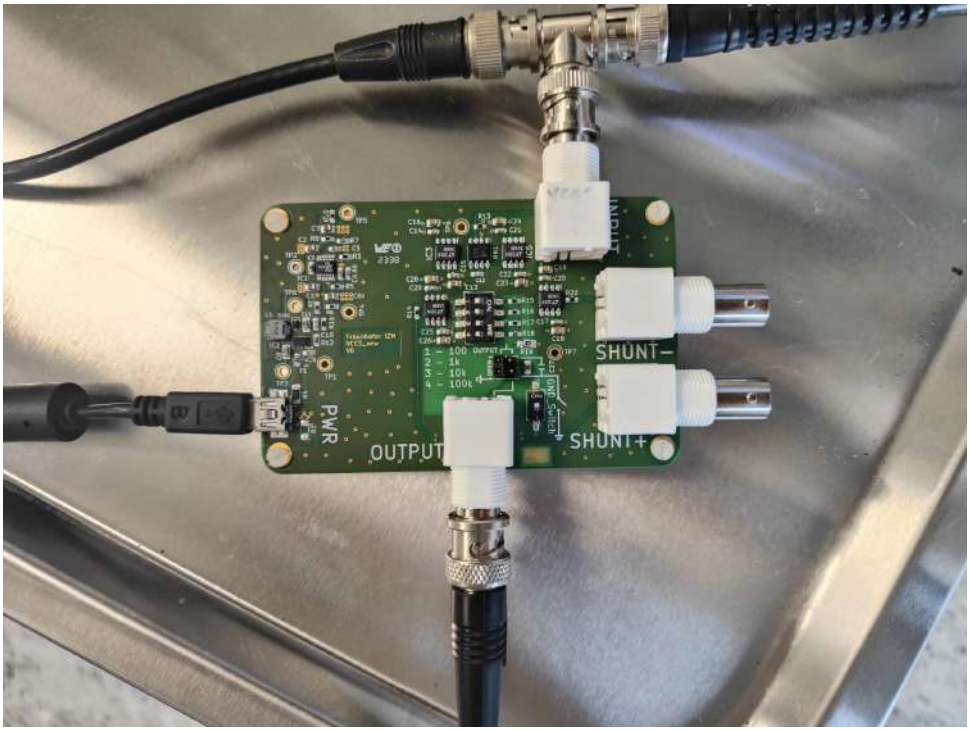

Figure 4.10: Final PCB configuration, ready to begin testing with.

To connect the PCB and Oscilloscope to the cage with the electrodes:

- Connect a BNC-to-banana cable at the end of the BNC cable coming from the PCB´s output.
- **With BNC cables, polarity is important!** Connect the **red** banana (carrying the signal) to the WE cage port (**black**).

- **With BNC cables, polarity is important!** Connect the **black** banana (shield and return signal) to the CE cage port (**red**).
- Connect an additional banana-hook cable at the WE port.
- At the hook end of this cable, connect the main oscilloscope´s probe for CH2 (also a hook!)
- Connect an additional banana-banana cable at the CE port
- At the banana end of this cable, you may use the large crocodile grippers of the cage to shield the whole connection
- Connect the remaining oscilloscope probe for CH2 to GND. This is done by connecting to the exposed metal of the CE banana cable. Anywhere along the cable is okay: either connect to the inside of the banana connector at the port passing through directly to the cage, or at the end of the additional banana cable as shown in Figure 4.11.

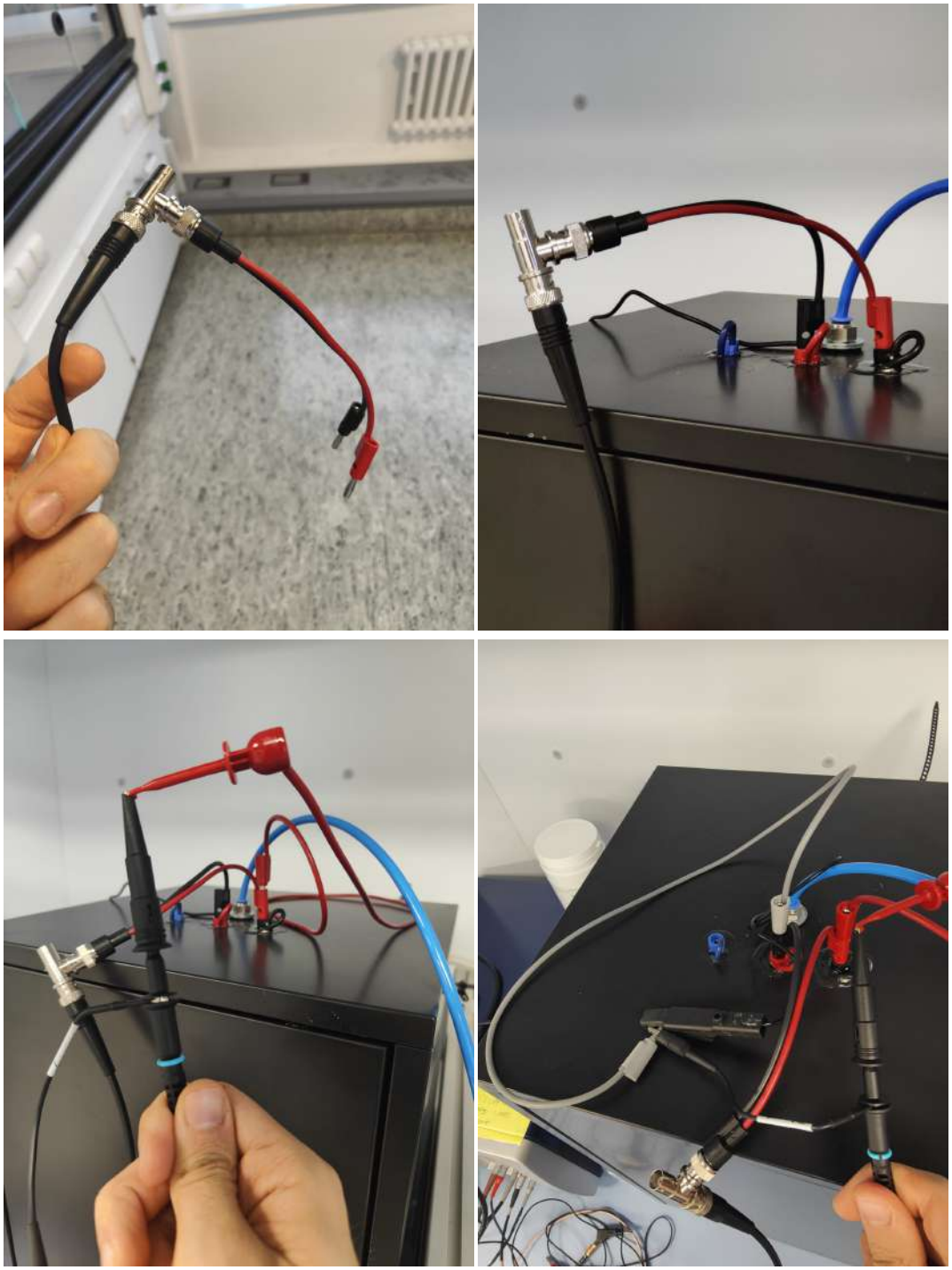

Figure 4.11: To correctly connect electrically the VT setup, both the output from the PCB and the Oscilloscope´s probes need to be connected. Pay attention, as the colour code between the cage and the BNC cable is switched. You may use additional banana cables to set all connections. And remember to ground the cage on the CE signal.

With the cage set up, it should look like this:

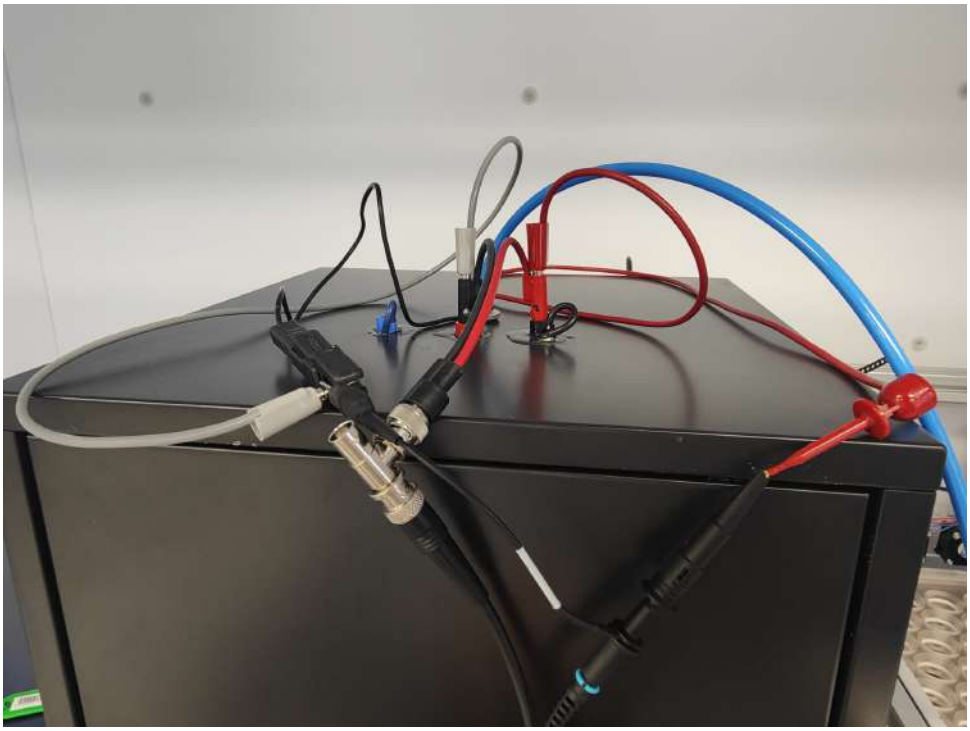

Figure 4.12: Final Cage configuration. Again, observe how the PCB output cables, the Oscilloscopes CH2 probes, the additional banana cables and the cage´s grounding grippers are all interconnected.

Note that in VTs, the Ag|AgCl Reference Electrode is not needed. Thus there is no need to plug a cable into the blue cage port or to place it in the electrode holder.

Next, we need to connect the wire connections to the interior of the cage. For further reference, check Figure 4.13.

- The red wire shall be connected to the CE's banana port
- The black wire shall be connected to the sample electrode. It may be needed to attach some crocodile grippers to connect directly to exposed wires.
- Close the Cage's door.

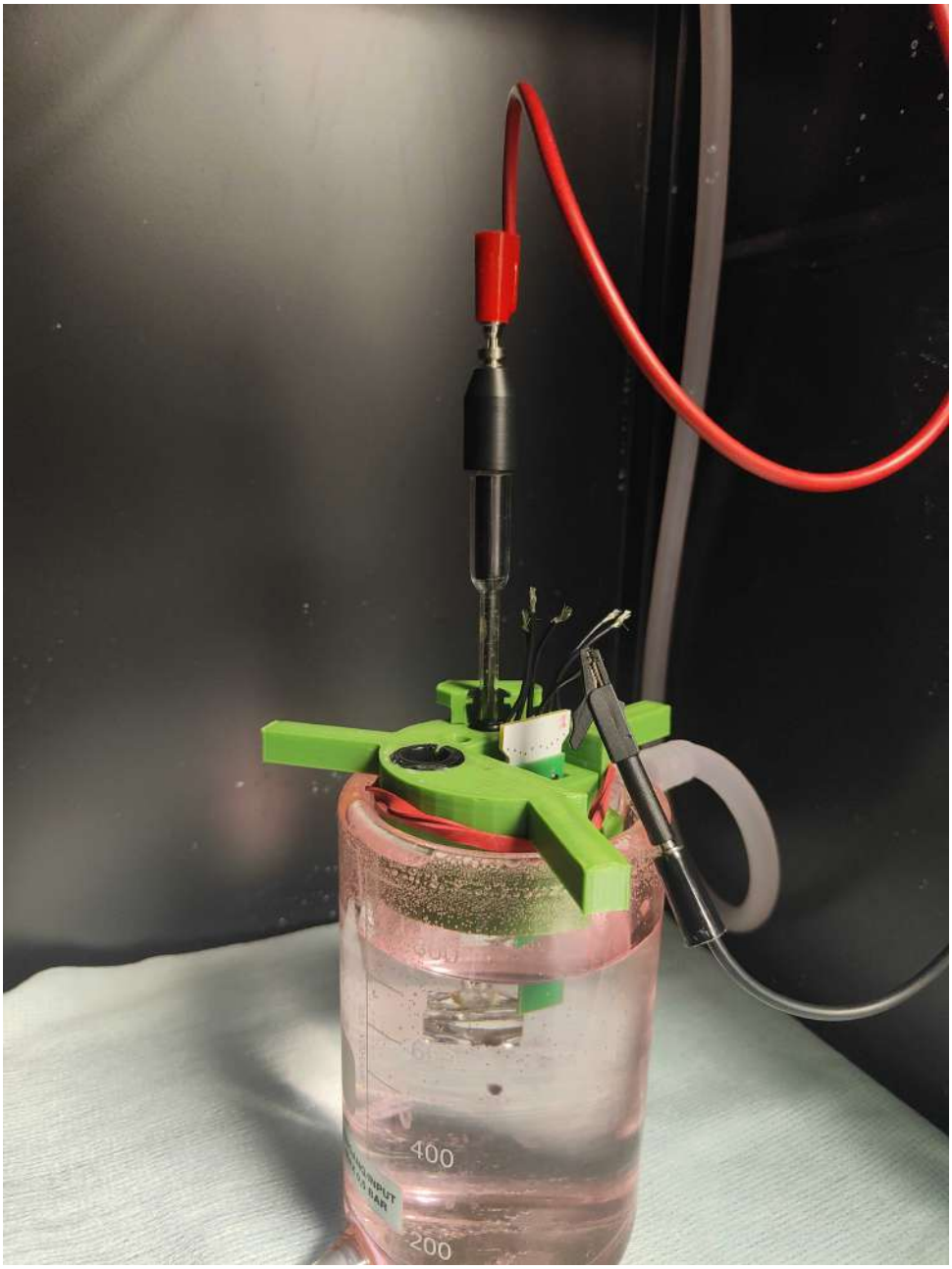

Figure 4.13: Internal Wiring for performing the VT tests. It only needs of the CE and the WE.

2.2 Computer & Python Preparation

Open the desktop folder named VTs. A Python code file with the name "voltage transient versionX.py" should be there. Open it with Visual Studio Code.

WARNING: TO AVOID DAMAGING ELECTRODE WHILE FIRST SETTING UP, DISCONNECT BOTH USB CABLES FROM THE LAPTOP WHILE ENSURING THE CODE CAN BE RUN

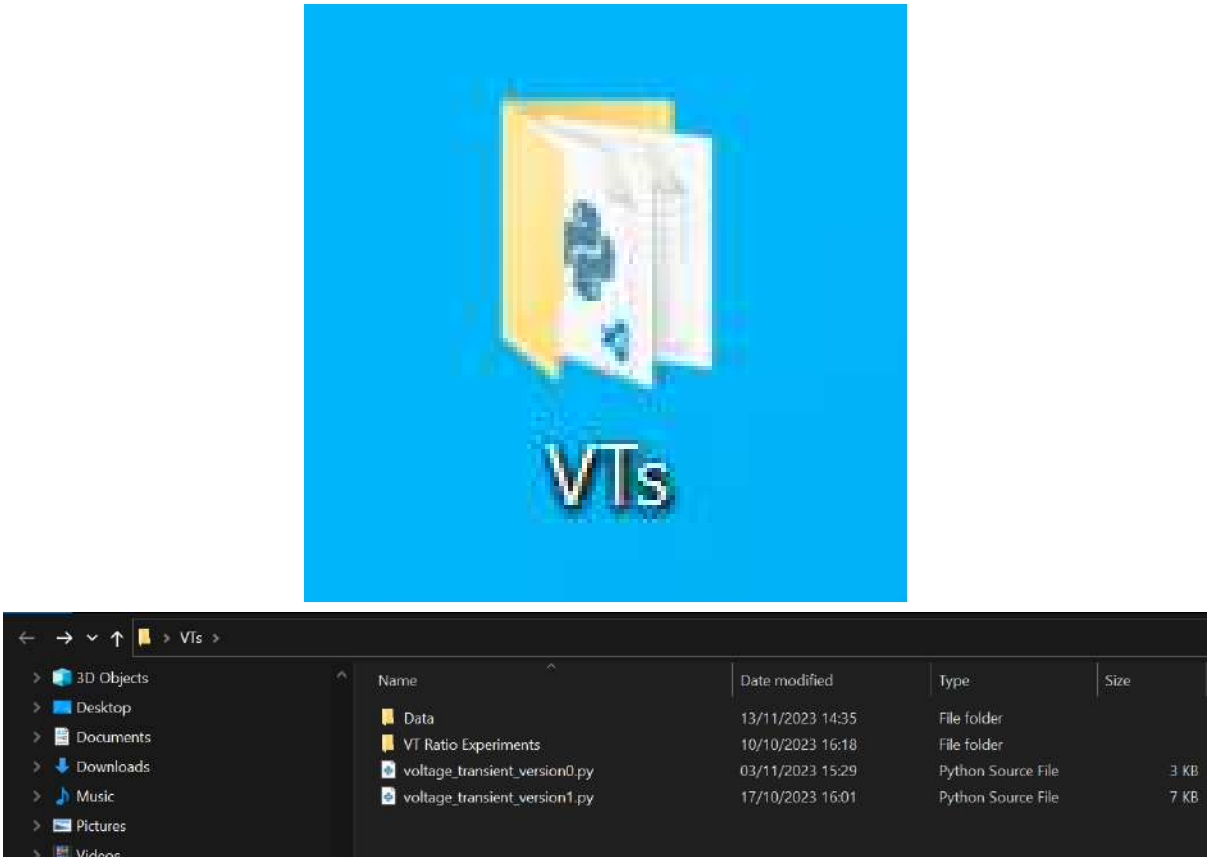

Figure 4.14: Folder in the desktop containing all files necessary to perform VTs. You may find the code files, with a .py extension there.

We first need to ensure that Python can run our code. If Python is loaded into VSC, it should show as a terminal when running the script. If it does not show, you need to route Python to VSC. To do this, start by changing the directory in the terminal. It can be done either in Powershell or VSC´s terminal. Start by copying the directory of the file from the folder on the desktop. Then type in the terminal:

CD STRG+V

This should paste the directory of the folder. Hit enter. Now the directory is changed.

To run the code, it may also be necessary to do so from the Terminal. To execute the file with Python, type:

PY "FILE NAME.PY"

The code may now be run from Visual Studio Code.

For a correct export of the data, make sure that the folder with the python files is added to the directory within VSC, as it will be here where the data files are created.

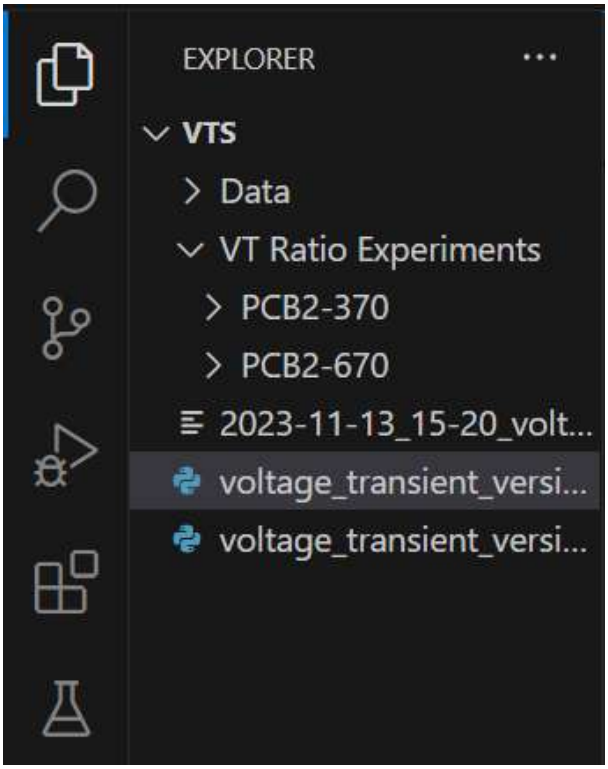

Figure 4.15: Once the file directory is set to the VTs folder on the desktop, it should appear as in the screenshot. If this step is omitted, the files will NOT be saved correctly.

The following diagram summarizes the whole setup configuration for performing VT experiments.

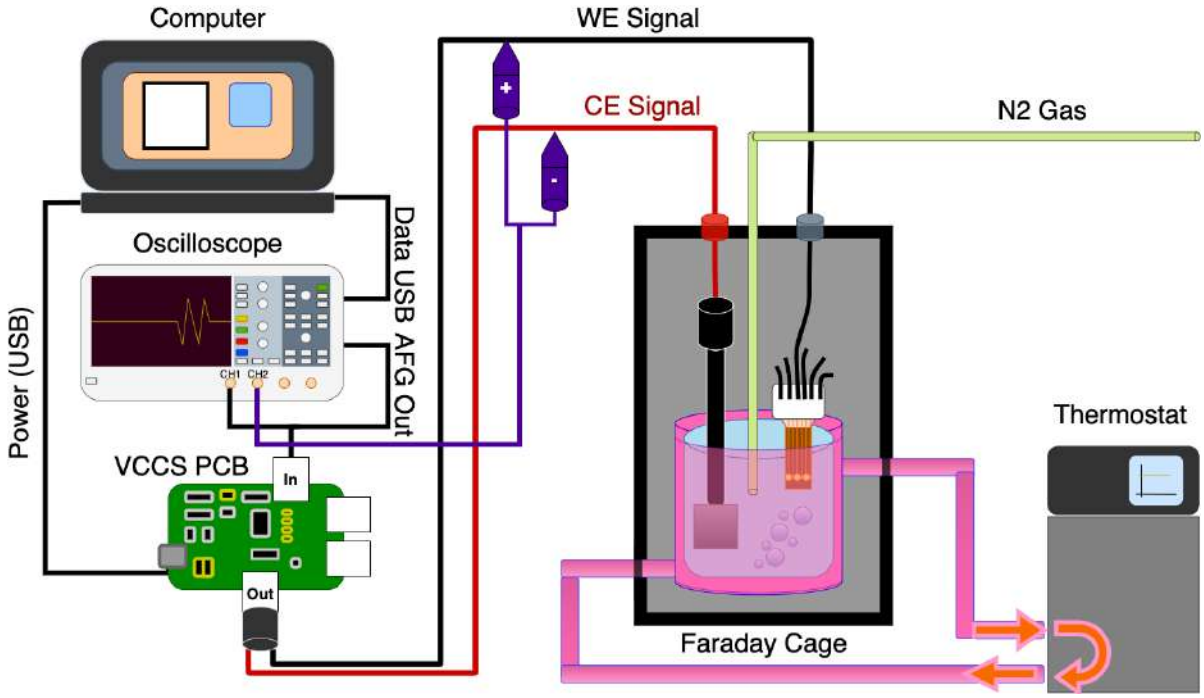

Figure 4.16: Schematic of the experiment setup for VTs

3 Electrode Characterization - VTs

To perform the VT tests, the Python code is run from the computer. This code sends the biphasic **voltage** pulse to the MDO34´s AFG, which then sends it to our VCCS PCB. The PCB uses one of the four conversion resistors to transform the voltage pulse into a **current** pulse, with a set current amplitude based on the parameter 'cathodic current' and the conversion resistor. This current pulse is run through our electrode pair, and the output generated (in Voltage) is measured to determine Va and the CIC.

To obtain Voltage Transients, the current method implies manual editing of the code script and manual analysis of the oscilloscope to determine Va. A code for automatizing these two tasks is under construction.

When a sample is tested, and a new one wants to be experimented with, follow this procedure:

- Plug the USB in if it was not connected already.
- Start by turning ON the switch next to the output of the PCB. This will ground your whole output signal, protecting the electrodes.
- Turn off the AFG from the oscilloscope. This way, it won´t send a high current pulse to the new sample
- Change to the sample of interest
- Turn OFF (to "1") the switch at the output, removing the ground.
- The AFG will be turned on when running the code again.

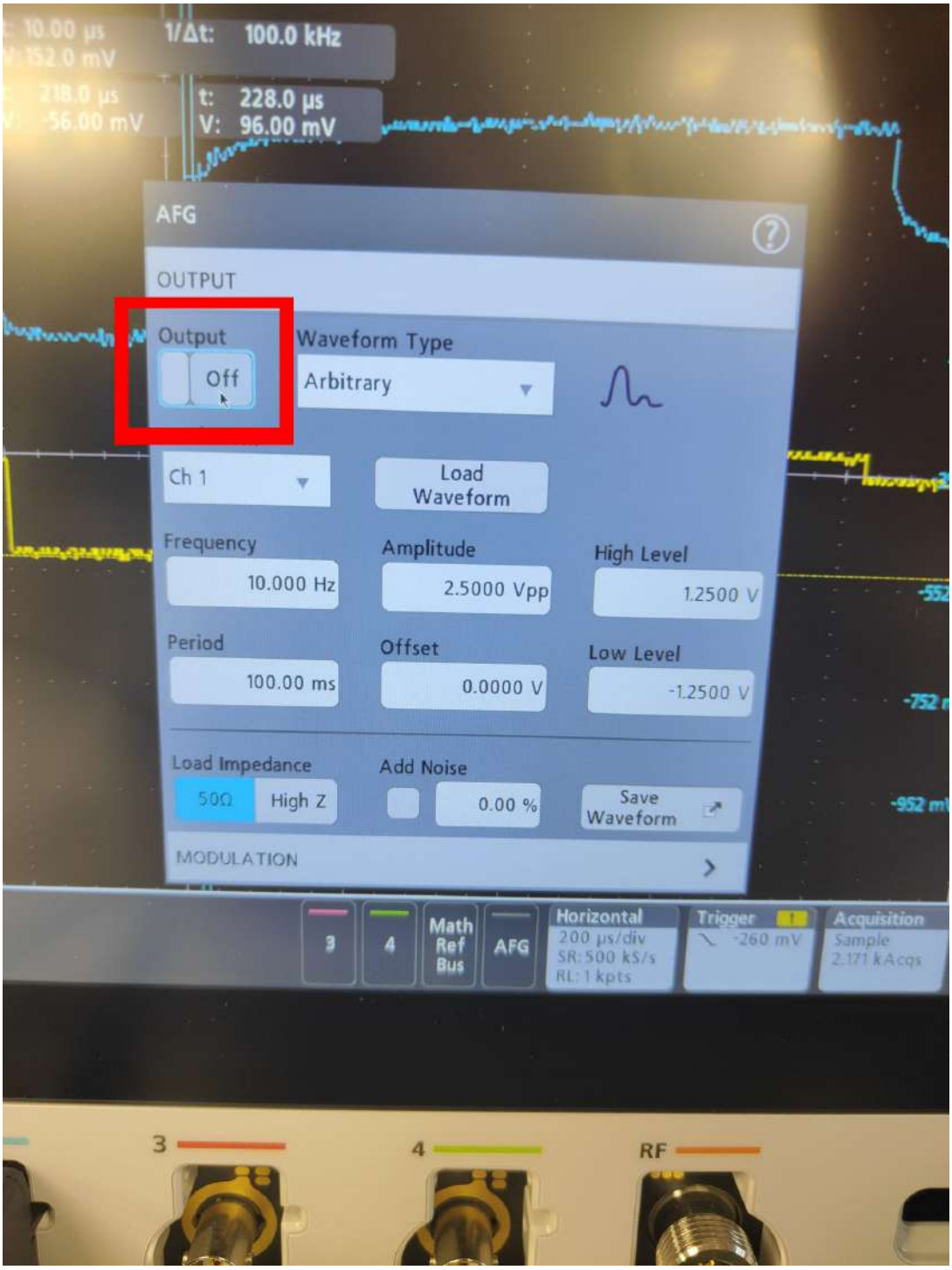

Figure 4.17: Long press the AFG icon in the oscilloscope´s touch screen, and this menu shall pop up. On the top left, you may toggle the digital switch to turn off the AFG directly. This is important while not actively running tests to avoid excessive damage to the sample.

3.1 Running the test with the Manual Code

The overall flow with the Manual VT code is as follows:

- Input cathodic current, both cathodic and anodic pulse duration and interpulse delay parameters to create a biphasic current pulse. See Figure

4.18. Note that the maximum value possible for cathodic current is 1e-3.

voltage_transient_version0.py

C: > Users > ERTS > Desktop > VTs > voltage_transient_version0.py > main

```
1   from alab import tektronix
2   from alab.tools.signal_generation import generate_bipolar_pulse
3   import numpy as np
4   import matplotlib.pyplot as plt
5   import datetime
6
7   def main():
8       # pulse parameters, all durations are in seconds, all currents in amperes.
9       pulse_repetition_period = 100e-3
10      cathodic_duration = 200e-6
11      cathodic_current = 0.1e-3
12      inter_phase_delay = 20e-6
13      anodic_duration = 800e-06
14      anodic_current = cathodic_current * (cathodic_duration / anodic_duration)
15
```

Figure 4.18: Section of code where parameters dictaminating the pulse´s profile can be set. The most important parameter, cathodic current, has a maximum value of 1e-3.

- Run the code
- If no output is shown, it may be because the trigger value is too high for the pulse sent. Play with the trigger until the signal in CH1 is detected.
- Use the measurement tools to determine Va at both pulses´rising edges. See Figure 4.19 for an example.
- Note that the latest manual code continuously sends pulses. If damage to the sample is to be reduced, stop the pulses by turning off the AFG while performing measurements.
- If at neither edge Va (the WW limit at that end) is reached, increase again the cathodic current parameter and repeat.
- If Va is exceeded, a smaller value for cathodic current is needed. **WARNING** If an electrode exceeds its WW Va, it may start overcharging and drifting, outputting increased voltage transients, and posing additional risks to the integrity of the electrode. When decreasing the cathodic current after exceeding Va, do so significantly and wait for the voltage transient output to settle back to its normal response before increasing the cathodic current parameter again.
- Although finer resolution steps are possible, I would type in code increments no smaller than 0.001.

- If the cathodic current is set to the maximum value (1e-3) and the maximum voltage is still not reached, it is necessary to go to a lower conversion resistance (R1<R2<R3<R4). For more on this, check the subsection 'Modifying the PCB configuration'
- If maximum Voltage is reached, first ensure the axis of the oscilloscope is correct (they will determine which data is exported), and then type 'y' when prompted in Visual Studio Code to save the data.

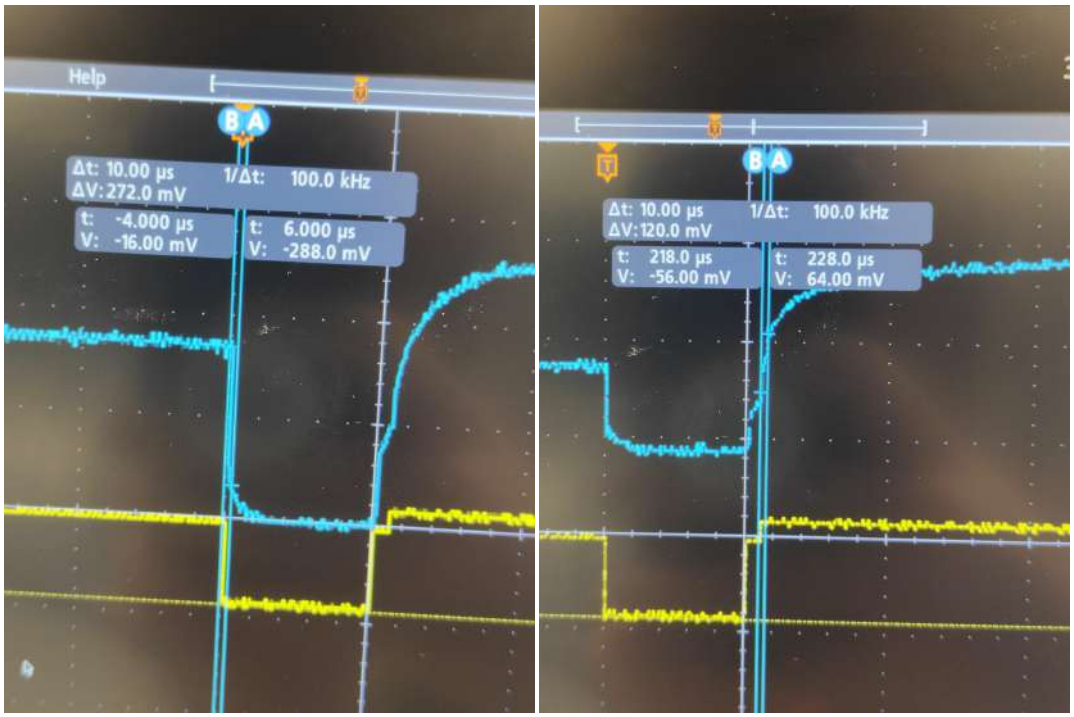

Figure 4.19: Manual detection of Va is done with the measurement tool within the oscilloscope. Always perform the measurement of the voltage drop over the same time span (10µs here), with a point previous to the drop measured against a point immediately after the drop. Do this on both the cathodic and anodic edges.

```
PS C:\Users\ERTS> & C:/Users/ERTS/AppData/Local/Programs/Python/Python311/python.exe c:/Users/ERTS/Desktop/VTs/voltage_transient_version0.py
Total sample count: 100000
CH1
CH2
Save? [y/N]y
```

Figure 4.20: If the set pulse has maximized the injected current, type y in the terminal when prompted to save the pulse´s measurement. A .txt file will be created in the file directory chosen in VSC.

3.2 Modifying the PCB configuration

Operating the VCCS PCB is an integral part of VT testing. Misuse of the PCB may lead to damage in both the sample and the PCB.

DISCLAIMER: This protocol is written with the VCCS PCB V0 in mind. Any further versions may differ slightly in build, and thus in operation

VCCS PCB Elements

The PCB offers the following possibilities

- Switches: To be turned ON or OFF. For easier operation, use a tool, preferably one made out of a non-conductive material.
- Output Jumpers: Two pairs of jumpers offer different configurations when connected or not. You need a jumper connector.
- Shunts: For electrical testing, they provide signal information before and after the current conversion through resistors R1-R4

Figure 4.21: Shunt connectors can be used to test the signal before and after the current conversion happens at resistors R1-R4

Specifically, these elements are the ones used in regular VT testing:

- **Output Switch:** Turning it ON grounds the whole output signal. Use it to isolate the sample from whatever output the PCB is sending.
- **Conversion Resistance Switches R1 to R4:** Turning ON these switches makes the PCB use the resistor associated with each switch when converting voltage to current. Resistor values grow in decades, with values

stated in subsection 'VCCS PCB, Oscilloscope and Cage Preparation'. If more than one switch is turned on, the one with lower resistance will dominate over the rest, so there really is no point in doing this.

- **Right Side Jumpers:** If these jumpers are connected, the capacitor in series with the output will be shorted. This is very likely to introduce a DC Voltage offset, capable of damaging samples when done with Resistors R2, R3, R4. But it is necessary when testing with R1.
- **Left Side Jumpers:** Indicated by the symbol on the board, it grounds the circuit previous to the output stage. This is useful for discharging elements and should be used as a safety measure when changing resistors.

Common Practices with the VCCS PCB

A common scenario in VT testing is that a resistor needs to be changed to a lower/higher resistance one due to the sample having a lower/higher resistance than initially assumed. If changing to R1, please follow the procedure described after this one.

To perform the resistor switch safely:

Procedure to change to resistors R2, R3 & R4

- Start by turning OFF the AFG.
- Turn OFF all resistor switches
- Turn ON the output switch, grounding the signal sent to the samples.
- Optionally, place a jumper on the LEFT side pins, grounding the internal circuitry. Then, immediately remove the jumper
- Turn OFF the output switch
- Turn ON the resistance switch of interest
- Return to section 3.1 Running the test with the Manual Code to continue experiments.

Procedure to change to R1

- Start by turning OFF the AFG.
- Turn OFF all resistor switches.
- Turn ON the output switch, grounding the signal sent to the samples.
- Optionally, place a jumper on the LEFT side pins, grounding the internal circuitry.

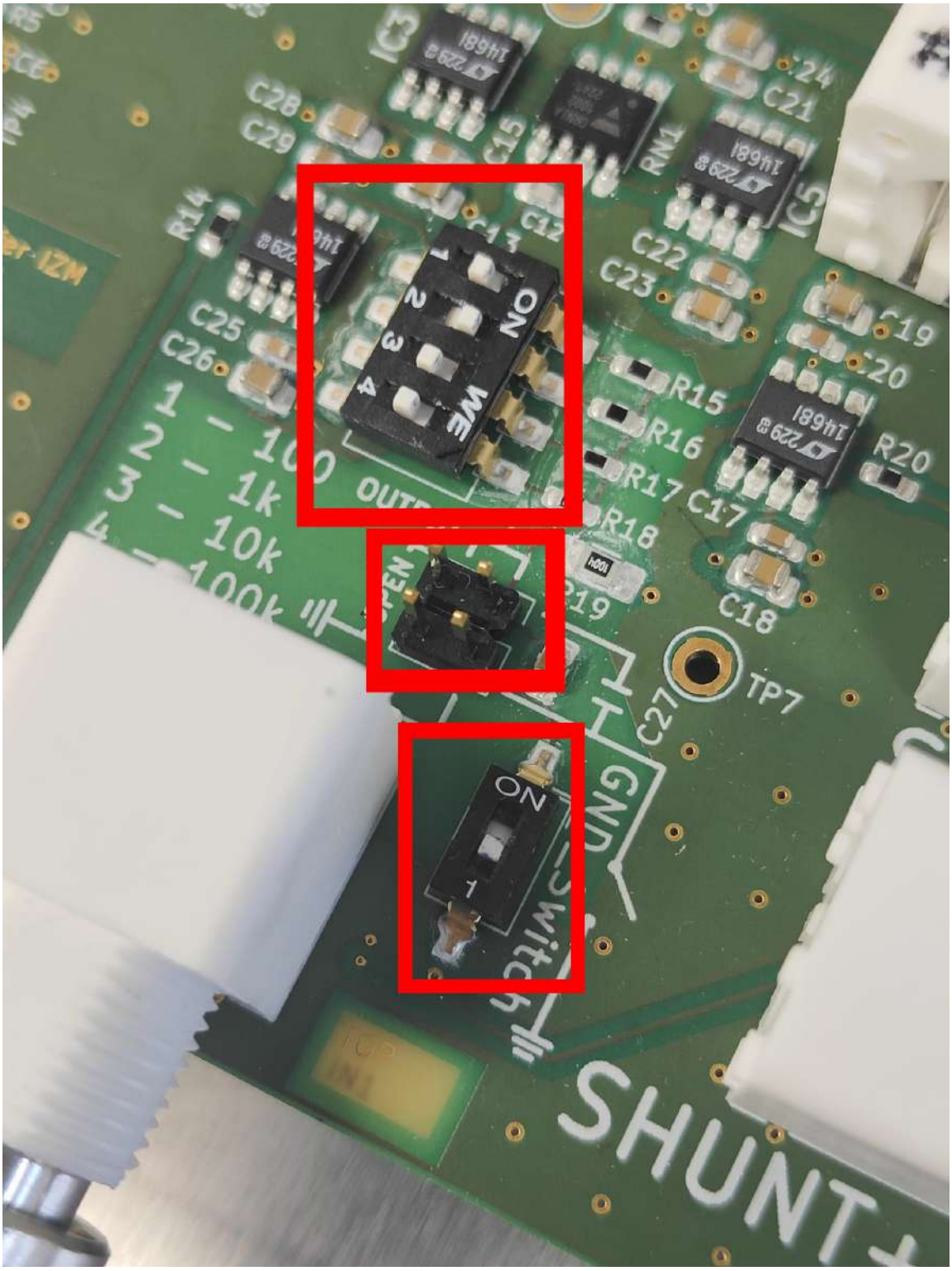

Figure 4.22: Common board elements that need to be interacted with throughout testing. From top to bottom in the picture: Conversion Resistor bay 4-switch, Jumper pin pairs and Output GND switch.

- Move the jumper to the two RIGHT side pins.
- Turn OFF the output switch

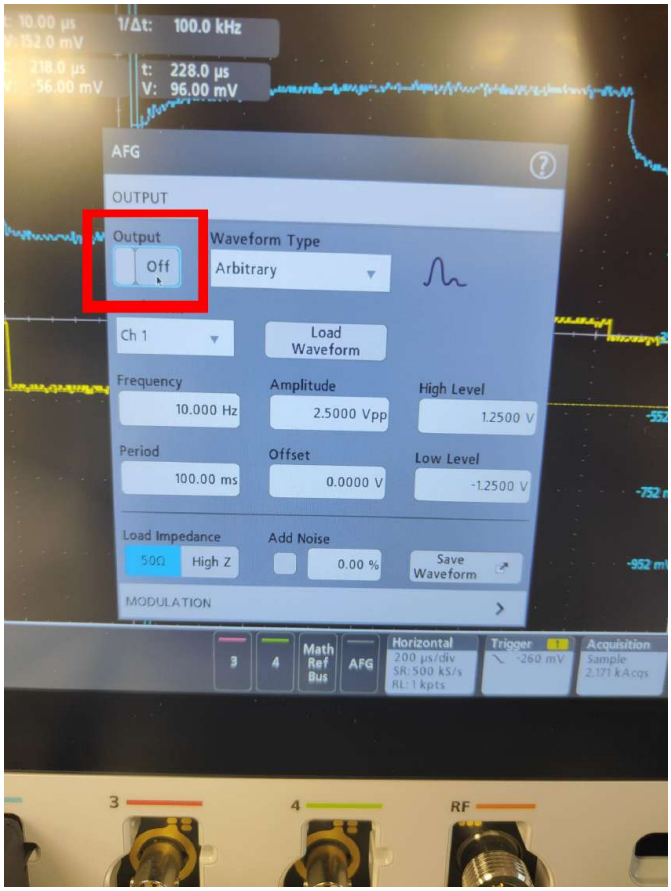

Figure 4.23: Again, to switch off the AFG, long press the AFG icon on the Oscilloscope´s screen, and switch it off with the digital toggle switch.

- Turn ON the resistance switch of interest

4 Clean Up

Clean-up specific to VT tests implies disconnecting and storing the VCCS PCB and the Oscilloscope.

Start by powering off the AFG of the oscilloscope, if you have not done it before. It can be done from the oscilloscope´s screen: long press the AFG box in the bottom bar of the screen, then select the option to turn it off.

Next, power off the oscilloscope and the PCB. The oscilloscope is powered off by pressing the power button, found at the bottom left corner of its front side. The VCCS PCB is powered off by removing the USB cable from both the PCB and the laptop. If the mini USB cable was borrowed, return it to where it belongs.

Disconnect any other BNC cables connected to the PCB. These should be the input Y-splitter and the output cable. If there are BNC cables connected to the shunts, disconnect these too. To store the PCB, it is a good idea to store it with its jumper to avoid losing the latter. Store the jumper by connecting it to the two TOP pins (**DO NOT CONNECT IT TO TWO SIDE PINS**) and it should be safe.

Proceed by disconnecting any probes from the oscilloscope. In the case of CH1, this would be done by unscrewing the BNC cable. For CH2, press the release button of the probe connector and pull it back. Then make sure that the measuring ends of CH2 are disconnected from the rest of the cables, and store the probe in the probe bag that should be attached to the handle of the Oscilloscope.

The other Oscilloscope cables connected to its backside can also be stored. This is the case for the USB to USB-A cable, which should be disconnected from the laptop first; the power cable, which should be unplugged first; and the AFG Out BNC cable can be disconnected too. Set aside the USB and power cables, as these should be stored with the Oscilloscope in lab 231.

Now you should be left with the Output BNC cable carrying the connections to the Faraday Cage. Start by releasing the crocodile grippers grounding the negative signal (black cable in the BNC, red port in the cage) to the cage. Then, for ease of setting up, you may disconnect the banana cables from the cage, while keeping them connected to each other in the same configuration. You may store the BNC cable like this. This also applies to the two BNC cables joined by the T-splitter. Take them and store them without dismantling them for a faster setup.

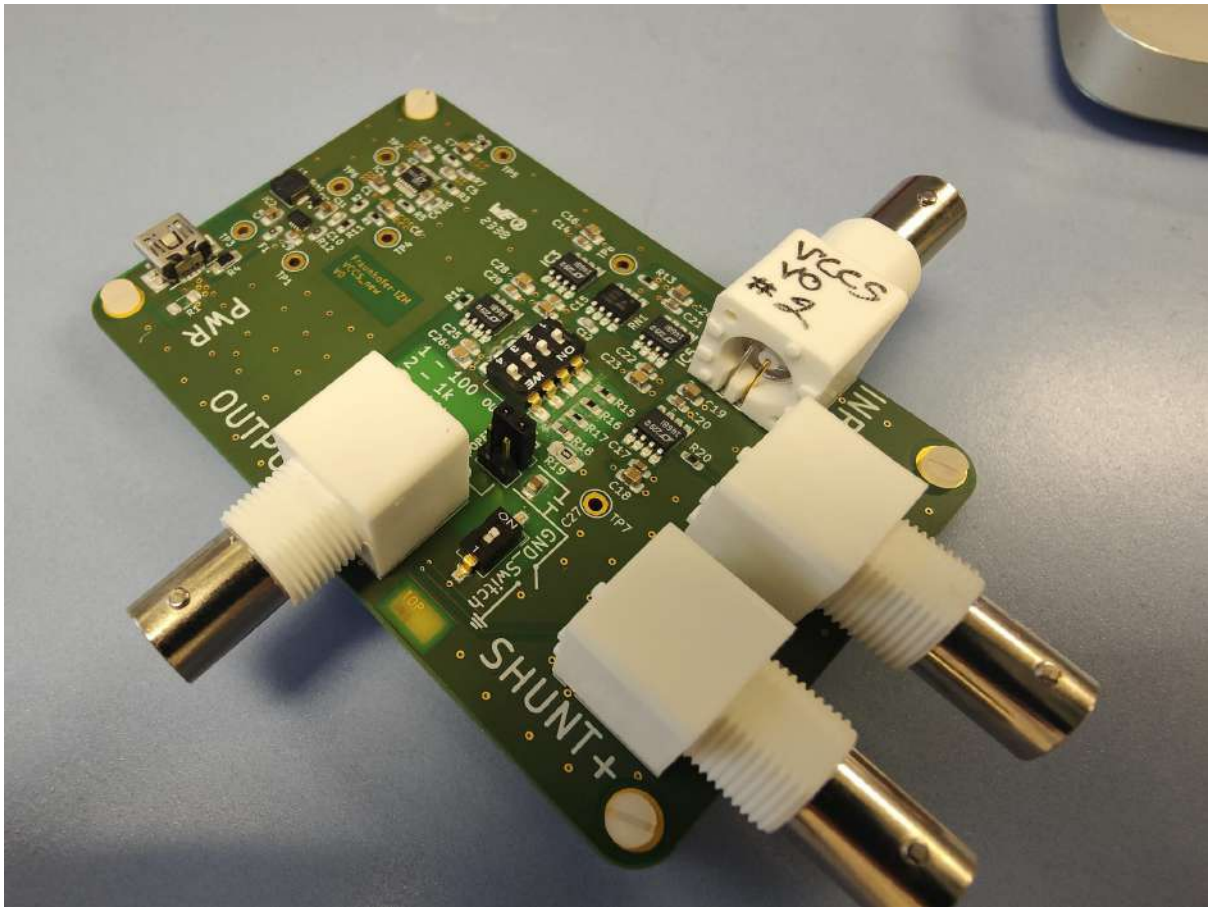

Figure 4.24: To store correctly the PCB, do the following: Turn off all conversion resistances, place the jumper on the two top pins, and set the Output switch to On, effectively grounding the output.

5 Data Retrieval & Processing

In the same folder, VTs found in the Desktop, .txt files with the timestamp of the text as names should have been generated.

Rename them according to the sample and test performed, and copy them onto an external USB drive.

Before analysis, it is important to transform the .txt file into a file we can work with, in this case, .xlsx. To do this, open the .txt file from Excel and follow these steps:

- File > Open > Choose .txt file
- A window for the import configuration of the file will appear.
- In the first screen, select "Delimited" (Default). Then click Next.
- Choose the following Delimiters: Tabulation, ; , Space and = (in custom delimiters). Then click Finalize

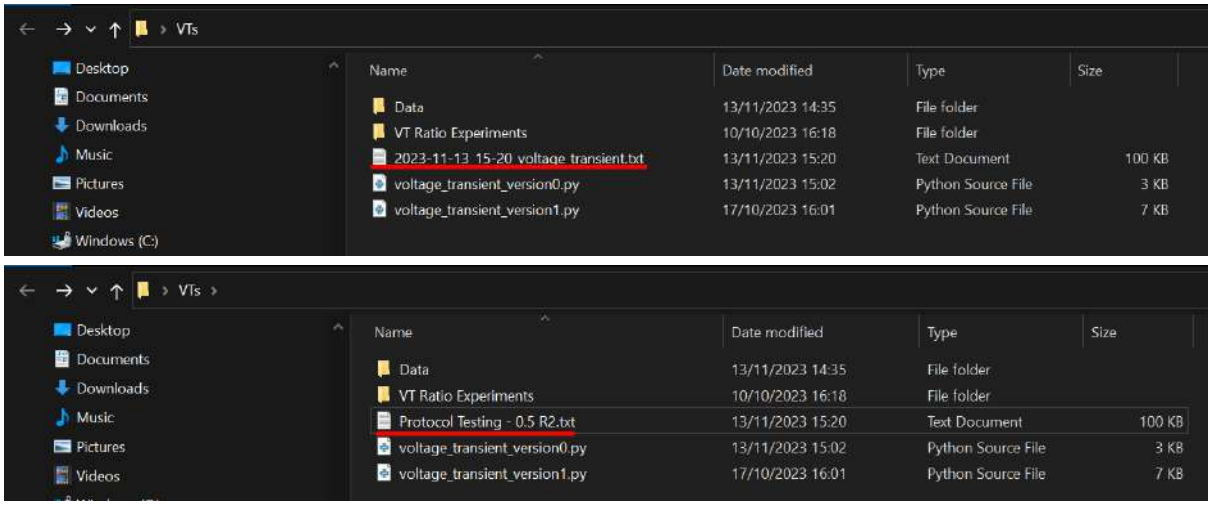

Figure 4.25: The data .txt file should have been exported to the VTs file folder (if this was chosen as the file directory in VSC). Rename it accordingly.

- In the new file, four rows should be filled with data for our four arrays. In row 6, input the following data: Cathodic Current value in cell A6, Cathodic Duration in cell B6, and Resistor value in cell C6.
- Delete all values from row 1. It should be empty.
- Save as an .xlsx file

To analyze the data, the Matlab code in the file "VTsNtests" will be used. Run the code to import the .xlsx files and indicate their diameter opening. The code will output plots for the data, as well as metrics such as CIC.

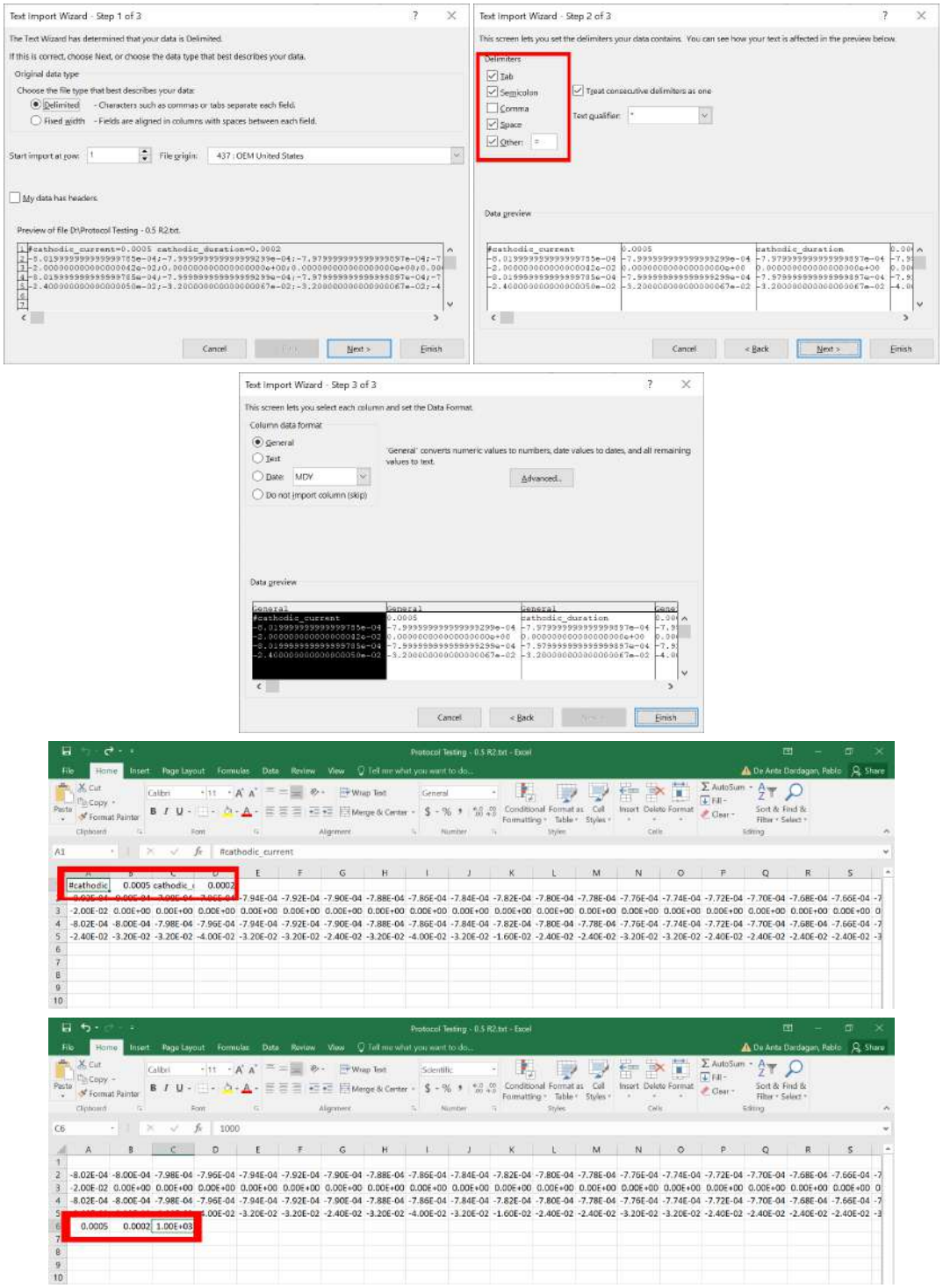

Figure 4.26: Procedure to convert the .txt file into an .xlsx file that the Matlab script can process.

5

ONE-TIME EXPERIMENTS

1 WATER-WINDOW TESTING

1.1 INTRODUCTION & SETUP

Water-Window (WW) testing is a specific type of Cyclic Voltammetry experiment used to determining the voltage range of an electrode´s material for its safe operation. For further information on the Water-Window, check the relevant literature ([1, 2]) or the Literature Review by P. de Anta.

The experiment setup is identical to that of CV. Follow Chapter 2 Protocol for EIS & CV, Section 1 Setup Preparation.

1.2 WW TEST

To conduct a WW test, two separate CV experiments must be performed. Ideally, each test shall be performed with a different sample, as the test leads to the irreversible modification of the sample. One test is to determine the positive bound of the WW, which will be referred to as the WW+ test. The other test is to determine the negative bound of the WW, which will be referred to as the WW- test.

To perform the WW+ test, the following parameters are needed:

- **Voltage Window** Starting voltage is set to 0V, and the other bound shall be a voltage point clearly exceeding the theoretical WW. Usually, 1.5V suffices, but research into the material´s reported window is needed in case such voltage still lies within its WW. **For scenarios like this, choose a higher voltage than that of the WW+ bound**
- **Scan Rate** Slow rates are necessary for adequate WW testing. 50mV/s is a good standard.
- **Cycle Count** Set to 1. As the sample will be modified when taken to excessive Voltage values, there is no point in repeating the voltammetry experiment.

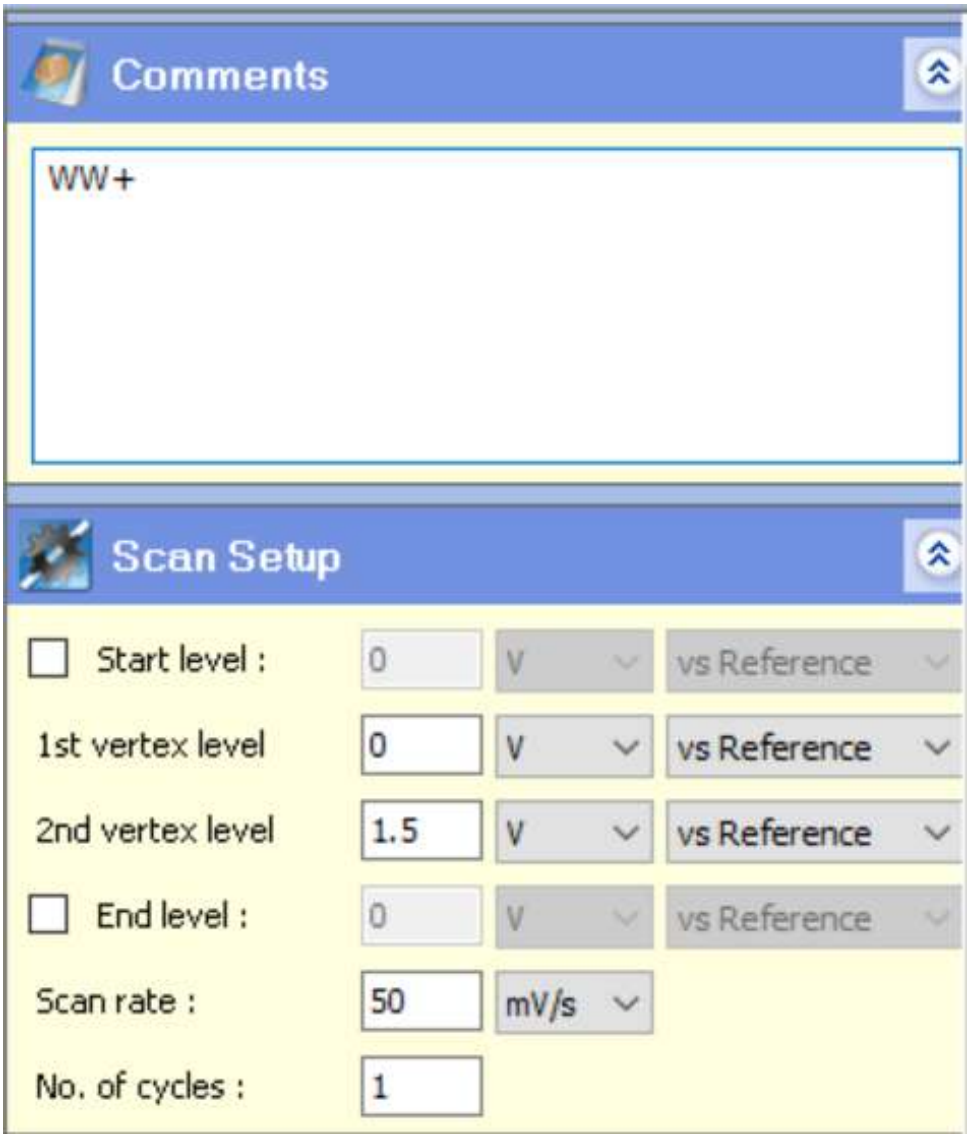

Figure 5.1: Settings in the CV experiment menu to conduct the WW+ test.

To perform the WW- test, the following parameters are needed:

- **Voltage Window** Starting voltage is set to 0V, and the other bound shall be a voltage point clearly exceeding the theoretical WW. Usually, -1.5V suffices, but research into the material´s reported window is needed in case such voltage still lies within its WW. **For scenarios like this, choose a lower voltage than that of the WW- bound**
- **Scan Rate** Slow rates are necessary for adequate WW testing. 50mV/s is a good standard.
- **Cycle Count** Set to 1. As the sample will be modified when taken to excessive Voltage values, there is no point in repeating the voltammetry experiment.

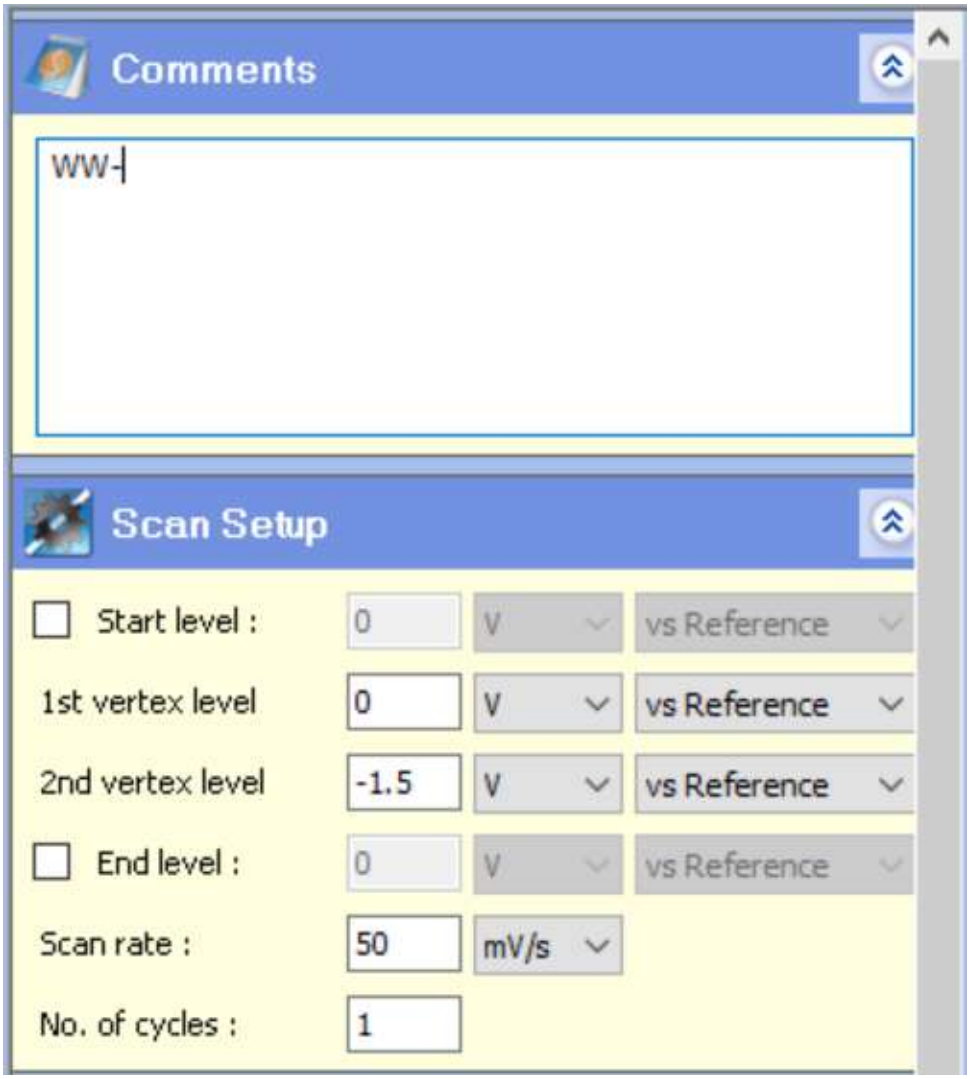

Figure 5.2: Settings in the CV experiment menu to conduct the WW- test.

1.3 WW Test Analysis

To determine the WW bounds, examine both experiments´ voltammograms. A peak in current density happens as the reaction voltage for water hydrolysis is approached, indicating the point past which our sample electrode is undergoing irreversible, damaging reactions. Set your WW bounds to a voltage between 0.1V and 0.2V smaller than the voltage measured at the peak of each bound.

NOTE: Subsequent CV testing at this WW is recommended to ensure survivability of the sample, as well as no signs of major surface modifications (which indicate irreversible reactions are happening)

2 Noise Characterization

6

GUIDELINES FOR A FULL SAMPLE CHARACTERIZATION

1 JUSTIFICATION AND THEORETICAL BASIS FOR A PREFERRED TESTING ORDER

In order to obtain accurate characterization data from a sample, it is important to be able to know its state prior to the test performed.

It has been established in the literature that some of the characterization tests described in this protocol (CV for instance) can potentially damage the electrode. Said damage may become visible under the microscope, or it may be simply subtle electrochemical changes in the electrode´s surface.

2 IDEAL GUIDELINE FOR A FULL CHARACTERIZATION

In order to minimize the potential risks of damaging these electrodes, and to obtain information from them throughout the process that would allow us to identify where things went wrong, the following testing guidelines are proposed:

1. **Avoid probing the electrodes with a tool** such as a multi-meter, as it will most likely damage the surface. If this step is needed, account for it by both imaging the sample (next step) and avoiding testing this sample.
2. Start by **imaging the sample electrode under the optical microscope.** This step is important to first measure the opening area and get an accurate approximation of the GSA of the sample. However, it is also important to have images of the sample prior to any testing to track potential future structural and surface modifications.
    - Other imaging methods may also be done here, such as Interferometry, or SEM.
3. **Begin ECM testing by running an EIS test.** EIS is highly unlikely to damage the sample and will also serve as an indicator of the health of the sample throughout testing
4. **Follow up with the VT test.** As the electrode voltage output is taken to

maximize its WW, potentially inducing non-reversible reactions, a risk of damage exists. Yet, the quick nature of the test usually implies no major damage happens.

5. At this point, **a sample check may be performed.** Repeat steps 2 and 3, imaging the sample and getting more EIS data. Modifications observed shall be attributed to the VT test.
6. **Finish with the CV testing.** As the sample is subjected to electrochemical stress, cycling back and forth from bound to bound of its WW, for a lengthy amount of time, it is the test with higher chances of damaging samples. Especially if WW bounds are not defined correctly.
    - If performing multiple CV tests at different scan rates, it is important to **do them from the fastest rate experiment to the slowest rate experiment.**
7. **A final sample check** is necessary to determine whether the CV scans damaged the electrode in any way. Microscopy and EIS are recommended, as there should be a record of previous measurements to compare to.

3 Ideal Guideline for a Time-Efficient Characterization

If pressed with time, but still wish to do a full characterization protocol that finds the optimum trade-offs between sample protection and testing time, follow these guidelines:

1. **Avoid probing the electrodes with a tool** such as a multi-meter, as it will most likely damage the surface. If this step is needed, account for it by both imaging the sample (next step) and avoiding testing this sample.
2. Start by **imaging the sample electrode under the optical microscope.** This step is important to first measure the opening area and get an accurate approximation of the GSA of the sample. However, it is also important to have images of the sample prior to any testing to track potential future structural and surface modifications.
3. **Begin ECM testing with the VT test.** Testing begins with VT as it requires a dedicated setup, Minimizing the overall preparation time. Again, as the electrode voltage output is taken to maximize its WW, potentially inducing non-reversible reactions, a risk of damage exists. Yet, the quick nature of the test usually implies no major damage happens.

4. **Follow up with the EIS test.** As performing an EIS will require setting up the Modulab XM, it will be more time-efficient and convenient for its later use in CV testing. EIS is highly unlikely to damage the sample, but it is important to note that running this experiment after the VT test would mean that possible modifications expressed in the electrochemical measurements will not be accounted for.
5. **Finish with the CV testing.** As the sample is subjected to electrochemical stress, cycling back and forth from bound to bound of its WW, for a lengthy amount of time, it is the test with higher chances of damaging samples. Especially if WW bounds are not defined correctly.
    - If performing multiple CV tests at different scan rates, it is important to **do them from the fastest rate experiment to the slowest rate experiment.**
6. **A final Microscopy sample check** is necessary to determine whether the whole characterization procedure damaged the electrode.

7

CLEAN UP - GENERAL

1 CAGE CLEAN UP

After cleaning up the specific instruments needed for the different tests, specified under the Clean Up sections of Chapters II and III, there should still be some common instruments left to clean up.

Start by stopping the thermostat from pumping liquid. To do this, press the STOP button on the bottom right corner of the thermostat's screen (figure 7.1), and then the OK button that pops up.

DO NOT ATTEMPT TO DISMANTLE THERMOSTAT BEFORE STOPPING THE THERMOSTAT FROM PUMPING HEATING LIQUID

Figure 7.1: Turn off the thermostat´s pump to stop the heating liquid from circulating the tubing. Press the stop button (bottom right corner) and then the Ok button that will show on the screen

Ensure all electrical connection cables from the inside of the cage are safely put away by placing them on the inside of the door, using the metal beam as a holder. Use Figure 7.7 for further reference.

Figure 7.2: Use the thin beam on metal door of the faraday cage to hold and store all of the internal cabling. The N2 probe can also be held out of the way for easier operation with the cables´ support, shown in the picture.

Remove the electrode holder and place it outside of the cage, on the loading support.

Grab a 1L glass beaker and place it inside the cage. We will pour the PBS from the double glass walled beaker into this 1L beaker. For best results, place the 1L beaker at the back of the cage, and pour the PBS away from you. If there are any spills, clean them up.

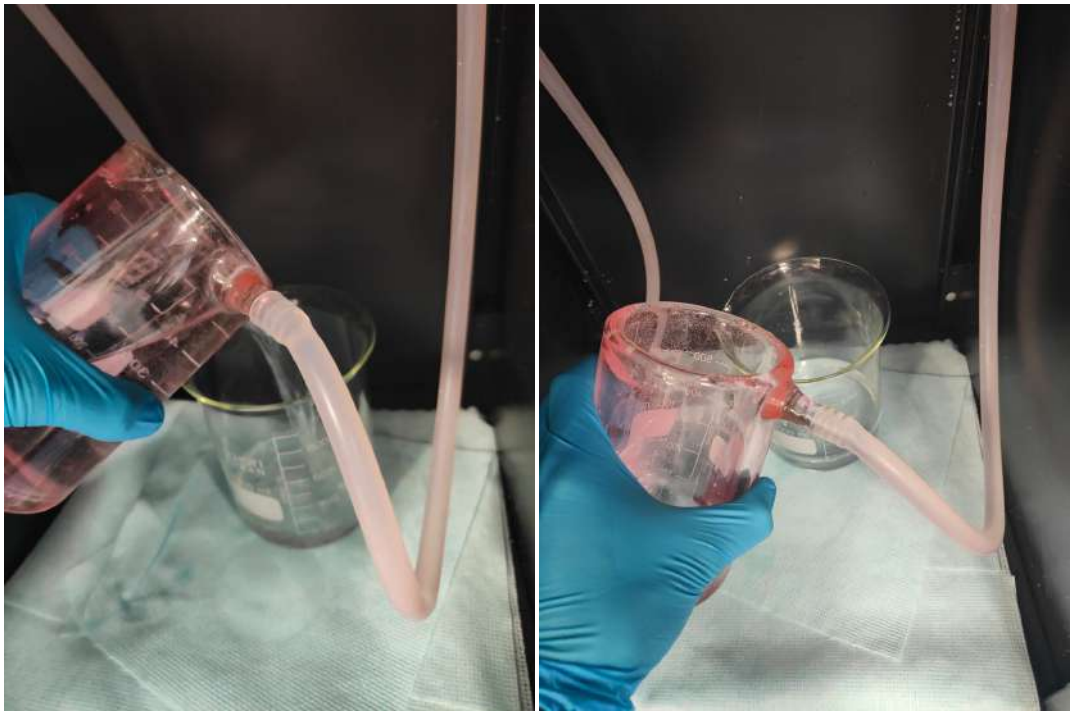

Figure 7.3: The PBS in the double glass walled beaker must be emptied before dismantling the thermostat´s tubing. To avoid spills, it is easier to pour the PBS away from you than towards you. Place a large beaker at the back of the cage and transfer the PBS

You may now take the beaker and empty the PBS in the basin. Rinse and dry the beaker (or place it in the dishwasher), and store it back in its cabinet.

Disassembling the double glass walled beaker and its heating liquid can be a bit tricky. Still, you must have gotten an introduction to using the thermostat. The way described here attempts to make this step as safe and foolproof as possible. Please see Figures 7.4 and 7.5 for additional pictures of each of the process´s steps.

- To ensure that there are no spills when disconnecting the thermostat tubing, start by picking up the doubles-glass-walled beaker and hold it high enough so that the connections are higher than the ports of the cage. This will ensure the liquid flows through the port, and not through the opened connection. (7.4 top left)
- Slowly pull out the tube from the connection. It is helpful to start by using your nail to pull back the first centimetres (7.4 top right). Once the tube is close to being pulled out, its grip loosens considerably.
- Additionally, try to pull it back from different sides of the circumference. This will help with breaking the seal.

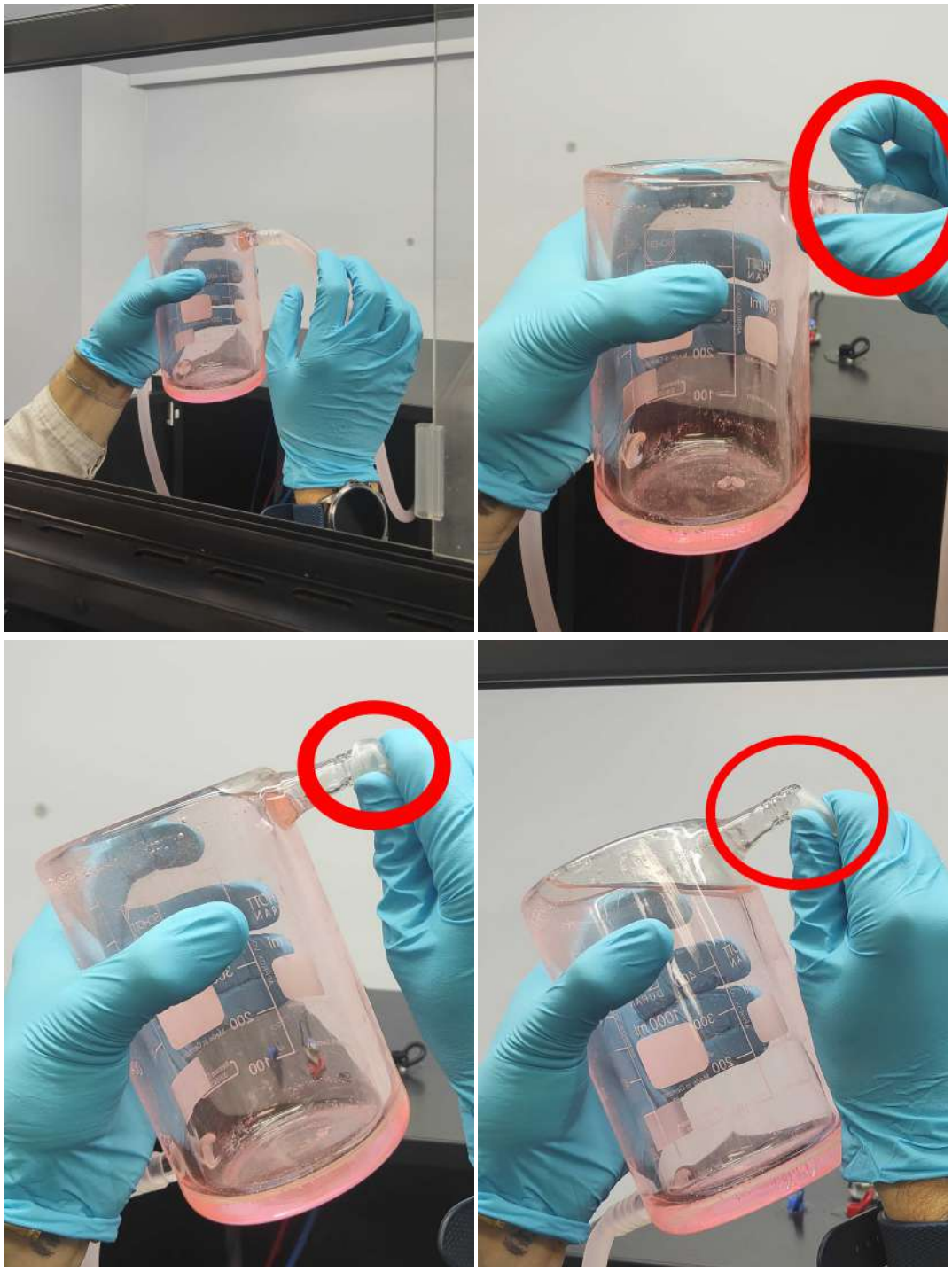

Figure 7.4: (Top Left) By holding the double-glass walled beaker in a high position while dismantling it, the risk of heating liquid flowing back and spilling is reduced. (Top Right) Use your nail to break the seal and pull back the tube. (Bottom Left) As the tube is pulled, bend it. (Bottom Right) If bent at almost 90º, air will come in, allowing for the liquid to flow back, without the risk of spilling.

- If before the tube comes out, you bend it at almost 90°, air will come in, and the liquid will start to flow back into the thermostat, ensuring no liquid spills (7.4 bottom right).
- With the top connection's tube disconnected, hold both beaker and tube

high, and ensure the thermostat liquid flows back through both of the cage's ports (7.5 Left).

- You do not have to disconnect the bottom port of the beaker. To avoid heating liquid from leaking out of the top connection tubing, you may leave the whole setup as in the picture 7.5, or reconnect it to its port again.

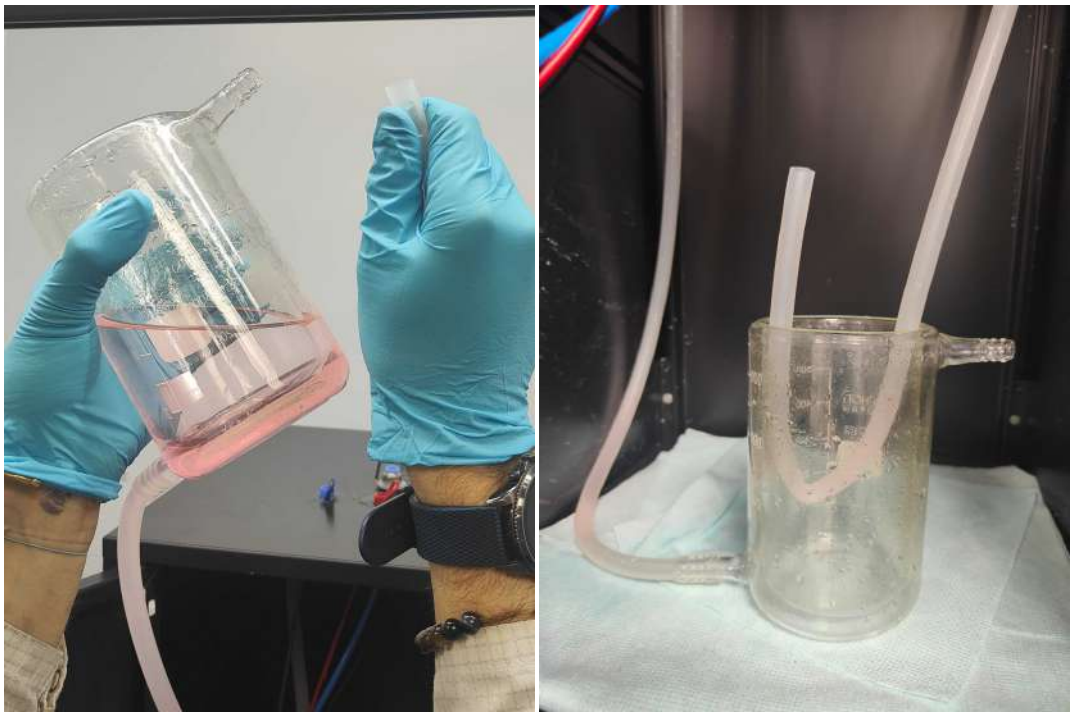

Figure 7.5: (Left) Hold both the beaker and the tube in a high position to allow the liquid to flow back into the thermostat. (Right) One can keep the cage´s inner tube as in the picture to avoid potential spills from leftover heating liquid. Alternatively, the top port´s tube could be reconnected to the beaker.

Ensure the thermostat liquid has flown out of the whole tubing section, especially the outer tubing circuit. If there is some liquid stuck, it is as simple as lifting the previous section and letting gravity do the rest.

With the tubes empty, the outer tube connections may be undone. Open the plastic fasteners, and pull the tubes apart. Store both fasteners and the thermostat's tubes in the white plastic tray to avoid losing anything.

Turn off and unplug the thermostat. Then it may be stored between the two digestoriums using its cart.

You may also disconnect the N2 probe. To pull it out of the port, first press down on the outer rim of the port to release the tube. Store it nicely behind the ERTS setup.

Figure 7.6: Loosen the plastic fasteners and disconnect the tubing sections. The tubes connected directly to the thermostat may be kept within the tray, to keep minor spills from falling on the floor

If not done yet, now is as good of a time as any to clean your electrodes before storage. Use DI water and IPA. And if the electrodes can withstand pressurized air (flexible electrodes may be damaged), use the pressurized N2.

2 Computer

If all the test files have been transferred to a USB drive, you may close all programs and turn off the computer. Please also make sure to disconnect and store the computer's charger next to the Modulab XM+.

3 Electrode Holder

Place any kind of leftover holder, equipment or miscellaneous item in the storage box labelled **Electrode Characterization**. This box may then be kept in the second tray of the metal cart situated left of the workbench.

4 PBS & Final Remarks

In order to ensure that fresh PBS is always available, it is recommended to have it dissolve overnight.

Figure 7.7: Equipment needed to make and store fresh PBS according to the protocol. It is best to make fresh PBS when two of the 0.5L jars are empty, as each tablet is meant for 1L of DI water.

If the two 0.5L blue-cap jars of PBS are empty, you may start by filling them up with the previously PBS-filled 1L blue-cap jar. For easier pouring, you may use the large glass funnel (it tends to move around a lot in the lab, common places are the glass cabinet, and the workbench by the windows looking to the building's corridor)

With the 1L blue-cap jar empty, we may use it to make PBS. Pick the white tub of CarlRoth ROTI PBS pH 7.4, 1L, 0.1 Molar tablets. We only use the large blue-cap jar because the tablets are meant for dissolving in 1L of DI Water.

Figure 7.8: (Left) Large glass funnel, optional (but useful) for safely transferring PBS between jars. (Right) CarlRoth ROTI PBS pH 7.4 tablets are meant for 1L of DI water.

Fill the blue-cap jar with 1L of DI water. For cleaner water, start running the DI water tap (green valve), and then start the additional filter by pulling out the round lever. Fill it up to 1L, then drop one tablet of PBS and close it off.

Store the jar. At the end of the process, you should have at least two 0.5L jars of PBS (two test mediums), and a 1L jar of PBS dissolving overnight.

Store the PBS in the digestorium. You may now close off the glass shield using the screen on the right side of the digestorium.

Before exiting the CoALab, if nobody else is working there, ensure that the air ventilation is turned off.

Figure 7.9: Two types of DI water may be used in CoALab. Open the regular DI Water for the same DI water that is found across the institute. Pull the pin by the faucet to drive the flow through the additional filtering station.

BIBLIOGRAPHY

[1] S. F. Cogan, "Neural stimulation and recording electrodes," *Annual Review Biomedical Engineering*, 2008.

[2] C. Boehler *et al.*, "Tutorial: guidelines for standardized performance tests for electrodes intended for neural interfaces and bioelectronics," *Nature Protocols*, 2022.